Development of Dynamic Equivalent Models for Large Scale Wind Power Plants

Dong-Eok Kim

A dissertation

submitted in partial fulfillment of the

requirements for the degree of

Doctor of Philosophy

University of Washington

2014

Reading Committee:

Mohamed A. El-Sharkawi, Chair

Daniel S. Kirschen

Richard D. Christie

Program Authorized to Offer Degree:

Electrical Engineering

University of Washington

Abstract

Development of Dynamic Equivalent Models for Large Scale Wind Power Plants

Dong-Eok Kim

Chair of the Supervisory Committee:
Professor Mohamed A. El-Sharkawi
Electrical Engineering

An individual wind turbine has trivial influence on existing power systems owing to its very small percentage of the total generation. In contrast, wind power plants (WPPs) that have large numbers of wind turbines in relatively small areas have significant impacts on the power systems, and thus their influence must be considered in the studies. This dissertation is of developing suitable dynamic models of WPPs for power system dynamics study.

In this dissertation, dynamic equivalent models (DEMs) for large scale WPPs are proposed for the dynamics study. As the dynamics of a WPP are the resultant dynamics of interconnected multiple wind turbines, its DEM is developed based on the knowledge of individual wind turbines and their interactions. In addition, as the dynamics of individual wind turbines are related to their control scheme, this study explains how to achieve an optimized control scheme for them with the use of the DEM.

For a certain purpose in which a WPP is considered as an external system for dynamics study of a power system, its DEM can be developed based on measurements at point of interconnection without any pre-knowledge of the WPP. For the case, this dissertation also proposes a DEM developed using an adaptive system identification method.

In addition, this study explains how to model an adequate power system for simulation tests. The validities of the proposed DEMs developed in this dissertation are verified by the simulation results with the power system model.

Contents

Chapter 1

Introduction

1.1 Background

Interconnected power systems cover large geographical areas and comprise thousands of devices. In addition, real power systems consist of numerous models, such as generators, excitation systems, control parts, and etc. That complexity makes it very difficult to perform studies for power systems, especially studies concerned with the stability of whole system, such as electromagnetic transient studies, on-line dynamic security assessments, off-line stability studies, and control design studies. Making those studies with fully detailed models requires a huge computation effort and a large amount of time. Thus, the studies are often performed with power systems broken down into several sub systems [1]–[7], where the sub system to be studied (internal system) is connected with other sub systems (external systems) by points of interconnection (POIs). If the dynamics at the POIs are retained, each of the power units in the external system is not important for internal system studies, and thus the external system can be replaced with its simplified equivalent model.

Wind farms have grown rapidly over the past couple of decades [8]–[13] and, in the USA, wind capacity in some regions has increased several-fold [10] in the past several years. Wind farms with capacities similar to that of conventional mid-size to large thermal power plants are called wind power plants (WPPs), and an increasing number of WPPs have begun to have a significant impact on existing power systems. Thus, WPPs are required to contribute stable operation of power systems with grid codes as do conventional power plants [14]–[19]. As an understanding of dynamics is essential for maintaining the stable operation of power systems, a proper dynamic model of the WPPs needs to be developed.

However, the WPPs differ significantly from the conventional power plants in terms of structure, operation, and dynamics, so a dynamic model of WPPs must account for their differences. Unlike dynamic modeling of conventional generation systems [20], the modeling of WPPs poses a unique set of problems: 1) a WPP consists of several small generators with limited dispatching capabilities; 2) each wind turbine includes multiple components that cause damping in electromechanical dynamics; 3) the wind turbines stand irregularly over a large area and their energy source (wind) varies stochastically, so the turbines operate differently; and 4) the turbines are mutually interconnected by cables so that they are affected by the operation of each. These problems make modeling WPPs a complicated process in which high-order models will necessarily be produced; it is therefore necessary to develop low-order dynamic equivalent model that can provide the same dynamic performance as the WPP models.

The development of a dynamic equivalent model for conventional power plants has been carried out over numerous studies [21]–[31], and they typically followed three procedures: coherency identification, network reduction, and generation aggregation. Similarly, dynamic equivalent models for WPPs have been developed over several researches [32]–[43]. These researches were accomplished in terms of: comparatively small-scale WPPs [34], [35], equivalent network construction [36], [37], use of a specific type of wind turbines [38]–[41], and relatively fast dynamics [42], [43]. However, a dynamic equivalent model (DEM) should be developed on the basis of comprehensive attributes of WPPs, not just one of them. Furthermore, it should be focused on slow electromechanical dynamics rather than fast dynamics when studying interaction between power systems [6], [24]. Therefore, an accurate slow dynamic DEM development technique, which could be applied regardless of the size, configuration, and complexity of WPPs, and even the use of multiple types of wind turbines in the WPPs, is still required.

1.2 Research Objective

A DEM should be developed to serve the purpose. If a DEM is meant to be for the study of WPPs themselves, such as WPP design, control, and stability study, it is important to identify their parameters and configuration inside the WPP. Although it requires huge efforts to identify them owing to the high degree of variability in wind as well as the switching of the turbines, they are directly correlated to the stable operation of WPPs. Therefore, a DEM, especially concerned with the stable operation of WPPs, should be derived on the basis of these parametric and configuration information of WPPs.

On the other hand, if a DEM is meant to be an imitation of external dynamics for the study of other systems, another approach could be made. An effective DEM for this purpose must have the following attributes: low order, yet accurate for dynamic studies, adaptability, to accommodate variations in wind and turbine switching; and ease of use, with no need for hard-to-find parameters within the WPP. Several attempts were made to develop lower-order DEMs for wind farms [44]–[48]. Most of these techniques, however, are based on the identification of the coherent performance of the turbines. Hence, they can be developed only when several parameters within the WPP are always available. This is a major hurdle because wind variability can change the operating status of individual turbines without the knowledge of the control centers of the utilities. Therefore, a DEM needs to be developed without knowledge of parametric or configuration information inside the WPP. Instead, it would be better to use measurements at the POI. Because the WPP is frequently subjected to natural disturbances due to wind variations and wind gusts, there is no need to disturb the system intentionally to acquire a dynamic response. In addition, the model needs to be adaptive to track the variability in wind seasons and any large changes within the farm.

This study proposes two types of DEM development methods: 1. a DEM of a WPP using aggregation technique, 2. a DEM of a WPP using parameter identification. For the first method, a DEM of a WPP based on aggregation techniques is derived. Separate models of wind-torque characteristics, drive trains, generators, and power converters are introduced and then combined to model a wind turbine. The constituent turbines of the WPP are clustered into several groups depending on type and operational conditions and slow dynamic models for the various groups and matching equivalent static network models in their respective local frames are developed. Then, the slow dynamic models are combined with the network models in order to express the WPP DEM as a single low-order system. For the second method, a DEM for WPP is developed on the basis of measurements. First, some data are measured and the measured data are properly processed for use in the identification process. Then, the DEM parameters are derived in the process, and the DEM is properly expressed with the parameters in a form of state-space equation to represent a low-order WPP system.

1.3 Outline of the Research

The study follows this configuration:

- In chapter 2, a detailed model of a WPP is first developed. In this chapter, separate models of wind-torque characteristics, drive trains, generators, back-to-back converters are introduced and then combined in order to model a complete wind turbine. Next, several types of network models are developed. Last, wind turbine and network models are combined to represent a wind power plant in a single large system.
- In chapter 3, a WPP DEM is developed using an aggregation technique, on the basis of the knowledge derived in the chapter 2. First, aggregation technique is briefly introduced. Then, slow dynamic model of wind turbines is developed. Equivalent slow dynamic models representing groups of the models are derived and the matching equivalent network model is also derived. The equivalent slow dynamic models are combined with the equivalent network model in order to express the WPP DEM as a single low-order system. Through simulation, the performance of the proposed method is verified.
- In chapter 4, a control design for wind turbines is performed. The control design is carried out using linear programming in the frame of linear matrix inequality (LMI). In doing the control design, a model in the form

of state space equation is required and the DEM introduced in the chapter 3 is used for it. The control method introduced in this chapter is used to control wind turbines.

- In chapter 5, a WPP DEM is developed on the basis of measurements at the POI. First, it is explained how the measured data is properly processed for use in the identification process. Then, the DEM parameters are derived in the process, and the DEM is properly expressed with the parameters in a state-space representation. In the simulation, an identification technique is used to obtain the DEM, and its performance is verified.
- In chapter 6, a power system modeling is explained. Generating units are modeled in the dq-representation and they are combined with a network model to represent a power system. IEEE 39 bus power system is modeled using the method introduced in this chapter and tested.
- In chapter 7, the DEMs developed in the chapter 3 and 5 are tested by interacting with a power system. A part of IEEE 39 bus power system is used as a power system. The power system is modeled as explained in chapter 6. The DEMs are integrated to the power system and its validity is proven by comparing the dynamics between the WPP and DEM.

Chapter 2

Modeling of Wind Power Plants

Wind power plants (WPP) consist of numerous wind turbines, and each wind turbine includes multiple components. Moreover, the wind turbines interconnect such that modeling WPP becomes a complicated process. To model large WPP, separate components of WPP should be modeled first and should then be combined.

The main components of a wind turbine are the drive train, generator, and power converter systems. Among these components, the generator and converter systems are nonlinear and therefore must be linearized. Once this is done, they can be combined to represent a complete wind turbine model. Then, multiple wind turbine models combine with a network model to represents a detailed model of WPP.

In this chapter, separate models of wind-torque characteristics, drive trains, generators, back-to-back converters are introduced and then combined in order to model a complete wind turbine. Depending on the wind turbine type, the combining process is slightly different, which this chapter shows as well. Further, several types of network models are developed. Last, wind turbine and network models are combined so that a wind power plant is expressed in a single large system. Once the wind power plant model is developed, the stability of the system could be analyzed by observing the eigenvalues.

Note that all the nonlinear models to be introduced in this chapter are linearized and used for the modeling of wind power plants. Although linearized models are merely available within certain operating ranges, they have distinctive advantages as far as networked systems are concerned such as wind power plant systems: easy to combine the models to a single complete system, so thus easy to check the stability of the complete system.

2.1 Wind Turbine Models

A wind turbine consists of several components such as the rotor blade, drive train, gear, generator, power conversion equipment such as back-to-back converters, step-up transformer, etc. These components are absorbed into three dynamic sub-models of the generator, drive train, and converters – including control parts – to represent a complete wind turbine.

2.1.1 Wind – Torque Characteristic

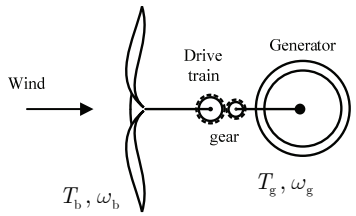

Fig. 1.1 A wind turbine

For a fixed speed wind turbine, the blade-captured wind power mainly varies by wind speed and pitch angle. On

the other hand, for a variable speed wind turbine, the captured power varies with the angular speed of rotor blade. The rotor speed can change up to 30 percent around synchronous speed. For both fixed and variable speed wind turbines, however, the captured power (blade power) is, on average, mainly regulated by pitch angle control.

The torque of rotor blade (blade torque) equals blade power divided by the angular speed of rotor blade. The relationship between wind speed and blade power was introduced in [49]. Using the relationships, the blade torque is given

$$T_b = g(\omega_b, w, \vartheta) = \frac{\rho}{2\omega_b} c_p(\lambda, \vartheta) A_R w^3 ; \qquad (\lambda = \omega_b R / w) \tag{2.1–1}$$

where ω_b is angular speed of rotor blade, ρ is air density, c_p is performance coefficient, λ is tip-speed ratio, A_R is swept area, ϑ is pitch angle, and w is wind speed. The performance coefficient relates to blade design and it might differ by the type of wind turbine. For fixed-speed wind turbines, blades (including gears) might be better designed to obtain the maximum performance around (or slightly over) synchronous speed, since generation is made with negative slip. On the other hand, for variable speed wind turbines, the maximum performance could happen under the synchronous speed.

For modelling of variable speed wind turbines using maximum power point tracking (MPPT) control, it might be necessary to calculate how much power a wind turbine can capture at a given wind speed. Thus, the operating conditions regarding (2.1–1) are calculated if necessary. Assuming the function of performance coefficient c_p is given, the corresponding pitch angle ϑ_o and tip-speed ratio λ_o can be obtained by using the newton-raphson method, where the solution is obtained at a point that the derivative of the function of performance coefficient with respect to the tip speed ratio is zero. The pitch angle is zero under the rated wind speed while not zero over the rated wind speed. After having the pitch angle, tip-speed ratio, and performance coefficient using the newton-raphson method, the rotor blade angular speed and blade torque are calculated.

Linearizing equation (2.1–1) and expressing it in per unit produces the following:

$$\Delta T_{bu} = \kappa_\omega \Delta\omega_{bu} + \kappa_w \Delta w_u + \kappa_\vartheta \Delta\vartheta_u \tag{2.1–2}$$

where

$$\kappa_\omega = \frac{\omega_{bB}}{T_{bB}} \frac{\partial g}{\partial \omega_b}\bigg|_{\omega_b=\omega_{bo}}, \quad \kappa_w = \frac{w_B}{T_{bB}} \frac{\partial g}{\partial w}\bigg|_{w=w_o}, \quad \kappa_\vartheta = \frac{\vartheta_B}{T_{bB}} \frac{\partial g}{\partial \vartheta}\bigg|_{\vartheta=\vartheta_o}$$

This equation could be used to model a wind turbine with wind speed input. Additionally, the dynamics of the pitch angle mechanism could be modeled with a first-order low-pass filter if necessary.

$$\dot{\vartheta} = -\frac{1}{\tau_\vartheta}\vartheta + \frac{1}{\tau_\vartheta}\vartheta_{ref} \tag{2.1–3}$$

where ϑ_{ref} is the pitch angle reference given by the pitch angle controller and ϑ is real pitch angle. τ_ϑ is time constant of the pitch angle mechanism.

2.1.2 Drive Train

Drive train model embodies the dynamics of the energy transfer from rotor blade by shaft to generator. In a one-mass lumped model of drive train, the angular speeds of generator and rotor blade are assumed to be the same ($\omega_{gu} = \omega_{bu}$).

$$\dot{\omega}_{gu} = \frac{D_u}{J_u}\omega_{gu} + T_{eu} - T_{bu} \tag{2.1–4}$$

On the other hand, by using a two-mass model of this process, the torsion effect of the shaft can be taken into account [50], [51], so that the angular speeds of the rotor blade and generator are different in a transient state. The two-mass type of drive train model is represented in per unit form:

$$\begin{pmatrix}\dot{\omega}_{gu}\\ \dot{\omega}_{bu}\\ \dot{T}_{su}\end{pmatrix}=\begin{pmatrix}-\frac{D_{gu}}{J_{gu}} & 0 & -\frac{1}{J_{gu}}\\ 0 & -\frac{D_{bu}}{J_{bu}} & \frac{1}{J_{bu}}\\ \left(K_{bgu}-\frac{D_{bgu}D_{gu}}{J_{gu}}\right) & -\left(K_{bgu}-\frac{D_{bgu}D_{bu}}{J_{bu}}\right) & -\left(\frac{D_{bgu}}{J_{gu}}+\frac{D_{bgu}}{J_{bu}}\right)\end{pmatrix}\begin{pmatrix}\omega_{gu}\\ \omega_{bu}\\ T_{su}\end{pmatrix}+\begin{pmatrix}\frac{1}{J_{gu}} & 0\\ 0 & -\frac{1}{J_{bu}}\\ \frac{D_{bgu}}{J_{gu}} & \frac{D_{bgu}}{J_{bu}}\end{pmatrix}\begin{pmatrix}T_{eu}\\ T_{bu}\end{pmatrix} \tag{2.1–5}$$

where the subscripts g and b signify generator and blade, respectively. D is damping coefficient, J is moment of inertia, and K is stiffness of shaft. Because of the gear ratio, the angular speed and torque are different at the side of the rotor blade and generator. Therefore, the base values for per-unit representation are also different depending on the side. They are given as:

$\omega_{bB} = \varepsilon\,\omega_{gB}$ (ε is gear ratio),

$J_{bB} = S_B \,/\, \omega_{bB}$, and $J_{gB} = S_B \,/\, \omega_{gB}$.

Equation (2.1–5) is expressed in the state space representation,

$$\dot{\boldsymbol{x}}_{dt} = \boldsymbol{A}_{dt}\boldsymbol{x}_{dt} + \boldsymbol{B}_{dt}\boldsymbol{u}_{dt} \tag{2.1–6}$$

where

$$\boldsymbol{x}_{dt} = \begin{pmatrix}\Delta\omega_{gu}\\ \Delta\omega_{bu}\\ \Delta T_{su}\end{pmatrix},\ \boldsymbol{u}_{dt} = \begin{pmatrix}\Delta T_{eu}\\ \Delta T_{bu}\end{pmatrix}$$

Subscript dt denotes drive train. It should be noted that, if the model is represented in the view of motoring, the generating torque will be indicated with negative sign.

2.1.3 Generators

The dynamic model used in this study applies to induction generators [52]–[60]. For wind turbines types 1 and 2, a stator current-rotor flux model is applied. For a type 3 wind turbine, a stator current-rotor current model is used while, for a type 4 wind turbine, rotor flux oriented (RFO) model is used.

2.1.3.1 Stator Current – Rotor Flux Model (Nonlinear Complex)

A model of induction machine (balanced) is expressed with state variables of stator current and rotor flux. It is represented in the nonlinear complex model in per unit form:

$$\frac{1}{\omega_B}\begin{pmatrix}\sigma L_{su} & \\ & 1\end{pmatrix}\begin{pmatrix}\dot{i}^c_{su}\\ \dot{\lambda}^c_{ru}\end{pmatrix}=\begin{pmatrix}-(R_{su}+a^2R_{ru})-j\omega_{su}\sigma L_{su} & a\frac{R_{ru}}{L_{ru}}\\ aR_{ru} & -\frac{R_{ru}}{L_{ru}}-j\omega_{su}\end{pmatrix}\begin{pmatrix}i^c_{su}\\ \lambda^c_{ru}\end{pmatrix}+\begin{pmatrix}1 & -a & -ja\\ 0 & 1 & j\end{pmatrix}\begin{pmatrix}v^c_{su}\\ v^c_{ru}\\ \omega_{ru}\lambda^c_{ru}\end{pmatrix} \tag{2.1–7}$$

where $i^c_{su} = i_{sd} + ji_{sq}$, $\lambda^c_{ru} = \lambda_{rd} + j\lambda_{rq}$, $v^c_{su} = v_{sd} + jv_{sq}$, $v^c_{ru} = v_{rd} + jv_{rq}$,

$L_{ru} = L_{mu} + L_{rl}$, $L_{su} = L_{mu} + L_{sl}$, $a = \frac{L_{mu}}{L_{ru}}$, $\sigma = \left(1 - \frac{L^2_{mu}}{L_{su}L_{ru}}\right)$, $\omega_{su} = 1$

Superscript c denotes complex. It should be noted that the model is developed in the view of motoring so that stator current into the machine is indicated with a positive sign.

The nonlinear model is often used for rotor field-oriented vector control (RFOC) of the induction motor. When

the model is re-expressed in rotor flux-oriented frame, the d-axis is aligned with the rotor flux ($\lambda_{ru} = \lambda_{rd}$) and the electrical torque is:

$$T_{eu} = \frac{p}{2}(\lambda_{rq}(=0) i_{rd} - \lambda_{rd} i_{rq}) = \frac{p}{2} a \lambda_{rd} i_{sq} \tag{2.1–8}$$

As seen in the equation (2.1–8), if the rotor flux is regulated at a constant value by controlling the d-axis stator current, toque can be instantaneously regulated by controlling the q-axis stator current. The nonlinear term $\omega_{ru}\lambda_{ru}$ is instantaneously feedback-compensated in the advanced servo control scheme. This control method can be applied to a type 4 wind turbine, and, in this case, the frequency of stator is not constant so that ω_{su} is not just 1 and varies depending on wind speed to capture maximum wind power.

2.1.3.2 Stator Current – Rotor Flux Model (Linear Complex)

A nonlinear model can be linearized at steady-state operating points. For instance, a first-order nonlinear model with single input is given as

$$\dot{h}(t) = f(h(t), v(t)) \tag{2.1–9}$$

where $h(t)$ is a state variable and $v(t)$ is an input variable. Linearizing results in the following:

$$\Delta\dot{h} = \left(\frac{\partial f}{\partial h}\Big|_{h=h_o}\right)\Delta h + \left(\frac{\partial f}{\partial v}\Big|_{v=v_o}\right)\Delta v \tag{2.1–10}$$

where

$$\Delta h = h(t) - h_o\,,\ \Delta v = v(t) - v_o$$

Likewise, nonlinear model of (2.1–7) is linearized and expressed in the form of complex state space equation,

$$\dot{\boldsymbol{x}}^c_{gf} = \boldsymbol{A}^c_{gf}\boldsymbol{x}^c_{gf} + \boldsymbol{B}^c_{gf}\boldsymbol{u}^c_g \tag{2.1–11}$$

where

$$\boldsymbol{A}^c_{gf} = \begin{pmatrix} -\frac{\omega_B(R_{su}+a^2R_{ru})}{\sigma L_{su}} - j\omega_B\omega_{suo} & \frac{\omega_B a(R_{ru}/L_{ru} - j\omega_{ruo})}{\sigma L_{su}} \\ \omega_B a R_{ru} & -\frac{\omega_B R_{ru}}{L_{ru}} - j\omega_B(\omega_{suo} - \omega_{ruo}) \end{pmatrix},$$

$$\boldsymbol{B}^c_{gf} = \begin{pmatrix} \frac{\omega_B}{\sigma L_{su}} & -\frac{\omega_B}{\sigma L_{su}}a & -j\frac{\omega_B\lambda_{ruo}}{\sigma L_{su}}a & \begin{pmatrix} -j\omega_B i_{suo} \\ -j\omega_B\lambda_{ruo} \end{pmatrix} \\ 0 & \omega_B & j\omega_B\lambda_{ruo} & \end{pmatrix},\ \boldsymbol{x}^c_{gf} = \begin{pmatrix} \Delta i^c_{su} \\ \Delta\lambda^c_{ru} \end{pmatrix},\ \boldsymbol{u}^c_g = \begin{pmatrix} \Delta v^c_{su} \\ \Delta v^c_{ru} \\ \Delta\omega_{ru} \\ (\Delta\omega_{su} = 0) \end{pmatrix}.$$

Subscript o denotes the operating points. Subscripts *g* and *f* signify generator and rotor-flux, respectively. Note that the stator electrical speed (synchronous speed) ω_{su} is assumed constant or hardly change so $\Delta\omega_{su} = 0$. This assumption is remained for generator modeling of type 1, 2, and 3 wind turbines except type 4 wind turbines until it needs to be retracted.

2.1.3.3 Stator Current – Rotor Flux Model (Dq-representation)

A generator transforms mechanical power to electrical power. This transforming process is typically embodied by torque that is represented with real variables. Hence, the complex model of generator is transformed into a model with real variables, to be subsequently interconnected with the drive train model.

For instance, simple state space equation with complex vector is shown below

$$\dot{x}^c = a^c x^c\,, \text{where } a^c = a_d + ja_q\,,\ x^c = x_d + jx_q \tag{2.1–12}$$

This simple complex model can be expressed in the dq-representation of state space equation as

$$\begin{pmatrix} \dot{x}_d \\ \dot{x}_q \end{pmatrix} = \begin{pmatrix} a_d & -a_q \\ a_q & a_d \end{pmatrix} \begin{pmatrix} x_d \\ x_q \end{pmatrix} = \left(a_d \otimes \boldsymbol{I} + a_q \otimes \boldsymbol{J} \right) \begin{pmatrix} x_d \\ x_q \end{pmatrix} \tag{2.1–13}$$

where $\otimes$ is Kronecker product, $\boldsymbol{I}$ is the identity matrix, and $\boldsymbol{J} = \begin{pmatrix} 0 & -1 \\ 1 & 0 \end{pmatrix}$. In the dq-representation, the d- and q-axis components, both real variables, represent real and imaginary components, respectively.

As seen, a complex model is easily transformed into the dq-representation of state space equation by using Kronecker product. The complex model (2.1–11) becomes

$$\dot{\boldsymbol{x}}_{gf} = \boldsymbol{A}_{gf} \boldsymbol{x}_{gf} + \boldsymbol{B}'_{gf} \boldsymbol{u}'_g \tag{2.1–14}$$

where

$$\boldsymbol{A}_{gf} = \left(\boldsymbol{A}_{gf}^{c(\text{real})} \otimes \boldsymbol{I} \right) + \left(\boldsymbol{A}_{gf}^{c(\text{imag})} \otimes \boldsymbol{J} \right),$$

$$\boldsymbol{B}'_{gf} = \left(\boldsymbol{B}_{gf}^{c(\text{real})} \otimes \boldsymbol{I} \right) + \left(\boldsymbol{B}_{gf}^{c(\text{imag})} \otimes \boldsymbol{J} \right),$$

$$\boldsymbol{x}_{gf} = \begin{pmatrix} \Delta \boldsymbol{i}_{su} \\ \Delta \boldsymbol{\lambda}_{ru} \end{pmatrix} \text{ where, } \boldsymbol{i}_{su} = \begin{pmatrix} i_{sd} \\ i_{sq} \end{pmatrix}, \ \boldsymbol{\lambda}_{ru} = \begin{pmatrix} \lambda_{rd} \\ \lambda_{rq} \end{pmatrix},$$

$$\boldsymbol{u}'_g = \begin{pmatrix} \boldsymbol{u}_g \\ 0 \end{pmatrix} \text{ where, } \boldsymbol{u}_g = \begin{pmatrix} \Delta \boldsymbol{v}_{su} \\ \Delta \boldsymbol{v}_{ru} \\ \Delta \omega_{ru} \end{pmatrix}, \ \boldsymbol{v}_{su} = \begin{pmatrix} v_{sd} \\ v_{sq} \end{pmatrix}, \ \boldsymbol{v}_{ru} = \begin{pmatrix} v_{rd} \\ v_{rq} \end{pmatrix}.$$

Superscript (real) and (imag) signify the real and imaginary components of the matrices, respectively. Removing the last column of input matrix $\mathbf{B}'_{gf}$ regarding to the zero term in the $\boldsymbol{u}'_g$, the transformation process is finalized.

$$\dot{\boldsymbol{x}}_{gf} = \boldsymbol{A}_{gf} \boldsymbol{x}_{gf} + \boldsymbol{B}_{gf} \boldsymbol{u}_g \tag{2.1–15}$$

where

$$\boldsymbol{B}_{gf} = \boldsymbol{B}'_{gf\,(1,2,3,4,5)}.$$

Here, the number in the subscript round brackets denotes the corresponding column matrix. It should be noted that, while the model can be represented more simply in the complex frame, the torque and power equations can be easily represented with real variables in the dq-frame, as seen in equation (2.1–8).

The process of transformation from the complex to the dq-representation will be usefully applied to converters and network modeling later.

2.1.3.4 Stator Current – Rotor Current Model (Dq-representation)

For certain type of wind turbines such as type 3, whose rotor currents are controlled, it might be better to express the model with rotor currents instead of rotor fluxes. A stator current–rotor flux model can be transformed to stator–rotor current model. Using the relation of $\lambda_{ru} = L_{ru} i_{ru} + L_{mu} i_{su}$, the transformation matrix is given as

$$\boldsymbol{T} = \begin{pmatrix} 1 & 0 \\ -a & 1/L_{ru} \end{pmatrix} \otimes \boldsymbol{I} \tag{2.1–18}$$

Using the transformation matrix, the stator–rotor current model is obtained:

$$\dot{\boldsymbol{x}}_g = \boldsymbol{A}_g \boldsymbol{x}_g + \boldsymbol{B}_g \boldsymbol{u}_g \tag{2.1–19}$$

where

$$\boldsymbol{A}_g = \boldsymbol{T} \boldsymbol{A}_{gf} \boldsymbol{T}^{-1}, \ \boldsymbol{B}_g = \boldsymbol{T} \boldsymbol{B}_{gf},$$

$$\boldsymbol{x}_g = \begin{pmatrix} \Delta \boldsymbol{i}_{su} \\ \Delta \boldsymbol{i}_{ru} \end{pmatrix} \text{ where, } \boldsymbol{i}_{ru} = \begin{pmatrix} i_{rd} \\ i_{rq} \end{pmatrix}.$$

For this model, the electrical torque is given as

$$T_{eu} = \tfrac{p}{2} L_{mu} \left(i_{sq} i_{rd} - i_{sd} i_{rq} \right) \tag{2.1–20}$$

Linearizing equation (2.1–20),

$$\Delta T_{eu} = \tfrac{p}{2} L_{mu} \left(-i_{rqo} \Delta i_{sd} + i_{rdo} \Delta i_{sq} + i_{sqo} \Delta i_{rd} - i_{sdo} \Delta i_{rq} \right) \tag{2.1–21}$$

The stator power, if stator and rotor resistances are ignored, is the same as the electrical torque. Thus, controlling stator power has the same control result as that of the electrical torque.

- Relation between Torque and Stator Real Power

For type 3 turbines, stator real power is often controlled instead of electrical torque, and controlling stator real power in the stator voltage-oriented frame has the same effect as controlling the electrical torque. It is simply proven.

In the q-axis oriented local frame, the rotor currents in the steady state are given by ignoring the stator resistance,

$$i_{rd} = \left(v_{sq} - L_{su} i_{sd} \right) / L_{mu} \text{ and } i_{rq} = -\tfrac{L_{su}}{L_{mu}} i_{sq}. \tag{2.1–22}$$

Assuming the pole number is 2 and substituting the equations of the rotor currents into (2.1–20), it is shown that the torque equation is the same as the stator power equation in per unit.

$$T_{eu} = L_{mu} \left(i_{sq} i_{rd} - i_{sd} i_{rq} \right) = v_{sq} i_{sq} = P_{su}. \tag{2.1–23}$$

2.1.3.5 Rotor Flux Oriented (RFO) Model

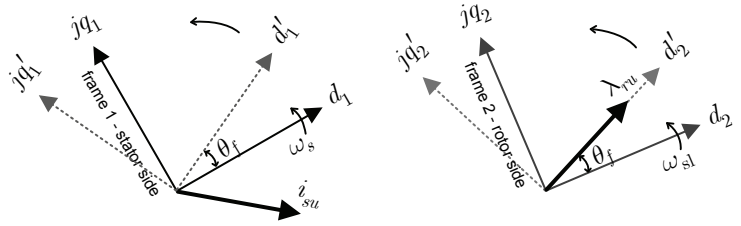

Fig. 1.2 Frames for generator model in dq-representation

The stator current – rotor flux model in the dq-representation of generator has been introduced in sub-subsection 2.1.3.3. To be clear, it is reminded that the quantities of the stator side and rotor side, which are the stator current and rotor flux, are expressed in different frames as shown in figure 1.2. The frame for stator side (frame 1) rotates in the synchronous speed ω_s and the frame for rotor side (frame 2) rotates in the speed ω_{sl}, which is the slip times the synchronous speed. The position angles of the frames are given $\theta_s = \omega_s t + \theta_{s0}$ and $\theta_{\text{sl}} = \omega_{\text{sl}} t + \theta_{\text{sl0}}$, respectively, where θ_{s0} and θ_{sl0} are their initial angles. As the slip is a function of the synchronous speed and the rotor speed, the frames are coupled by the rotor speed, where the position angle of the rotor is given $\theta_r = \theta_s - \theta_{\text{sl}}$. The frames can be rotationally shifted to have the quantities in the frames altered, which is equivalent to projecting the quantities to other frames. For instance, the rotor flux can be expressed in real value (d-axis component) by aligning the frame 2 with the rotor flux. Here, it should be noted that the rotor angle does not change with respect to either the original frames or the shifted frames; $\theta_r = \theta_s' - \theta_{\text{sl}}'$ where $\theta_s' = \theta_s + \theta_f$ and $\theta_{\text{sl}}' = \theta_{\text{sl}} + \theta_f$, and thus the frame 1 and 2

are shifted with the same angle θ_f.

In sub-subsection 2.1.3.1, a model represented in a frame whose q-axis is instantaneously aligned with the rotor flux so that the d-axis component is always zero, was briefly mentioned. Here, it is explained how the RFO model is derived from an original model of (2.1–15), where the rotor voltage is assumed zero. As the rotor flux angle is required for the creation of the RFO frame and the correspondingly altered frame for stator side, the following relation is derived by linearizing $\theta_f = \tan^{-1}(\lambda_{rq} / \lambda_{rd})$

$$\Delta\theta_f = \boldsymbol{K}_f \Delta\boldsymbol{\lambda}_{ru} \text{ where } \boldsymbol{K}_f = \frac{1}{(\lambda_{rdo}^2 + \lambda_{rqo}^2)}\begin{pmatrix} -\lambda_{rqo} & \lambda_{rdo} \end{pmatrix} \tag{2.1–24}$$

By linearizing the transformation process of $(z'_d + jz'_q) = e^{-j\theta_f}(z_d + jz_q)$; it transforms d- and q-axis components in a frame to those in the altered frames

$$\begin{pmatrix} \Delta z'_d \\ \Delta z'_q \end{pmatrix} = \begin{pmatrix} z'_{qo} \\ -z'_{do} \end{pmatrix} \Delta\theta_f + \begin{pmatrix} \cos\theta_{fo} & \sin\theta_{fo} \\ -\sin\theta_{fo} & \cos\theta_{fo} \end{pmatrix} \begin{pmatrix} \Delta z_d \\ \Delta z_q \end{pmatrix} \tag{2.1–25}$$

where subscript d and q signify the d- and q-axis components of the state and input variables, and the variables with superscript prime represents those in the altered frames. Transforming the input variable of stator voltage to that in the corresponding altered frame using (2.1–25), equation (2.1–15) changes to

$$\dot{\boldsymbol{x}}_{gf} = \bar{\boldsymbol{A}}_{gf}\boldsymbol{x}_{gf} + \bar{\boldsymbol{B}}_{gf}\boldsymbol{u}'_g, \text{ where } \boldsymbol{u}'_g = \begin{pmatrix} \Delta\boldsymbol{v}'_{su} \\ \Delta\omega_{ru} \end{pmatrix} \tag{2.1–26}$$

Now, the state variables of state current and rotor flux need to be transformed to those in the corresponding altered frames, and, for that, the transformation matrix is derived using (2.1–25)

$$\boldsymbol{T} = \begin{pmatrix} \bar{\boldsymbol{T}}_{3\times4} \\ \boldsymbol{0}_{1\times4} \end{pmatrix};\ \boldsymbol{x}'_{gf\,(3\times1)} = \bar{\boldsymbol{T}}\boldsymbol{x}_{gf\,(4\times1)} \tag{2.1–27}$$

The transformation matrix of which the rank is 3 is not invertible, and thus the model is equivalently derived using the right inverse matrix of the transformation matrix. Then, the original model is completely changed to the RFO model:

$$\dot{\boldsymbol{x}}'_{gf} = \boldsymbol{A}'_{gf}\boldsymbol{x}'_{gf} + \boldsymbol{B}'_{gf}\boldsymbol{u}'_g \tag{2.1–28}$$

where

$$\boldsymbol{A}'_{gf} = \bar{\boldsymbol{T}}\bar{\boldsymbol{A}}_{gf}\bar{\boldsymbol{T}}^{-1}_{\text{right}},\ \boldsymbol{B}'_{gf} = \bar{\boldsymbol{T}}\bar{\boldsymbol{B}}_{gf},\ \boldsymbol{x}'_{gf} = \begin{pmatrix} \Delta\boldsymbol{i}'_{su} \\ \Delta\lambda'_{rd} \end{pmatrix}$$

Figure 1.3 shows a conceptualized model transformation from a model represented in a frame to its modified RFO model.

- Model in a frame loosely aligned with rotor flux

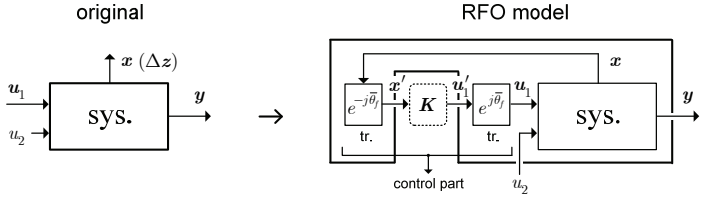

Fig. 1.3 Model represented in a frame and its modified RFO model

When control matter considered, rotor flux needs to be observed or estimated for coordinate transformation. In this case, a filtering might be necessary to eliminate some high frequency components that might occur in the estimation. Taking into consideration the filtering process in control part, the model can be expressed in a frame whose q-axis is loosely aligned with the rotor flux using a filtered quantity of the rotor flux angle. The dynamics of the filtered rotor flux angle is given with using (2.1–24)

$$\Delta\dot{\overline{\theta}}_f = -\frac{1}{\tau}\Delta\overline{\theta}_f + \frac{1}{\tau}\Delta\theta_f \tag{2.1–29}$$

where $\overline{\theta}_f$ is the filtered rotor flux angle and τ is the time constant of the low-pass filtering. This angle is included as an additional state variable in (2.1–15), so the model order increases to five. By transforming the input and state variables to those in the altered frames accordingly using (2.1–25), then, the model represented in the loosely rotor flux oriented frame is finalized. The q-axis component of the rotor flux in this model is not always zero but converged to zero after transients. This model could be useful to test controllers that are designed using the RFOC method. For this model, the linearized equation from original torque equation including the q-axis component of the rotor flux is used: $\Delta T_{eu} = \frac{p}{2}a\left(-\lambda_{rqo}\Delta i_{sd} + \lambda_{rdo}\Delta i_{sq} + i_{sqo}\Delta\lambda_{rd} - i_{sdo}\Delta\lambda_{rq}\right)$.

2.1.4 Back-to-back Converters

For the power converters used in type 3 and 4 wind turbines, back-to-back converters based on Pulse Width Modulation (PWM) are used [61]-[64]. The back-to-back converters are modeled by two main dynamic models of the dc-link voltage and the converter input currents.

2.1.4.1 DC–Link Voltage Model

DC – link voltage dynamics are obtained on the basis of instantaneous real power balance. The derivative of energy stored in a dc-link capacitor is same as the instantaneous difference between converter input and output powers,

$$\frac{d}{dt}\left(\frac{1}{2}C_{dcu}v_{dcu}^2\right) = P_{in} - P_{out} \tag{2.1–30}$$

where

$$P_{in} = v_{cd}i_{cd} + v_{cq}i_{cq},$$
$$P_{out} = v_{cd}^{(o)}i_{cd}^{(o)} + v_{cq}^{(o)}i_{cq}^{(o)}.$$

As seen in (2.1–30), while both sides of the dc-link are coupled by real power balance, imaginary power flow is decoupled by the dc-link. Linearizing equation (2.1–30) results in:

$$\begin{aligned}\frac{d}{dt}\Delta v_{dcu} = {} & \frac{1}{C_{dcu}v_{dcu}}\left(-v_{cdo}^{(o)}\Delta i_{cd}^{(o)} - v_{cqo}^{(o)}\Delta i_{cq}^{(o)} + v_{cdo}\Delta i_{cd} + v_{cqo}\Delta i_{cq}\right) \\ & + \frac{1}{C_{dcu}v_{dcu}}\left(-i_{cdo}^{(o)}\Delta i_{cd}^{(o)} - i_{cqo}^{(o)}\Delta v_{cq}^{(o)} + i_{cdo}\Delta v_{cd} + i_{cqo}\Delta v_{cq}\right)\end{aligned} \tag{2.1–31}$$

Damping is determined by power difference between the input and the output of dc-link voltage. Thus, a crow bar is necessary to increase the damping of dc-link voltage dynamics.

- Enhanced Damping in Dc-link Voltage Dynamics by Crowbar Application

A crowbar is designed to limit excessive energy in the equipment. For wind turbines, crowbar is generally used for two main purposes. One is to prevent the dc-link voltage from exceeding over a certain level by absorbing excessive energy, which is often called ‘chopper,’ and the other is to prevent excessive energy from flowing into rotor side.

The former case is generally applied when diode rectifier is connected to the grid side because the dc-link voltage

needs to be restricted. But, this chopper is also necessary to properly regulate the back-to-back converters by dissipating excessive energy at a faulted condition. The crow bar is connected in parallel at the dc-link capacitor by power electronics switch that is rapidly turned on and off. The crowbar resistance can work as a new control input. Since the resistance is nothing but the ratio of voltage and current, the crowbar resistance in average can be instantaneously altered by using power electronics device with control such as bandwidth control method. For the crowbar in parallel at the dc-link capacitor, the dc-link model is re-expressed

$$\frac{d}{dt}\left(\frac{1}{2}C_{dcu}v_{dcu}^2\right) = P_{in} - P_{out} - v_{dcu}^2 \;/\; R_{crow} \tag{2.1–32}$$

Although the crowbar resistance in normal condition is zero because the crowbar is disconnected, it can be thought that the crow bar is controlled for dc-link voltage to enhance the damping of dc-link voltage dynamics. Thus, linearizing it and assuming the crowbar resistance is sort of an input variable, the following is obtained.

$$v_{dco}^2 R_{crow}^{-2}\Delta R_{crow} \text{ , where } \Delta R_{crow} = K\Delta v_{dcu} \tag{2.1–33}$$

As seen, a crow bar controlled with power electronics can provide more damping capability for dc-link voltage model. Although the dc-link voltage is controlled by the input side converter, the crow bar can provide more damping by actively controlling it.

On the other case, the crow bar is connected in parallel at the output side of the back-to-back converters. For the crowbar in parallel at the side of converter output, the converter output is re-expressed

$$P_{out} = v_{cd}^{(o)}i_{cd}^{(o)} + v_{cq}^{(o)}i_{cq}^{(o)} - ((v_{cd}^{(o)})^2 + (v_{cq}^{(o)})^2) \;/\; R_{crow} \tag{2.1–34}$$

This type of crowbar could also provide additional damping for the dc-link voltage dynamics when controlled with respect to dc-link voltage. However, the damping capability of crowbar connected at the side of converter output depends on the rotor voltage while the other directly depends on dc-link voltage. For instance, when type 3 - wind turbine operates at the rated wind speed, most real power flows through the stator side and the rotor voltage is so small that the crow bar provides less damping ability compared to the other case. In addition, if the crowbar resistance is large, most currents flow into the rotor side even if the crow bar is connected, i.e. unsatisfying the purpose of rotor side protection. The worst case is that the frequency of output converter voltages is almost dc so that the rotor impedance is almost same as rotor resistance (although the main purpose of this crowbar is against faulted conditions that mainly cause high frequency transients). Therefore, the minimum resistance of the crow bar might need to be as small or at least several times as the rotor resistance.

- Restriction of Converter Input and Output Voltages by PWM Part

The magnitude of converter output voltages is limited by dc-link voltage [65]. Assuming the modulation index is 1, the magnitude of converter output voltages in average cannot exceed 1/2 times the dc-link voltage. Thus, the output voltage is restricted in every sample time by

$$v_{cu}^{\lim} = e^{j\theta_v}\min(e^{-j\theta_v}v_{cu}, k_{MI}v_{dcu}) \tag{2.1–35}$$

This effect can be ignored if the output voltage is very small, as in the case of a type 3 wind turbines being operated at rated working points. In contrast, a type 4 wind turbine has high stator voltage at rated operating points so the effect must be considered. However, the equation (2.1–35) is not appropriate to apply for linearized models, and thus a different approach is used.

Assuming the magnitude of converter output voltage is controllable by the rate to dc-link voltage, the following can be derived

$$\Delta v_{\text{cmag}}^{(o)} = k_{Mo}\Delta v_{dcu} + v_{dco}\Delta k_M \tag{2.1–36}$$

where k_M is the ratio between converter output voltage and dc-link voltage. A term regarding dc-link voltage $k_{Mo}\Delta v_{dc}$ is provided and the magnitude of output voltages can be controlled by the other term $v_{dco}\Delta k_M$, which

would not exist if k_M was considered constant. The magnitude and angle of output voltages can be expressed in terms of the d- and q-axis components by linearizing them, then the following relation is obtained and used as coupling terms for dc-link voltage effect in type 3 and 4 wind turbine models

$$\begin{pmatrix} \Delta v_{cd}^{(o)} \\ \Delta v_{cq}^{(o)} \end{pmatrix} = \boldsymbol{K}_{dc}^{(o)} \Delta v_{dcu} \tag{2.1–37}$$

By using (2.1–37), the coupling effect between the converter output voltage and the dc-link voltage is applied. Because the magnitude of the converter output voltage is remained controllable by the term $v_{dco}\Delta k_M$ and the angle of the converter output voltage is available to be controlled, the d- and q-axis components of the converter output voltage, which will be used as control variables, are preserved. This approach can be applied the same for the converter input voltage.

2.1.4.2 Converter Input Current Model

Considering resistance and leakage inductance of tap-transformer in the side of converter input, the dynamics (voltage equation) are expressed as

$$\tfrac{1}{\omega_B} L_{cu} \tfrac{d}{dt} i_{cu}^c = -R_{cu} i_{cu}^c - j\omega_u L_{cu} i_{cu}^c + v_{tu}^c - v_{cu}^c \tag{2.1–38}$$

where i_{cu}^c, v_{cu}^c, and v_{tu}^c are converter input current, converter input voltage, and terminal source voltage in complex, respectively. R_{cu} and L_{cu} are resistance and inductance on the converter input side, respectively. For type 3, the terminal source voltage is assumed to be the same as stator voltage ($v_{tu}^c = v_{su}^c$). This complex equation is transformed in the dq-representation the same as (2.1–14).

2.1.4.3 Back-to-back Converter Model

Models of dc-link and converter input side are combined and represented in the state space as

$$\dot{\boldsymbol{x}}_{cv} = \boldsymbol{A}_{cv}\boldsymbol{x}_{cv} + \boldsymbol{B}_{cv}\boldsymbol{u}_{cv} \tag{2.1–39}$$

where,

$$\boldsymbol{x}_{cv} = \begin{pmatrix} \Delta \boldsymbol{i}_{cu} \\ \Delta v_{dcu} \end{pmatrix} \text{ where, } \boldsymbol{i}_{cu} = \begin{pmatrix} i_{cd} \\ i_{cq} \end{pmatrix}.$$

The converter input and output sides link to different points of wind turbines, depending on the type.

- For type 3 turbines, converter input and output sides are connected to the terminal and rotor side of generator, respectively. Converter output voltages and currents are the same as generator rotor voltages and currents, respectively; $\boldsymbol{v}_{cu}^{(o)} = \boldsymbol{v}_{ru}$, $\boldsymbol{i}_{cu}^{(o)} = \boldsymbol{i}_{ru}$. The stator of generator is also connected to the terminal so that the source voltage of converter is assumed to be the same as the stator voltage; $\boldsymbol{v}_{tu} = \boldsymbol{v}_{su}$.

  $$\boldsymbol{u}_{cv} = (\ \Delta \boldsymbol{i}_{ru}^T \quad \Delta \boldsymbol{v}_{su}^T \quad \Delta \boldsymbol{v}_{ru}^T \quad \Delta \boldsymbol{v}_{cu}^T\ )^T .$$

- For type 4 turbines, converter input and output sides are connected to the terminal and stator of the generator, respectively. Converter output voltages and currents are the same as generator stator voltages and currents, respectively; $\boldsymbol{v}_{cu}^{(o)} = \boldsymbol{v}_{su}$, $\boldsymbol{i}_{cu}^{(o)} = \boldsymbol{i}_{su}$.

  $$\boldsymbol{u}_{cv} = (\ \Delta \boldsymbol{i}_{su}^T \quad \Delta \boldsymbol{v}_{tu}^T \quad \Delta \boldsymbol{v}_{su}^T \quad \Delta \boldsymbol{v}_{cu}^T\ )^T .$$

2.1.5 Complete Wind Turbine Models

Type 1, 2, 3, and 4 wind turbine models are developed by combining generator, drive train, and converters models. These four types of wind turbines have different characteristics and configurations. A Type 1 wind turbine consists of a drive train and a generator connected to the grid, and thus the electrical torque is uncontrollable. A type 2 wind turbine is similar as the type 1, but it has varying external rotor resistances so the electrical torque is controllable by changing the resistances. Type 3 and 4 wind turbines have additional power converters so they have capability of the electrical torque control over large ranges but they have different configuration regarding the converters from each other, which will be shown in the following subsections.

2.1.5.1 Type 1

One input of the drive train model is electrical torque, which can be expressed by the state variables of generator model according to (2.1–21). The two models of drive train and generator can be combined by relating the state variables of generator model to the input variables of drive train model. Using (2.1–6), (2.1–19) and (2.1–21), the model of type-1 wind turbine is obtained:

$$\dot{\boldsymbol{x}}_{\text{tp1}} = \boldsymbol{A}_{\text{tp1}}\boldsymbol{x}_{\text{tp1}} + \boldsymbol{B}_{\text{tp1}}\boldsymbol{u}_{\text{tp}} \tag{2.1–40}$$

$$\boldsymbol{y}_{\text{tp1}} = \boldsymbol{C}_{\text{tp1}}\boldsymbol{x}_{\text{tp1}} + \boldsymbol{D}_{\text{tp1}}\boldsymbol{u}_{\text{tp}} \tag{2.1–41}$$

where

$$\boldsymbol{A}_{\text{tp1}} = \begin{pmatrix} \boldsymbol{A}_{gf} & (\boldsymbol{B}_{gf(5)} \quad \boldsymbol{0}_{4\times 2}) \\ \boldsymbol{B}_{dt(1)}\boldsymbol{K}_{\text{t}} & \boldsymbol{A}_{dt} \end{pmatrix};\ \boldsymbol{K}_{\text{t}} = \tfrac{p}{2}a\begin{pmatrix} -\lambda_{rq} & \lambda_{rd} & i_{sq} & -i_{sd} \end{pmatrix}$$

$$\boldsymbol{B}_{\text{tp1}} = \begin{pmatrix} \boldsymbol{B}_{gf(1,2)} & \boldsymbol{0}_{4\times 1} \\ \boldsymbol{0}_{3\times 2} & \boldsymbol{B}_{dt(2)} \end{pmatrix},\ \boldsymbol{x}_{\text{tp1}} = \begin{pmatrix} \boldsymbol{x}_{gf} \\ \boldsymbol{x}_{dt} \end{pmatrix},\ \boldsymbol{u}_{\text{tp}} = \begin{pmatrix} \Delta\boldsymbol{v}_{tu} \\ \Delta T_{bu} \end{pmatrix};\ \boldsymbol{v}_{tu} = \boldsymbol{v}_{su}\,.$$

Subscript "tp1" signifies a type1 wind turbine. The system outputs can be either of stator (terminal) currents or powers. Assuming that the outputs are the variations of terminal (stator) powers, the output matrix and feed-through matrix are obtained by applying the instantaneous powers of $P_{tu} = v_{sd}i_{sd} + v_{sq}i_{sq}$ and $Q_{tu} = v_{sq}i_{sd} - v_{sd}i_{sq}$

$$\boldsymbol{C}_{\text{tp1}} = \begin{pmatrix} v_{sdo} & v_{sqo} & \boldsymbol{0}_{1\times 5} \\ v_{sqo} & -v_{sdo} & \boldsymbol{0}_{1\times 5} \end{pmatrix},\ \boldsymbol{D}_{\text{tp1}} = \begin{pmatrix} i_{sdo} & i_{sqo} & 0 \\ -i_{sqo} & i_{sdo} & 0 \end{pmatrix},\ \boldsymbol{y}_{\text{tp1}} = \begin{pmatrix} \Delta P_{tu} \\ \Delta Q_{tu} \end{pmatrix}.$$

Additionally, leakage inductance and resistance, especially at the low-voltage side, of a step-up transformer is not small so their dynamics are not negligible. Thus, the leakage inductance and resistance will be added up in the stator's leakage inductance and resistance, respectively.

2.1.5.2 Type 2

For a type 2 wind turbine, external variable resistances (that could be controlled with power electronics) are connected to internal rotor resistances in series through slip-rings to control the electrical torque. The varying rotor resistance is considered as an additional input variable. Equation (2.1–40) is modified to:

$$\dot{\boldsymbol{x}}_{\text{tp2}} = \boldsymbol{A}_{\text{tp2}}\boldsymbol{x}_{\text{tp2}} + \boldsymbol{B}_{\text{tp2}}\boldsymbol{u}_{\text{tp2}} \tag{2.1–42}$$

where

$$\boldsymbol{u}_{\text{tp2}} = (\Delta\boldsymbol{v}_{su}^{T} \quad \Delta T_{bu} \quad \Delta R_{ru}^{\text{ext}})^{T}$$

2.1.5.3 Type 3

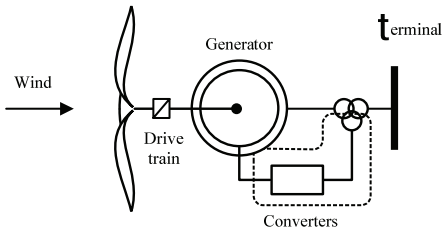

Fig. 1.4 Type 3 Wind Turbine

Type-3 wind turbines have back-to-back converters to control stator real (or electrical torque) and reactive power. The terminal voltages are assumed to be the same as stator voltages. The terminal currents are the sum of stator currents and converter input currents. In addition, leakage inductance and resistance of the step-up transformer are absorbed into the leakage inductance and resistance of the stator and the side of converters. Considering these, the model is expressed in the form of state space equation as

$$\dot{\boldsymbol{x}}_{\text{tp3}} = \boldsymbol{A}^{\text{u}}_{\text{tp3}}\boldsymbol{x}_{\text{tp3}} + \boldsymbol{B}^{\text{u}}_{\text{tp3}}\boldsymbol{u}_{\text{tp3}} \tag{2.1–43}$$

where

$$\boldsymbol{A}^{\text{u}}_{\text{tp3}} = \begin{pmatrix} \boldsymbol{A}_g & (\boldsymbol{0}_{4\times2} \quad \boldsymbol{B}_{g(3,4)}\boldsymbol{K}_{dc}) & (\boldsymbol{B}_{g(5)} \quad \boldsymbol{0}_{4\times2}) \\ (\boldsymbol{0}_{3\times2} \quad \boldsymbol{B}_{cv(1,2)}) & \boldsymbol{A}_{cv} + (\boldsymbol{0}_{3\times2} \quad \boldsymbol{B}_{cv(3,4)}\boldsymbol{K}_{dc} + \boldsymbol{B}_{cv(5,6)}\boldsymbol{K}^{(o)}_{dc}) & \boldsymbol{0}_{3\times3} \\ \boldsymbol{B}_{dt(1)}\boldsymbol{K}_{\text{t}} & \boldsymbol{0}_{3\times3} & \boldsymbol{A}_{dt} \end{pmatrix};$$

$$\boldsymbol{K}_{\text{t}} = \frac{p}{2}L_{mu}\begin{pmatrix} -i_{rqo} & i_{rdo} & i_{sqo} & -i_{sdo} \end{pmatrix}$$

$$\boldsymbol{B}^{\text{u}}_{\text{tp3}} = \begin{pmatrix} \boldsymbol{B}_{g(1,2)} & \boldsymbol{B}_{g(3,4)} & \boldsymbol{0}_{4\times2} & \boldsymbol{0}_{4\times1} \\ \boldsymbol{B}_{cv(3,4)} & \boldsymbol{B}_{cv(5,6)} & \boldsymbol{B}_{cv(7,8)} & \boldsymbol{0}_{3\times1} \\ \boldsymbol{0}_{3\times2} & \boldsymbol{0}_{3\times2} & \boldsymbol{0}_{3\times2} & \boldsymbol{B}_{dt(2)} \end{pmatrix},\ \boldsymbol{x}_{\text{tp3}} = \begin{pmatrix} \boldsymbol{x}_g \\ \boldsymbol{x}_{cv} \\ \boldsymbol{x}_{dt} \end{pmatrix},\ \boldsymbol{u}_{\text{tp3}} = \begin{pmatrix} \Delta\boldsymbol{v}_{tu} \\ \Delta\boldsymbol{v}_{ru} \\ \Delta\boldsymbol{v}_{cu} \\ \Delta T_{bu} \end{pmatrix};\ \boldsymbol{v}_{tu} = \boldsymbol{v}_{su}\,.$$

The above is an uncontrolled system. Assuming that the converters are feedback controlled using the method to be introduced in chapter 4, the controlled system is expressed as

$$\dot{\boldsymbol{x}}_{\text{tp3}} = \boldsymbol{A}_{\text{tp3}}\boldsymbol{x}_{\text{tp3}} + \boldsymbol{B}_{\text{tp3}}\boldsymbol{u}_{\text{tp}} \tag{2.1–44}$$

$$\boldsymbol{y}_{\text{tp3}} = \boldsymbol{C}_{\text{tp3}}\boldsymbol{x}_{\text{tp3}} + \boldsymbol{D}_{\text{tp3}}\boldsymbol{u}_{\text{tp}} \tag{2.1–45}$$

where

$$\boldsymbol{A}_{\text{tp3}} = \boldsymbol{A}^{\text{u}}_{\text{tp3}} - \boldsymbol{B}^{\text{u}}_{\text{tp3(3:6)}}\boldsymbol{K}_{con}\,,$$

$$\boldsymbol{B}_{\text{tp3}} = \boldsymbol{B}^{\text{u}}_{\text{tp3(1,2,7)}}\,,$$

Again, the outputs of system can be either of currents or powers. The terminal powers are chosen as the outputs.

$$\boldsymbol{C}_{\text{tp3}} = \begin{pmatrix} v_{sdo} & v_{sqo} & \boldsymbol{0}_{1\times2} & v_{sdo} & v_{sqo} & \boldsymbol{0}_{1\times3} \\ v_{sqo} & -v_{sdo} & \boldsymbol{0}_{1\times2} & v_{sqo} & -v_{sdo} & \boldsymbol{0}_{1\times3} \end{pmatrix},$$

$$\boldsymbol{D}_{\text{tp3}} = \begin{pmatrix} (i_{sdo} + i_{cdo}) & (i_{sqo} + i_{cqo}) & 0 \\ -(i_{sqo} + i_{cqo}) & (i_{sdo} + i_{cdo}) & 0 \end{pmatrix},\ \boldsymbol{y}_{\text{tp3}} = \begin{pmatrix} \Delta P_{tu} \\ \Delta Q_{tu} \end{pmatrix}.$$

2.1.5.4 Type 4

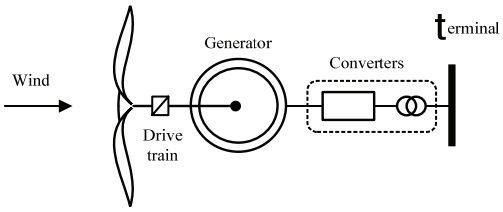

Fig. 1.5 Type 4 Wind Turbine

For type 4 wind turbines, either the synchronous (PMSG) or induction generators can be used. Generally, type 4 wind turbines represent those with generators having many magnetic poles, so they do not require the gear boxes. However, in this work, turbines with induction generators, but with gear boxes, are used and will be called type 4 wind turbines. As mentioned earlier, the generator model is expressed in rotor flux-oriented frame ($\lambda_{rqo} = 0$, $\lambda_{ru}^{c} = \lambda_{rd}$). The generator model's state variables are

$$\boldsymbol{x}_{gf}' = (\Delta \boldsymbol{i}_{su}^{T} \quad \Delta\lambda_{rd})^{T} \tag{2.1–46}$$

In this sub-subsection, the prime signifies that the variables and matrices are expressed with respect to the rotor flux-oriented frame. Then, the type 4 wind turbine model is expressed in the dq-representation of state space equation as

$$\dot{\boldsymbol{x}}_{\text{tp4}} = \boldsymbol{A}_{\text{tp4}}^{\text{u}} \boldsymbol{x}_{\text{tp4}} + \boldsymbol{B}_{\text{tp4}}^{\text{u}} \boldsymbol{u}_{\text{tp4}} \tag{2.1–47}$$

where

$$\boldsymbol{A}_{\text{tp4}}^{\text{u}} = \begin{pmatrix} \boldsymbol{A}_{gf}' & (\boldsymbol{0}_{3\times2} \quad \boldsymbol{B}_{gf(1,2)}'\boldsymbol{K}_{dc}) & (\boldsymbol{B}_{gf(5)}' \quad \boldsymbol{0}_{3\times2}) \\ (\boldsymbol{B}_{cv(1,2)} \quad \boldsymbol{0}_{3\times1}) \quad \boldsymbol{A}_{cv} + (\boldsymbol{0}_{3\times2} \quad \boldsymbol{B}_{cv(3,4)}\boldsymbol{K}_{dc} + \boldsymbol{B}_{cv(5,6)}\boldsymbol{K}_{dc}^{(o)}) & \boldsymbol{0}_{3\times3} \\ \boldsymbol{B}_{dt(1)}\boldsymbol{K}_{\text{t}} & \boldsymbol{0}_{3\times3} & \boldsymbol{A}_{dt} \end{pmatrix},$$

$$\boldsymbol{K}_{\text{t}} = \frac{p}{2} a \begin{pmatrix} 0 & \lambda_{rdo} & i_{sqo} \end{pmatrix}.$$

$$\boldsymbol{B}_{\text{tp4}}^{\text{u}} = \begin{pmatrix} \boldsymbol{0}_{3\times2} & \boldsymbol{B}_{gf(1,2)}' & \boldsymbol{0}_{3\times2} & \boldsymbol{0}_{3\times1} \\ \boldsymbol{B}_{cv(3,4)} & \boldsymbol{B}_{cv(5,6)} & \boldsymbol{B}_{cv(7,8)} & \boldsymbol{0}_{3\times1} \\ \boldsymbol{0}_{3\times2} & \boldsymbol{0}_{3\times2} & \boldsymbol{0}_{3\times2} & \boldsymbol{B}_{dt(2)} \end{pmatrix}, \ \boldsymbol{x}_{\text{tp4}} = \begin{pmatrix} \boldsymbol{x}_{gf}' \\ \boldsymbol{x}_{cv} \\ \boldsymbol{x}_{dt} \end{pmatrix}, \ \boldsymbol{u}_{\text{tp4}} = \begin{pmatrix} \Delta \boldsymbol{v}_{tu} \\ \Delta \boldsymbol{v}_{su} \\ \Delta \boldsymbol{v}_{cu} \\ \Delta T_{bu} \end{pmatrix}.$$

Assuming that the converters are feedback-controlled,

$$\dot{\boldsymbol{x}}_{\text{tp4}} = \boldsymbol{A}_{\text{tp4}} \boldsymbol{x}_{\text{tp4}} + \boldsymbol{B}_{\text{tp4}} \boldsymbol{u}_{\text{tp}} \tag{2.1–48}$$

$$\boldsymbol{y}_{\text{tp4}} = \boldsymbol{C}_{\text{tp4}} \boldsymbol{x}_{\text{tp4}} + \boldsymbol{D}_{\text{tp4}} \boldsymbol{u}_{\text{tp}} \tag{2.1–49}$$

where

$$\boldsymbol{A}_{\text{tp4}} = \boldsymbol{A}_{\text{tp4}}^{\text{u}} - \boldsymbol{B}_{\text{tp4(3:6)}}^{\text{u}} \boldsymbol{K}_{con},$$

$$\boldsymbol{B}_{\text{tp4}} = \boldsymbol{B}_{\text{tp4(1,2,7)}}^{\text{u}},$$

$$\boldsymbol{C}_{\text{tp4}} = \begin{pmatrix} \boldsymbol{0}_{1\times3} & v_{tdo} & v_{tqo} & \boldsymbol{0}_{1\times4} \\ \boldsymbol{0}_{1\times3} & v_{tqo} & -v_{tdo} & \boldsymbol{0}_{1\times4} \end{pmatrix},$$

$$\boldsymbol{D}_{\text{tp4}} = \begin{pmatrix} i_{cdo} & i_{cqo} & 0 \\ -i_{cqo} & i_{cdo} & 0 \end{pmatrix}, \ \boldsymbol{y}_{\text{tp4}} = \begin{pmatrix} \Delta P_{tu} \\ \Delta Q_{tu} \end{pmatrix}.$$

Note that, for type 4, the stator electrical speed ω_{su} varies by control, and thus $\Delta\omega_{su} \neq 0$. Refer to subsection 4.3.2.2. It is assumed that $\Delta\omega_{su}$ was controlled as said in the subsection and absorbed into the model.

2.1.5.5 Model with Wind Speed

The model can be further developed so that it uses wind speed as an input. For a type-1 wind turbine, using equations (2.1–2) and (2.1–40),

$$\dot{\boldsymbol{x}}_{\mathrm{tp1}} = \boldsymbol{A}^{w}_{\mathrm{tp1}}\boldsymbol{x}_{\mathrm{tp1}} + \boldsymbol{B}^{w}_{\mathrm{tp1}}\boldsymbol{u}^{w}_{\mathrm{tp}} \tag{2.1–50}$$

where

$$\boldsymbol{A}^{w}_{\mathrm{tp1}} = \begin{pmatrix} \boldsymbol{A}_{g} & (\boldsymbol{B}_{g(5)} \quad \boldsymbol{0}_{4\times 2}) \\ \boldsymbol{B}_{dt(1)}\boldsymbol{K}_{\mathrm{t}} & \boldsymbol{A}_{dt} + \boldsymbol{B}_{dt(2)}\begin{pmatrix} 0 & \kappa_{\omega} & 0 \end{pmatrix} \end{pmatrix},$$

$$\boldsymbol{B}^{w}_{\mathrm{tp1}} = \begin{pmatrix} \boldsymbol{B}_{g(2)} & \boldsymbol{0}_{4\times 2} \\ \boldsymbol{0}_{3\times 1} & \boldsymbol{B}_{dt(2)}\begin{pmatrix} \kappa_{\vartheta} & \kappa_{w} \end{pmatrix} \end{pmatrix},\ \boldsymbol{u}^{w}_{\mathrm{tp}} = \begin{pmatrix} \Delta \boldsymbol{v}_{tu} \\ \Delta \vartheta_{u} \\ \Delta w_{u} \end{pmatrix}.$$

Now the model of type-1 wind turbine has wind speed and pitch angle as inputs instead of blade torque. When wind is under the rated speed, the pitch angle is kept at constant or zero ($\Delta\vartheta_{u} = 0$). In this case, both the pitch angle input and the related input matrix can be removed from the model.

2.1.5.6 Terminal Voltage-oriented Model

The models in the previous sub-sections are developed in a global dq-frame. Models can also be developed in local dq-frames, where either their d-axes or q-axes are aligned with their specific vectors such as stator (terminal) voltages. The locally framed models are especially important when control matters are concerned because power converters are generally controlled in local frames. In this subsection, models that are locally framed in terms of their terminal voltages are introduced.

- Models represented in Terminal Voltage-oriented Local Frames

The locally framed model can be developed in two different ways. First, all operating points for linearization are set with respect to a local frame (local-frame model 1). The model representation is exactly same as the ones developed in the previous sub-subsections, but all operating points have been altered. For example, when a type 3 wind turbine is modeled in the stator (terminal) voltage-oriented frame, the operating point of d-axis stator voltage is considered zero ($v^{\mathrm{vo}}_{sdo} = 0$). In this case, the output matrix is given as

$$\boldsymbol{C}_{\mathrm{tp3}} = \begin{pmatrix} 0 & v_{sqo} & \boldsymbol{0}_{1\times 2} & 0 & v_{sqo} & \boldsymbol{0}_{1\times 3} \\ v_{sqo} & 0 & \boldsymbol{0}_{1\times 2} & v_{sqo} & 0 & \boldsymbol{0}_{1\times 3} \end{pmatrix},$$

Also, in the voltage-oriented frame, the converter d-axis input current is controlled at zero to regulate reactive power at the converter input side. The result is that the operating point is also zero. The feed-through matrix is rewritten as

$$\boldsymbol{D}_{\mathrm{tp3}} = \begin{pmatrix} i_{sdo} & (i_{sqo} + i_{cqo}) & 0 \\ -(i_{sqo} + i_{cqo}) & i_{sdo} & 0 \end{pmatrix}.$$

Here, it is assumed that the local-frame model 1 is represented in a local frame whose q-axis is 'initially' aligned at the stator voltage but the frame could be out of the alignment in either transient or steady states.

On the other hand, the model (local-frame model 2) can be obtained by further assuming that stator voltage is 'instantaneously' aligned with the q-axis of the local frame. Since the d-axis component of stator voltage is always

zero in the frame ($v_{sd}^{\text{vo}} = 0 , v_{sdo}^{\text{vo}} = 0$), the inputs of the d- and q-axis stator voltages are reduced to voltage in magnitude. These two locally framed models are basically the same in terms of the system parameters, but they are completed differently as explained the above by applying their agreeable network models, which will be introduced in sub-subsection 2.2.2.2.

For this modeling, it should be clear of a point, that is, the synchronous speed variation in the stator (terminal) voltage-oriented frame $\Delta\omega_{su}^{\text{vo}}$ changes by the differential of terminal voltage variation even if the synchronous speed in a global frame is constant:

$$\Delta\omega_{su}^{\text{vo}} = \Delta\omega_{su}(=0) + \Delta\omega^{\text{vo}} ; \Delta\omega^{\text{vo}} = \frac{1}{\omega_B}\Delta\dot{\theta}^{\text{vo}} ; \Delta\dot{\theta}^{\text{vo}} = -\boldsymbol{K}_{\theta}^{\text{vo}} \begin{pmatrix} \Delta\dot{v}_{sd} \\ \Delta\dot{v}_{sq} \end{pmatrix} \tag{2.1–51}$$

where $\Delta\theta^{\text{vo}}$ is the angle of terminal voltage in a global frame, which is used to align instantaneously the local frame's q-axis at the terminal voltage. If the differential term changes, the added term $\Delta\omega^{\text{vo}}$ also change so the synchronous speed variation in the local frame is not zero. However, if the dynamics of the terminal voltage can be neglected, the differential of the terminal voltage is assumable zero. This assumption is reasonable because a static network model, which will be introduced in sub-section 2.2.2.2, is on the basis of neglecting the dynamics of capacitor voltages (voltages across capacitive elements at the buses) of which one is the terminal voltage, and thus the added term can be ignored as well.

- Control in the stator flux-oriented frame

For control matter in a real, stator flux-oriented frame (where the d-axis is aligned with stator flux) might be preferred to the stator voltage-oriented frame. The reason is as follows. The stator voltage-oriented frame is obtained with the angle of three-phase components of stator voltages. The problem is that the frame experiences a transient response when the stator voltages are abruptly changed. In this case, all states in the frame are in a transient state even if they are not actually changed. The frame where control is performed should be insensitive to transient states. For this reason, a flux-oriented frame could be preferably applied. A stator flux in a three-phase frame is given as

$$\lambda_{abcs} = \int (v_{abcs} - R_{su} i_{abcs}) dt$$

As seen, assuming that stator resistance is very small, stator flux is the integrated stator voltages. Since stator flux does not quickly respond to the stator voltage change, the stator flux-oriented frame is robust against a voltage transient response. The integration produces a 90-degree phase delay. Hence, the d-axis of stator flux is equivalent to the q-axis of stator voltage in the steady state. This is shown below:

$$\lambda_{sd} = (v_{sq} - R_{su} i_{sq}) / \omega_u$$

Here, it is expected that the stator flux oriented frame is equivalent to a frame whose q-axis is loosely aligned with the stator voltage by using a filter with a cut-off frequency of nearly zero. Thus the dynamics of a model represented in the stator flux-oriented frame is similar to one represented in the loosely stator voltage oriented frame. When the voltage-oriented frame is applied, the PLL (phase-locked-loop) technique is generally required to detect the angle of the source voltage [86], [87].

2.2 Network Model

Two types of network model are developed in this section. One is a dynamic network model developed in the form of state space equation. The other is a static network model developed by using instantaneous power theory in the steady state. While the former includes the dynamics of bus voltages and line currents, it increases the complexity of the WPP model combined with the network model. The latter does not provide the dynamics, but the complexity can be reduced. Note that, however, to study more in detail the dynamics and stability of the network, the dynamic network model will be necessary as the static network model does not explain dynamics regarding the voltages and currents in the network.

2.2.1 Dynamic Network Models

2.2.1.1 State Space Equation 1 (Complex)

According to Kirchhoff's current and voltage laws (KCL and KVL), a network can be represented in the form of complex state space equation.

The buses are connected with each other via resistance and inductance. In addition, the buses are assumed to be connected to the ground by capacitive susceptance. In this case, the capacitor voltage is same as the bus voltage. The state of connectivity can be found with an incidence matrix of the network. The method of developing the model is shown with a simple example. For instance, a network with five buses is expressed in the directed graph as shown in figure 1.6.

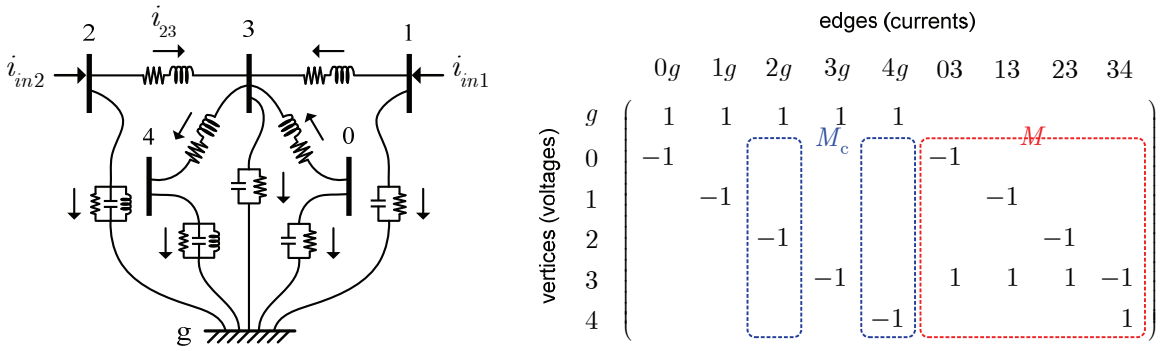

Fig. 1.6 Network model and its incidence matrix

All five buses have capacitive susceptance. The network's incidence matrix is given. Using the incidence matrix, a complex dynamic model is obtained (in per-unit form)

$$\frac{1}{\omega_B}\begin{pmatrix} \boldsymbol{C} & & \\ & \boldsymbol{L}_{\text{line}} & \\ & & \boldsymbol{L} \end{pmatrix}\begin{pmatrix} \dot{\boldsymbol{v}}^c \\ \dot{\boldsymbol{i}}^c \\ \dot{\boldsymbol{i}}_L^c \end{pmatrix} = \begin{pmatrix} -(\boldsymbol{R}^{-1}+j\omega_u\boldsymbol{C}) & \boldsymbol{M} & \boldsymbol{M}_{\text{c}} \\ -\boldsymbol{M}^T & -(\boldsymbol{R}_{\text{line}}+j\omega_u\boldsymbol{L}_{\text{line}}) & \boldsymbol{0} \\ -\boldsymbol{M}_{\text{c}}^T & \boldsymbol{0} & -j\omega_u\boldsymbol{L} \end{pmatrix}\begin{pmatrix} \boldsymbol{v}^c \\ \boldsymbol{i}^c \\ \boldsymbol{i}_L^c \end{pmatrix} + \begin{pmatrix} \boldsymbol{B}_{\text{in}} \\ \boldsymbol{0} \\ \boldsymbol{0} \end{pmatrix}\boldsymbol{i}_{in}^c \tag{2.2–1}$$

where

$$\boldsymbol{R} = \text{diag}\{(\, R_0 \quad R_1 \quad R_2 \quad R_3 \quad R_4 \,)\},$$

$$\boldsymbol{C} = \mathrm{diag}\{(\,C_0 \quad C_1 \quad C_2 \quad C_3 \quad C_4\,)\}\,,$$

$$\boldsymbol{L} = \mathrm{diag}\{(\,L_3 \quad L_4\,)\}\,,$$

$$\boldsymbol{R}_{\mathrm{line}} = \mathrm{diag}\{(\,R_{\mathrm{line02}} \quad R_{\mathrm{line12}} \quad R_{\mathrm{line24}} \quad R_{\mathrm{line32}}\,)\}\,,$$

$$\boldsymbol{L}_{\mathrm{line}} = \mathrm{diag}\{(\,L_{\mathrm{line02}} \quad L_{\mathrm{line12}} \quad L_{\mathrm{line24}} \quad L_{\mathrm{line32}}\,)\}\,,$$

$$\boldsymbol{v}^c = (\,v_0^c \quad v_1^c \quad v_2^c \quad v_3^c \quad v_4^c\,)^T \text{ where, } v^c = v_d + jv_q\,,$$

$$\boldsymbol{i}^c = (\,i_{02}^c \quad i_{12}^c \quad i_{24}^c \quad i_{32}^c\,)^T,\ \boldsymbol{i}_L^c = (\,i_{L3}^c \quad i_{L4}^c\,)^T,\ \boldsymbol{i}_{in}^c = (\,i_{in1}^c \quad i_{in2}^c\,)^T.$$

where, $i^c = i_d + ji_q$.

Since most networks include transformers, a new network with transformers is introduced. The figure below shows a network with four transformers.

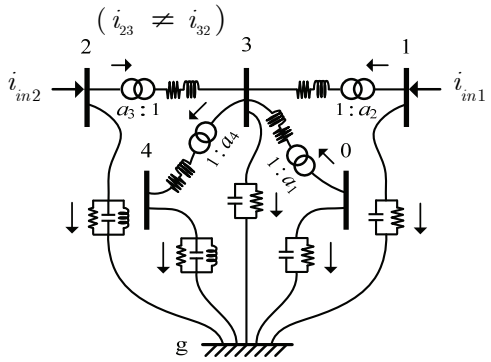

Fig. 1.7 Network model with transformers

In this case, the matrix *M* obtained from the incidence matrix should be changed according to transformer's turn-ratio:

$$\frac{1}{\omega_B}\begin{pmatrix} \boldsymbol{C} & & \\ & \boldsymbol{L}_{\mathrm{line}}\boldsymbol{T}r & \\ & & \boldsymbol{L} \end{pmatrix}\begin{pmatrix} \dot{\boldsymbol{v}}^c \\ \dot{\boldsymbol{i}}^c \\ \dot{\boldsymbol{i}}_L^c \end{pmatrix} = \begin{pmatrix} -(\boldsymbol{R}^{-1} + j\omega_u\boldsymbol{C}) & \boldsymbol{M}_{\mathrm{a}} & \boldsymbol{M}_{\mathrm{c}} \\ -\boldsymbol{M}_{\mathrm{b}}^T & -(\boldsymbol{R}_{\mathrm{line}} + j\omega_u\boldsymbol{L}_{\mathrm{line}})\boldsymbol{T}r & \boldsymbol{0} \\ -\boldsymbol{M}_{\mathrm{c}}^T & \boldsymbol{0} & -j\omega_u\boldsymbol{L} \end{pmatrix}\begin{pmatrix} \boldsymbol{v}^c \\ \boldsymbol{i}^c \\ \boldsymbol{i}_L^c \end{pmatrix} + \begin{pmatrix} \boldsymbol{B}_{\mathrm{in}} \\ \boldsymbol{0} \\ \boldsymbol{0} \end{pmatrix}\boldsymbol{i}_{in}^c \tag{2.2–2}$$

where

$$\boldsymbol{T}r = \mathrm{diag}\{(a_1 \quad a_2 \quad a_3 \quad a_4)\},\ \boldsymbol{M}_{\mathrm{a}} = \begin{pmatrix} -a_1 & & & \\ & -a_2 & & \\ & & -a_3 & \\ 1 & 1 & 1 & -a_4 \\ & & & 1 \end{pmatrix},\ \boldsymbol{M}_{\mathrm{b}} = \begin{pmatrix} -1/a_1 & & & \\ & -1/a_2 & & \\ & & -1/a_3 & \\ 1 & 1 & 1 & -1/a_4 \\ & & & 1 \end{pmatrix}$$

Expressing the complex model in the form of complex state space equation that has currents injected into the network as the inputs and bus voltages as the outputs,

$$\dot{\boldsymbol{x}}_{\mathrm{nt1}}^c = \boldsymbol{A}_{\mathrm{nt1}}^c\boldsymbol{x}_{\mathrm{nt1}}^c + \boldsymbol{B}_{\mathrm{nt1}}^c\boldsymbol{u}_{\mathrm{nt1}}^c \tag{2.2–3}$$

$$\boldsymbol{y}_{\mathrm{nt1}}^c = \boldsymbol{C}_{\mathrm{nt1}}^c\boldsymbol{x}_{\mathrm{nt1}}^c \tag{2.2–4}$$

where

$$\boldsymbol{x}^c_{\mathrm{nt1}} = ((\boldsymbol{v}^c)^T \quad (\boldsymbol{i}^c)^T \quad (\boldsymbol{i}^c_L)^T)^T,\ \boldsymbol{u}^c_{\mathrm{nt1}} = \boldsymbol{i}^c_{in},$$

$$\boldsymbol{C}^c_{\mathrm{nt1}} = (\boldsymbol{I}_{5\times5} \quad \boldsymbol{0}_{5\times6}),\ \boldsymbol{y}^c_{\mathrm{nt1}} = \boldsymbol{v}^c.$$

In the steady state, since the derivative terms are zeroes, the relation between the network inputs and the network outputs is expressed as

$$\boldsymbol{y}^c_{\mathrm{nt1}} = \boldsymbol{Z}\,\boldsymbol{u}^c_{\mathrm{nt1}} \tag{2.2–5}$$

where

$$\boldsymbol{Z} = -\boldsymbol{C}_{\mathrm{nt1c}}\boldsymbol{A}^{-1}_{\mathrm{nt1c}}\boldsymbol{B}_{\mathrm{nt1c}}$$

The matrix $\boldsymbol{Z}$ represents the relation between bus voltages and injected currents (that is, the impedance matrix—inverting this results in the admittance matrix ($\boldsymbol{Y} = \boldsymbol{Z}^{-1}$)).

2.2.1.2 State Space Equation 2 (complex)

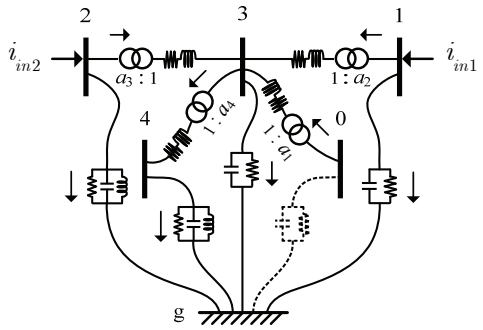

Fig. 1.8 Network model with a constant voltage bus

If the voltage of a certain bus is assumed to be ideally controlled, capacitive voltage dynamics at the bus can be ignored. In this case, the bus voltage can be expected to be an additional network input. Assuming that bus-0 is infinite bus, the network can be changed as shown in figure 1.8.

The state variable of bus 0 voltage is the first-row component of $\boldsymbol{x}^c_{\mathrm{nt1}}$. A new system matrix $\boldsymbol{A}^c_{\mathrm{nt2}}$ is obtained by removing the first row of $\boldsymbol{A}^c_{\mathrm{nt1}}$ matrix and the first column of the remained $\boldsymbol{A}^c_{\mathrm{nt1}}$ matrix. A new input matrix $\boldsymbol{B}^c_{\mathrm{nt2}}$ is obtained by removing the first row of $\boldsymbol{B}^c_{\mathrm{nt1}}$ matrix and adding the first column of the remaining $\boldsymbol{A}^c_{\mathrm{nt1}}$ matrix to the $\boldsymbol{B}^c_{\mathrm{nt1}}$. Components regarding to resistance and capacitive susceptance at the bus 0 is included in the feed-through matrix. $\boldsymbol{D}^c_{\mathrm{nt1}}$ matrix is obtained by adding the corresponding (1, 1) component of $\boldsymbol{A}^c_{\mathrm{nt1}}$ into spot with respect to the input v_0. This process is shown below.

$$\boldsymbol{A}^c_{\mathrm{nt1}} = \begin{pmatrix} (1,1) & \\ (:,1) & \boldsymbol{A}^c_{\mathrm{nt2}} \end{pmatrix} \begin{matrix} \text{Col 1st} \\ \\ \text{Row 1st} \end{matrix} \qquad \begin{matrix} \text{Row 1st} \\ \boldsymbol{B}^c_{\mathrm{nt1}} = \end{matrix} \begin{pmatrix} & \\ \boldsymbol{B}^c_{\mathrm{nt2}(1,2)} & \end{pmatrix}$$

$$\boldsymbol{B}^c_{\mathrm{nt2}(3)} = \begin{matrix} \text{Col 1st} \\ \end{matrix} \begin{pmatrix} (:,1) \\ \end{pmatrix} \qquad \boldsymbol{D}^c_{\mathrm{nt2}} = \begin{pmatrix} 0 & \\ 0 & (1,1) \end{pmatrix}$$

.

The new complex state space equation is represented as

$$\dot{\boldsymbol{x}}^c_{\mathrm{nt2}} = \boldsymbol{A}^c_{\mathrm{nt2}}\boldsymbol{x}^c_{\mathrm{nt2}} + \boldsymbol{B}^c_{\mathrm{nt2}}\boldsymbol{u}^c_{\mathrm{nt2}} \tag{2.2–6}$$

$$\boldsymbol{y}^c_{\mathrm{nt2}} = \boldsymbol{C}^c_{\mathrm{nt2}}\boldsymbol{x}^c_{\mathrm{nt2}} + \boldsymbol{D}^c_{\mathrm{nt2}}\boldsymbol{u}^c_{\mathrm{nt2}} \tag{2.2–7}$$

where

$$\boldsymbol{B}^c_{\text{nt2}} = \begin{pmatrix} \boldsymbol{B}^c_{\text{nt2(1,2)}} & \boldsymbol{B}^c_{\text{nt2(3)}} \end{pmatrix}$$

$$\boldsymbol{x}^c_{\text{nt2}} = \begin{pmatrix} (\overline{\boldsymbol{v}}^c)^T & (\boldsymbol{i}^c)^T & (\boldsymbol{i}^c_L)^T \end{pmatrix}^T \text{ where, } \overline{\boldsymbol{v}}^c = \begin{pmatrix} v^c_1 & v^c_2 & v^c_3 & v^c_4 \end{pmatrix}^T$$

$$\boldsymbol{u}^c_{\text{nt2}} = \begin{pmatrix} v^c_0 & (\boldsymbol{i}^c_{in})^T \end{pmatrix}^T, \ \boldsymbol{y}^c_{\text{nt2}} = \begin{pmatrix} i^c_0 & (\overline{\boldsymbol{v}}^c)^T \end{pmatrix}^T ; \ i_0 \text{ is total current at bus 0.}$$

For generalization, it will be clearer to explain the process above with matrix manipulation. Let us say that network's original complex state space equation is given

$$\begin{pmatrix} \dot{\boldsymbol{x}}^c_{\text{nt1a}} (= 0) \\ \dot{\boldsymbol{x}}^c_{\text{nt1b}} \end{pmatrix} = \begin{pmatrix} \boldsymbol{A}^c_{\text{nt1a}} & \boldsymbol{A}^c_{\text{nt1b}} \\ \boldsymbol{A}^c_{\text{nt1c}} & \boldsymbol{A}^c_{\text{nt1d}} \end{pmatrix} \begin{pmatrix} \boldsymbol{x}^c_{\text{nt1a}} \\ \boldsymbol{x}^c_{\text{nt1b}} \end{pmatrix} + \begin{pmatrix} \boldsymbol{B}^c_{\text{nt1a}} & \boldsymbol{B}^c_{\text{nt1b}} \\ \boldsymbol{B}^c_{\text{nt1c}} & \boldsymbol{B}^c_{\text{nt1d}} \end{pmatrix} \begin{pmatrix} \boldsymbol{u}^c_{\text{nt1a}} \\ \boldsymbol{u}^c_{\text{nt1b}} \end{pmatrix} \tag{2.2–8}$$

where, $\dot{\boldsymbol{x}}^c_{\text{nt1a}} = 0$ by assuming $\boldsymbol{x}^c_{\text{nt1a}}$ being the vector of bus voltages whose dynamics are ignored. Then, $\boldsymbol{u}^c_{\text{nt1a}}$ is expressed as a function of $\boldsymbol{x}^c_{\text{nt1a}}$, $\boldsymbol{x}^c_{\text{nt1b}}$, and $\boldsymbol{u}^c_{\text{nt1b}}$ by proper matrix manipulation, where which $\boldsymbol{x}^c_{\text{nt1a}}$ will be used as a new input variable. By substituting $\boldsymbol{u}^c_{\text{nt1a}}$ into the original state space equation, the original is re-expressed with states of $\dot{\boldsymbol{x}}^c_{\text{nt1b}}$ and inputs of $\boldsymbol{x}^c_{\text{nt1a}}$ and $\boldsymbol{u}^c_{\text{nt1b}}$, where $\boldsymbol{x}^c_{\text{nt1a}}$ are the vector of respective bus voltages. The results would be the same as (2.2–6) and (2.2–7) if $\boldsymbol{x}^c_{\text{nt1a}} = v^c_0$.

This complex state space equation can be transformed into the dq-representation of state space equation using Kronecker product, as in equation (2.1–8) in sub-section 2.1.3.3.

2.2.1.3 State Space Equation 3 (Dq-representation)

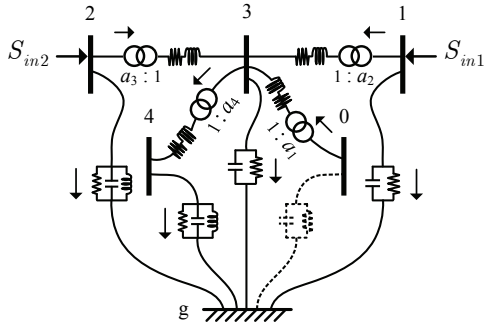

Fig. 1.9 Network model with power injection

It is now assumed that powers are the inputs into the networks. The complex models of equations (2.2–6) and (2.2–7) are transformed into dq-representations:

$$\dot{\boldsymbol{x}}_{\text{nt2}} = \boldsymbol{A}_{\text{nt2}} \boldsymbol{x}_{\text{nt2}} + \boldsymbol{B}_{\text{nt2-1}} \Delta \boldsymbol{i}_{in} + \boldsymbol{B}_{\text{nt2-2}} \Delta \boldsymbol{v}_0 \tag{2.2–9}$$

$$\Delta \boldsymbol{v}_{1,2} = \boldsymbol{c}\, \boldsymbol{x}_{\text{nt2}} \tag{2.2–10}$$

where

$$\boldsymbol{x}_{\text{nt2}} = \begin{pmatrix} \Delta \overline{\boldsymbol{v}}^T & \Delta \boldsymbol{i}^T & \Delta \boldsymbol{i}_L^T \end{pmatrix}^T, \ \Delta \boldsymbol{v}_{1,2} = \begin{pmatrix} \Delta \boldsymbol{v}_1^T & \Delta \boldsymbol{v}_2^T \end{pmatrix}^T.$$

Using the instantaneous power theory [66], the following is obtained from the relation of $P_{ink} = v_{kd} i_{inkd} + v_{kq} i_{inkq}$ and $Q_{ink} = v_{kq} i_{inkd} - v_{kd} i_{inkq}$:

$$\Delta \boldsymbol{i}_{in} = \boldsymbol{q}_1 \Delta \boldsymbol{S}_{in} - \boldsymbol{q}_2 \Delta \boldsymbol{v}_{1,2} \tag{2.2–11}$$

where

$$\boldsymbol{q}_1 = \begin{pmatrix} \boldsymbol{V}_{\mathrm{o}}^{(1)} & \\ & \boldsymbol{V}_{\mathrm{o}}^{(2)} \end{pmatrix}^{-1},\ \boldsymbol{q}_2 = \boldsymbol{q}_1 \begin{pmatrix} \boldsymbol{I}_{\mathrm{o}}^{(1)} & \\ & \boldsymbol{I}_{\mathrm{o}}^{(2)} \end{pmatrix},$$

$$\text{where, } \boldsymbol{V}_{\mathrm{o}}^{(k)} = \begin{pmatrix} v_{kdo} & v_{kqo} \\ v_{kqo} & -v_{kdo} \end{pmatrix},\ \boldsymbol{I}_{\mathrm{o}}^{(k)} = \begin{pmatrix} i_{kdo} & i_{kqo} \\ -i_{kqo} & i_{kdo} \end{pmatrix},$$

Substituting (2.2–11) into (2.2–9), a new network model with power injection is obtained:

$$\dot{\boldsymbol{x}}_{\mathrm{nt2}} = (\boldsymbol{A}_{\mathrm{nt2}} - \boldsymbol{B}_{\mathrm{nt2\text{-}1}}\, \boldsymbol{q}_2\, \boldsymbol{c}\,)\, \boldsymbol{x}_{\mathrm{nt2}} + \boldsymbol{B}_{\mathrm{nt2\text{-}1}}\, \boldsymbol{q}_1\, \Delta \boldsymbol{S}_{in} + \boldsymbol{B}_{\mathrm{nt2\text{-}2}}\, \Delta \boldsymbol{v}_0 \tag{2.2–12}$$

If the powers at the bus 0 are to be chosen as the output, the corresponding output matrix $\boldsymbol{C}_0$ and feed-through matrix $\boldsymbol{D}_0$ are obtained from the following two equations

$$\Delta \boldsymbol{i}_0 = \boldsymbol{c}_0 \boldsymbol{x}_{\mathrm{nt2}} (= \Delta \boldsymbol{i}_{03}) + \boldsymbol{d}_0 \Delta \boldsymbol{v}_0 \text{ and } \Delta \boldsymbol{S}_0 = \boldsymbol{V}_{\mathrm{o}}^{(0)} \Delta \boldsymbol{i}_0 + \boldsymbol{I}_{\mathrm{o}}^{(0)} \Delta \boldsymbol{v}_0 \tag{2.2–13}$$

Then, the output equation is expressed

$$\boldsymbol{y}_0 = \boldsymbol{C}_0 \boldsymbol{x}_{\mathrm{nt2}} + \boldsymbol{D}_0 \Delta \boldsymbol{v}_0 \tag{2.2–14}$$

where

$$\boldsymbol{y}_0 = \Delta \boldsymbol{S}_0,\ \boldsymbol{C}_0 = \boldsymbol{V}_{\mathrm{o}}^{(0)} \boldsymbol{c}_0,\ \text{and } \boldsymbol{D}_0 = \boldsymbol{V}_{\mathrm{o}}^{(0)} \boldsymbol{d}_0 + \boldsymbol{I}_{\mathrm{o}}^{(0)}.$$

2.2.2 Static Network Models

2.2.2.1 Power Equations 1 (using a Global Frame)

It is now assumed that network consists of *n* buses instead of five buses, as in the previous section. Power equations of the network model are derived using the instantaneous power theory and the admittance matrix. The dynamics of voltages and currents are ignored, unlike in the dynamic network model. Also, the network is assumed to be reduced so that all buses are linked with terminals of wind turbines, except POI bus 0.

The instantaneous power theory expresses powers injected to bus k in the network:

$$\boldsymbol{S}_k = \begin{pmatrix} P_k \\ Q_k \end{pmatrix} = \begin{pmatrix} v_{kd} i_{kd} + v_{kq} i_{kq} \\ v_{kq} i_{kd} - v_{kd} i_{kq} \end{pmatrix} \tag{2.2–15}$$

By linearizing this,

$$\Delta \boldsymbol{S}_k = \begin{pmatrix} \Delta P_k \\ \Delta Q_k \end{pmatrix} = \begin{pmatrix} v_{kdo} & v_{kqo} \\ v_{kqo} & -v_{kdo} \end{pmatrix} \begin{pmatrix} \Delta i_{kd} \\ \Delta i_{kq} \end{pmatrix} + \begin{pmatrix} i_{kdo} & i_{kqo} \\ -i_{kqo} & i_{kdo} \end{pmatrix} \begin{pmatrix} \Delta v_{kd} \\ \Delta v_{kq} \end{pmatrix} \tag{2.2–16}$$

Using (2.2–16), injected powers at n buses are expressed in simple matrix form:

$$\Delta \boldsymbol{S} = \boldsymbol{V}_{\mathrm{o}} \Delta \boldsymbol{I} + \boldsymbol{I}_{\mathrm{o}} \Delta \boldsymbol{V} \tag{2.2–17}$$

where

$$\boldsymbol{S} = \begin{pmatrix} \boldsymbol{S}_0 \\ \vdots \\ \boldsymbol{S}_n \end{pmatrix},\ \boldsymbol{I} = \begin{pmatrix} \boldsymbol{I}_0 \\ \vdots \\ \boldsymbol{I}_n \end{pmatrix},\ \boldsymbol{V} = \begin{pmatrix} \boldsymbol{V}_0 \\ \vdots \\ \boldsymbol{V}_n \end{pmatrix};$$

$$\boldsymbol{S}_k = \begin{pmatrix} P_k \\ Q_k \end{pmatrix},\ \boldsymbol{I}_k = \begin{pmatrix} i_{kd} \\ i_{kq} \end{pmatrix},\ \boldsymbol{V}_k = \begin{pmatrix} v_{kd} \\ v_{kq} \end{pmatrix},$$

$$\boldsymbol{V}_{\mathrm{o}} = \mathrm{diag}\left\{ \boldsymbol{V}_{\mathrm{o}}^{(0)}, \ldots, \boldsymbol{V}_{\mathrm{o}}^{(n)} \right\},\ \boldsymbol{I}_{\mathrm{o}} = \mathrm{diag}\left\{ \boldsymbol{I}_{\mathrm{o}}^{(0)}, \ldots, \boldsymbol{I}_{\mathrm{o}}^{(n)} \right\};$$

$$\boldsymbol{V}_{\mathrm{o}}^{(k)} = \begin{pmatrix} v_{kdo} & v_{kqo} \\ v_{kqo} & -v_{kdo} \end{pmatrix},\ \boldsymbol{I}_{\mathrm{o}}^{(k)} = \begin{pmatrix} i_{kdo} & i_{kqo} \\ -i_{kqo} & i_{kdo} \end{pmatrix}$$

Using the admittance matrix that is represented in the dq-frame (referring to (2.2–5)), equation (2.2–17) is changed to a function of bus voltages as

$$\Delta \boldsymbol{S} = \boldsymbol{F} \Delta \boldsymbol{V}\text{, where } \boldsymbol{F} = \boldsymbol{V}_{\mathrm{o}} \boldsymbol{Y} + \boldsymbol{I}_{\mathrm{o}} \tag{2.2–18}$$

The matrix $\boldsymbol{F}$ is similar to the Jacobian matrix of the power flow problem but is represented in the dq-frame. Decomposing (2.2–18) into two components of bus 0 (POI bus) and terminal buses, the result is:

$$\begin{pmatrix} \Delta \boldsymbol{S}_0 \\ \Delta \boldsymbol{S}_{\mathrm{ts}} \end{pmatrix} = \begin{pmatrix} \boldsymbol{F}_{11} & \boldsymbol{F}_{12} \\ \boldsymbol{F}_{21} & \boldsymbol{F}_{22} \end{pmatrix} \begin{pmatrix} \Delta \boldsymbol{V}_0 \\ \Delta \boldsymbol{V}_{\mathrm{ts}} \end{pmatrix} \tag{2.2–19}$$

The inputs and outputs of static network model are bus voltages and powers injected to the buses, respectively. The equation (2.2–19) can be differently expressed by matrix manipulation, where the inputs and outputs of the model are, bus 0 voltages and powers injected to the other buses, and powers injected to bus 0 and the other bus voltages, respectively,

$$\begin{pmatrix} \Delta \boldsymbol{S}_0 \\ \Delta \boldsymbol{V}_{\mathrm{ts}} \end{pmatrix} = \begin{pmatrix} \boldsymbol{H}_{11} & \boldsymbol{H}_{12} \\ \boldsymbol{H}_{21} & \boldsymbol{H}_{22} \end{pmatrix} \begin{pmatrix} \Delta \boldsymbol{V}_0 \\ \Delta \boldsymbol{S}_{\mathrm{ts}} \end{pmatrix} \tag{2.2–20}$$

The static network model developed on the basis of the power equations in this sub-subsection is for wind turbine models developed in a global frame. For wind turbine models developed in their local frames, the power equations should be modified. That is introduced in the next sub-subsection.

- Mixture of Current and Power Equations

If necessary, the static network model can be modified to have both current and power equations by replacing sets of powers with sets of d- and q-axis components of currents: if powers injected to bus-k is intended to be replaced with the corresponding currents, $\boldsymbol{V}_{\mathrm{o}}^{(k)}$ and $\boldsymbol{I}_{\mathrm{o}}^{(k)}$ are simply exchanged with the identity matrix and zero matrix, respectively. For instance, if the POI powers are exchanged with d- and q-axis components of POI currents, the changed static network model is obtained by modifying the matrix $\boldsymbol{F}$ as the following:

$$\boldsymbol{F} = \boldsymbol{V}_{\mathrm{o}} \boldsymbol{Y} + \boldsymbol{I}_{\mathrm{o}}\text{, where } \boldsymbol{V}_{\mathrm{o}} = \mathrm{diag}\left\{ \boldsymbol{I}_{2\times 2}, \boldsymbol{V}_{\mathrm{o}}^{(1)}, \ldots, \boldsymbol{V}_{\mathrm{o}}^{(n)} \right\},\ \boldsymbol{I}_{\mathrm{o}} = \mathrm{diag}\left\{ \boldsymbol{0}_{2\times 2}, \boldsymbol{I}_{\mathrm{o}}^{(0)}, \ldots, \boldsymbol{I}_{\mathrm{o}}^{(n)} \right\}$$

where $\boldsymbol{I}_{2\times 2}$ and $\boldsymbol{0}_{2\times 2}$ are 2 by 2 identity matrix and zero matrix, respectively.

2.2.2.2 Power Equations 2 (using Local Frames)

Power equations suitable for the local-frame model 1 are developed using dq-frame transformation. The dq-frame transformation process can be expressed in two ways based on different assumptions.

$$(v_d + jv_q) = e^{-j\theta_o'}(v_d^{\mathrm{vo}} + jv_q^{\mathrm{vo}}) \tag{2.2–21}$$

$$\text{where } \theta_o' = \tan^{-1}\left(\frac{v_{do}}{v_{qo}}\right)$$

$$(v_d + jv_q) = e^{-j\theta'}(v_d^{\mathrm{vo}} + jv_q^{\mathrm{vo}}) \tag{2.2–22}$$

$$\text{where } \theta' = \tan^{-1}\left(\frac{v_d}{v_q}\right)$$

Here, v and v^{vo} represent voltages in a global frame and in a voltage-oriented local frame, respectively. Figure 1.10 shows the transformation process of equations (2.2–21) and (2.2–22).

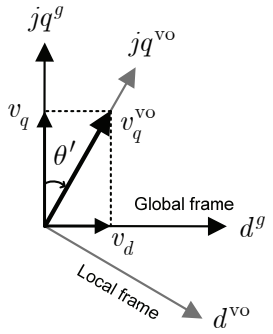

Fig. 1.10 Local and global frames

It needs to be noted that $e^{-j\theta'_o}$ is constant while $e^{-j\theta'}$ is a function of the voltage. For the equation (2.2–21), because the local frame maintains constant angle position to the global frame, the d-axis component of voltage is not instantaneously zero but its value in average is zero as long as the voltage varies around the initial point. On the other hand, for the equation (2.2–22), the local frame is instantaneously aligned with the voltage so that the d-axis component of the voltage is always zero.

By using either of the equation (2.2–21) or (2.2–22), voltages can be projected (transformed) from a global frame to their local frames. Expressing the transformation function with respect to the voltage at bus k in dq-representation,

$$\begin{pmatrix} \Delta v_{kd}^{\mathrm{vo}} \\ \Delta v_{kq}^{\mathrm{vo}} \end{pmatrix} = \boldsymbol{T}_{kv} \begin{pmatrix} \Delta v_{kd} \\ \Delta v_{kq} \end{pmatrix} \tag{2.2–23}$$

For the various buses that multiple wind turbines are connected, a transformation matrix $\boldsymbol{T}^{\mathrm{vo}}$, which transforms voltages in a global frame to those of their local frames, can be properly obtained using sets of $\boldsymbol{T}_{kv}$. Then, applying the transformation matrix to the equations (2.2–19) or (2.2–20), new power equations in terms of the local frames are obtained. As there are two different transformation matrixes, the locally framed power equations will be derived in two ways.

- Local-frame network model 1:

First, transformation matrix $\boldsymbol{T}_{kvA}$ by linearizing equation (2.2–21) is,

$$\boldsymbol{T}_{kvA} = \begin{pmatrix} \cos\theta'_{ko} & -\sin\theta'_{ko} \\ \sin\theta'_{ko} & \cos\theta'_{ko} \end{pmatrix} \tag{2.2–24}$$

Using this matrix, power equations for local frame with respect to (2.2–21) is derived,

$$\begin{pmatrix} \Delta \boldsymbol{S}_0 \\ \Delta \boldsymbol{S}_{\mathrm{ts}} \end{pmatrix} = \begin{pmatrix} \boldsymbol{F}_{11} & \boldsymbol{F}_{12}^{\mathrm{vo}} \\ \boldsymbol{F}_{21}^{\mathrm{vo}} & \boldsymbol{F}_{22}^{\mathrm{vo}} \end{pmatrix} \begin{pmatrix} \Delta \boldsymbol{V}_0 \\ \Delta \boldsymbol{V}_{\mathrm{ts}}^{\mathrm{vo}} \end{pmatrix} \tag{2.2–25}$$

where

$$\begin{pmatrix} \boldsymbol{F}_{11} & \boldsymbol{F}_{12}^{\mathrm{vo}} \\ \boldsymbol{F}_{21}^{\mathrm{vo}} & \boldsymbol{F}_{22}^{\mathrm{vo}} \end{pmatrix} = \begin{pmatrix} \boldsymbol{F}_{11} & \boldsymbol{F}_{12} \\ \boldsymbol{F}_{21} & \boldsymbol{F}_{22} \end{pmatrix} \begin{pmatrix} \boldsymbol{I} & \\ & \boldsymbol{T}_A^{\mathrm{vo}} \end{pmatrix}^{-1};$$

$$\boldsymbol{T}_A^{\mathrm{vo}} = \mathrm{diag}\{\boldsymbol{T}_{1vA}, \ldots, \boldsymbol{T}_{nvA}\}.$$

- Local-frame network model 2:

On the other hand, another transformation matrix $\boldsymbol{T}_{kvB}$ by linearizing equation (2.2–22),

$$\boldsymbol{T}_{kvB} = \begin{pmatrix} \cos\theta'_{ko} & -\sin\theta'_{ko} \\ \sin\theta'_{ko} & \cos\theta'_{ko} \end{pmatrix} \begin{pmatrix} 1 - av_{kqo}^2 & av_{kdo}v_{kqo} \\ av_{kdo}v_{kqo} & 1 - av_{kdo}^2 \end{pmatrix}, \text{ where } a = \frac{1}{|v_{ko}|^2} \tag{2.2–26}$$

The transformation obtained by (2.2–26) has rank 1, where components in the first row are zeroes and components in the second row are identical to ones obtained by linearizing the terminal voltage magnitude of $(v_{kd}^2 + v_{kq}^2)^{1/2}$. Using this matrix, the other power equations for local frame with respect to (2.2–22) is derived

$$\begin{pmatrix} \Delta \boldsymbol{S}_0 \\ \Delta \boldsymbol{V}_{\text{ts}}^{\text{vo}} \end{pmatrix} = \begin{pmatrix} \boldsymbol{H}_{11} & \boldsymbol{H}_{12}^{\text{vo}} \\ \boldsymbol{H}_{21}^{\text{vo}} & \boldsymbol{H}_{22}^{\text{vo}} \end{pmatrix} \begin{pmatrix} \Delta \boldsymbol{V}_0 \\ \Delta \boldsymbol{S}_{\text{ts}} \end{pmatrix} \tag{2.2–27}$$

where

$$\begin{pmatrix} \boldsymbol{H}_{11} & \boldsymbol{H}_{12}^{\text{vo}} \\ \boldsymbol{H}_{21}^{\text{vo}} & \boldsymbol{H}_{22}^{\text{vo}} \end{pmatrix} = \begin{pmatrix} \boldsymbol{I} & \\ & \boldsymbol{T}_B^{\text{vo}} \end{pmatrix} \begin{pmatrix} \boldsymbol{H}_{11} & \boldsymbol{H}_{12} \\ \boldsymbol{H}_{21} & \boldsymbol{H}_{22} \end{pmatrix};$$

$$\boldsymbol{T}_B^{\text{vo}} = \text{diag}\{\boldsymbol{T}_{1vB}, \ldots, \boldsymbol{T}_{nvB}\}.$$

2.3 Wind Power Plant Model

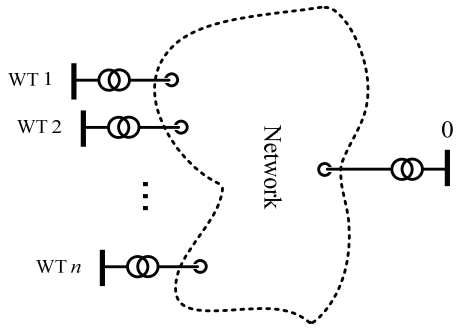

Fig. 1.11 N wind turbines connected to 0 (POI) bus though network

A full detailed WPP model includes multiple wind turbines and networks, which requires a full knowledge of the WPP system. In addition, separate linearized models need to be developed depending on various operating points. This requires huge efforts in developing WPP model. Nevertheless, a full detailed WPP is still essential, especially, to compare the performance of a WPP's equivalent with it. For this reason, this subsection introduces a full detailed (linearized) WPP model.

Figure 1.11 shows n wind turbines (WTs) are connected to corresponding (terminal) buses which are linked through transformers and networked lines to the point of interconnection (POI). The transformer in the figure represents ideal transformer of which turn ratio is only considered. The leakage inductance and resistance of step-up transformers are assumed absorbed into wind turbine models, and thus they are not considered when modeling network.

The subsequent sections will complete a WPP model by combining wind turbine models with a network model, which have been developed in the previous sections.

2.3.1 WPP Model using a Global Frame

As shown in figure 1.11, n wind turbines are linked to the network model. The types are not specified, so they could be any types of wind turbines. The inputs of wind turbine are d- and q-axis components of terminal voltage and either of blade torque or wind speed. The outputs are chosen terminal powers of wind turbines in motoring view.

$$\dot{\boldsymbol{x}}_{\text{ts}} = \boldsymbol{A}_{\text{ts}}\boldsymbol{x}_{\text{ts}} + \boldsymbol{B}^1_{\text{ts}}\boldsymbol{u}^1_{\text{ts}} + \boldsymbol{B}^2_{\text{ts}}\boldsymbol{u}^2_{\text{ts}} \tag{2.3–1}$$

$$\boldsymbol{y}_{\text{ts}} = \boldsymbol{C}_{\text{ts}}\boldsymbol{x}_{\text{ts}} + \boldsymbol{D}_{\text{ts}}\boldsymbol{u}^1_{\text{ts}} \tag{2.3–2}$$

where

$$\boldsymbol{A}_{\text{ts}} = \text{diag}\left\{\boldsymbol{A}_{\text{t-1}}, \cdots, \boldsymbol{A}_{\text{t-n}}\right\},$$

$$\boldsymbol{B}^1_{\text{ts}} = \text{diag}\left\{\boldsymbol{B}^1_{\text{t-1}}, \cdots, \boldsymbol{B}^1_{\text{t-n}}\right\},\ \boldsymbol{B}^2_{\text{ts}} = \text{diag}\left\{\boldsymbol{B}^2_{\text{t-1}}, \cdots, \boldsymbol{B}^2_{\text{t-n}}\right\},$$

$$\boldsymbol{C}_{\text{ts}} = \text{diag}\left\{\boldsymbol{C}_{\text{t-1}}, \cdots, \boldsymbol{C}_{\text{t-n}}\right\},$$

$$\boldsymbol{D}_{\text{ts}} = \text{diag}\left\{\boldsymbol{D}_{\text{t-1}}, \cdots, \boldsymbol{D}_{\text{t-n}}\right\},$$

$$\boldsymbol{x}_{\text{ts}} = \begin{pmatrix} \boldsymbol{x}_{\text{t-1}} \\ \vdots \\ \boldsymbol{x}_{\text{t-n}} \end{pmatrix},\ \boldsymbol{y}_{\text{ts}} = \begin{pmatrix} \Delta\boldsymbol{S}_{\text{t-1}} \\ \vdots \\ \Delta\boldsymbol{S}_{\text{t-n}} \end{pmatrix}.$$

Here, subscript "ts" denotes a set of n wind turbines. $\boldsymbol{u}^2_{\text{ts}}$ is the input vector that consists of either blade torques or wind speeds. The system matrix $\boldsymbol{A}_{\text{ts}}$ and input matrix $\boldsymbol{B}_{\text{ts}}$ are formed in blocked diagonal matrices, and it means wind turbines are not coupled with each other yet.

A network model is developed in the dq-representation as done in equations (2.2–6) and (2.2–7). Network inputs are injected powers from wind turbines to the network and voltage at bus 0 (POI bus). The bus 0 voltage is emphasized with capital $\boldsymbol{V}$.

$$\dot{\boldsymbol{x}}_{\text{net}} = \boldsymbol{A}_{\text{net}}\boldsymbol{x}_{\text{net}} + \boldsymbol{B}^1_{\text{net}}\boldsymbol{u}^1_{\text{net}} + \boldsymbol{B}^2_{\text{net}}\Delta\boldsymbol{V}_0 \tag{2.3–3}$$

$$\boldsymbol{y}_{\text{net}} = \boldsymbol{C}_{\text{net}}\boldsymbol{x}_{\text{net}} + \boldsymbol{D}_{\text{net}}\Delta\boldsymbol{V}_0 \tag{2.3–4}$$

No load is assumed connected at bus 0 ($\boldsymbol{D}_{\text{net}} = \boldsymbol{0}$). One of the two inputs of the multiple wind turbine model (a set of turbines' terminal voltages) is equivalent to the network model outputs (a set of voltages at buses that the turbines are connected) ($\boldsymbol{u}^1_{\text{ts}} = \boldsymbol{y}_{\text{net}}$) and vice versa ($\boldsymbol{u}^1_{\text{net}} = -\boldsymbol{y}_{\text{ts}}$), so the two models can be combined:

$$\begin{pmatrix} \dot{\boldsymbol{x}}_{\text{ts}} \\ \dot{\boldsymbol{x}}_{\text{net}} \end{pmatrix} = \begin{pmatrix} \boldsymbol{A}_{\text{ts}} & \boldsymbol{B}^1_{\text{ts}}\boldsymbol{C}_{\text{net}} \\ -\boldsymbol{B}^1_{\text{net}}\boldsymbol{C}_{\text{ts}} & \bar{\boldsymbol{A}}_{\text{net}} \end{pmatrix} \begin{pmatrix} \boldsymbol{x}_{\text{ts}} \\ \boldsymbol{x}_{\text{net}} \end{pmatrix} + \begin{pmatrix} \boldsymbol{B}^2_{\text{ts}} & \boldsymbol{0} \\ \boldsymbol{0} & \boldsymbol{B}^2_{\text{net}} \end{pmatrix} \begin{pmatrix} \boldsymbol{u}^2_{\text{ts}} \\ \Delta\boldsymbol{V}_0 \end{pmatrix} \tag{2.3–5}$$

where $\bar{\boldsymbol{A}}_{\text{net}} = \boldsymbol{A}_{\text{net}} - \boldsymbol{B}^1_{\text{net}}\boldsymbol{D}_{\text{ts}}\boldsymbol{C}_{\text{net}}$

Here, the wind turbines are coupled with each other via the network model. Additionally, in this model development:

- it should be noted that all states are expressed in a global dq frame. Therefore, operating points of each wind turbine might differ by the terminal voltages not only in magnitude but also in angle.
- the model (2.3–5) can be reduced if able to assume that the dynamics of network are much faster than those of the wind turbines. Assuming the derivative terms of $\boldsymbol{x}_{\text{net}}$ are zeroes,

$$\boldsymbol{x}_{\text{net}} = \bar{\boldsymbol{A}}^{-1}_{\text{net}}\boldsymbol{B}^1_{\text{net}}\boldsymbol{C}_{\text{ts}}\boldsymbol{x}_{\text{ts}} - \bar{\boldsymbol{A}}^{-1}_{\text{net}}\boldsymbol{B}^2_{\text{net}}\Delta\boldsymbol{V}_0 \tag{2.3–6}$$

Substituting it into equation (2.3–5), the result is:

$$\dot{\boldsymbol{x}}_{\rm ts} = (\boldsymbol{A}_{\rm ts} + \boldsymbol{B}^1_{\rm ts}\boldsymbol{C}_{\rm net}\bar{\boldsymbol{A}}^{-1}_{\rm net}\boldsymbol{B}^1_{\rm net}\boldsymbol{C}_{\rm ts})\boldsymbol{x}_{\rm ts} - \boldsymbol{B}^1_{\rm ts}\boldsymbol{C}_{\rm net}\bar{\boldsymbol{A}}^{-1}_{\rm net}\boldsymbol{B}^2_{\rm net}\Delta\boldsymbol{V}_0 + \boldsymbol{B}^2_{\rm ts}\boldsymbol{u}^2_{\rm ts} \qquad (2.3\text{–}7)$$

The result would be the same when the static network model completed in sub-subsection 2.2.2.1, power equations 1 is applied. Unless the dynamics of network is considered, it would be proper to develop WPP model with the static network model.

2.3.2 WPP Model using Local Frames

In this subsection, wind turbines are assumed to be modeled in the voltage-oriented local dq-frames, where each local frame's q-axis is aligned with each turbine's terminal voltage. In addition, static network model is applied instead of dynamic network model. The WPP model development can be achieved in two ways depending on the choice of the models of wind turbine and static network. The first is to use local-frame model 1 for wind turbines and the static network model completed in sub-subsection 2.2.2.2, local-frame network model 1, by which it is assumed that the turbines' terminal voltages are initially aligned with the q-axes of their local frames but they could deviate from the alignment. The second is to use local-frame model 2 for wind turbines and static network model completed in sub-subsection 2.2.2.2, local-frame network model 2, by which it is assumed that the turbines' terminal voltages are instantaneously aligned with the q-axes of their local frames.

The model of wind turbines in their local frames, which are not interconnected, is expressed in the same form of (2.3–1) and (2.3–2), but with slightly different parameters. The output is: $\boldsymbol{y}_{\rm ts} = \Delta\boldsymbol{S}_{\rm ts}$ and the input is: $\boldsymbol{u}^1_{\rm ts} = \Delta\boldsymbol{V}^{\rm vo}_{\rm ts}$. Using equations (2.3–2) and (2.2–24) or (2.2–26), the following is obtained.

$$\boldsymbol{u}^1_{\rm ts} = \boldsymbol{L}_a\boldsymbol{x}_{\rm ts} + \boldsymbol{L}_b\Delta\boldsymbol{V}_0 \qquad (2.3\text{–}8)$$

where the matrixes $\boldsymbol{L}_a$ and $\boldsymbol{L}_b$ are different depending on the choice of network models.

With local-frame network mode 1: $\boldsymbol{L}_a = -(\boldsymbol{F}^{\rm vo}_{22} + \boldsymbol{D}^{\rm vo}_{\rm ts})^{-1}\boldsymbol{C}_{\rm ts}$, $\boldsymbol{L}_b = -(\boldsymbol{F}^{\rm vo}_{22} + \boldsymbol{D}_{\rm ts})^{-1}\boldsymbol{F}^{\rm vo}_{21}$.

With local-frame network mode 2: $\boldsymbol{L}_a = -(\boldsymbol{I} + \boldsymbol{H}^{\rm vo}_{22}\boldsymbol{D}^{\rm vo}_{\rm ts})^{-1}\boldsymbol{H}^{\rm vo}_{22}\boldsymbol{C}_{\rm ts}$, $\boldsymbol{L}_b = (\boldsymbol{I} + \boldsymbol{H}^{\rm vo}_{22}\boldsymbol{D}_{\rm ts})^{-1}\boldsymbol{H}^{\rm vo}_{21}$.

Wind turbines are interconnected to completes WPP model development by combining the equation (2.3–8) into the model of turbines developed in the local frames

$$\dot{\boldsymbol{x}}_{\rm ts} = \bar{\boldsymbol{A}}_{\rm ts}\boldsymbol{x}_{\rm ts} + \bar{\boldsymbol{B}}^1_{\rm ts}\Delta\boldsymbol{V}_0 + \boldsymbol{B}^2_{\rm ts}\boldsymbol{u}^2_{\rm ts} \qquad (2.3\text{–}9)$$

$$\Delta\boldsymbol{S}_0 = \bar{\boldsymbol{C}}_0\boldsymbol{x}_{\rm ts} + \bar{\boldsymbol{D}}_0\Delta\boldsymbol{V}_0 \qquad (2.3\text{–}10)$$

where

$\bar{\boldsymbol{A}}_{\rm ts} = \boldsymbol{A}_{\rm ts} + \boldsymbol{B}^1_{\rm ts}\boldsymbol{L}_a$,

$\bar{\boldsymbol{B}}^1_{\rm ts} = \boldsymbol{B}^1_{\rm ts}\boldsymbol{L}_b$,

With local-frame network model 1: $\bar{\boldsymbol{C}}_0 = -\boldsymbol{F}^{\rm vo}_{12}\boldsymbol{L}_a$, $\bar{\boldsymbol{D}}_0 = -(\boldsymbol{F}_{11} + \boldsymbol{F}^{\rm vo}_{12}\boldsymbol{L}_b)$.

With local-frame network model 2: $\bar{\boldsymbol{C}}_0 = -\boldsymbol{H}^{\rm vo}_{12}(\boldsymbol{C}_{\rm ts} + \boldsymbol{D}_{\rm ts}\boldsymbol{L}_a)$, $\bar{\boldsymbol{D}}_0 = (\boldsymbol{H}_{11} - \boldsymbol{H}^{\rm vo}_{12}\boldsymbol{D}_{\rm ts}\boldsymbol{L}_b)$.

The results obtained in this section will be used to develop a dynamic equivalent model for WPP using aggregation technique in the next chapter.

2.3.3 Frequency-related Modeling

The WPP models developed in this chapter were on the basis of the assumption that the angular speed ω^g of the global dq-rotating frame (frequency) is constant, and thus ω_{su} and ω_u in the generators (excepting type 4), back-to-back converters, and network models were also assumed constant: $\Delta\omega^g = 0$. This implies that the WPPs are only affected by other power systems through POI voltage variations with constant frequency.

When other power systems are considered into modeling problem, ω^g is no longer constant and treated as an additional variable. In consequence, the current equations of the network model becomes nonlinear and its linearization results

$$\boldsymbol{I} = \boldsymbol{Y}(\omega^g)\boldsymbol{V}\,;\ \Delta\boldsymbol{I} = \boldsymbol{Y}(\omega_o^g)\Delta\boldsymbol{V} + \boldsymbol{K}_Y\boldsymbol{V}\Delta\omega^g \tag{2.3–11}$$

Also, the power equations should change accordingly by (2.3–11). These require complicated calculations but contribute a little for modeling accuracy if ω^g varies within small range. Therefore, for simplicity, it is assumed that system and network impedance changes regarding the angular speed are negligible; the second term in (2.3–11) is discarded. However, the synchronous speed regarding turbine dynamic models still need to be taken into consideration, which can be carried out in the following way.

- Modeling in POI Voltage-oriented Frame

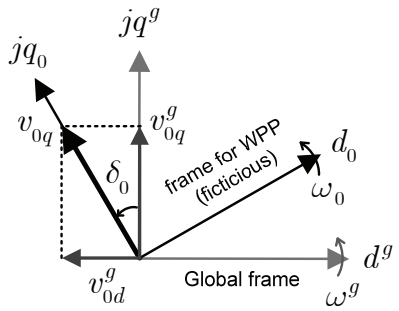

Fig. 1.12 a POI voltage in a fictitious frame and its corresponding in the global frame

The synchronous speed ω_{su} in the generator models and ω_u in the input side of the back-to-back converter models are equal to the angular speed ω_0 of a fictitious frame where a WPP system is modeled, and thus the following relations are obtained

$$\Delta\omega_{su} = \Delta\omega_0 \text{ and } \Delta\omega_u = \Delta\omega_0 \tag{2.3–12}$$

Then, the ignored terms by the assumption of $\Delta\omega_{su} = 0$ in (2.1–11) are re-emerged and the terms regarding $\Delta\omega_u$ in the converter models are obtained properly. Using some matrix manipulations, the WPP model of (2.3–9) changes to

$$\dot{\boldsymbol{x}}_{\text{ts}} = \bar{\boldsymbol{A}}_{\text{ts}}\boldsymbol{x}_{\text{ts}} + \bar{\boldsymbol{B}}_{\text{ts}}^1\Delta\boldsymbol{V}_0 + \boldsymbol{B}_{\text{ts}}^2\boldsymbol{u}_{\text{ts}}^2 + \boldsymbol{B}_{\text{ts}}^3\Delta\omega_0 \tag{2.3–13}$$

The key to this modeling is properly changing the angular speed of the frame. The voltage-oriented frame whose q-axis is aligned at POI voltage of the fictitious frame rotates in the speed of ω_0 which is the sum of ω^g, which is the angular speed of the global frame, and a supplementary speed ω_{ad}, which is happened by the POI voltage change. The angular speed variation of the voltage-oriented frame is given

$$\Delta\omega_0 = \Delta\omega^g + \Delta\omega_{ad} \tag{2.3–14}$$

Assuming that the fictitious frame is loosely aligned with the POI voltage of the global frame, the differential equation of the angle is given by using low-pass filtering,

$$\Delta\dot{\delta}_0 = -a_c\Delta\delta_0 + a_c\boldsymbol{K}_{0\delta}\Delta\boldsymbol{V}_0^g \tag{2.3–15}$$

where a_c is the cut-off frequency of the low-pass filtering and $\boldsymbol{K}_\delta$ is obtained by linearizing $\tan^{-1}(-v_{0d}^g / v_{0q}^g)$. The supplementary speed is equal to the time differential of the angle, so it is given

$$\Delta\omega_{ad} = \frac{1}{\omega_B}\Delta\dot{\delta}_0 \tag{2.3–16}$$

Here, it is expected that $\Delta\omega_{ad}$ is assumable zero when the cut-off frequency is chosen very large because its dynamics could be ignored; it is not when the cut-off frequency is chosen very small. This is, actually, the same concept used to develop the terminal voltage-oriented turbine model; refer to (2.1–51).

Now, the POI voltage of the global frame is projected to that of the fictitious frame as

$$\Delta \boldsymbol{V}_0 = \boldsymbol{K}_{0v}\Delta\delta_0 + \boldsymbol{T}^{-1}(\delta_{0o})\Delta \boldsymbol{V}_0^g \tag{2.3–17}$$

Recalling that powers are conserved between the transformation processes, the frequency-related modeling is finalized by applying the equations of (2.3–14, 15, 16, and 17) to (2.3–13),

$$\dot{\boldsymbol{x}}_{\text{ts-}\delta} = \bar{\boldsymbol{A}}_{\text{ts-}\delta}\boldsymbol{x}_{\text{ts-}\delta} + \bar{\boldsymbol{B}}^1_{\text{ts-}\delta}\Delta \boldsymbol{V}_0^g + \boldsymbol{B}^2_{\text{ts-}\delta}\boldsymbol{u}^2_{\text{ts}} + \boldsymbol{B}^3_{\text{ts-}\delta}\Delta\omega^g \tag{2.3–18}$$

$$\Delta \boldsymbol{S}_0 = \bar{\boldsymbol{C}}_{0\text{-}\delta}\boldsymbol{x}_{\text{ts-}\delta} + \bar{\boldsymbol{D}}_{0\text{-}\delta}\Delta \boldsymbol{V}_0^g \tag{2.3–19}$$

where $\boldsymbol{x}_{\text{ts-}\delta} = (\, \boldsymbol{x}_{\text{ts}}^T \quad \Delta\delta_0 \,)^T$. Compare (2.3–9) and (2.3–18). It will be noticed that (2.3–18) has an additional input variable of $\Delta\omega^g$. This frequency-related modeling should be used to combine the WPP model into power systems. Note that generating unit models in power systems generally require differential equations of power angles to be interfaced each other, while the WPP model of (2.3–18) does not because the WPP consists of asynchronous generators. Refer to subsection 6.1.1. This subsection will show the differential equations of power angles for power system modeling with synchronous generators.

2.4 Summary

Chapter 2 has been assigned to develop a dynamic model of wind power plants. First, dynamic sub-models such as drive train, generator, and back-to-back converters were developed. Several components of wind-torque characteristics, gear ratios, step-up transformers, crowbars, pulse width modulation parts were absorbed into the sub-models. The sub-models were properly combined to represent four types of complete models of wind turbines. This chapter showed that the complete turbine models could be changed on the basis of their input types and the frames where they were developed. Second, networked cables in wind power plants were modeled. By using KVL and KCL, the networked cables were dynamically modeled. The dynamic network models were altered by the input types: current injection, constant bus voltage, and power injection. Also, this chapter introduced static network models using the instantaneous power theory. Furthermore, as wind turbines, especially variable speed wind turbines, are feedback controlled in their local frames and thus modeled in the frames, the static network models matching for the dynamic models of the turbines were developed. Lastly, the models of wind turbines and network were combined to complete a dynamic model of wind power plants.

Chapter 3

Dynamic Equivalent Model of WPP using Aggregation Technique

Wind power generation has emerged as an effective alternative energy source over the past couple of decades, with successful research and industry development leading to the construction of wind power generation systems that approach the scale of conventional mid- to large-size thermal power plants. This large scale of wind power generation systems is referred to as wind power plants (WPPs), and an increasing number of WPPs have begun to have a significant impact on existing power systems. However, the WPPs differ significantly from the conventional power plants in terms of structure, operation, and dynamics. As an understanding of dynamics is essential for maintaining the stable operation of power systems, a proper dynamic model of the WPPs must be developed.

The dynamic modeling of WPP systems poses a unique set of problems unlike those of conventional generation systems in that 1) a WPP consists of numerous small wind turbines with limited dispatching capabilities; 2) each wind turbine includes multiple components that cause damping in electromechanical dynamics; 3) the wind turbines are placed irregularly over a large area and their energy source (wind) varies stochastically, so the turbines are operated differently; and 4) the turbines are mutually interconnected by cables so that they are affected by the operation of each. These four problems make modeling WPPs a complicated process in which high-order models will necessarily be produced; it is therefore necessary to develop low-order dynamic equivalent model (DEM) that can provide the same dynamic performance as the original WPP models.

In this chapter, a DEM for WPP is developed using aggregation technique. First, the aggregation technique is briefly introduced. Then, slow dynamic models of wind turbines are developed, which is important for developing a proper WPP DEM. The slow dynamic models are combined with the network models to express the WPP DEM as a single low-order system. The performance of the proposed method is verified through simulation.

3.1 Introduction of Aggregation Technique

Notes [67]–[69] explain the main concept of model equivalencing. The model equivalencing can be categorized into two cases: 1) a detailed model is reduced to its low-order equivalent model, where the detailed model's slow dynamics are equivalently preserved, 2) a single form of multiple models, which is obtained by 'model combining', is simplified to its low-order equivalent model by the model equivalencing. The figure below shows the concept of 'aggregation technique'. For clear understanding, specific terms are used. 'Model combining' will refer to the process of combining separated multiple models into a single form of the multiple models, where model complexity does not change, and 'model equivalencing' refers to the process of simplifying a single complex model into an equivalent model, respectively. 'Aggregation technique' refers to the process including the both. In figure 2.1 (a), a detailed model is simplified to its low-order equivalent model by neglecting fast dynamics. Figure 2.1 (b) shows that separate models are interconnected and combined into a single form of the models, and then the model is simplified to its low-order equivalent model. The model equivalencing used in the figure (a) and the ones used in the part of (2) to (3) (or (5) to (6)) in the figure (b) are different, where the former is to neglect fast dynamics and the latter is to lump a single form of 'multiple models' into the form of a 'single model'. The part of (1) represents separate detailed models interconnected and the part of (4) represents separate low-order equivalent models interconnected, where the dynamics of interconnection is ignored. The model of (1) or (4) is combined to be one of (2) or (5) by

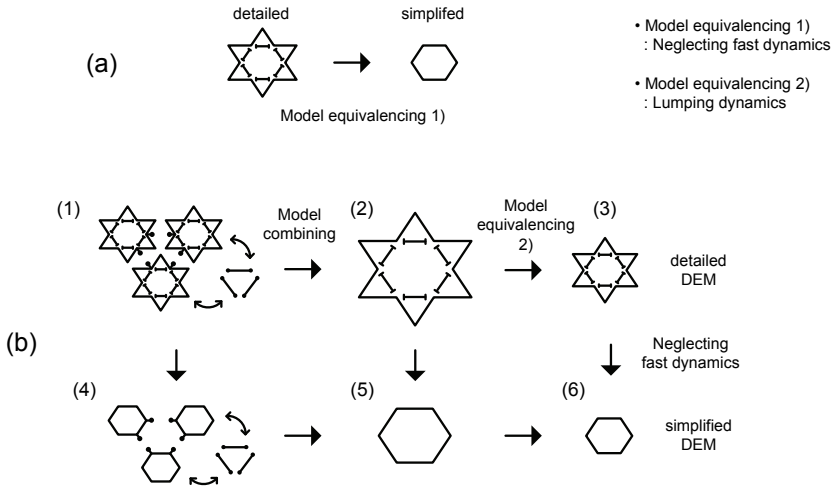

Fig. 2.1 Aggregation technique (a) single detailed model simplified to its low-order equivalent model (b) multiple models aggregated to its low-order equivalent model and it is simplified to its equivalent model

model combining, then to be one of (3) or (6) by model equivalencing. Dynamic equivalent model of (6) can be obtained by any sequence preferred. An efficient procedure to develop the dynamic equivalent model might follow the sequence of (1)-(2)-(3)-(6) because a procedure starting from (4) requires multiple low-order equivalent models to be developed. For an example of a DEM for a WPP, this process could be performed as: assuming that wind turbines in a WPP are pre-identified into a single group on the basis of their operational conditions, the wind turbine models are combined with a static network model into a single form of WPP model by model combining. Then, the WPP model is lumped into a form of single wind turbine model by model equivalencing, which represents a simplified WPP equivalent model, and the WPP equivalent model is further simplified by neglecting fast dynamics, significantly reducing the resultant WPP equivalent model's complexity.

In the subsequent subsection, the model equivalencing will be introduced accordingly.

3.1.1 Slow Dynamic Equivalent Model

To simplify a detailed model to its equivalence with preserved slow dynamics, the detailed model needs to be decomposed into the components in terms of slow and fast dynamics. Let us assume that a system's detailed model is expressed as

$$\dot{\boldsymbol{x}}_{n\times 1} = \boldsymbol{A}\boldsymbol{x} + \boldsymbol{B}\boldsymbol{u} \tag{3.1–1}$$

$$\boldsymbol{y} = \boldsymbol{C}\boldsymbol{x} + \boldsymbol{D}\boldsymbol{u} \tag{3.1–2}$$

When a model is developed from physical concept, it could be easily known which state variables are related to slow and fast dynamics. However, the dynamics might be uncertain in many cases. In the cases, the state variables should be properly altered with a transformation matrix. Here, for instance, it is assumed that the system is transformed using Gramian matrix so that the states have been decomposed into probable slow and fast (quick) states [69]:

$$\begin{pmatrix} \dot{\boldsymbol{x}}_q \\ \dot{\boldsymbol{x}}_s \end{pmatrix} = \begin{pmatrix} \boldsymbol{A}_{11} & \boldsymbol{A}_{12} \\ \boldsymbol{A}_{21} & \boldsymbol{A}_s \end{pmatrix} \boldsymbol{x} + \begin{pmatrix} \boldsymbol{B}_1 \\ \boldsymbol{B}_s \end{pmatrix} \boldsymbol{u} \tag{3.1–3}$$

$$\boldsymbol{y} = \begin{pmatrix} \boldsymbol{C}_1 & \boldsymbol{C}_s \end{pmatrix} \boldsymbol{x} + \boldsymbol{D}\boldsymbol{u} \tag{3.1–4}$$

According to the minimal realization theory, there is an exact order model if and only if the subsystem

$(\boldsymbol{A}_s, \boldsymbol{B}_s, \boldsymbol{C}_s)$ has the same impulse response as the full model. This can be satisfied if the states of $\boldsymbol{x}_s$ and $\boldsymbol{x}_q$ are weakly coupled and the dynamics related to the states $\boldsymbol{x}_q$ are damped out so fast that the eigenvalues of $\boldsymbol{A}_s$ are almost same as those of a reduced equivalent model. Thus, it is important to know which state variables relate to slow dynamics to develop a proper slow dynamic equivalent model. If the dynamics for state variables are known and they are separable, the dynamics of state variables related to fast dynamics can be easily removed. If not, state variables related to fast dynamics will be found by eigenvalue-sorting method (modal analysis) and the dynamics of the corresponding state variables can be neglected. These are explained in the following two sub-subsections, respectively.

3.1.1.1 Model Equivalencing by Neglecting Fast Dynamics

If the states can be completely separated in terms of fast and slow dynamics, either of the two dynamics can be ignored. First, if fast dynamics are interested, it can be assumed that the changes of slow dynamics are almost constant compared to those of the fast dynamics so that the derivatives of the states with respect to the slow dynamics are to be near zero. Conversely, if the slow dynamics are the subject of interest, the states related to the fast dynamics are assumed to reach the steady state much faster than those for the slow dynamics, so that the derivatives of the states with respect to the fast dynamics can be assumed to be zero. Here, what to be interested is to the latter case.

Assuming that a system's state variables are decomposed according to physically presumable slow and fast dynamics, the system is simply expressed by neglecting the respective fast dynamics as

$$\begin{pmatrix} \boldsymbol{0} \\ \dot{\boldsymbol{x}}_s \end{pmatrix} = \begin{pmatrix} \boldsymbol{A}_{11} & \boldsymbol{A}_{12} \\ \boldsymbol{A}_{21} & \boldsymbol{A}_s \end{pmatrix} \boldsymbol{x} + \begin{pmatrix} \boldsymbol{B}_1 \\ \boldsymbol{B}_s \end{pmatrix} \boldsymbol{u} \tag{3.1–5}$$

In this case, the state variables of fast dynamics can be written in the function of the state variables of slow dynamics

$$\boldsymbol{x}_q = -\boldsymbol{A}_{11}^{-1}\boldsymbol{A}_{12}\boldsymbol{x}_s - \boldsymbol{A}_{11}^{-1}\boldsymbol{B}_1\boldsymbol{u} \tag{3.1–6}$$

Then, the equivalent model regarding only the slow dynamics is given as

$$\dot{\boldsymbol{x}}_s = (\boldsymbol{A}_s - \boldsymbol{A}_{21}\boldsymbol{A}_{11}^{-1}\boldsymbol{A}_{12})\boldsymbol{x}_s + (\boldsymbol{B}_s - \boldsymbol{A}_{21}\boldsymbol{A}_{11}^{-1}\boldsymbol{B}_1)\boldsymbol{u} \tag{3.1–7}$$

Although this method is very simple and effective, it presumes that the state variables are properly altered in terms of slow and fast dynamics. However, it might be sometimes difficult to decompose states in terms of probable slow and fast dynamics. In this case, eigenvalue-sorting method could provide a useful solution, which following sub-subsection explains.

3.1.1.2 Model Equivalencing with Eigenvalue-sorting Method

The eigenvalue-sorting method is performed by modal analysis, which is carried out by converting a state space equation to the respective modal form and properly removing some of the eigenvalues. Let us say a transformation matrix $\boldsymbol{V}$ (matrix of eigenvectors) exists:

$$\boldsymbol{x} = \boldsymbol{V}\boldsymbol{h} \tag{3.1–8}$$

It is assumed that the matrix $\boldsymbol{V}$ transforms system matrix $\boldsymbol{A}$ in the equation (3.1–1) into matrix $\boldsymbol{F}$ that consists of eigenvalues, ordered in largest to smallest:

$$\dot{\boldsymbol{h}}_{n\times 1} = \boldsymbol{F}\boldsymbol{h} + \boldsymbol{G}\boldsymbol{u} \tag{3.1–9}$$

where

$$\boldsymbol{F} = \boldsymbol{V}^{-1}\boldsymbol{A}\,\boldsymbol{V}\,,\ \boldsymbol{G} = \boldsymbol{V}^{-1}\boldsymbol{B}$$

The slow and fast states are completely decoupled in (3.1–10) under the assumption of $\left|\lambda_{real}(\boldsymbol{F}_s)\right| \ll \left|\lambda_{real}(\boldsymbol{F}_q)\right|$; assuming that the damping ratios of all the eigenvalues are similar, the states can be said separable into two groups if the absolute values of the eigenvalues regarding a group (the fast states) are, at least, ten times larger than those of the other group (the slow states),

$$\begin{pmatrix} \dot{\boldsymbol{h}}_q \\ \dot{\boldsymbol{h}}_s \end{pmatrix} = \begin{pmatrix} \boldsymbol{F}_q & 0 \\ 0 & \boldsymbol{F}_s \end{pmatrix} \begin{pmatrix} \boldsymbol{h}_q \\ \boldsymbol{h}_s \end{pmatrix} + \begin{pmatrix} \boldsymbol{G}_q \\ \boldsymbol{G}_s \end{pmatrix} \boldsymbol{u} \tag{3.1–10}$$

Noting the following,

$$\lambda(\Lambda) = \lambda(\bar{\Lambda}) \tag{3.1–11}$$

where

$$\Lambda = \begin{pmatrix} \alpha + j\beta & 0 \\ 0 & \alpha - j\beta \end{pmatrix}, \ \bar{\Lambda} = \begin{pmatrix} \alpha & -\beta \\ \beta & \alpha \end{pmatrix}$$

It is assumed that the matrices of $\boldsymbol{F}_s$, $\boldsymbol{F}_q$, $\boldsymbol{G}_s$, and $\boldsymbol{G}_q$ consist of real components, which is called 'modal form'. Assuming that the dynamics of fast states are neglected, the following is obtained

$$\boldsymbol{h}_q = -\boldsymbol{F}_q^{-1}\boldsymbol{G}_q\boldsymbol{u} \tag{3.1–12}$$

From (3.1–8),

$$\boldsymbol{x} = \boldsymbol{V}\boldsymbol{h} = \begin{pmatrix} \boldsymbol{V}_q & \boldsymbol{V}_s \end{pmatrix} \begin{pmatrix} \boldsymbol{h}_q \\ \boldsymbol{h}_s \end{pmatrix} = \boldsymbol{V}_q\boldsymbol{h}_q + \boldsymbol{V}_s\boldsymbol{h}_s \tag{3.1–13}$$

The equivalent model of slow dynamics with eigenvalue-sorting is expressed as

$$\dot{\boldsymbol{h}}_s = \boldsymbol{F}_s\boldsymbol{h}_s + \boldsymbol{G}_s\boldsymbol{u} \tag{3.1–14}$$

$$\boldsymbol{y} = \boldsymbol{C}_s\boldsymbol{h}_s + \boldsymbol{D}_s\boldsymbol{u} \tag{3.1–15}$$

where

$$\boldsymbol{C}_s = \boldsymbol{C}\boldsymbol{V}_s, \ \boldsymbol{D}_s = \boldsymbol{D} - \boldsymbol{C}\boldsymbol{V}_q\boldsymbol{F}_q^{-1}\boldsymbol{G}_q$$

Thus, it has been shown that a high-order model can be simplified to a lower-order one.

3.1.2 Equivalent Model of Multiple Systems

If multiple models have the same dynamics, its equivalent model can be obtained by lumping them into a single model. This part corresponds to the process of (2) to (3) (or (4) to (6)) in the figure 2.1 (b). Since the concept of this method is to merging systems' dynamics that are identical kind, it can be effective and easily applied for such wind turbine systems of which the types are identical.

Let us assume that two systems are interconnected and can be expressed in the following state space equation by model combining:

$$\begin{pmatrix} \dot{\boldsymbol{x}}_A \\ \dot{\boldsymbol{x}}_B \end{pmatrix} = \begin{pmatrix} \boldsymbol{A}_{11} & \boldsymbol{A}_{12} \\ \boldsymbol{A}_{21} & \boldsymbol{A}_{22} \end{pmatrix} \begin{pmatrix} \boldsymbol{x}_A \\ \boldsymbol{x}_B \end{pmatrix} + \begin{pmatrix} \boldsymbol{B}_A \\ \boldsymbol{B}_B \end{pmatrix} \boldsymbol{u} \tag{3.1–16}$$

If the two systems' dynamic responses are similar and they are weakly coupled, the following assumption can be satisfied.

$$\boldsymbol{x}_{e\,(n\times 1)} = \boldsymbol{R}_{(n\times 2n)} \begin{pmatrix} \boldsymbol{x}_{A(n\times 1)} \\ \boldsymbol{x}_{B(n\times 1)} \end{pmatrix} \tag{3.1–17}$$

As seen, the state variables of $\boldsymbol{x}_A$ and $\boldsymbol{x}_B$ are lumped into the state variable $\boldsymbol{x}_e$ by matrix $\boldsymbol{R}$. The matrix $\boldsymbol{R}$ will be called 'aggregation matrix'. If the types of two systems are identical so that their state variables are describing the same dynamics, respectively, the aggregation matrix can be simply chosen $\boldsymbol{R} = \frac{1}{2}\mathbf{1}^T_{(2\times1)} \otimes \boldsymbol{I}_{(n\times n)}$. Then, the model is simplified to an equivalent model without compromising performance:

$$\dot{\boldsymbol{x}}_e = \boldsymbol{A}_e\boldsymbol{x}_e + \boldsymbol{B}_e\boldsymbol{u} \tag{3.1–18}$$

where

$$\boldsymbol{A}_e = \boldsymbol{R}\boldsymbol{A}\boldsymbol{R}^{-1}_{\text{right}},\ \boldsymbol{B}_e = \boldsymbol{R}\boldsymbol{B}.$$

However, it should be noted that, if two systems' dynamics, otherwise referred to as their eigenvalues, are far different, the equivalent model can still be obtained but its dynamics will be different from those of the originals.

3.2 Equivalent Models of Wind Turbines

In this section, slow dynamic equivalent models of wind turbines are developed not only to reduce the model complexity but to maintain their slow electromechanical dynamics. This procedure is important in developing a proper WPP DEM so that the DEM is sufficient for slow dynamics stability analysis of the power system.

Fast dynamics ignored in slow dynamics study do not represent states just oscillating fast but being damped out fast. How fast oscillation is damped out depends on the damping ratio, i.e., ratio of real value of eigenvalue and natural frequency, where the natural frequency is given as the absolute value of eigenvalue. Thus, states being damped out fast oscillate fast as well, but the opposite is not true. Some states oscillating fast might be damped out very slow. Let us say some states include fast oscillating dynamics, such as high frequency components. The high frequency components could be damped out either fast or slowly depending on system structures. However, if high frequency components created from a system are not properly damped, they might affect the other system in negative ways relating to stability. Thus, for slow dynamics stability analysis of power systems, it is justified the high frequency components were damped out fast owing to the system being properly designed and controlled and thus as if they did not exist.

Wind turbines often have properly designed power capacitors with small damping resistance at their terminals. The capacitance of power capacitor and line inductance work as filters that quickly damp out high frequency components in terminal voltage (input) and current (output), as it does in terminal power. This filtering effect occurs by the dynamics of voltages and currents related to line inductance and capacitance with damping resistance at the terminals as well as in the network. If the dynamics of the voltages and currents are ignored and the parameters of line inductance and capacitance are lumped so that a lumped (reduced) static network model is used in modeling, the filtering effect will appear compromised. In this case, high frequency components generated from wind turbines are

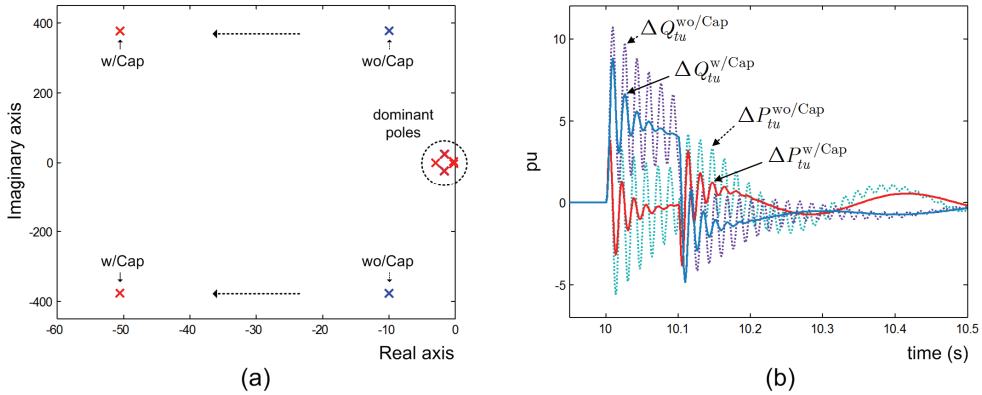

Fig. 2.2 (a) Poles and (b) output power variations - with and without taking dynamics of capacitance with damping resistance at terminal into account (Type 1)

transferred without being properly damped out by the filtering effect into other wind turbines and into generating units in power systems. Therefore, the use of the static network model ignoring the dynamics of voltages and currents inside the network will only be justified with the assumption of: the high frequency components that might be generated from wind turbine are properly damped out before being injected to the main network, so the dominant electromechanical dynamics generated from wind turbines are slow enough compared to the dynamics of voltages and currents in the network. This is the reason why the slow dynamic equivalent model of wind turbine is necessary in addition to reducing the model's order.

Figure 2.2 shows the poles of a type 1 wind turbine system and its terminal power variations, with and without taking into account the dynamics related to the use of capacitance with 10% damping resistance (assumed naturally existing) and small inductance at the terminal. (How to include damping resistance is explained in chapter 6) When the dynamics are considered, poles except the dominant poles move further away from the imaginary axis so that high frequency components are damped out much faster. As seen in the example, it would be appropriate to ignore fast dynamics related to the non-dominant poles for the study of slow electromechanical dynamics.

3.2.1 Slow Dynamic Models of Wind Turbines

The model with wind speed was introduced in chapter 2, sub-section 2.1.5.5. Pitch angle was added for an additional input in this model. The pitch angle is constant or changed to capture maximum power when wind speed is under the rated value. When wind speed is over the rated, the wind power captured by blade (blade power) is regulated to be the rated power by the pitch angle change. In this case, the pitch angle can be expressed as a function of wind speed. Under this assumption, the model can be represented with two inputs of terminal voltage and wind speed. Otherwise, blade power can be the input in place of wind speed, disregarding the characteristics of wind speed and blade power. The model development in this subsection is carried out with using the blade power as one of the inputs.

Rotor drive train is expected to have the slowest dynamics in a wind turbine system. So, the slow dynamic equivalent model could be developed by ignoring fast dynamics related to some states of generator and power converters, where the states regarding fast dynamics are replaced as damping factors for slow dynamics. However, if the states in a turbine model are strongly coupled and disturbed by the same inputs, they are not decoupled and the corresponding fast dynamics cannot be ignored. Thus, finding a proper model representation will be important. For type 1 turbines, stator and rotor currents are strongly coupled and disturbed by the same terminal voltage so they cannot be decoupled. On the other hand, because rotor flux is mainly disturbed indirectly through stator current, the dynamics of stator current can be ignored if the generator model is represented in the stator current-rotor flux form. Furthermore, when rotor flux is regulated by rotor voltage injection, the dynamics of rotor flux could be additionally ignored: the electrical torque is a function of rotor flux and rotor current, or rotor flux and stator current. To control the electrical torque adequately, it is important to control the rotor flux consistently so that oscillation in rotor flux dynamics is fast damped out. For type 3 turbines, electrical torque is regulated by rotor current control which makes rotor flux fast damped out. In this case, generator speed is more coupled to blade torque in terms of slow dynamics so that the dynamics of the generator can be ignored. For type 4 turbines, electrical torque is controlled with constant rotor flux control by stator current in the rotor flux oriented frame so that the dynamics of the generator could be ignored as well. In addition, for type 3 and 4 turbines with power converters comprehensively feedback controlled with integrators, the corresponding integrated states for the integral control should be included in the equivalent model.

Using a one-mass or a two-mass drive train model, the wind turbine models can be expressed as

$$\begin{pmatrix} \mathbf{0} \\ \Delta\dot{\boldsymbol{\omega}}_{+} \end{pmatrix} = \begin{pmatrix} \boldsymbol{A}_{\mathrm{t}11} & \boldsymbol{A}_{\mathrm{t}12} \\ \boldsymbol{A}_{\mathrm{t}21} & \boldsymbol{A}_{\mathrm{t}22} \end{pmatrix} \begin{pmatrix} \boldsymbol{x}_{q} \\ \Delta\boldsymbol{\omega}_{+} \end{pmatrix} + \begin{pmatrix} \boldsymbol{B}_{\mathrm{t}11} & \mathbf{0} \\ \boldsymbol{B}_{\mathrm{t}21}(=\mathbf{0}) & \boldsymbol{B}_{\mathrm{t}22} \end{pmatrix} \begin{pmatrix} \Delta\boldsymbol{v}_{tu} \\ \Delta P_{bu} \end{pmatrix} \tag{3.2–1}$$

where, $\Delta\boldsymbol{\omega}_{+}$ is the vector of state variables concerning slow dynamics, which is different depending on the types of wind turbines and drive train model.

For type 1 wind turbine: $\Delta\boldsymbol{\omega}_{+}^{\mathrm{tp1}} = \begin{pmatrix} \Delta\boldsymbol{\lambda}_{ru(2\times1)} \\ \Delta\boldsymbol{\omega}_{t} \end{pmatrix}$,

For type 3 wind turbine: $\Delta\boldsymbol{\omega}_{+}^{\mathrm{tp3}} = \boldsymbol{\kappa}^{\mathrm{tp3}}$, and $\Delta\boldsymbol{\omega}_{+}^{\mathrm{tp3}} = \begin{pmatrix} \boldsymbol{\kappa}^{\mathrm{tp3}} \\ \Delta\boldsymbol{x}_{I} \end{pmatrix}$;

$\boldsymbol{\kappa}^{\mathrm{tp3}} = \begin{pmatrix} \Delta\boldsymbol{\lambda}_{ru(2\times1)} \\ \Delta\boldsymbol{\omega}_{t} \end{pmatrix}$, If rotor flux is fast damped by control: $\boldsymbol{\kappa}^{\mathrm{tp3}} = \Delta\boldsymbol{\omega}_{t}$,

For type 4 wind turbine: $\Delta\boldsymbol{\omega}_{+}^{\mathrm{tp4}} = \boldsymbol{\kappa}^{\mathrm{tp4}}$, and $\Delta\boldsymbol{\omega}_{+}^{\mathrm{tp4}} = \begin{pmatrix} \boldsymbol{\kappa}^{\mathrm{tp4}} \\ \Delta\boldsymbol{x}_{I} \end{pmatrix}$;

$\boldsymbol{\kappa}^{\mathrm{tp4}} = \begin{pmatrix} \Delta\lambda_{rd} \\ \Delta\boldsymbol{\omega}_{t} \end{pmatrix}$, If rotor flux is fast damped by control: $\boldsymbol{\kappa}^{\mathrm{tp4}} = \Delta\boldsymbol{\omega}_{t}$.

where, $\Delta\boldsymbol{\omega}_{t} = \Delta\omega_{gu}$ for one mass drive train, and $\Delta\boldsymbol{\omega}_{t} = (\Delta\omega_{gu} \;\; \Delta\omega_{bu} \;\; \Delta T_{s})^{T}$ for two mass drive train. By ignoring the dynamics of generator and converters, the states $\boldsymbol{x}_{q}$ are

$$\boldsymbol{x}_{q} = -\boldsymbol{A}_{\mathrm{t}11}^{-1}\boldsymbol{A}_{\mathrm{t}12}\Delta\boldsymbol{\omega}_{+} - \boldsymbol{A}_{\mathrm{t}11}^{-1}\boldsymbol{B}_{\mathrm{t}11}\Delta\boldsymbol{v}_{tu} \tag{3.2–2}$$

Using (3.2–2), the model of which the state variables are $\Delta\boldsymbol{\omega}_{+}$, is be obtained. The outputs could be either currents or powers. The powers are functions of terminal voltages and currents, where the currents are two state variables in $\boldsymbol{x}_{q}$. Then, the outputs are expressed as

$$\Delta\boldsymbol{S}_{\mathrm{t}} = \boldsymbol{C}_{\mathrm{t}}\Delta\boldsymbol{\omega}_{+} + \boldsymbol{D}_{\mathrm{t}}\Delta\boldsymbol{v}_{tu} \tag{3.2–3}$$

where $\boldsymbol{S}_{\mathrm{t}} = (P_{tu} \;\; Q_{tu})^{T}$. The similarity of slow dynamics between an original model and the corresponding reduced model can be confirmed by eigenvalue observation. If dominant poles of the two models are identical, it is considered that the two models would produce identical slow dynamics. The tables below offer some results.

Table 1 Result with one-mass drive train model

Parameters	Moment of Inertia: J_{gen} = 50.1 kg·m^2, J_{blade} = 3.1×10^6 kg·m^2, Damping due to friction: $D_{gen,blade}$ = 0.1 N·m/rad, Gear ratio: 1/100	
Type 1	– 9.98 ± *j*376.92, (dominant) – 2.98, – 1.60 ± *j*8.68	– 2.98, – 1.61 ± *j*8.68
Type 3 (w/ P control: LQR)	– 1208.73 ± *j*392, – 215.94 ± *j*9.86, – 126.12, – 4.69 ± *j*372.37, (dominant) – 0.49	– 0.49
Type 4 (w/ P control: LQR)	– 474 ± *j*1072.4, – 1068.73, – 891.12, – 222.19, (– 5.01), (dominant) – 0.105	(– 4.95), – 0.105

Table 2 Result with two-mass drive train model

Parameters	Moment of Inertia: J_{gen} = 50.1 kg·m^2, J_{blade} = 3.1×10^6 kg·m^2, Damping due to friction: $D_{gen,blade}$ = 0.1 N·m/rad, D_{shaft} = 2.53×10^5 N·m/rad, Stiffness of shaft: K_{shaft} = 3.34×10^7 N·m/rad/s, Gear ratio: 1/100	
Type 1	(dominant) – 2.98, – 1.66 ± *j*24.98, – 0.21 ± *j*3.09	– 2.98, – 1.71 ± *j*24.97, – 0.21 ± *j*3.09
Type 3 (w/ P control: LQR)	(dominant) – 1.71 ± *j*8.60, – 0.499	– 1.68 ± *j* 8.55, – 0.498
Type 4 (w/ P control: LQR)	(dominant) – 0.53 ± *j*8.75, – 0.105	– 0.51 ± *j*8.77, – 0.105

The parameters in table 1 and 2 are slightly but arbitrarily tuned on the basis of ones picked from [?]. The pole in the bracket for type 4 in table 1 is one related to state variable of d-axis rotor flux. It appears that the corresponding dynamics is fast enough to be ignored without affecting the dominant pole and it is proved so as shown in table 2.

If it is difficult to discern the relationship between state variables and slow dynamics, the eigenvalue-sorting method could be useful. However, in this case, the state variables obtained by the method might be less meaningful because the state variables of generator and rotor blade speeds are not preserved. It is still possible to recover the state variables of the speeds under some assumptions, but it requires complicated process of matrix manipulation.

- Model Reformation

The model could be freely modified into different forms by using matrix manipulation. For instance, in the case of slow dynamic equivalent model of type 3 wind turbine with one mass drive train, the model could be represented to make it more physically meaningful by using the concept of power balance.

Using the wind turbine model developed in its local frame and decomposing power outputs of (3.2–3) into real and imaginary powers results in

$$\Delta P_{tu} = C_{\mathrm{t}}^{(1)} \Delta \omega_{gu} + D_{\mathrm{t}}^{(1)} \Delta v_{\mathrm{mag}} \tag{3.2–4}$$

$$\Delta Q_{tu} = C_{\mathrm{t}}^{(2)} \Delta \omega_{gu} + D_{\mathrm{t}}^{(2)} \Delta v_{\mathrm{mag}} \tag{3.2–5}$$

The terminal voltage can be expressed as a function of terminal real power and generator speed:

$$\Delta v_{\mathrm{mag}} = \frac{1}{D_t^{(1)}} \Delta P_{tu} - \frac{1}{D_t^{(1)}} C_t^{(1)} \Delta \omega_{gu} \tag{3.2–6}$$

Using equations (3.2–1) and (3.2–6) and selecting the input of blade power instead of wind speed, the model with one-mass drive train is modified to one with the inputs of terminal real power and blade power:

$$\Delta \dot{\omega}_{gu} = \bar{A}_{\mathrm{t}} \Delta \omega_{gu} + \bar{B}_{\mathrm{t}}^{1} \Delta P_{tu} + B_{\mathrm{t}}^{2} \Delta P_{bu} \tag{3.2–7}$$

The system output would be the terminal reactive power obtained from equations (3.2–4) and (3.2–5):

$$\Delta Q_{tu} = \bar{C}_{\mathrm{t}}^{(2)} \Delta \omega_{gu} + \bar{D}_{\mathrm{t}}^{(2)} \Delta P_{tu} \tag{3.2–8}$$

The model in the form of an inertia model (in the view of motoring) to make it physically meaningful can be expressed,

$$J_{\mathrm{int}} \Delta \dot{\omega}_{gu} = D_{\mathrm{dmp}} \Delta \omega_{gu} + \Delta P_{tu} - \Delta P_{bu} - \Delta P_{\mathrm{dmp}} \tag{3.2–9}$$

where

$$J_{\mathrm{int}} = \frac{1}{B_{\mathrm{t}}^{2}},\ D_{\mathrm{dmp}} = \frac{\bar{A}_{\mathrm{t}}}{B_{\mathrm{t}}^{2}},\ \Delta P_{\mathrm{dmp}} = \frac{B_{\mathrm{t}}^{2} - \bar{B}_{\mathrm{t}}^{1}}{B_{\mathrm{t}}^{2}} \Delta P_{tu}$$

Also, taking the terminal voltage angle into account, the original model can be reformed so that it has real power and voltage magnitude as inputs or reactive power and terminal voltage angle as inputs, etc. This model reformation might be useful to confirm input variables adequate for system control.

However, the reformed models require a network model in agreement with them, which involves more process of matrix manipulation. Besides, when they are combined with external systems by the corresponding network models, their dynamic characteristics would appear the same as those of the original models. Thus, the model reformation will remain as a meaningful example, but not used for WPP DEM development.

3.3 Equivalent Model of WPP (using a Global Frame)

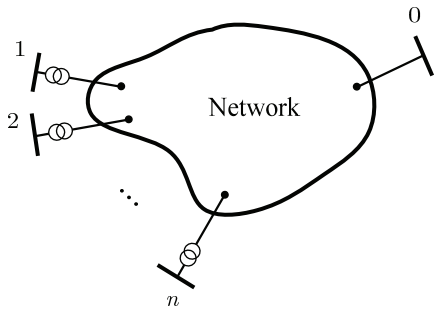

Fig. 2.3 N-WTs connected to bus 0 (POI bus) through network

In this section, the way of reducing a WPP model to its equivalent model by using the aggregation technique will be introduced, where wind turbine models developed in a global frame are used. For simplicity, it is assume that all wind turbines in a WPP are of the same type and being operated in the same operational conditions in terms of wind speeds. (More complicated case that includes different types and operational conditions are considered in the next section.) Wind turbines are connected to the central bus 0 (POI bus) through networked cables, as shown in figure 2.3. While the detailed WPP model introduced in (2.3–5) included the network dynamics, a static network model is used in this section. An advantage of developing WPP model in a global frame is that the outputs could be either of currents or powers without a transformation process. Assuming the currents are chosen as the outputs, a state space equation of slow dynamic models of n wind turbines without including a static network model can be expressed using equations (2.3–1, 2) and (3.2–1, 2)

$$\dot{\boldsymbol{x}}_{\text{ts}} = \boldsymbol{A}_{\text{ts}}\boldsymbol{x}_{\text{ts}} + \boldsymbol{B}^1_{\text{ts}}\boldsymbol{u}^1_{\text{ts}} + \boldsymbol{B}^2_{\text{ts}}\boldsymbol{u}^2_{\text{ts}} \tag{3.3–1}$$

$$\boldsymbol{y}_{\text{ts}} = \boldsymbol{C}_{\text{ts}}\boldsymbol{x}_{\text{ts}} + \boldsymbol{D}_{\text{ts}}\boldsymbol{u}^1_{\text{ts}} \tag{3.3–2}$$

where

$$\boldsymbol{x}_{\text{ts}} = \begin{pmatrix} \Delta\boldsymbol{\omega}_{+1} \\ \vdots \\ \Delta\boldsymbol{\omega}_{+n} \end{pmatrix},\ \boldsymbol{u}^1_{\text{ts}} = \Delta\boldsymbol{V}_{1\text{-}n},\ \boldsymbol{u}^2_{\text{ts}} = \Delta\boldsymbol{w}_{1-n},\ \boldsymbol{y}_{\text{ts}} = \Delta\boldsymbol{I}_{1\text{-}n}.$$

Because wind turbines are modeled in a global frame, the system parameters of the models will be slightly different due to the differences in the inputs of terminal voltages. Wind speed is assumed to be constant so that its variation is zero. The DEM can be developed in either as: 1) a slow dynamic model of n wind turbines in a state space representation is combined with a static network model, then reduced to the DEM, or 2) a slow dynamic model of n wind turbines in a state space representation is reduced to its equivalent, and then the equivalent is combined with a static network model to represent the DEM. The both procedures give the same result. Here, the model development is carried out by the second procedure. By model equivalencing with the use of aggregation matrix $\boldsymbol{R}$,

$$\boldsymbol{x}_{wd} = \boldsymbol{R}\boldsymbol{x}_{\text{ts}}, \text{ where } \boldsymbol{R} = \tfrac{1}{n}\boldsymbol{1}^T \otimes \boldsymbol{I}$$

Then,

$$\dot{\boldsymbol{x}}_{wd} = \boldsymbol{A}_{wd}\boldsymbol{x}_{wd} + \boldsymbol{B}^1_{wd}\boldsymbol{u}^1_{\text{ts}}, \text{ where } \boldsymbol{A}_{wd} = \boldsymbol{R}\boldsymbol{A}_{\text{ts}}\boldsymbol{R}^{-1}_{\text{right}} \tag{3.3–3}$$

$$\boldsymbol{y}_{\text{ts}} = \boldsymbol{C}_{wd}\boldsymbol{x}_{wd} + \boldsymbol{D}_{\text{ts}}\boldsymbol{u}^1_{\text{ts}}, \tag{3.3–4}$$

where the subscript wd denotes WPP DEM. The equivalent model has n terminal voltage inputs and current outputs. By combining it with a state network model, it has the POI voltage input and current output. Using an admittance matrix or the equation (2.2–5), the admittance matrix is expressed in the dq-representation.

$$\begin{pmatrix} \Delta \boldsymbol{I}_0 \\ \Delta \boldsymbol{I}_{1\text{-}n} \end{pmatrix} = \begin{pmatrix} \boldsymbol{Y}_{11} & \boldsymbol{Y}_{12} \\ \boldsymbol{Y}_{21} & \boldsymbol{Y}_{22} \end{pmatrix} \begin{pmatrix} \Delta \boldsymbol{V}_0 \\ \Delta \boldsymbol{V}_{1\text{-}n} \end{pmatrix}, \text{ where } \boldsymbol{V}_j = \begin{pmatrix} v_{jd} \\ v_{jq} \end{pmatrix}, \ \boldsymbol{I}_j = \begin{pmatrix} i_{jd} \\ i_{jq} \end{pmatrix} \tag{3.3–5}$$

As done in subsection 2.3.2 with the admittance matrix, the model is combined with the static network model to complete the WPP DEM,

$$\dot{\boldsymbol{x}}_{wd} = \bar{\boldsymbol{A}}_{wd}\boldsymbol{x}_{wd} + \bar{\boldsymbol{B}}^1_{wd}\Delta \boldsymbol{V}_0 \tag{3.3–6}$$

$$\Delta \boldsymbol{I}_0 = \bar{\boldsymbol{C}}_{wd}\boldsymbol{x}_{wd} + \bar{\boldsymbol{D}}_{wd}\Delta \boldsymbol{V}_0 \tag{3.3–7}$$

where

$$\bar{\boldsymbol{A}}_{wd} = \boldsymbol{A}_{wd} + \boldsymbol{A}_{ad}\,,\ \boldsymbol{A}_{ad} = \boldsymbol{B}^1_{wd}(\boldsymbol{Y}_{22} - \boldsymbol{D}_{\text{ts}})^{-1}\boldsymbol{C}_{wd}\,.$$

It is noted from $\boldsymbol{Y}_{22}^{-1}$ that if the wind turbines are strongly connected, that is, the impedance between them is low, they can be assumed to be weakly coupled. Recall that this method implies,

$$\boldsymbol{R}\boldsymbol{A}_{\text{ts}} = \boldsymbol{A}_{wd}\boldsymbol{R} \tag{3.3–8}$$

The relation of (3.3–8) might not be true if the wind turbines are not identical. However, this method provides proper DEM with comparatively simple matrix manipulation.

In this section, WPP dynamic equivalent model has been obtained by the method introduced in the section 3.1. However, WPP dynamic equivalent model can also be obtained in another way that uses the concept of coherent inputs and tied buses, and it is explained in the next section.

- Common (Tied) bus

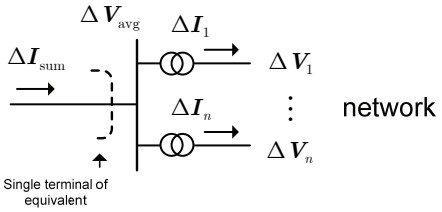

Fig. 2.4 Equivalent with single terminal

This aggregation technique is often explained with the concept of ‘common bus’ [25]. If the wind turbines are identical and their terminals are connected by cables, the dynamics of the terminal voltages are coherent so that the dynamics of currents from the wind turbines are also coherent. Consequently, it is satisfied,

$$\Delta \boldsymbol{V}_{1\text{-}n} = \boldsymbol{U}^T \Delta \boldsymbol{V}_{\text{avg}},\ \Delta \boldsymbol{I}_{\text{sum}} = \boldsymbol{U}\Delta \boldsymbol{I}_{1\text{-}n} \tag{3.3–9}$$

where $\boldsymbol{U} = \boldsymbol{1}^T \otimes \boldsymbol{I}$ is an aggregation matrix. By substituting (3.3–9) into (3.3–3) and (3.3–4), the model is changed to have a single terminal. There is an advantage of using this concept, that is, the equivalents of wind turbines and the equivalent static network model can be separately developed.

3.4 Equivalent Model of WPP (using Local Frames)

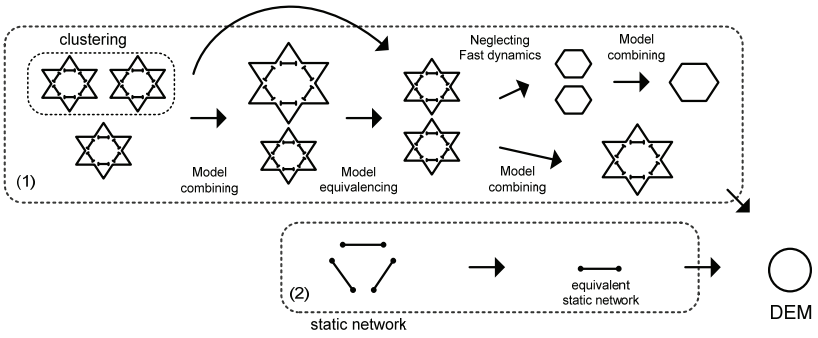

Fig. 2.5 Procedure of WPP DEM development

In the section, wind turbine models developed in their local frame will be used. In addition, the case of different types of wind turbines working in different operational conditions is taken into account.

The method to be introduced in this section is basically the same as found in section 3.3, but it proceeds in different steps. In figure 2.5, the part of (1) shows that separate multiple wind turbines that are not interconnected are combined into a single form of the models by model combining and it is simplified to its equivalent by model equivalencing. The part of (2) shows that static network model is lumped, and it is absorbed into the equivalent model, which achieves the DEM.

It is noted that the equivalent model of wind turbines and the equivalent static network are developed, separately. That is possible if two assumptions are satisfied: 1) wind turbines can be properly grouped depending on their types and operational conditions; 2) wind turbines in the same group have coherent inputs of terminal voltages and wind speeds.

3.4.1 Clustering

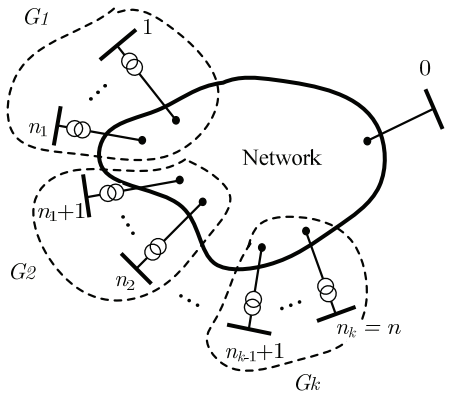

Fig. 2.6 Clustering n wind turbines into k groups

To develop a proper equivalent model of a given system, the system inputs must be coherent. As the terminals of the constituent wind turbines are electrically interconnected via cables, the dynamics of the terminal voltages will be coherent; however, the wind speeds (or blade powers) will not be coherent owing to the separate locations of wind

turbines. Although the patterns of wind speed in average, which the individual wind turbines experience, can be assumed to be identical, the instantaneous speeds will be relatively displaced in time. In addition, as the turbulence generated behind blades can persist over a non-trivial distance, the wind speed faced at each turbine can differ. For these reasons, it is more realistic to assume that each turbine experiences wind speeds that are randomly distributed around the average pattern of wind speed, making the modeling of wind speeds experienced by a multiple wind turbine array a problem involving non-coherent dynamics. Nevertheless, this problem can be solved by the use of equivalent wind speed. Because the output of multiple grouped wind turbines is the sum of their individual powers at a certain bus, such as the point of interconnection (POI) bus, there exists a probable equivalent wind speed corresponding to the sum of the individual powers. Assuming that the wind turbines within a group are identical, the equivalent wind speed for the group is simply given by averaging all of the wind speeds:

$$\Delta \overline{w}_G^{(k)}(t) = \frac{1}{m_k} \sum_{i=1}^{m_k} \Delta w_{(n_{k-1}+i)}(t) \tag{3.4–1}$$

where m_k is the number of wind turbines in the group *k*. In the case where blade power is used instead of wind speed, the equivalent blade power is given as the same.

As the variations of terminal voltages and wind speeds over a given group are coherent, each can be assumed to be identical, which implies that the variations in power produced by all of the wind turbines are also coherent. However, some wind turbines might face unique average wind speeds owing to the wind wake effect, in which case it should be assumed that the operating points of these wind turbines are also unique. Because the equivalent wind speed assumption is only valid in the case in which all average wind speeds are similar, the wind turbines should be grouped by similarity in terms of average experienced wind speed:

$$\Delta \boldsymbol{w}_{Gk} = \begin{pmatrix} \Delta w_{(n_{k-1}+1)} \\ \vdots \\ \Delta w_{(n_k)} \end{pmatrix} = \boldsymbol{U}_k^T \Delta \overline{w}_G^{(k)} \tag{3.4–2}$$

where, $\boldsymbol{U}_k = (\mathbf{1}_{m_k \times 1})^T \otimes \boldsymbol{I}$, $\otimes$ is the Kronecker product operator, $\boldsymbol{I}$ is the 2×2 identity matrix. $\overline{w}_G^{(k)}$ and $m_k (= n_k - n_{k-1})$ are the equivalent wind speed and the number of wind turbines in group k, respectively. Thus, the wind turbines in the WPP model developed in this section are clustered based on their respective turbine types and by the amount of wind power that they experience.

In general, the equivalent of a set of multiple models can be developed by aggregating and simplifying the respective models into the form of a single model. For the case shown in figure 2.6, this aggregation and simplification process can be denoted by

$$\boldsymbol{x}_G^{(k)} = \boldsymbol{R}_k \boldsymbol{x}_{Gk} \text{ , where } \boldsymbol{x}_{Gk} = \begin{pmatrix} \boldsymbol{x}_{\mathrm{t}(n_{k-1}+1)} \\ \vdots \\ \boldsymbol{x}_{\mathrm{t}(n_k)} \end{pmatrix} \tag{3.4–3}$$

where $\boldsymbol{x}_G^{(k)}$ and $\boldsymbol{x}_{Gk}$ are the state variable vectors of the equivalent representing a group k and the wind turbines in the group k, respectively, and $\boldsymbol{R}_k$ is an aggregation matrix for the group k. This method incorporates the process of developing and properly aggregating all multiple turbine models, which can be burdensome unless the wind power plant is properly clustered; this can be accomplished by obtaining the equivalents representing the respective groups of turbines with using the corresponding equivalent inputs, i.e., the terminal voltages and wind speeds averaged over each group. The respective equivalent model for each group will satisfy the following relations,

$$\begin{aligned} \boldsymbol{A}_G^{(k)} &= \boldsymbol{R}_k \boldsymbol{A}_{Gk} (\boldsymbol{R}_k)_{\mathrm{rigth}}^{-1}, \\ \boldsymbol{B}_G^{(k)} &= \boldsymbol{R}_k \boldsymbol{B}_{Gk} \boldsymbol{U}_k^T, \\ \boldsymbol{C}_G^{(k)} &= \boldsymbol{U}_k \boldsymbol{C}_{Gk} (\boldsymbol{R}_k)_{\mathrm{rigth}}^{-1}, \end{aligned}$$

$$\boldsymbol{D}_G^{(k)} = \boldsymbol{U}_k \boldsymbol{D}_{Gk} \boldsymbol{U}_k^T .$$

where the subscript Gk signify blocked diagonal matrix that is composed of respective matrices of m_k systems in the group k.

- Wind Wake Effect

When developing DEM based on aggregation, operating condition is a critical aspect for adequate DEM development. If groups of wind turbines are operated on largely different conditions, they have to be developed in different equivalent models. Especially, the difference in wind speed for each wind turbine could be important factor. Generally, it could be considered that all wind turbines have same wind speed in average. However, groups

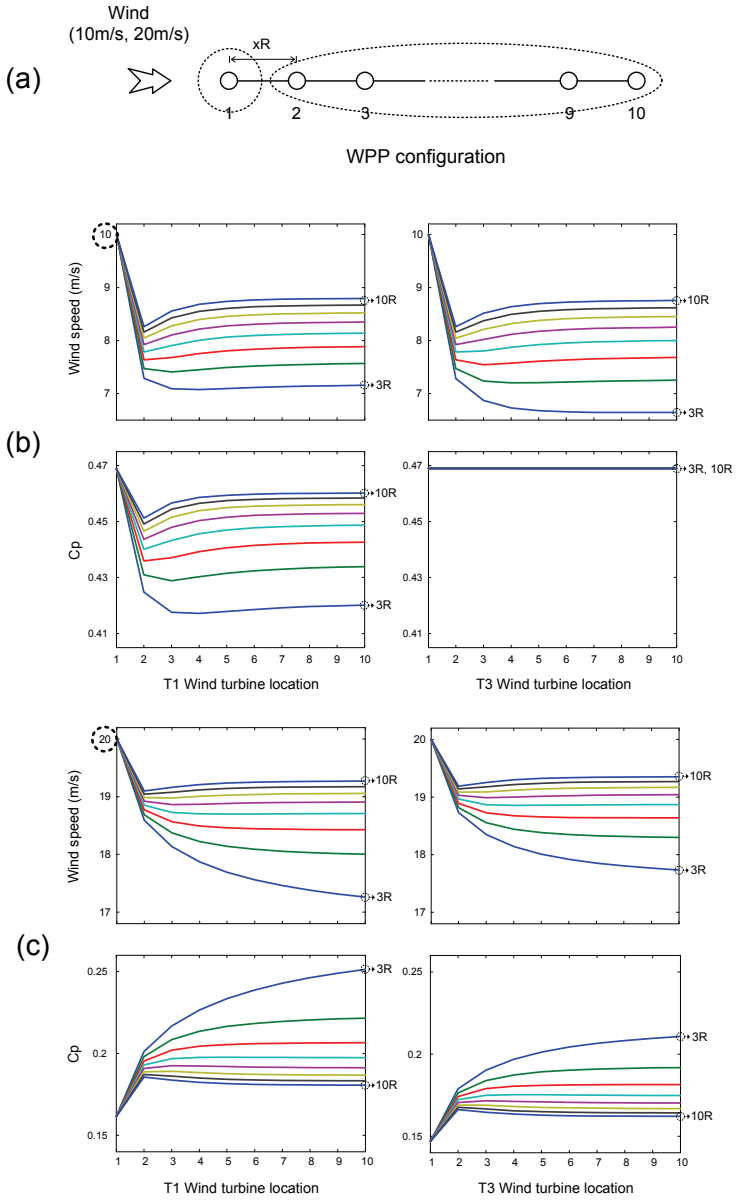

Fig. 2.7 Wind speed on different WT locations (1D)
(a) WT locations, (b), and (c) wind speeds that type 1 and 3 (or 4) WTs face

of wind turbines in WPP are actually operated on different conditions in wind speed due to wind wake effect [70]-[72]. Therefore, clustering of wind turbines that have possibly same wind speed in average is necessary.

To clarify the difference wind wake effect makes in wind speed that wind turbines face, figure 2.7 offers some examples. Wind speed for each wind turbine is calculated with the method described in [73].

$$w_j(t) = w_{j0}(t) + \sqrt{\sum_{k=1,k\neq j}^{n} \beta_k \left(w_k(\mathrm{x}_{kj}, t) - w_{j0}(t) \right)^2} \qquad (3.4\text{–}4)$$

where w_j is the resultant wind speed for an arbitrary turbine j, $w_k(\mathrm{x}_{kj})$ is the speed of the wind approaching turbine j with turbine k as the shadowing turbine, w_{j0} is the incoming wind at the turbine location j without any shadowing, the quotient β_k represents the ratio of that part of the area of turbine j under the shadow of turbine k to its total area, and n is the total number of turbines.

First, wind speed that wind turbines would have depending on the distance between them is calculated. The front wind speed is chosen 10 m/s under the rated wind speed (14 m/s). It is assumed that 10 wind turbines are located equally in distance. The distance has been changed from 3R to 10R and the respective wind speed for every wind turbine is observed, where R is the radius of swept area. It is observed that wind speed decreases passing the first wind turbine and further decreases or recovers near the original value depending on the distance between them. Additionally, it is observed what differences are made by different wind turbine types and 20 m/s wind speed over the rated. It is shown that, because type 3 wind turbines are controlled at maximum coefficient of performance (CP), the CP for type 3 wind turbines are all the same, unlike type 1 wind turbines. In contrast, if wind speed is over the rated, pitch angle is controlled to make excessive wind power passing through so that CP is decreased and downstream wind speed is less decreased. The results in different circumstances could be dissimilar. But, the important observation in developing DEM is that, if wind turbine types are identical, wind turbines could be clustered in groups that have similar wind speed. For instance, if the distance between the wind turbines is set 10R, then first wind turbine has 10 m/s upstream wind speed and the other wind turbines have around 8 m/s downstream wind speed. We conclude that WPP can be generally clustered into at least two groups: one with wind turbine facing wind speed without obstacles and the other with wind turbines facing wind speed by wake effect. Depending on wind wake condition, the number of clustering could increase. Furthermore, WPP is configured two-dimensionally in irregular positions and it does not that differ from the 1D case. With assumption of wind direction fixed, the WPP can be clustered into at least two groups: that is wind turbine 'without or with less wake effect' and those 'with more wake effect'.

- Clustering Rule

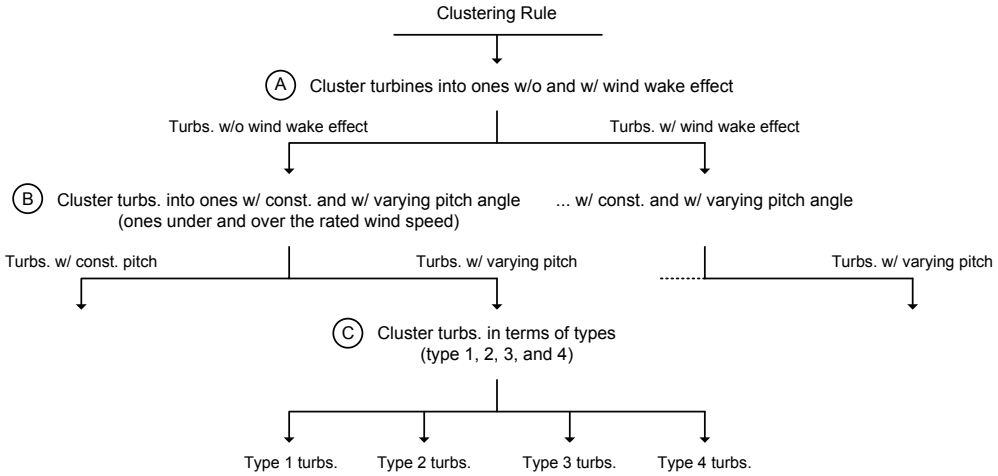

Fig. 2.8. Clustering turbines in terms of the operating conditions regarding wind wake effect and types

Clustering is performed on the basis of the types of turbines and their operating conditions regarding the wind wake effect, and thus a simple rule of the clustering can be generated and shown in figure 2.8.

First, by sloving the equation (3.4–4), wind speeds that each turbines face can be known. As mentioned, the wind speeds that turbines without and with experiencing the wake effect are quite different. So, the turbines are clustered into two groups; one without experiencing wind wake effect and the others; step A. Second, turbines in each group are clustered into two groups of ones having constant pitch angles, which are operated under the rated wind speed, and ones having varying pitch angles to maintain their captured wind powers at the rated values; step B. Third, turbines in each group are clustered into groups on the basis of their types; step C which is the most important because the control and dynamics of turbines are very different depending on their types.

In addition, if the wind wake effect is not considered into the modeling problem and thus all turbines in the WPP experience the same averaged wind speed, then the step A and B can be ignored so that the turbines will be clustered in terms of their types only.

3.4.2 WPP Dynamic Equivalent Model

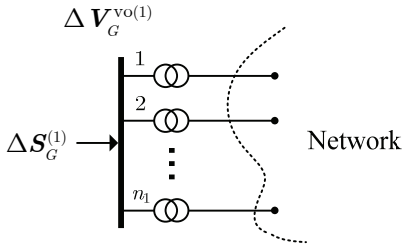

Fig. 2.8 Group 1 of WTs expressed with common bus

Assuming that wind turbines in WPP are properly clustered, the respective equivalents for k groups are expressed in a single space state representation,

$$\dot{\boldsymbol{x}}_{wd} = \boldsymbol{A}_{wd}\boldsymbol{x}_{wd} + \boldsymbol{B}^1_{wd}\boldsymbol{u}^1_{wd} + \boldsymbol{B}^2_{wd}\boldsymbol{u}^2_{wd} \tag{3.4–1}$$

$$\boldsymbol{y}_{wd} = \boldsymbol{C}_{wd}\boldsymbol{x}_{wd} + \boldsymbol{D}_{wd}\boldsymbol{u}^1_{wd}, \tag{3.4–2}$$

where

$$\boldsymbol{A}_{wd} = \mathrm{diag}\left\{\boldsymbol{A}_G^{(1)}, \dots, \boldsymbol{A}_G^{(k)}\right\},$$

$$\boldsymbol{B}^1_{wd} = \mathrm{diag}\left\{\boldsymbol{B}_G^{1(1)}, \dots, \boldsymbol{B}_G^{1(k)}\right\},\ \boldsymbol{B}^2_{wd} = \mathrm{diag}\left\{\boldsymbol{B}_G^{2(1)}, \dots, \boldsymbol{B}_G^{2(k)}\right\}$$

$$\boldsymbol{C}_{wd} = \mathrm{diag}\left\{\boldsymbol{C}_G^{(1)}, \dots, \boldsymbol{C}_G^{(k)}\right\},$$

$$\boldsymbol{D}_{wd} = \mathrm{diag}\left\{\boldsymbol{D}_G^{(1)}, \dots, \boldsymbol{D}_G^{(k)}\right\},$$

$$\boldsymbol{x}_{wd}=\begin{pmatrix}\Delta\boldsymbol{\omega}_+^{(1)}\\ \vdots \\ \Delta\boldsymbol{\omega}_+^{(k)}\end{pmatrix},\ \boldsymbol{y}_{wd}=\begin{pmatrix}\Delta\boldsymbol{S}_G^{(1)}\\ \vdots \\ \Delta\boldsymbol{S}_G^{(k)}\end{pmatrix},\ \boldsymbol{u}^1_{wd}=\begin{pmatrix}\Delta\boldsymbol{V}_G^{\mathrm{vo}(1)}\\ \vdots \\ \Delta\boldsymbol{V}_G^{\mathrm{vo}(k)}\end{pmatrix},\ \boldsymbol{u}^2_{wd}=\begin{pmatrix}\Delta w_G^{(1)}\\ \vdots \\ \Delta w_G^{(k)}\end{pmatrix}.$$

$\Delta \boldsymbol{V}_G^{\mathrm{vo}(k)}$ and $\Delta \boldsymbol{S}_G^{(k)}$ are the terminal voltage and wind speed averaged over group k. Then, equivalent static network model is developed and combined with (3.4–1) and (3.4–2) to represent the DEM.

The concept of coherent voltages and powers can be simply expressed with nodes tied at the same bus. In figure 2.8, buses of 1 to n_1 in the group 1 are tied so that the voltages at the buses are assumed to be identical. Thus, using this concept, the terminal voltages in the group k are related to the equivalent voltage,

$$\Delta \boldsymbol{V}_{Gk}^{\mathrm{vo}} = \boldsymbol{U}_k^T \Delta \boldsymbol{V}_G^{\mathrm{vo}(k)} \tag{3.4–3}$$

where

$$\Delta \boldsymbol{V}_{Gk}^{\mathrm{vo}} = \begin{pmatrix} \Delta \boldsymbol{V}_{\mathrm{t}(n_{k-1}+1)}^{\mathrm{vo}} \\ \vdots \\ \Delta \boldsymbol{V}_{\mathrm{t}(n_k)}^{\mathrm{vo}} \end{pmatrix},$$

$\boldsymbol{U}_k = (\mathbf{1}_{m_k \times 1})^T \otimes \boldsymbol{I}_{2\times 2}$, and $m_k = n_k - n_{k-1}$

Also, for the powers from wind turbines in the group k,

$$\Delta \boldsymbol{S}_G^{(k)} = \boldsymbol{U}_k \Delta \boldsymbol{S}_{Gk} \tag{3.4–4}$$

where

$$\Delta \boldsymbol{S}_{Gk} = \begin{pmatrix} \Delta \boldsymbol{S}_{\mathrm{t}(n_{k-1}+1)} \\ \vdots \\ \Delta \boldsymbol{S}_{\mathrm{t}(n_k)} \end{pmatrix},$$

Expressing the above into simple matrix forms,

$$\Delta \boldsymbol{V}_{\mathrm{ts}}^{\mathrm{vo}} = \boldsymbol{X}^T \Delta \boldsymbol{V}_{wd}^{\mathrm{vo}} \tag{3.4–5}$$

$$\Delta \boldsymbol{S}_{wd} = \boldsymbol{X} \Delta \boldsymbol{S}_{\mathrm{ts}}, \tag{3.4–6}$$

where

$$\Delta \boldsymbol{V}_{\mathrm{ts}}^{\mathrm{vo}} = \begin{pmatrix} \Delta \boldsymbol{V}_{G1}^{\mathrm{vo}} \\ \vdots \\ \Delta \boldsymbol{V}_{Gk}^{\mathrm{vo}} \end{pmatrix}, \ \Delta \boldsymbol{V}_{wd}^{\mathrm{vo}} (= \boldsymbol{u}_{wd}^1) = \begin{pmatrix} \Delta \boldsymbol{V}_G^{\mathrm{vo}(1)} \\ \vdots \\ \Delta \boldsymbol{V}_G^{\mathrm{vo}(k)} \end{pmatrix},$$

$$\Delta \boldsymbol{S}_{wd} = \begin{pmatrix} \Delta \boldsymbol{S}_G^{(1)} \\ \vdots \\ \Delta \boldsymbol{S}_G^{(k)} \end{pmatrix}, \ \Delta \boldsymbol{S}_{\mathrm{ts}} = \begin{pmatrix} \Delta \boldsymbol{S}_{G1} \\ \vdots \\ \Delta \boldsymbol{S}_{Gk} \end{pmatrix},$$

$\boldsymbol{X} = \mathrm{diag}\{ \boldsymbol{U}_1, \ldots, \boldsymbol{U}_k \}$.

From equations (2.2–15) and (2.2–26) or (2.2–29), the followings are obtained:

1. For local-frame network model 1:

$$\begin{pmatrix} \Delta \boldsymbol{S}_0 (\mathrm{or}\, \Delta \boldsymbol{I}_0) \\ \Delta \boldsymbol{S}_{wd} \end{pmatrix} = \begin{pmatrix} \boldsymbol{F}_{11} & \bar{\boldsymbol{F}}_{12}^{\mathrm{vo}} \\ \bar{\boldsymbol{F}}_{21}^{\mathrm{vo}} & \bar{\boldsymbol{F}}_{22}^{\mathrm{vo}} \end{pmatrix} \begin{pmatrix} \Delta \boldsymbol{V}_0 \\ \Delta \boldsymbol{V}_{wd}^{\mathrm{vo}} \end{pmatrix}, \tag{3.4–7}$$

where

$$\bar{\boldsymbol{F}}_{12}^{\mathrm{vo}} = \boldsymbol{F}_{12}^{\mathrm{vo}} \boldsymbol{X}^T,$$
$$\bar{\boldsymbol{F}}_{21}^{\mathrm{vo}} = \boldsymbol{X} \boldsymbol{F}_{21}^{\mathrm{vo}},$$
$$\bar{\boldsymbol{F}}_{22}^{\mathrm{vo}} = \boldsymbol{X} \boldsymbol{F}_{22}^{\mathrm{vo}} \boldsymbol{X}^T.$$

2. For local-frame network model 2:

$$\begin{pmatrix} \Delta \boldsymbol{S}_0 (\mathrm{or}\, \Delta \boldsymbol{I}_0) \\ \Delta \boldsymbol{V}_{wd}^{\mathrm{vo}} \end{pmatrix} = \begin{pmatrix} \boldsymbol{H}_{11} & \bar{\boldsymbol{H}}_{12}^{\mathrm{vo}} \\ \bar{\boldsymbol{H}}_{21}^{\mathrm{vo}} & \bar{\boldsymbol{H}}_{22}^{\mathrm{vo}} \end{pmatrix} \begin{pmatrix} \Delta \boldsymbol{V}_0 \\ \Delta \boldsymbol{S}_{wd} \end{pmatrix}, \tag{3.4–8}$$

where

$$\bar{\boldsymbol{H}}_{12}^{\mathrm{vo}} = \boldsymbol{H}_{12}^{\mathrm{vo}} \boldsymbol{X}_{\mathrm{right}}^{-1},$$
$$\bar{\boldsymbol{H}}_{21}^{\mathrm{vo}} = (\boldsymbol{X}^{T})_{\mathrm{left}}^{-1} \boldsymbol{H}_{21}^{\mathrm{vo}},$$
$$\bar{\boldsymbol{H}}_{22}^{\mathrm{vo}} = (\boldsymbol{X}^{T})_{\mathrm{left}}^{-1} \boldsymbol{H}_{22}^{\mathrm{vo}} \boldsymbol{X}_{\mathrm{right}}^{-1}.$$

As seen in the equations (3.4–7, 8), POI current variations can be applied instead of POI power variations if necessary. Noting that $\Delta \boldsymbol{S}_{wd}$ and $\Delta \boldsymbol{V}_{wd}^{\mathrm{vo}}$ in (3.4–7, 8) are equal to $\boldsymbol{y}_{wd}$ and $\boldsymbol{u}_{wd}$ in (3.4–2), respectively, $\boldsymbol{u}_{wd}^{1}$ can be derived by matrix manipulation using the same procedure as was used in equations from (2.3–8) to (2.3–15) in the chapter 2. Using the local-frame network model 1,

$$\boldsymbol{u}_{wd}^{1} = \boldsymbol{L}_a \boldsymbol{x}_{wd} + \boldsymbol{L}_b \Delta \boldsymbol{V}_0, \tag{3.4–9}$$

where

$$\boldsymbol{L}_a = -(\bar{\boldsymbol{F}}_{22}^{\mathrm{vo}} + \boldsymbol{D}_{wd})^{-1} \boldsymbol{C}_{wd},$$
$$\boldsymbol{L}_b = -(\bar{\boldsymbol{F}}_{22}^{\mathrm{vo}} + \boldsymbol{D}_{wd})^{-1} \bar{\boldsymbol{F}}_{21}^{\mathrm{vo}}.$$

Recalling that the equivalent model given in (3.4–1, 2) is simply a set of separated slow dynamic equivalents representing k groups of wind turbines, the development of the WPP DEM is finalized by combining the equivalent model and the equivalent static network model by substituting $\boldsymbol{u}_{wd}^{1}$ into (3.4–1, 2) and using (3.4–7),

$$\dot{\boldsymbol{x}}_{wd} = \bar{\boldsymbol{A}}_{wd} \boldsymbol{x}_{wd} + \bar{\boldsymbol{B}}_{wd}^{1} \Delta \boldsymbol{V}_0 + \boldsymbol{B}_{wd}^{2} \Delta \boldsymbol{w}_{wd} \tag{3.4–10}$$
$$\Delta \boldsymbol{S}_0 (\text{or } \Delta \boldsymbol{I}_0) = \bar{\boldsymbol{C}}_0 \boldsymbol{x}_{wd} + \bar{\boldsymbol{D}}_0 \Delta \boldsymbol{V}_0, \tag{3.4–11}$$

where

$$\bar{\boldsymbol{A}}_{wd} = \boldsymbol{A}_{wd} + \boldsymbol{B}_{wd}^{1} \boldsymbol{L}_a,$$
$$\bar{\boldsymbol{B}}_{wd}^{1} = \boldsymbol{B}_{wd}^{1} \boldsymbol{L}_b,$$
$$\bar{\boldsymbol{C}}_0 = -\bar{\boldsymbol{F}}_{12}^{\mathrm{vo}} \boldsymbol{L}_a,$$
$$\bar{\boldsymbol{D}}_0 = -(\boldsymbol{F}_{11} + \bar{\boldsymbol{F}}_{12}^{\mathrm{vo}} \boldsymbol{L}_b).$$

The DEM outputs in (3.4–11) are chosen the same as in (3.4–7, 8), that is, either POI power variations or POI current variations.

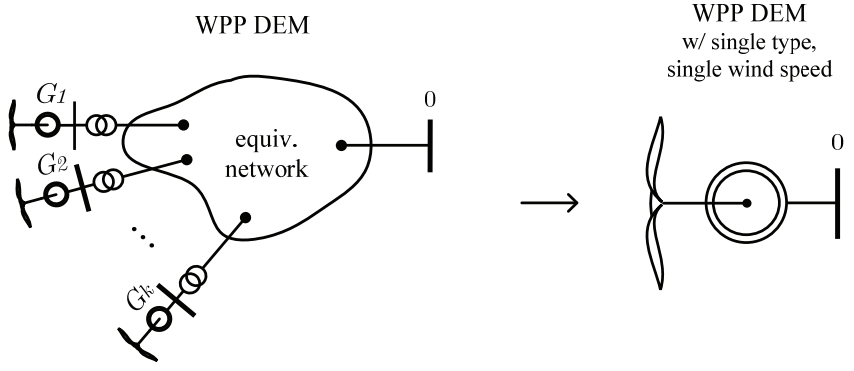

Fig. 2.9 WPP DEM

If it can be further assumed that all wind speeds are identical without wind wake effect, (3.4–10) can be changed to the following model with single wind speed input:

$$\dot{\boldsymbol{x}}_{wd} = \bar{\boldsymbol{A}}_{wd}\boldsymbol{x}_{wd} + \bar{\boldsymbol{B}}^1_{wd}\Delta \boldsymbol{V}_0 + \bar{\boldsymbol{B}}^2_{wd}\Delta \bar{w}\,, \text{ where } \bar{\boldsymbol{B}}^2_{wd} = \boldsymbol{B}^2_{wd}\mathbf{1} \tag{3.4–12}$$

Figure 2.9 shows WPP DEMs in simple representation. In the left figure, the WPP DEM consists of multiple equivalent models of turbines owing to different turbine types and operating conditions regarding wind power. If the types of all turbines in the WPP are the same and the wind wake effect is ignore so that all the turbines are in the same operating conditions regarding wind power, the WPP DEM can be represented in the form of a single turbine as shown in the right figure.

- Frequency-related Modeling

When the synchronous speed is not constant so it needs to be considered into the modeling, the equivalent model of clustered turbines (3.4–1 and 2) is properly changed to have an additional input of the fictitious frame's angular speed for WPP: refer to subsection 2.3.3,

$$\dot{\boldsymbol{x}}_{wd} = \boldsymbol{A}_{wd}\boldsymbol{x}_{wd} + \boldsymbol{B}^1_{wd}\boldsymbol{u}^1_{wd} + \boldsymbol{B}^2_{wd}\boldsymbol{u}^2_{wd} + \boldsymbol{B}^3_{wd}\boldsymbol{u}^3_{wd} \tag{3.4–13}$$

$$\boldsymbol{y}_{wd} = \boldsymbol{C}_{wd}\boldsymbol{x}_{wd} + \boldsymbol{D}_{wd}\boldsymbol{u}^1_{wd} + \boldsymbol{D}^3_{wd}\boldsymbol{u}^3_{wd}\,, \text{ where } \boldsymbol{u}^3_{wd} = \Delta\omega_0 \tag{3.4–14}$$

Note that the output equation has the additional input unlike the model of turbines (2.3–1 and 2). This is because some parameters of the additional input in the differential equations regarding fast dynamics equivalently are replaced into the output equation by the development process of the slow dynamic equivalent model. With the same process used in this section, the corresponding WPP DEM is finalized to have the additional input of the angular speed

$$\dot{\boldsymbol{x}}_{wd} = \bar{\boldsymbol{A}}_{wd}\boldsymbol{x}_{wd} + \bar{\boldsymbol{B}}^1_{wd}\Delta \boldsymbol{V}_0 + \boldsymbol{B}^2_{wd}\Delta \boldsymbol{w}_{wd} + \boldsymbol{B}^3_{wd}\Delta\omega_0 \tag{3.4–15}$$

$$\Delta \boldsymbol{S}_0 = \bar{\boldsymbol{C}}_0\,\boldsymbol{x}_{wd} + \bar{\boldsymbol{D}}_0\,\Delta \boldsymbol{V}_0 + \bar{\boldsymbol{D}}^3_0\Delta\omega_0\,, \tag{3.4–16}$$

where

$$\bar{\boldsymbol{D}}^3_0 = \bar{\boldsymbol{F}}^{\text{vo}}_{12}(\bar{\boldsymbol{F}}^{\text{vo}}_{22} + \boldsymbol{D}_{wd})^{-1}\boldsymbol{D}^3_{wd}$$

Then, by using the method introduced in subsection 2.3.3, the WPP DEM can be changed to have the POI voltage and angular speed of the global frame. In addition, it needs to be noted that, if the POI current was chosen as the output, an additional transformation process from the fictitious frame for WPP modeling to the global frame regarding the POI current would have been necessary: refer to (2.3–17).

- Model Structure Change

The WPP DEM developed in this chapter has the variations of variables, such as voltages, currents, powers, fluxes, angular speeds, and etc., as its input, output, and state variables. Sometimes, it might be needed to represent the WPP DEM in terms of the original variables, not their variations. It could be done in two ways. The first is to add offsets regarding operating conditions to both sides of the input and output. The other is to add the offsets equivalently to either side of the input or the output. Let's say the WPP DEM is expressed in the following form,

$$\dot{\boldsymbol{x}} = \boldsymbol{A}\boldsymbol{x} + \boldsymbol{B}\boldsymbol{u} \text{ and } \boldsymbol{y} = \boldsymbol{C}\boldsymbol{x} + \boldsymbol{D}\boldsymbol{u} \tag{3.4–17}$$

Recalling that the variables $\boldsymbol{x}$, $\boldsymbol{u}$, and $\boldsymbol{y}$ are the variations of some variables $\boldsymbol{z}$, $\boldsymbol{v}$, and $\boldsymbol{g}$,

$$\Delta\dot{\boldsymbol{z}} = \boldsymbol{A}\Delta\boldsymbol{z} + \boldsymbol{B}\Delta\boldsymbol{v} \text{ and } \Delta\boldsymbol{g} = \boldsymbol{C}\Delta\boldsymbol{z} + \boldsymbol{D}\Delta\boldsymbol{v} \tag{3.4–18}$$

where $\Delta\boldsymbol{z} = \boldsymbol{z} - \boldsymbol{z}_o$, $\Delta\boldsymbol{v} = \boldsymbol{v} - \boldsymbol{v}_o$, and $\Delta\boldsymbol{g} = \boldsymbol{g} - \boldsymbol{g}_o$. The input–output relation of the model in steady state is given by $\boldsymbol{\kappa}_o = (\boldsymbol{D} - \boldsymbol{C}\boldsymbol{A}^{-1}\boldsymbol{B})$. Assuming that $\boldsymbol{z}_o$, $\boldsymbol{v}_o$, and $\boldsymbol{g}_o$ are constant, (3.4–18) can be expressed as

$$\dot{\boldsymbol{z}} = \boldsymbol{A}\boldsymbol{z} + \boldsymbol{B}\boldsymbol{v} \text{ and } \boldsymbol{g} = \boldsymbol{C}\boldsymbol{z} + \boldsymbol{D}\boldsymbol{v} + \boldsymbol{K}_o \tag{3.4–19}$$

where $\boldsymbol{K}_o = \boldsymbol{g}_o - \boldsymbol{\kappa}_o\boldsymbol{v}_o$. The changed model structures of WPP DEM are shown in figure 2.10. Here, $\boldsymbol{K}_o$ is not

zeroes because the model (depicted as sys. in the second block diagram) is linearized from originally nonlinear ones. In contrast, $\boldsymbol{K}_o$ would have been zeroes if the model were originally linear.

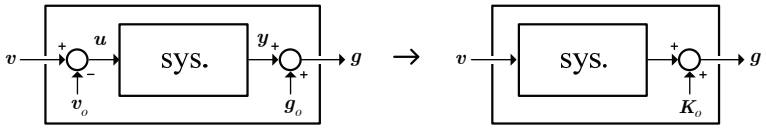

Fig. 2.10 Model structure change

In addition, as seen in the equations (3.4–7, 8) and (3.4–11), the POI current variations can be used as the outputs of the WPP DEM, instead of the POI power variations. Using this changed model structure, the output will be the POI currents. In this case, the POI powers are calculated using nonlinear power equations on the basis of the instantaneous power theory, which gives more nonlinearity into the dynamics of the powers. Nonetheless, it should be noted that the WPP DEM is developed on the basis of linearized models. When the operating conditions largely deviate from the initially given conditions, the WPP DEM should be updated accordingly.

3.5 Simulations

The performance of the proposed linear DEM is verified by simulation tests. The simulation tests in this chapter, however, are only focused on the dynamic performance of the DEM.

The validity of the DEM's interaction with power system will be verified in the chapter 7.

3.5.1 Test system

In the simulation, the WPP is directly connected by the POI bus to a variable ideal voltage source which represents a power system. The WPP consists of 49 wind turbines, where are 21 × types 1, 14 × type 3, and 14 × type 4 wind turbines, and they are irregularly placed, which is shown in figure 2.1s. Base power is 2 MVA and reactive power from type 3 or 4 wind turbine is controlled to be 0.3 pu. In the figure, the step-up transformers at the terminal buses of 52 to 100 have only the function of turn-ratio and their impedances are applied in the wind turbine models. The capacitances of power capacitors at the terminal buses are applied to the static network model. Wind turbines placed in the first column in the wind direction, face 15m/s wind speed and the other wind turbines face around 13m/s wind speed due to the wind wake effect. The rate wind speed for wind turbines is chosen 14m/s, so wind turbines have their pitch angle adjusted if the wind speed exceeds 14m/s. Wind turbines are accordingly clustered by the types and their wind speeds so that they are in: case.1 – 3 and case. 2 – 6 groups. The number of equivalent wind turbines is the same as the number of the groups.

Pitch angle mechanism is not included in the models of turbines, and integrators are not used for the control of turbines. Then, the model of type 1 turbine has 7 state variables while type 3 and type 4 have 10 and 9, respectively.

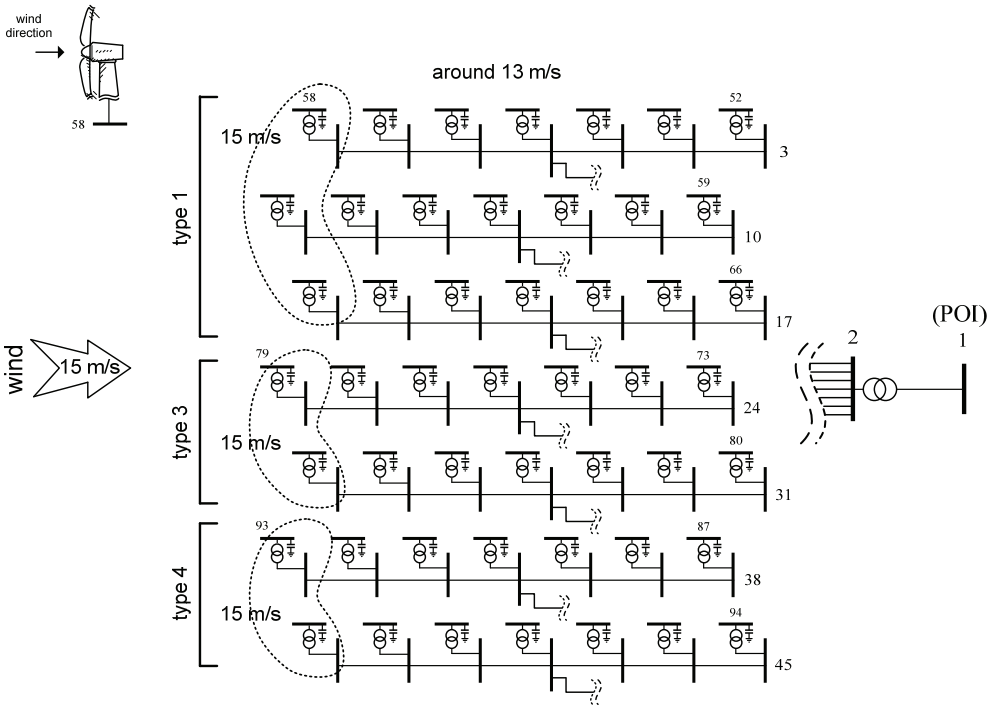

Fig. 2.1s. WPP clustered into 3 and 6 groups

On the other hand, the slow dynamics model of type 1 turbine has 5 state variables while type 3 and type 4 have 3 and 4, respectively. Therefore, the WPP has 413 state variables, while the DEM has the state variables of: case. 1 – 12 and case. 2 – 24.

3.5.2 Results

The dynamic performance of the DEM for wind speed variations is verified by comparing that of the WPP. The DEM has power variations as its outputs. 49 wind speeds are applied for the WPP and equivalent wind speeds are applied for the DEM. The variations of 49 wind speeds are randomly generated for the test and the variations of equivalent wind speeds are obtained by summing the 49 variations according to the clustered wind turbines in the

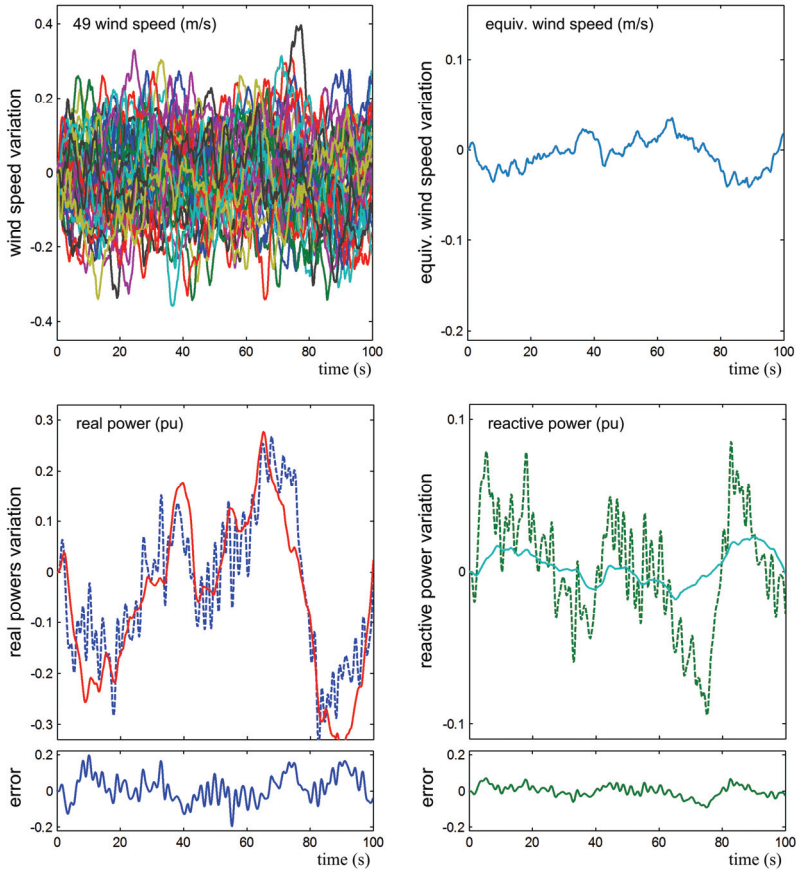

Fig. 2.2s. Dynamic performance comparison between the WPP and the DEM w/ 1 equivalent wind speed (1 group)

WPP. The POI voltage is maintained constant.

First, all turbines in the WPP are clustered into one group regardless their types and the wind speeds they are facing. Figure 2.2s shows the result. In the figure, it is shown that, the variations of 49 wind speeds for the WPP and 1 equivalent wind speeds for the DEM and the variations of powers at POI bus, which are generated by the WPP and the DEM. The DEM provides a poor performance because it is developed without considering the dynamics of different types of turbines by grouping all the turbines in the same group.

Second, the turbines are clustered into three groups by their types. Figure 2.3s shows the variations of 49 wind speeds for the WPP and 3 equivalent wind speeds for the DEM. The next figure demonstrates the variations of powers at POI bus, which are generated by the WPP and the DEM. The DEM provides much better performance than the first case.

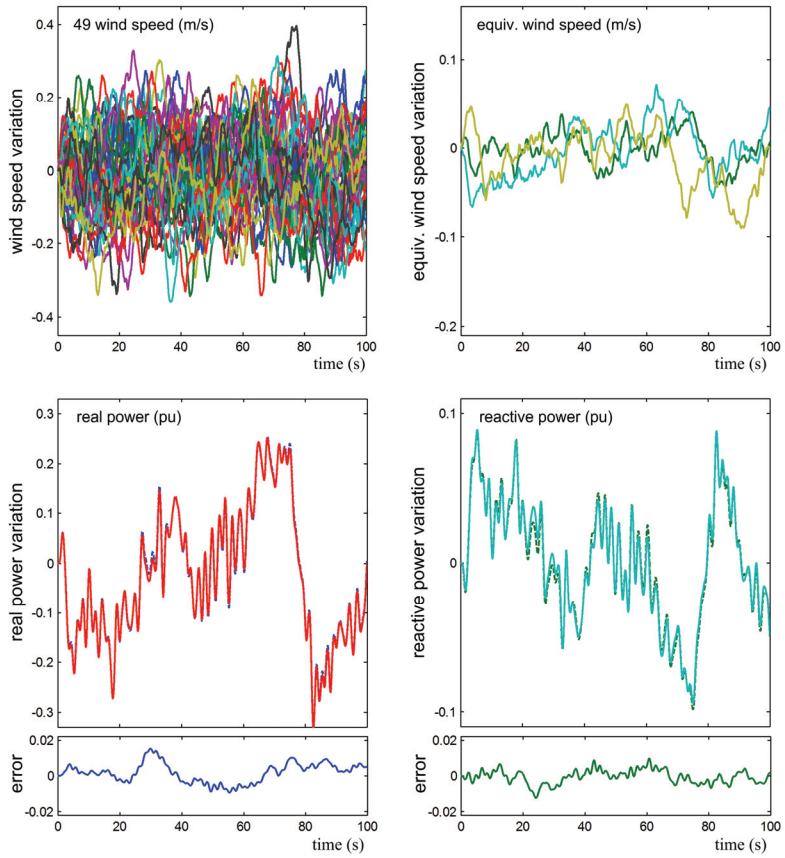

Fig. 2.3s. Dynamic performance comparison between the WPP and the DEM w/ 3 equivalent wind speeds (3 groups)

Third, the turbines are clustered into six groups by their types and the wind speeds they are facing. Figure 2.4s first shows the variations of 49 wind speeds for the WPP and 6 equivalent wind speeds for the DEM, in next compares the variations of powers at POI bus, which are generated by the WPP and the DEM. In the figure showing the equivalent wind speeds, the dotted lines represent the 3 equivalents of wind turbines with 15m/s upstream wind speed and the solid lines represent the 3 equivalents of wind turbines with around 13m/s downstream wind speed. Despite the significantly reduced model complexity of DEM with the use of equivalent wind speed, the DEM produces almost identical dynamics as the WPP. Also, the DEM obtained by clustering the WPP in 6 groups provides better performance than the DEM in figure 2.3s.

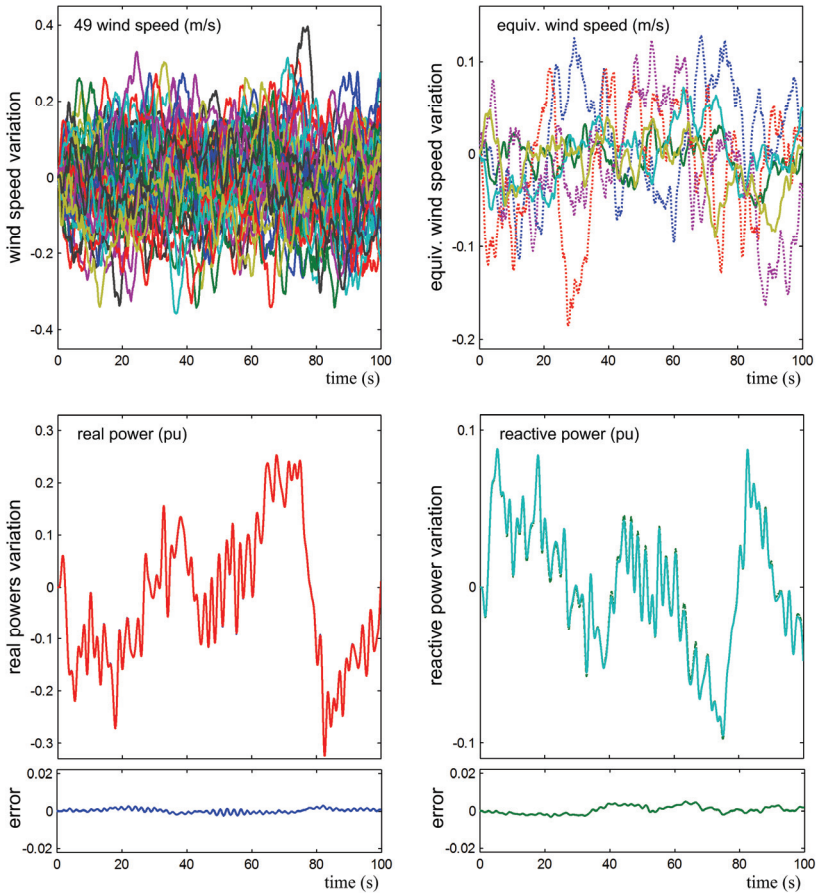

Fig. 2.4s. Dynamic performance comparison between the WPP and the DEM w/ 6 equivalent wind speeds (6 groups)

The dynamic performance of the DEM for POI voltage variation is verified by comparing that of the WPP. The variation of POI voltage in magnitude dropped to -1 in step for 0.1 second and recovered to 0, while the wind speeds were maintained constant. Figure 2.5s shows that, while the WPP creates fast oscillating dynamics, the DEM does not. As seen in the extended figure A, the DEM maintains the slow dynamics, which was mixed with the fast transients in the ones from the WPP. Also, the extended figure B reveals that the slow dynamics last for a long time, even after 10 seconds, and the DEM provides exactly same response regarding it. The results proved that the DEM provides the identical slow dynamic performance as the WPP model.

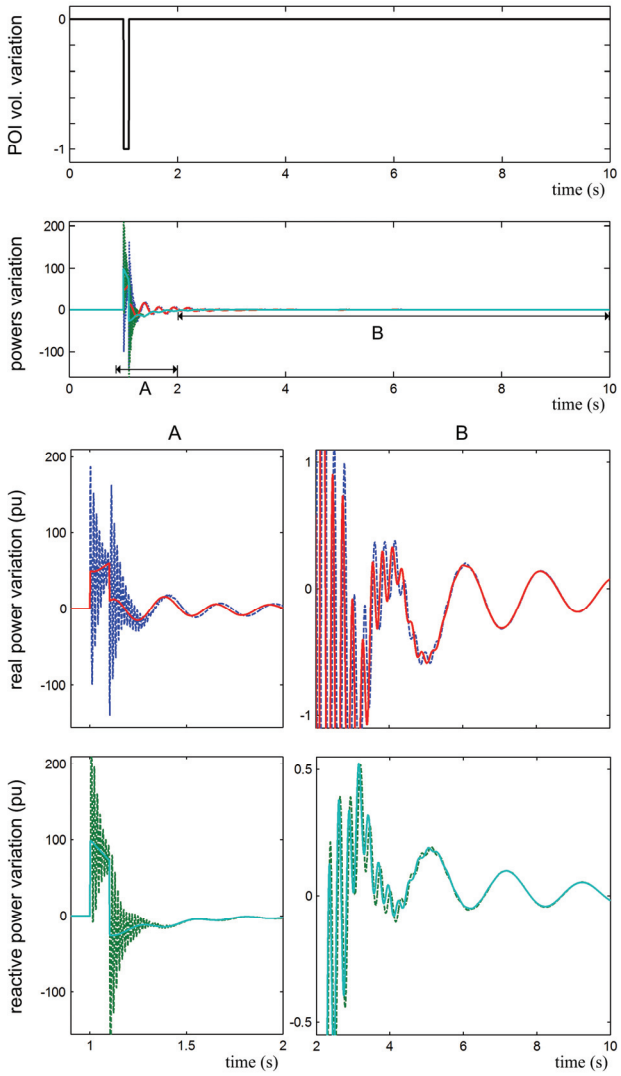

Fig. 2.5s. Dynamic performance comparison between the WPP and the DEM for a sudden POI voltage change

Additionally, the dynamics of the DEM, which have the same POI power variations as the outputs are compared to those of a DEM having the POI current variations as its outputs. As the latter DEM has the current variations as its output, the variations of POI powers are calculated to compare with those of the former DEM. The powers are calculated using nonlinear power equations and then their variations are obtained: $\Delta P_{0(\text{compr})} = P_0 - P_{0o}$ and $\Delta Q_{0(\text{compr})} = Q_0 - Q_{0o}$, where $P_0 = v_{0d}i_{0d} + v_{0q}i_{0q}$, $Q_0 = v_{0q}i_{0d} - v_{0d}i_{0q}$, $i_{0d} = \Delta i_{0d} + i_{0do}$, and $i_{0q} = \Delta i_{0q} + i_{0qo}$. The variation of POI voltage in magnitude dropped to -1 in step for 0.1 second and recovered to 0, which can be considered the same as the POI voltage in magnitude drops to almost zero and recovers to the original value (voltage sag). Figure 2.6s shows the results.

When the voltage drops to almost zero, it is expected that power also drops nearly to zero so the power variations are changed with negative sign. While the latter DEM meets this expectation, the former DEM does not since it uses power variations obtained by linearizing nonlinear power equations, which is valid within a certain amount of range from the given operating conditions for the linearization. However, both the DEM provide exactly the same dynamics after the voltage sag. Considering the voltage sag is used to trigger transients as, sort of, an impulsive input that hardly alters the initially given operating conditions, either of the DEMs can contribute to power system dynamics study.

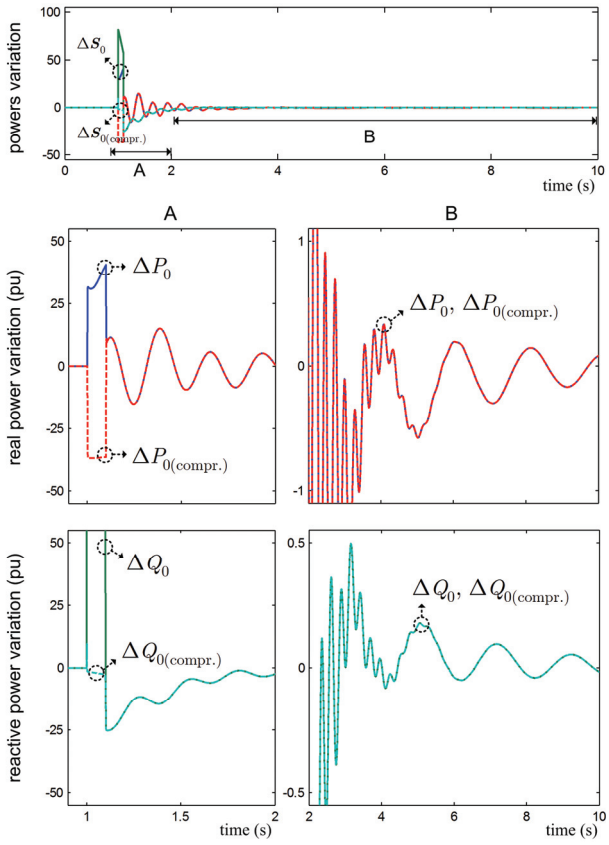

Fig. 2.6s. Dynamics performance comparison between
a DEM using power outputs and a DEM using current outputs
for a sudden POI voltage change

3.6 Conclusions

In this chapter, a DEM of a WPP has been developed using an aggregation technique. First, aggregation technique to develop equivalent models was conceptualized. Then, slow equivalent models of wind turbines were derived using the technique on the basis of dynamic models of wind turbines, which was introduced in chapter 2. Equivalent slow dynamic models for groups of wind turbines within the WPP were introduced and aggregated into an equivalent static network model to formulate a low-order WPP DEM. Finally, simulation testing of the DEM confirmed that it has identical dynamic performance as the WPP model. The usefulness of the DEM increases with the number of wind turbines in the WPP, and it is expected that the proposed DEM will be useful for WPP dynamic study.

There are remained tests to confirm the DEM has the same effects on power system dynamics as the WPP. This should be confirmed by simulation tests using the DEM interacted with power systems. The tests will be performed in chapter 7.

Chapter 4

Design of Wind Turbine Controllers using DEMs

As increasing number of WPPs have begun to have a significant impact on existing power systems, WPPs are asked to contribute the stable operation of the power system with grid codes as do conventional generating units [14]-[19]. The grid codes require WPPs to have capabilities of voltage control, reactive power control, active frequency adjustment, and fault ride through. To meet these requirements, WPPs need to be centrally controlled, i.e., proper references are centrally created and individual wind turbines in the WPPs should be able to effectively follow the references. Thus, wind turbines need to be regulated by properly designed controllers. Also, variable speed wind turbines with power converters become common types in these days. While these variable speed wind turbines provide improved efficiency of power transfer and reduced mechanical stresses, they requires more sophisticated control scheme [84], [85]. Furthermore, as wind turbines in a WPP are mutually interconnected by cables, controller design should be carried out from the perspective of the WPP operation, not from that of individual wind turbines. Consequently, chapter 4 deals with the control design for wind turbines.

This chapter presents a Proportional Integral (PI) control method as a conventional method. Then, it introduces a control design using Linear Quadratic Integral Regulator (LQIR) method. The control design is carried out using linear programming based on the linear matrix inequality (LMI). The control design requires a model in the form of state space equation and the DEMs introduced in chapter 3 are used for this purpose.

4.1 Proportional Integral Control

The Proportional Integral (PI) controller is a generic feedback control method widely used in industrial control systems, including wind turbine systems. It has historically been considered a great controller because it provided good performance with simple gain tunings. PI controllers generally regulate wind turbine systems such as back-to-back converters and pitch angle mechanisms. Thus, the subsequent section introduces PI control design as a conventional method.

4.1.1 PI Controller

PI controller design is introduced with a simple example. Let us say a model is given in the form of a 1st order state space equation,

$$\dot{x} = ax + bu \tag{4.1– 1}$$

Assuming the state is to be controlled, the error between the state and its objective (reference) needs to be defined,

$$e = x - x_{ref} \tag{4.1– 2}$$

If the state is intended to be controlled with an integrator, the integrated error is also defined,

$$e_I = \int e \; dt \tag{4.1– 3}$$

Applying the error and the integrated error into the original model,

$$\begin{pmatrix} \dot{x} \\ \dot{e}_I \end{pmatrix} = \boldsymbol{A}\begin{pmatrix} x \\ e_I \end{pmatrix} + \begin{pmatrix} \boldsymbol{b}_1 & \boldsymbol{b}_2 \end{pmatrix}\begin{pmatrix} x_{ref} \\ u \end{pmatrix}, \text{ where } \boldsymbol{A} = \begin{pmatrix} a & 0 \\ 1 & 0 \end{pmatrix}, \; \boldsymbol{b}_1 = \begin{pmatrix} 0 \\ -1 \end{pmatrix}, \; \boldsymbol{b}_2 = \begin{pmatrix} b \\ 0 \end{pmatrix} \tag{4.1– 4}$$

The control input - the properly adjusted states by gains - is fed back to the original model, where the gains are designed, for instance, using pole-zero cancellation method [74],

$$u = -\boldsymbol{K}\begin{pmatrix} x \\ e_I \end{pmatrix} + k_P x_{ref}, \text{ where } \boldsymbol{K} = \begin{pmatrix} k_P & k_I \end{pmatrix} \tag{4.1– 5}$$

By substituting the control input into the original model, a controlled model is

$$\begin{pmatrix} \dot{x} \\ \dot{e}_I \end{pmatrix} = (\boldsymbol{A} - \boldsymbol{b}_2\boldsymbol{K})\begin{pmatrix} x \\ e_I \end{pmatrix} + \boldsymbol{b}_2 k_P x_{ref} \tag{4.1– 6}$$

Now, the model has the reference x_{ref} as an auxiliary input.

4.1.2 Multi-loop Control

PI control method is often performed in multi-loop structures. In the case of back-to-back converter control, dc-link voltage is regulated by a multi-loop control scheme. In the (terminal) voltage oriented frame, real and reactive powers can be controlled by q-axis and d-axis converter input currents, respectively. Since the dc-link voltage varies by real power balance, it can be regulated by q-axis converter input current control. Thus, the output of dc-link voltage controller is equivalent to the reference of the q-axis converter input current controller, which creates a multi-feedback loop.

Take, for instance, a model of type 3 wind turbine, where the converter input and output currents are regulated by PI controllers so that the model's control inputs are now the references of converter input currents and stator powers. Yet, the dc-link voltage is not feedback-controlled. In addition, it is assumed that the d-axis converter input current and reactive power are controlled at constant values ($\Delta i_{cq(ref)} = 0$, $\Delta Q_{su(ref)} = 0$). Then, the model is expressed,

$$\dot{\boldsymbol{x}} = \boldsymbol{A}\boldsymbol{x} + \boldsymbol{B}\boldsymbol{u} + \boldsymbol{G}\boldsymbol{d}, \text{ where } \boldsymbol{u} = \begin{pmatrix} \Delta i_{cq(ref)} \\ \Delta P_{su(ref)} \end{pmatrix}, \; \boldsymbol{d} = \begin{pmatrix} \Delta \boldsymbol{v}_{tu} \\ \Delta w \end{pmatrix} \tag{4.1– 7}$$

Applying the dc-link voltage control without an integrator is performed by using the following feedback input,

$$\Delta i_{cq(ref)} = -k_{dcP}\Delta e_{dc}, \text{ where } \Delta e_{dc} = \Delta v_{dcu} - \Delta v_{dcu(ref)} (= 0) \tag{4.1– 8}$$

In addition, if the stator power is not controlled at a constant value but controlled based on generator speed to capture maximum power, the reference can be expressed as a function of generator speed,

$$\Delta P_{su(ref)} = K_g \Delta \omega_{gu} \tag{4.1– 9}$$

The control input variable $\boldsymbol{u}$ is now absorbed into the model by (4.1– 8) and (4.1– 9), and the disturbance input $\boldsymbol{d}$ is remained. The resultant model is given

$$\dot{\boldsymbol{x}} = \bar{\boldsymbol{A}}\boldsymbol{x} + \boldsymbol{G}\boldsymbol{d} \tag{4.1– 10}$$

4.2 Linear Quadratic Integral Regulator (LQIR)

Now, Linear Quadratic Integral Regulator (LQIR) is introduced. This is a modified version of Linear Quadratic Regulator (LQR) [75]. In addition to the system states, the integrated outputs are feedback-controlled to eliminate steady-state errors of the system outputs. In the perspective of the state variables being feedback controlled with proportional and integral gains, the LQIR method is similar to the PI control method, but the difference is, the PI controller controls chosen states separately while the LQIR controls simultaneously all states included in control design. In addition, the PI control method requires repetitive tuning process to obtain proper gains by trial and errors, while the LQIR method does not. The gains are derived by solving mathematical problems based on the corresponding system model represented in the form of state space equation, and thus it is possible to obtain more reliable optimized controllers for the model.

As an integrator works to eliminates only the local system output's steady-state error, reducing one system's steady-state error might increase the other systems' steady-state error in a networked system, and thus stability of the networked system could be eventually decrease. Therefore, if integrators are intended to be used in the control, the controller should be designed based on the models not only of local systems but also of the network system.

4.2.1 LQIR Structure

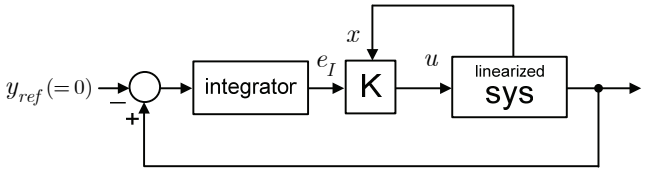

Fig. 3.1 LQIR structure

In the LQIR method, the integrated states are feedback-controlled to eliminate steady-state error of system output. To apply the LQIR method, the state space equation needs to be modified so that integrated system outputs are included in the states. For instance, a simple second-order state space equation is given as

$$\begin{pmatrix} \dot{x}_1 \\ \dot{x}_2 \end{pmatrix} = \boldsymbol{A}\begin{pmatrix} x_1 \\ x_2 \end{pmatrix} + \boldsymbol{B}\boldsymbol{u} \tag{4.2– 1}$$

Assuming that the state x_1 is chosen the system output to be controlled with an integrator, the integrated state is given as

$$e_I = \int e \; dt \tag{4.2– 2}$$

where $e = y - y_{ref}$ and $y = x_1$. By applying this result, the modified state space equation is obtained as

$$\begin{pmatrix} \dot{\boldsymbol{x}} \\ \dot{e}_I \end{pmatrix} = \begin{pmatrix} \boldsymbol{A} & \boldsymbol{0} \\ (1 \quad 0) & 0 \end{pmatrix}\begin{pmatrix} \boldsymbol{x} \\ e_I \end{pmatrix} + \begin{pmatrix} \boldsymbol{B} & \boldsymbol{0} \\ \boldsymbol{0} & -1 \end{pmatrix}\begin{pmatrix} \boldsymbol{u} \\ y_{ref}(=0) \end{pmatrix} \tag{4.2– 3}$$

Using (4.2–3), the control law is achieved by solving the corresponding Lyapunov equations,

$$\boldsymbol{u} = -\boldsymbol{K}\begin{pmatrix} \boldsymbol{x} \\ e_I \end{pmatrix} \tag{4.2– 4}$$

Applying the control input to the original model gives the controlled model. The next section explains how to obtain

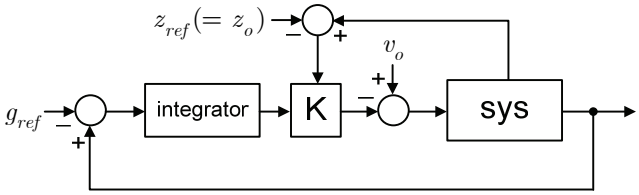

Fig. 3.2 Applying LQIR to nonlinear system

the gain matrix $\boldsymbol{K}$.

- Applying LQIR to Nonlinear System

When applying LQIR method, which is designed on the basis of a linearized model, to the corresponding original nonlinear model, some modifications might have to be made, unless making the nonlinear model work as a linear model by canceling the nonlinear terms by feedback compensation, such as the feedback linearization method [63]. The operating points used for linearization will be used for control references. Assuming that the states and inputs are variations of some variables:

$$\boldsymbol{x} = \Delta \boldsymbol{z} = \boldsymbol{z} - \boldsymbol{z}_o (= \boldsymbol{z}_{ref}),\ \boldsymbol{u} = \Delta \boldsymbol{v} = \boldsymbol{v} - \boldsymbol{v}_o,\ y = \Delta g = g - g_o (= g_{ref})$$

The control law is expressed as

$$\boldsymbol{v} = \boldsymbol{v}_o - \boldsymbol{K}_1(\boldsymbol{z} - \boldsymbol{z}_o) - \boldsymbol{K}_2 \int (g - g_o) dt \qquad (4.2\text{–}5)$$

where subscript "*o*" denotes operating points that are used as references in control matter. Figure 3.2 shows the control law.

4.2.2 Control Design in LMI Framework

Here, control design is simply referred as a process of obtaining a gain matrix. This section explains how to obtain the optimized gain matrix $\boldsymbol{K}$ in linear matrix inequality (LMI) framework. For this, a system's state space equation is assumed given as

$$\dot{\boldsymbol{x}} = \boldsymbol{A}\boldsymbol{x} + \boldsymbol{B}\boldsymbol{u} + \boldsymbol{G}\boldsymbol{d} \qquad (4.2\text{–}6)$$

where $\boldsymbol{u}$ denotes control inputs and $\boldsymbol{d}$ denotes disturbance inputs that are not controlled.

4.2.2.1 Method 1

When designing a state feedback controller, the system stability should be guaranteed first. The system (4.2–6) is asymptotically stable if the followings are satisfied:

$$V(\boldsymbol{x}) = \boldsymbol{x}^T \boldsymbol{P} \boldsymbol{x} > 0 \qquad (4.2\text{–}7)$$

$$\dot{V}(\boldsymbol{x}) = \boldsymbol{x}^T (\boldsymbol{A}^T \boldsymbol{P} + \boldsymbol{P}\boldsymbol{A}) \boldsymbol{x} + \boldsymbol{x}^T \boldsymbol{P} \boldsymbol{B} \boldsymbol{u} + \boldsymbol{u}^T \boldsymbol{B}^T \boldsymbol{P} \boldsymbol{x} < 0 \qquad (4.2\text{–}8)$$

where $\boldsymbol{P}$ is a symmetric matrix in (4.2–7) and is said to be positive by definition. The two equations are called Lyapunov stability equations. Adding a boundary condition of $(\boldsymbol{x}^T \boldsymbol{Q} \boldsymbol{x} + \boldsymbol{u}^T \boldsymbol{R} \boldsymbol{u})$ that is always positive, (4.2–8) can be expressed as

$$\boldsymbol{x}^T (\boldsymbol{A}^T \boldsymbol{P} + \boldsymbol{P}\boldsymbol{A}) \boldsymbol{x} + \boldsymbol{x}^T \boldsymbol{P} \boldsymbol{B} \boldsymbol{u} + \boldsymbol{u}^T \boldsymbol{B}^T \boldsymbol{P} \boldsymbol{x} = -(\boldsymbol{x}^T \boldsymbol{Q} \boldsymbol{x} + \boldsymbol{u}^T \boldsymbol{R} \boldsymbol{u}) \qquad (4.2\text{–}9)$$

Representing (4.2–9) in matrix form, the following is obtained:

$$\begin{pmatrix} \boldsymbol{x} \\ \boldsymbol{u} \end{pmatrix}^T \begin{pmatrix} \boldsymbol{A}^T\boldsymbol{P} + \boldsymbol{P}\boldsymbol{A} + \boldsymbol{Q} & \boldsymbol{P}\boldsymbol{B} \\ \boldsymbol{B}^T\boldsymbol{P} & \boldsymbol{R} \end{pmatrix} \begin{pmatrix} \boldsymbol{x} \\ \boldsymbol{u} \end{pmatrix} = 0 \tag{4.2–10}$$

By the Schur complement condition, the Riccati equation is obtained from (4.2–10), resulting in:

$$\boldsymbol{A}^T\boldsymbol{P} + \boldsymbol{P}\boldsymbol{A} + \boldsymbol{Q} - \boldsymbol{P}\boldsymbol{B}\boldsymbol{R}^{-1}\boldsymbol{B}^T\boldsymbol{P} = 0 \tag{4.2–11}$$

The Riccati equation can be numerically solved. However, in this work, the problem is solved in the LMI framework. The solution is obtained by maximizing the summation of positive eigenvalues of matrix $\boldsymbol{P}$. The sum of eigenvalues is same as the sum of the diagonal components of the corresponding matrix, called trace of the matrix. The optimization problem is configured in the form of linear programming based on LMI constraints as:

$$\begin{aligned} &\text{minimize} && \operatorname{trace}(\boldsymbol{Z}) \\ &\text{subject to} && \begin{pmatrix} \boldsymbol{A}_j^T\boldsymbol{P} + \boldsymbol{P}\boldsymbol{A}_j + \boldsymbol{Q} & \boldsymbol{P}\boldsymbol{B}_j \\ \boldsymbol{B}_j^T\boldsymbol{P} & \boldsymbol{R} \end{pmatrix} = 0\,, \ \begin{pmatrix} \boldsymbol{Z} & \boldsymbol{I} \\ \boldsymbol{I} & \boldsymbol{P} \end{pmatrix} > 0\,, \ \boldsymbol{P} > 0 \end{aligned} \tag{4.2–12}$$

where $\boldsymbol{Z}$ and $\boldsymbol{P}$ are variable matrices and they are obtained by solving (4.2–12). Subscript j denotes j operating conditions. System and input matrixes of multiple operating conditions could be added into the optimization problem. The weight matrices $\boldsymbol{Q}$ and $\boldsymbol{R}$ are chosen by designers, where $\boldsymbol{R}$ is generally chosen the identity matrix. Once $\boldsymbol{P}$ is obtained, then the control gain matrix $\boldsymbol{K}$ is given as [75]:

$$\boldsymbol{K} = \boldsymbol{R}^{-1}\boldsymbol{B}^T\boldsymbol{P} \tag{4.2–13}$$

4.2.2.2 Method 2

In the method 1, input energy is limited by choosing the input weigh matrix. The gain matrix can also be obtained without selecting input weight matrix. The process is as follows [6], [76]:

- An alternative symmetric variable matrix is chosen as $\boldsymbol{T} = \boldsymbol{P}^{-1}$.
- Using the state feedback of $\boldsymbol{u} = -\boldsymbol{K}\boldsymbol{x}$, the system matrix becomes $(\boldsymbol{A} - \boldsymbol{B}\boldsymbol{K})$.
- The gain matrix is given as $\boldsymbol{K} = \boldsymbol{L}\boldsymbol{T}^{-1}$ with an additional variable matrix $\boldsymbol{L}$.

Then, the following is obtained by the Lyapunov stability equations, as in (4.2–9)

$$\boldsymbol{T}(\boldsymbol{A} - \boldsymbol{B}\boldsymbol{K})^T + (\boldsymbol{A} - \boldsymbol{B}\boldsymbol{K})\boldsymbol{T} + \boldsymbol{T}\boldsymbol{Q}\boldsymbol{T} = 0 \tag{4.2–14}$$

Problem (4.2–9) is represented in the LMI framework.

$$\begin{aligned} &\text{minimize} && \operatorname{trace}(\boldsymbol{Z} + \boldsymbol{R}) \\ &\text{subject to} && \begin{pmatrix} \boldsymbol{T}\boldsymbol{A}_j^T - \boldsymbol{L}^T\boldsymbol{B}_j^T + \boldsymbol{A}_j\boldsymbol{T} - \boldsymbol{B}_j\boldsymbol{L} & \boldsymbol{T} \\ \boldsymbol{T} & -\boldsymbol{Q}^{-1} \end{pmatrix} = 0\,, \\ & && \begin{pmatrix} \boldsymbol{Z} & \boldsymbol{I} \\ \boldsymbol{I} & \boldsymbol{T} \end{pmatrix} > 0\,, \ \begin{pmatrix} \boldsymbol{R} & \boldsymbol{L}^T \\ \boldsymbol{L} & \boldsymbol{I} \end{pmatrix} > 0\,, \ \boldsymbol{T} > 0\,, \ \operatorname{trace}(\boldsymbol{Z}) < \sigma \end{aligned} \tag{4.2–15}$$

In this case, the gains are limited by reducing the energy of $\boldsymbol{L}^T\boldsymbol{L}$. To find the optimized gain matrix, the additional constraint $\operatorname{trace}(\boldsymbol{Z}) < \sigma$ is also added. The scalar σ is chosen as small as possible. If the disturbance in (4.2–6) is considered in the design problem, one of the LMI constraints is modified to:

$$\begin{pmatrix} \boldsymbol{T}\boldsymbol{A}_j^T - \boldsymbol{L}^T\boldsymbol{B}_j^T + \boldsymbol{A}_j\boldsymbol{T} - \boldsymbol{B}_j\boldsymbol{L} & \boldsymbol{T} & \boldsymbol{G}_j \\ \boldsymbol{T} & -\boldsymbol{Q}^{-1} & \\ \boldsymbol{G}_j^T & & -\boldsymbol{R}_G^{-1} \end{pmatrix} = 0$$

where $\boldsymbol{R}_G = \boldsymbol{I}$ and subscript j denotes j operating conditions. This LMI optimization problem is solved with the cvx program [77].

4.2.2.3 Decentralized Control

Typically, commands from upper control levels are centrally generated and are transmitted to the lower primary control part. The lowest primary control level, such as converter and governor control, should be decentralized. Therefore, each wind turbine needs to be controlled by its own state feedback without information from the other wind turbines. This is called decentralized control. If wind turbines to be controlled are different in terms of dynamics and structure, the gain matrix needs to be related only to the states of corresponding wind turbines. To do so, the gain matrix $\boldsymbol{K}$ is in the form of blocked diagonal matrix as:

$$\boldsymbol{K} = \mathrm{diag}\{\boldsymbol{K}_1, \ldots, \boldsymbol{K}_k\} \tag{4.2–16}$$

To make the gain matrix in the form of blocked diagonal, the following constraint is needed for method 1:

$$\boldsymbol{P} = \mathrm{diag}\{\boldsymbol{P}_1, \ldots, \boldsymbol{P}_k\} \tag{4.2–17}$$

For method 2, the following constraints are required:

$$\boldsymbol{T} = \mathrm{diag}\{\boldsymbol{T}_1, \ldots, \boldsymbol{T}_k\},\ \boldsymbol{L} = \mathrm{diag}\{\boldsymbol{L}_1, \ldots, \boldsymbol{L}_k\} \tag{4.2–18}$$

The other variable matrices $\boldsymbol{Z}$ and $\boldsymbol{R}$ with respect to $\boldsymbol{P}$, $\boldsymbol{T}$, and $\boldsymbol{L}$ would also be in the form of a blocked-diagonal matrix.

4.3 Converter Control

When doing the control design for the back-to-back (PWM) converters, the network parameters of power system must be taken into account because wind turbines are connected to the network by the converters. By using the equivalent model of the back-to-back converters, which is obtained by the aggregation method, it is possible to consider the network parameters into the control design problem.

The equivalent model of the back-to-back converters is represented in the form of state space equations as (4.2–6), and then the optimal gain matrix is derived by solving the corresponding optimization problem.

4.3.1 Control Design of Back-to-back Converters

For the control of back-to-back converters, a gain matrix with respect to the state variables such as stator currents, rotor currents, converter input currents, and dc-link voltage is required. The electrical torque (or stator real power) and stator reactive power are indirectly regulated by controlling the rotor or stator currents.

When doing the control design for back-to-back converters, the dynamics of drive train are ignored so that the equivalent model of the WPP contains only the equivalent state variables of generator and converters. In this case, generator angular speed is treated as a disturbance input and the generator angular speed is assumed not changing much due to enormous blade inertia: 1. $\Delta\omega_{gu} = 0$ (or it considered as a disturbance). In addition, the lumped network parameters between the POI bus and generating units in external power system are considered, where the

buses to which the generating units are connected are assumed as infinite buses of which the voltages are constant: 2. $\Delta \boldsymbol{V}_{POI} = \boldsymbol{K}_a \Delta \boldsymbol{S}_{POI} + \boldsymbol{K}_b \Delta \boldsymbol{V}_0 (= 0)$. Then, the equivalent model of back-to-back converters that absorbed the network parameters $\boldsymbol{K}_a$ into the system matrix can be expressed (without being controlled)

$$\dot{\boldsymbol{x}} = \boldsymbol{A}\boldsymbol{x} + \boldsymbol{B}\boldsymbol{u} \tag{4.3–1}$$

where

$$\boldsymbol{x} = \begin{pmatrix} \boldsymbol{x}_g^e \\ \boldsymbol{x}_{cv}^e \\ \boldsymbol{x}_I^e \end{pmatrix},\ \boldsymbol{u} = \begin{pmatrix} \Delta \boldsymbol{v}_{cu}^e \\ \Delta \boldsymbol{v}_{ru}^e \end{pmatrix} \text{ for type 3, } \boldsymbol{u} = \begin{pmatrix} \Delta \boldsymbol{v}_{cu}^e \\ \Delta \boldsymbol{v}_{su}^e \end{pmatrix} \text{ for type 4}$$

Superscript "*e*" denotes the equivalents obtained by the aggregation method as describe in chapter 3. $\boldsymbol{x}_g^e$ and $\boldsymbol{x}_{cv}^e$ are the equivalent state variables of generator and back-to-back converters, respectively, and $\boldsymbol{x}_I^e$ is the integrated of equivalent states chosen to be controlled with integrators. The state variables are fed back by a control law: $\boldsymbol{u} = -\boldsymbol{K}\boldsymbol{x}$, where the gain matrix $\boldsymbol{K}$ is obtained by solving an optimization problem with respect to (4.3–1). The gain matrix can directly be applied to back-to-back converters of individual wind turbines.

Additionally, in configuring an optimization problem, the following assumption could be useful: wind turbines in a WPP have slightly different operational conditions because of such wind wake effect. However, for the control design, it might be better to assume that all wind turbines are in the same operational conditions if the WPP consists of identical wind turbines (their type and system parameters are the same). By doing so, the WPP can be modeled into one equivalent model and thus the back-to-back converters are also modeled into one equivalent. Then, the optimization problem can be simple and requires less computation. If necessary, multiple equivalents for various operational conditions can be derived and they are included in the LMI constraints of the optimization problem.

4.3.2 Control References (Operating Points)

In the LQIR method, the gain matrix is obtained based on a linearized model. To apply the LQIR method to the original nonlinear model, the operating points need to be calculated. The operating points, which also represent control references, are obtained from the steady-state model of wind turbines. Here, the operating points for type 3 and 4 wind turbines are derived.

4.3.2.1 Generator for Type 3 wind turbines

Voltage equations in the steady state of stator and rotor side are given as

$$v_{su}^c = (R_{su} + j\omega_u L_{su}) i_{su}^c + j\omega_u L_{mu} i_{ru}^c \tag{4.3–2}$$

$$v_{ru}^c = (R_{ru} + j s_{\text{lip}} \omega_u L_{ru}) i_{ru}^c + j s_{\text{lip}} \omega_u L_{mu} i_{su}^c \tag{4.3–3}$$

where s_{lip} is slip and $\omega_u = 1$. Stator power is expressed as

$$s_{su} = v_{su}^c (i_{su}^c)^* \tag{4.3–4}$$

To derive the operating points, voltage equations and power equation are expressed in the dq-frame. From the stator voltage equation (4.3–2), we can derive:

$$\begin{pmatrix} i_{rd} \\ i_{rq} \end{pmatrix} = \frac{1}{L_{mu}} \begin{pmatrix} 0 & 1 \\ -1 & 0 \end{pmatrix} \begin{pmatrix} v_{sd} \\ v_{sq} \end{pmatrix} - \frac{1}{L_{mu}} \begin{pmatrix} L_{su} & R_{su} \\ -R_{su} & L_{su} \end{pmatrix} \begin{pmatrix} i_{sd} \\ i_{sq} \end{pmatrix} \tag{4.3–5}$$

Stator currents in the dq frame can be derived from power equation (4.3–4):

$$\begin{pmatrix} i_{sd} \\ i_{sq} \end{pmatrix} = \frac{1}{v_{sd}^2 + v_{sq}^2} \begin{pmatrix} v_{sd} & v_{sq} \\ v_{sq} & -v_{sd} \end{pmatrix} \begin{pmatrix} p_s \\ q_s \end{pmatrix} \quad (4.3\text{–}6)$$

Substituting (4.3–6) into (4.3–5), the reference of rotor currents is obtained:

$$i_{rd} = \frac{1}{L_{mu}} v_{sq} - \kappa_a p_s + \kappa_b q_s \quad (4.3\text{–}7)$$

$$i_{rq} = -\frac{1}{L_{mu}} v_{sd} + \kappa_b p_s + \kappa_a q_s \quad (4.3\text{–}8)$$

where

$$\kappa_a = \frac{1}{v_{sd}^2 + v_{sq}^2} \left(\frac{L_{su}}{L_{mu}} v_{sd} + \frac{R_{su}}{L_{mu}} v_{sq} \right), \; \kappa_b = \frac{1}{v_{sd}^2 + v_{sq}^2} \left(\frac{R_{su}}{L_{mu}} v_{sd} - \frac{L_{su}}{L_{mu}} v_{sq} \right)$$

If it is assumed that the control is made in the stator voltage-oriented frame and the small stator resistance is ignored, $\kappa_a = 0$. Therefore, (4.3–7) and (4.3–8) are simplified to:

$$i_{rd(ref)} = \frac{1}{L_{mu}} v_{sq} + \kappa_b' q_{s(ref)} \quad (4.3\text{–}9)$$

$$i_{rq(ref)} = \kappa_b' p_{s(ref)} \quad (4.3\text{–}10)$$

where $\kappa_b' = -\frac{L_{su}}{L_{mu} v_{sq}}$

From (4.3–9) and (4.3–10), it is shown that the imaginary and real powers can be independently controlled by the d-axis and q-axis currents, respectively. Also, the operating points of stator currents are obtained from (4.3–6):

$$i_{sd(o)} = \kappa_c q_{s(ref)} \quad (4.3\text{–}11)$$

$$i_{sq(o)} = \kappa_c p_{s(ref)} \quad (4.3\text{–}12)$$

where $\kappa_c = \frac{1}{v_{sq}}$

To derive the operating points of rotor voltages, equation (4.3–3) is expressed in the dq frame:

$$\begin{pmatrix} v_{rd} \\ v_{rq} \end{pmatrix} = \begin{pmatrix} R_{ru} & -s_{\text{lip}} L_{ru} \\ s_{\text{lip}} L_{ru} & R_{ru} \end{pmatrix} \begin{pmatrix} i_{rd} \\ i_{rq} \end{pmatrix} + \begin{pmatrix} 0 & -s_{\text{lip}} L_{mu} \\ s_{\text{lip}} L_{mu} & 0 \end{pmatrix} \begin{pmatrix} i_{sd} \\ i_{sq} \end{pmatrix} \quad (4.3\text{–}13)$$

Assuming that rotor resistance is small enough to be ignored, the operating points are given as

$$v_{rd(o)} = -s_{\text{lip}} L_{ru} i_{rq(ref)} - s_{\text{lip}} L_{mu} i_{sq(o)} \quad (4.3\text{–}14)$$

$$v_{rq(o)} = s_{\text{lip}} L_{ru} i_{rd(ref)} + s_{\text{lip}} L_{mu} i_{sd(o)} \quad (4.3\text{–}15)$$

4.3.2.2 Generator for Type 4 wind turbines

As the generator is modeled in the RFO frame, the rotor flux $\lambda_{ru(o)} = \lambda_{rd(o)}$. Then, the references of stator currents are given

$$i_{sd(ref)} = \lambda_{rd(o)} \; / \; L_{mu} \quad (4.3\text{–}16)$$

$$i_{sq(ref)} = T_{eu(o)} \; / \; (a \lambda_{rd(o)}) \quad (4.3\text{–}17)$$

If being assumed that the blade power is controlled on optimal points and the corresponding generator speeds are given, the operating points of electrical torque are

$$T_{eu(o)} = P_{bu(ref)} \,/\, \omega_{ru(ref)} \tag{4.3–18}$$

Then, the slip speed is calculated

$$\omega_{\mathrm{sl}(o)} = aR_{ru} i_{sq(ref)} \,/\, \lambda_{rd(o)} \tag{4.3–19}$$

After the slip speed is given, the angular speed of generator stator side is

$$\omega_{su(o)} = \omega_{ru(ref)} + \omega_{\mathrm{sl}(o)} \tag{4.3–20}$$

Once all of $i_{su(ref)}$, $\lambda_{ru(o)}$, $\omega_{ru(ref)}$, and $\omega_{su(o)}$ are given, $v_{su(o)}$ is calculated from the nonlinear equation (2.1–5).

4.3.2.3 Back-to-back Converters

In the voltage-oriented frame, the d-axis converter input current is controlled at zero to regulate the reactive power at zero:

$$i_{cd(ref)} = 0 \tag{4.2–21}$$

Assuming that the d-axis converter input current is controlled at zero, then the real power balance of converter output side (rotor side for type 3 and stator side for type 4) and converter input side is given as:

$$p_{out} = v_{cq} i_{cq} \tag{4.2–22}$$

Also, by ignoring small resistance and $\omega_u = 1$, the dq-voltage equations of converter input side are given as:

$$\begin{pmatrix} v_{sd}(=0) \\ v_{sq} \end{pmatrix} - \begin{pmatrix} v_{cd} \\ v_{cq} \end{pmatrix} = \begin{pmatrix} 0 & -L_{cu} \\ L_{cu} & 0 \end{pmatrix} \begin{pmatrix} i_{cd}(=0) \\ i_{cq} \end{pmatrix} \tag{4.2–23}$$

The following operating points of converter input voltages are obtained from (4.2–23):

$$v_{cd(o)} = L_{cu} i_{cq(o)} \tag{4.2–24}$$

$$v_{cq(o)} = v_{sq} \tag{4.2–25}$$

Using equations (4.2–22) and (4.2–25), the q-axis converter input current is obtained:

$$i_{cq(o)} = \kappa_c \, p_{out(o)} \tag{4.2–26}$$

where

for type 3: $p_{out(o)} = v_{rd(o)} i_{rd(ref)} + v_{rq(o)} i_{rq(ref)}$,

for type 4: $p_{out(o)} = v_{sd(o)} i_{sd(ref)} + v_{sq(o)} i_{sq(ref)}$

Last, the reference of dc-link voltage is chosen appropriately.

4.4 Turbine Governor Control

The wind turbine governor (blade power control by pitch angle change) is designed with a one-mass drive train model. The design of the pitch angle controller makes use of the slow dynamic equivalent model that has been developed in the subsection 3.2.1. The model is modified to have pitch angle input. In the one-mass drive train model, the angular speeds of rotor blade and generator are the same. Thus, the blade power is expressed as a function of wind speed, pitch angle, and the angular speed of generator:

$$\Delta P_{bu} = \kappa_{\omega}\Delta\omega_{gu} + \kappa_{w}\Delta w_{u} + \kappa_{\vartheta}\Delta\vartheta_{u} \tag{4.3–1}$$

By substituting (4.3–1) into (3.2–1), the model has the pitch angle input. For variable speed wind turbines (types 3 and 4), the rotor speed of generator $\Delta\omega_{gu}$ is controlled to regulate blade power. Then, by including the differential equation of integrated state of $\dot{x}_I = \Delta\omega_{gu}$, the slow dynamic equivalent model can be re-expressed, with the assumption of constant wind speed $\Delta w_{u} = 0$,

$$\dot{\boldsymbol{x}} = \boldsymbol{A}\boldsymbol{x} + \boldsymbol{B}\Delta\vartheta_{u} \tag{4.3–2}$$

where

$$\boldsymbol{x} = \begin{pmatrix} \Delta\omega_{gu}^{e} \\ x_{I}^{e} \end{pmatrix}$$

The model to be used for pitch angle control design is represented in 2nd order state space equation. Using this model, the gain matrix is derived by the LMI method.

On the other hand, for fixed speed wind turbine (type 1), terminal real power is feedback-controlled by pitch angle controller. Thus, the state of the angular speed of generator $\Delta\omega_{gu}^{e}$ needs to be transformed to the terminal real power ΔP_{tu}. By manipulating matrices of the output equation and network power equations, the following relation is derived.

$$\Delta P_{tu} = \boldsymbol{K}_{c}\boldsymbol{x} + \boldsymbol{K}_{d}\Delta\boldsymbol{V}_{0}(=0) \tag{4.3–3}$$

By using (4.3–3), a transformation matrix that transforms the state of $\Delta\omega_{gu}^{e}$ to ΔP_{tu} can be derived, and thus a pitch angle controller with respect to the terminal real power can be developed. In addition, as the equivalent model includes rotor fluxes, the rotor fluxes might have to be taken into consideration for the control design. Deriving and applying the transformation matrix will be explained more in detail in chapter 6, which is similarly used to develop a power system stabilizer (PSS).

4.5 Summary

For a WPP to operate stably or support the stable operation of power systems, we should guarantee that individual wind turbines are regulated by correctly tracking the references created from the control center of the WPP. Therefore, chapter 4 has been assigned to design controllers for wind turbines. First, the chapter briefly mentioned a conventional PI control method, and then introduced the LQIR method. Optimal gain matrix for LQIR method was derived by solving an optimization problem in LMI frame, which was configured using the equivalent models introduced in the chapter 3. In case that the method was applied to control a nonlinear model of turbines, the way of generating control references was also explained. This control method can be applied for both linear and nonlinear models of turbines. The control method was or will be used for simulation tests in the study.

Chapter 5

Dynamic Equivalent Model of WPP using Parameter Identification

Unlike dynamic modeling of conventional generation systems, the modeling of WPPs poses a unique set of problems. A WPP consists of several small generators with limited dispatching capabilities. Adding all of the WPP's turbines to a single cumulative model would produce a very high-order model, even for a small number of turbines. Furthermore, it is often difficult for the utility to determine the operating status of the individual turbines within the WPP. Therefore, detailed models of all generators will not always provide an accurate representation for the WPP. In addition, the high degree of variability and stochasticity in the wind seasons and the switching of the turbines require an adaptive model. These problems make the development of an aggregated and low-order adaptive model for the WPP a challenging task indeed.

An effective dynamic equivalent model (DEM) must have the following attributes:

- low order, yet accurate for dynamic studies
- adaptive to accommodate variations in wind and turbine switching
- developed without the need for hard-to-find parameters within the WPP.

The dynamic model used in this study applies to induction generators.

Several attempts have been made to develop lower-order DEMs for WPPs. However, most of these techniques are based on the identification of the coherent performance of the turbines. Therefore, they can be developed only when several parameters within the WPP are always available. This is a major hurdle because wind variability can change the operating status of individual turbines without the knowledge of the control centers of the utilities.

A better DEM should not be developed on the basis of parametric or configuration information inside the WPP. Instead, it should use measurements at the point of interconnection (POI). Because the WPP is frequently subjected to natural disturbances due to wind variations and wind gusts, there is no need to intentionally disturb the system to acquire its dynamic response. The DEM should be adaptive in order to track the variability in wind seasons and any large changes within the WPP.

In this chapter, a DEM for WPP is developed on the basis of measurements. First, it is explained how the measured data is properly processed for use in the identification process. Then, the DEM parameters are derived in the process, and the DEM is properly expressed with the parameters in a state-space representation. In the simulation, an identification technique is used to obtain the DEM, and its performance is verified.

5.1 Measurements

Figure 4.1 shows a WPP interconnected with a simplified external system by a point of interconnection (POI). In the figure, the load or generation change of the external system is represented by current injection that is randomly and continuously varying. The current injection has an important role for the DEM identification: Currents cause voltage drops across lines, where the voltage drops are equivalent to voltage differences between bus voltages. Thus, with the assumption of constant voltage at the infinite bus, the POI bus voltage is determined by currents injected from the WPP and the external systems, where the currents reflect the dynamics of the systems. If the external current injection is zero or constant, the POI voltage is only varied by the current injected from the WPP, which is

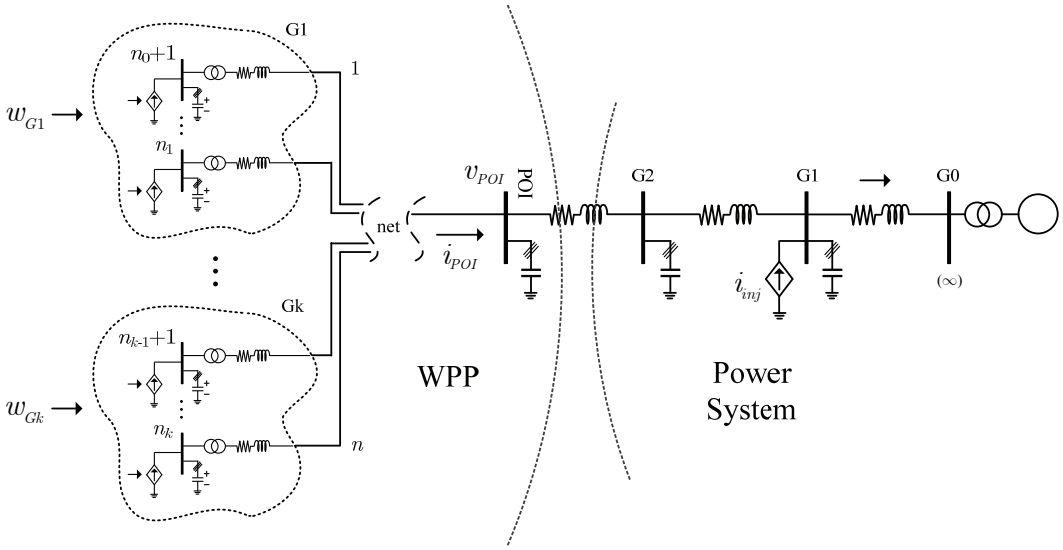

Fig. 4.1 WPP (clustered in *k* groups of wind turbines) interconnected with an external power system by a point of interconnection.

the POI current. The POI voltage and current are the input and output of the WPP system, respectively. As the POI voltage is now a function of the POI current, the input and output create a feedback loop. This means that the POI voltage does not reflect the dynamics of the external system, thus a proper DEM cannot be developed by the measurement of the POI voltage. This can be proved from:

$$\Delta v_{POI}(t) = h_a \Delta v_{G0}(t) + z_a \Delta i_{POI}(t) + z_b \Delta i_{inj}(t)$$
$$\Delta i_{POI}(t) = H(q^{-1}) \Delta v_{POI}(t),$$

where v_{POI} and v_{G0} are the voltages of POI bus and the infinite bus, respectively, i_{POI} and i_{inj} are the currents injected from the WPP and the external systems, respectively, and $H(q^{-1})$ is a transfer function of the WPP system. In the case of $\Delta v_{G0} = 0$ and $\Delta i_{inj} = 0$, the transfer function between Δv_{POI} and Δi_{POI} is expressed,

$$H(q^{-1}) = z_a^{-1}.$$

The transfer function is now just a constant, which does not include any dynamics. This clarifies that the DEM cannot be developed by the measurements of the POI voltage unless the external current injection sufficiently varies. Therefore, it is assumed that the current (or power) injected from the external power system is sufficiently varying.

5.1.1 Voltage and Power at POI Bus

The voltage at the POI bus and the current injected to the bus are measured in three phase quantities, and they are transformed into direct- and quadrature-axis components by dq transformation:

$$\boldsymbol{f}_{dqo} = \boldsymbol{T}(\theta(t)) \boldsymbol{f}_{abc} \tag{5.1–1}$$

where

$$\theta(t) = \omega t + \theta_0, \ \boldsymbol{f}_{dqo} = \begin{pmatrix} f_d \\ f_q \\ f_o \end{pmatrix}, \ \boldsymbol{f}_{abc} = \begin{pmatrix} f_a \\ f_b \\ f_c \end{pmatrix}$$

where ω is the angular speed of rotating dq-axis frame and θ_0 is the initial angle of $\theta(t)$. $\boldsymbol{f}_{dqo}$ and $\boldsymbol{f}_{abc}$ are the vectors of dq-components including zero sequence component and three phase components, respectively. The zero sequence component f_o in a balanced system is always zero, thus it is ignored.

Using the dq-transformation, the POI voltages and currents are obtained. The powers injected to the POI bus are calculated from the voltages and currents:

$$S^c_{POI} = v^c_{POI}(i^c_{POI})^* = P_{POI} + jQ_{POI} \tag{5.1–2}$$

where

$$v^c_{POI} = v_{POId} + jv_{POIq},\ i^c_{POI} = i_{POId} + ji_{POIq}$$

v_{POId} and v_{POIq} are d- and q-axis components of the POI voltage, respectively, and i_{POId} and i_{POIq} are d- and q-axis components of the POI current, respectively.

For the inputs and outputs of the DEM, the variations of the POI voltages and powers are applied. The measurements are compared to the corresponding moving averages that represent the operating conditions at the WPP. The moving average allows us to model the WPP for wide range of operation. In this case, variations in POI voltage measurements with respect to the moving averages can be written as:

$$\Delta \boldsymbol{V}_{POI} = \begin{pmatrix} \Delta v_{POId} \\ \Delta v_{POIq} \end{pmatrix} = \begin{pmatrix} v_{POId} - v_{POIdo} \\ v_{POIq} - v_{POIqo} \end{pmatrix} \tag{5.1–3}$$

And, variations in POI powers are given either

$$\Delta \boldsymbol{S}_{POI} = \begin{pmatrix} \Delta P_{POI} \\ \Delta Q_{POI} \end{pmatrix} = \begin{pmatrix} P_{POI} - P_{POIo} \\ Q_{POI} - Q_{POIo} \end{pmatrix} \tag{5.1–4}$$

or
$$\Delta \boldsymbol{S}_{POI} = \begin{pmatrix} \Delta P_{POI} \\ \Delta Q_{POI} \end{pmatrix} = \begin{pmatrix} v_{POIdo} & v_{POIqo} \\ v_{POIqo} & -v_{POIdo} \end{pmatrix} \begin{pmatrix} \Delta i_{POId} \\ \Delta i_{POIq} \end{pmatrix} + \begin{pmatrix} i_{POIdo} & i_{POIqo} \\ -i_{POIqo} & i_{POIdo} \end{pmatrix} \begin{pmatrix} \Delta v_{POId} \\ \Delta v_{POIq} \end{pmatrix} \tag{5.1–5}$$

where the subscript "*o*" means the operating condition of the WPP. It is expected that (5.1–5) is less nonlinear than (5.1–4) because equation (5.1–5) is a purely linear function. However, (5.1–5) is more computationally burdensome, so (5.1–5) is applied for the DEM identification process.

The POI voltage can also be represented by the magnitude and angle. When the measured voltage is aligned on the q-axis, the d-axis component is zero so that the q-axis POI voltage can be considered as voltage in magnitude,

$$\Delta \boldsymbol{V}_{POI} = \begin{pmatrix} \Delta v_{\text{mag}} \\ \Delta \theta_v \end{pmatrix}, \tag{5.1–6}$$

where

$$v_{\text{mag}} = \text{Im}\left(v^c_{POI} e^{-j(\theta_v)}\right) \text{ or } \sqrt{v^2_{POId} + v^2_{POIq}},$$
$$\theta_v = \tan^{-1}\left(\frac{v_{POId}}{v_{POIq}}\right).$$

It is noted that, from the equations (5.1-6), both information of voltage magnitude and angle at POI bus would be necessary for accurate DEM identification. Although the response of each wind turbine is mainly correlated to wind speed and terminal voltage in magnitude, the angle of terminal voltage also affects the response, especially in transient state. As the angle variation at POI bus is related to the variations in the magnitude and angle of wind turbines' terminal voltages, the angle information at POI bus is necessary.

- Measurements for Frequency-related Identification

In this chapter, the frequency will be assumed constant and ignored in the DEM development process. However, when the frequency needs to be considered for the DEM development, the frequency matter is simply taken into the

development process by measuring the angular frequency ω_0 at the POI and including it as an additional input of $\Delta\omega_0 = \omega_0 - \omega_{0o}$ into the identification process.

When the frequency is not only inconstant also uncertain, a Phase Locked Loop (PLL) method is typically used to detect the angular frequency ω and angle $\theta(t)$ of the equation (5.1–1): a frame in which the POI voltage is represented in the d-and q-axis components rotates in the angular speed ω and the frame's d-axis is positioned by the angle. The POI voltage can be represented in various ways in terms of different frames. For instance, let say the angle $\theta(t)$ of (5.1–1) is obtained by using a PLL method so that the d-axis component of the POI voltage in the corresponding frame is maintained nearly zero. In this case, it can be thought that the POI voltage is represented in a POI voltage-oriented frame whose angular speed is ω: the angular speed is equal to the differential of $\theta(t)$ and considered as ω_0. In this way, the d-and q-axis components of the POI voltage and the angular frequency ω_0 can be obtained and used for the identification process.

5.1.2 Equivalent Wind Speed

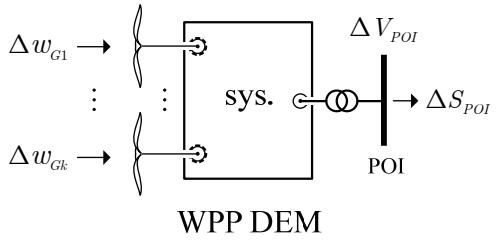

Fig. 4.2 WPP DEM with inputs of multiple equivalent wind speeds

Wind is decomposed of three vector components, where the *x*-axis is vertical to the blades. It is assumed that only the *x*-axis component of wind is effective and the others do not contribute to power generation. Here, the wind speed indicates the speed of the *x*-axis wind component.

While the wind pattern could be assumed to be the same at a certain height in some areas because wind is spatially continuous, the instantaneous patterns of wind that wind turbines experience are not identical. There are two main reasons for it. First, because the moment at which the wind reaches the wind turbines varies due to the separate location of the wind turbines, the speed of wind blowing to wind turbines appears to be delayed depending on their location. Wind turbines are typically located more than 100m from each other. In this case, the time delay could be more than 5 sec in rated wind speed. This time delay is critical in identifying DEM based on wind speed measurement. Second, due to the wind wake effect and turbulence by it, wind turbines have different wind speed in either or both average and instantaneity. If the wind turbines in the area are located far enough from each other, turbulence effect in average caused by blades might be small, but turbulence effect in instantaneity still cannot be ignored. Therefore, it would be better to assume that all wind turbines have different pattern of wind speed. Because the instantaneous patterns of wind that wind turbines experience are not identical because of the separate locations of the wind turbines and the wind wake effect [70]–[73], the data regarding the wind speeds for all wind turbines in a WPP are necessary to develop a proper WPP DEM. Thus, it is assumed that each wind turbine is equipped with a wind speed sensor so that the instantaneous wind speed of the wind turbine can be measured.

However, if the WPP consists of a large number of wind turbines, it is not proper to use the all wind speeds as the inputs of the DEM in the identification because too many input parameters have to be identified. Thus, it would be appropriate to cluster wind turbines into several groups and to use equivalent wind speeds for the groups as the inputs of the DEM. The wind turbines are properly clustered by their types and operational conditions on the basis of the wind power that they experience. The equivalent wind speed for group *k* of the wind turbines is expressed as

$$w_{Gk}(t) = \frac{1}{m_k}\sum_{i=1}^{m_k} w_{(n_{k-1}+i)}(t) \tag{5.1–7}$$

where $m_k (= n_k - n_{k-1})$ is the number of wind turbines in group *k*. For the inputs of the DEM, the variation of the equivalent wind speeds Δw_{Gk} is used. The figure 4.2 shows a WPP DEM with multiple equivalent wind speeds.

5.1.3 Filtering Process

The DEM deals mainly with the slow electromechanical dynamics and neglects the fast electric dynamics. However, improper rational transfer functions amplify the high-frequency noise so does the same the DEM improperly developed; therefore, low-pass filters are used to eliminate these high-frequency components. The filters on the inputs and outputs must have the same structure in order to ensure equal phase delays:

$$y_f(t) = H(q^{-1})u_f(t) \tag{5.1–8}$$

where $y_f(t) = G(q^{-1})^n y(t)$ and $u_f(t) = G(q^{-1})^n u(t)$ are the filtered output and input, respectively. $G(q^{-1})$ is the filter transfer function and *n* denotes the number of filtering. The filtering can be done as many times as required to eliminate the fast dynamics and to maintain the slow dynamics. Note that using filters does not affect the identification of DEM transfer function $H(q^{-1})$ because the filter transfer functions are cancelled. In this work, the cutoff frequency of the infinite impulse response filters is approximately 1.5 Hz.

5.2 Linear DEM Development

5.2.1 MIMO Structure of DEM Transfer Function

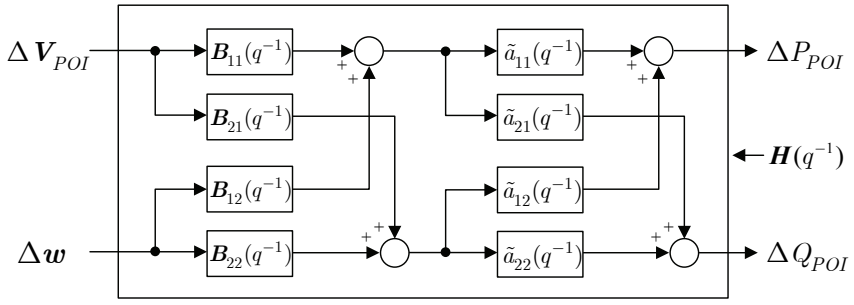

Fig. 4.3 MIMO structure of DEM transfer function

In this subsection, multi-inputs multi-outputs (MIMO) structure of the DEM transfer function is introduced. This is not directly associated with the DEM identification, but it gives an intuitive conception of the DEM structure. The MIMO relationship of the DEM is

$$\boldsymbol{A}(q^{-1})\boldsymbol{y}(t) = \boldsymbol{B}(q^{-1})\boldsymbol{u}(t) \tag{5.2–1}$$

where

$$\boldsymbol{y}(t) = \Delta \boldsymbol{S}_{POI}\,,\ \boldsymbol{u}(t) = \begin{pmatrix} \Delta \boldsymbol{V}_{POI}(t) \\ \Delta \boldsymbol{w}(t) \end{pmatrix}_{(2+k)\times 1}.$$

where $\boldsymbol{w}(t) = (\, w_{G1}(t) \quad \dots \quad w_{Gk}(t))^T$ that is the vector of k multiple equivalent wind speeds, q^{-1} is the backward shift operator. $\boldsymbol{A}(q^{-1})$ and $\boldsymbol{B}(q^{-1})$ are the system polynomials given by

$$\boldsymbol{A}(q^{-1}) = \begin{pmatrix} a_{11}(q^{-1}) & a_{12}(q^{-1}) \\ a_{21}(q^{-1}) & a_{22}(q^{-1}) \end{pmatrix} = \boldsymbol{I} + \boldsymbol{A}_1 q^{-1} + \cdots + \boldsymbol{A}_p q^{-p} \tag{5.2–2}$$

$$\boldsymbol{B}(q^{-1}) = \begin{pmatrix} \boldsymbol{B}_{11}(q^{-1}) & \boldsymbol{B}_{12}(q^{-1}) \\ \boldsymbol{B}_{21}(q^{-1}) & \boldsymbol{B}_{22}(q^{-1}) \end{pmatrix} = \boldsymbol{B}_0 + \boldsymbol{B}_1 q^{-1} + \cdots + \boldsymbol{B}_p q^{-p} \tag{5.2–3}$$

where

$$\boldsymbol{A}_i = \begin{pmatrix} a_{i\text{-}11} & a_{i\text{-}12} \\ a_{i\text{-}21} & a_{i\text{-}22} \end{pmatrix}_{2\times 2}, \; \boldsymbol{B}_i = \begin{pmatrix} (\boldsymbol{B}_{i\text{-}11})_{1\times 2} & (\boldsymbol{B}_{i\text{-}12})_{1\times k} \\ (\boldsymbol{B}_{i\text{-}21})_{1\times 2} & (\boldsymbol{B}_{i\text{-}22})_{1\times k} \end{pmatrix}_{2\times(2+k)}.$$

The roots of equation (5.2–2) are the poles of the MIMO DEM transfer function model, where the DEM transfer function is

$$\boldsymbol{H}(q^{-1}) = \boldsymbol{A}^{-1}(q^{-1})\boldsymbol{B}(q^{-1}) \tag{5.2–4}$$

where

$$\boldsymbol{A}^{-1}(q^{-1}) = \begin{pmatrix} \tilde{a}_{11}(q^{-1}) & \tilde{a}_{12}(q^{-1}) \\ \tilde{a}_{21}(q^{-1}) & \tilde{a}_{22}(q^{-1}) \end{pmatrix}$$

Figure 4.3 shows the block diagram of the DEM transfer function.

5.2.2 DEM Identification

Now, a basic form of DEM identification is introduced [78]. To identify the parameters of the DEM, the DEM is written in the form of deterministic autoregressive moving average (DARMA) model:

$$\hat{\boldsymbol{y}}(t) = \sum_{i=1}^{p} \boldsymbol{R}_i^T \boldsymbol{F}(t-i) + \boldsymbol{B}_0 \boldsymbol{u}(t) + \boldsymbol{k}(t) \tag{5.2–7}$$

where

$$\boldsymbol{R}_i^T = \begin{pmatrix} \boldsymbol{A}_i & \boldsymbol{B}_i \end{pmatrix}, \; \boldsymbol{F}(t) = \begin{pmatrix} \boldsymbol{y}(t) \\ \boldsymbol{u}(t) \end{pmatrix}$$

$\boldsymbol{u}(t)$ and $\boldsymbol{y}(t)$ are the measured values for the input and output of the model at time instance t, respectively, and $\hat{\boldsymbol{y}}(t)$ is the estimated value of $\boldsymbol{y}(t)$. $\boldsymbol{A}$ and $\boldsymbol{B}$ are the parameter matrixes of the model, p is the degree of the model, and $\boldsymbol{k}(t)$ is a biased vector. Equation (5.2–7) can be expressed by

$$\hat{\boldsymbol{y}}(t) = \boldsymbol{\vartheta}^T \boldsymbol{\psi}(t) \tag{5.2–8}$$

where

$$\boldsymbol{\vartheta}^T = (\, \boldsymbol{k} \quad \boldsymbol{B}_0 \quad \boldsymbol{R}_1^T \quad \cdots \quad \boldsymbol{R}_p^T), \; \boldsymbol{\psi}(t) = \begin{pmatrix} \boldsymbol{1} \\ \boldsymbol{u}(t) \\ \boldsymbol{F}(t-1) \\ \vdots \\ \boldsymbol{F}(t-p) \end{pmatrix}$$

$2p$ is the DEM order. The DEM order is chosen on the basis of the complexity of the original system dynamics. The parameter vector ϑ is identified by minimizing the cost function $J(\vartheta)$:

$$J(\vartheta) = \sum_{i=1}^{2}\sum_{j=0}^{n} \lambda^j \left(\boldsymbol{e}_s^{(i)}(t-j)\, \boldsymbol{e}_s^{(i)}(t-j)^T \right) \tag{5.2–9}$$

where

$$\boldsymbol{e}_s(t-j) = \boldsymbol{y}_s(t-j) - \boldsymbol{\vartheta}^T \boldsymbol{\psi}_s(t-j),$$
$$\boldsymbol{y}_s(t) = \begin{pmatrix} \boldsymbol{y}(t) & \cdots & \boldsymbol{y}(t-s+1) \end{pmatrix},\ \boldsymbol{\psi}_s(t) = \begin{pmatrix} \boldsymbol{\psi}(t) & \cdots & \boldsymbol{\psi}(t-s+1) \end{pmatrix}.$$

λ is the forgetting factor, and $0 \ll \lambda \leq 1$. $\boldsymbol{e}_s(t)$ is the error between the measured $\boldsymbol{y}_s(t)$ and the estimated $\hat{\boldsymbol{y}}_s(t)$, and s is the size of the samples in the batch. The cost index is minimized by a recursive least-squares (RLS) method. In this study, the forgetting factor and the number of the samples in the batch are chosen as 0.99 and 50, respectively. The covariance matrix $\boldsymbol{P}(t)$ is updated by solving equation (5.2–10) using the Woodbury matrix identity (binomial inverse theorem):

$$\boldsymbol{P}(t) = \left(\lambda \boldsymbol{P}(t-1)^{-1} + \boldsymbol{\psi}_s(t) \boldsymbol{\psi}_s(t)^T \right)^{-1} \tag{5.2–10}$$

The Woodbury matrix identity is processed,

$$\left(\boldsymbol{\kappa}(t) + \boldsymbol{\psi}_s(t) \boldsymbol{\psi}_s(t)^T \right)^{-1} = \boldsymbol{\kappa}(t) - \boldsymbol{\kappa}(t) \boldsymbol{\psi}_s(t) \left(\boldsymbol{I} + \boldsymbol{\psi}_s(t)^T \boldsymbol{\kappa}(t) \boldsymbol{\psi}_s(t) \right)^{-1} \boldsymbol{\psi}_s(t)^T \boldsymbol{\kappa}(t) \tag{5.2–11}$$

where

$$\boldsymbol{\kappa}(t) = \lambda^{-1} \boldsymbol{P}(t-1)$$

The parameters of the DEM are updated according to

$$\boldsymbol{\vartheta}(t) = \boldsymbol{\vartheta}(t-1) + \boldsymbol{K}(t) \left(\boldsymbol{y}_s(t)^T - \boldsymbol{\psi}_s(t)^T \boldsymbol{\vartheta}(t-1) \right) \tag{5.2–12}$$

where $\boldsymbol{K}(t) = \boldsymbol{P}(t) \boldsymbol{\psi}_s(t)$ is the RLS gain. The covariance matrix is reset to a predetermined matrix when needed. One way to choose the initial covariance matrix is to set it a very large value times the identity matrix. The estimated parameters are bounded within a given threshold to ensure stable convergence, which is introduced in section 5.2.4.

- Modified Identification Process

The DEM identification can be processed differently depending on the data manipulation. For instance, the DEM for a WPP system can be represented into two DARMA models depending on the choice of POI voltage input. In this case, the characteristic responses of the two models should be the same and so possibly does the parameters corresponding to recursive terms. Then, the two models can be simultaneously developed with two types of terminal voltage inputs. Two DAMRA equations representing the same system can be given as

$$\hat{\boldsymbol{y}}(t) = \sum_{i=1}^{p} \boldsymbol{A}_i \boldsymbol{y}(t-i) + \sum_{j=1}^{2}\sum_{i=0}^{p} \boldsymbol{b}_i^{(j)} \boldsymbol{u}_{(j)}(t-i) + \boldsymbol{k}(t)$$
$$\hat{\boldsymbol{y}}'(t) = \sum_{i=1}^{p} \boldsymbol{A}_i' \boldsymbol{y}'(t-i) + \sum_{j=1}^{2}\sum_{i=0}^{p} \boldsymbol{b}_i'^{(j)} \boldsymbol{u}'_{(j)}(t-i) + \boldsymbol{k}'(t)$$

Both the models represent the same system, that is, if the two models are developed in a same condition and they have the same autoregressive terms (outputs), the system characteristics or dynamics regarding to the autoregressive terms could be the same. Therefore, by choosing the powers as the outputs, it leads to

$$\boldsymbol{A}_i = \boldsymbol{A}_i'$$

Powers for the two models are not necessarily the same as far as they vary around the same operating conditions. However, for simplicity, it is assumed that

$$\boldsymbol{y}(t) = \boldsymbol{y}'(t)$$

As both the models have wind speeds as one of the inputs, the following is obtained from the same reason above: $\boldsymbol{b}_i^{(2)} = \boldsymbol{b}_i'^{(2)}$ and $\boldsymbol{u}_{(2)} = \boldsymbol{u}'_{(2)}$. The voltage inputs for the two DARMA models are different, but the problem can be solved with linearization. The voltage inputs of magnitude and angle are transformed by linearization. Newly obtained dq-axis voltages are

$$\hat{\boldsymbol{u}}_{(1)} = \begin{pmatrix} \Delta\hat{v}_{POId} \\ \Delta\hat{v}_{POIq} \end{pmatrix} = \boldsymbol{T}_o \begin{pmatrix} \Delta v_{\text{mag}} \\ \Delta\theta_v \end{pmatrix}, \text{ where } \boldsymbol{T}_o = \begin{pmatrix} k\,v_{POIdo} & k\,v_{POIqo} \\ -k^2 v_{POIqo} & k^2 v_{POIdo} \end{pmatrix}^{-1} \text{ and } k = \frac{1}{|v_{POIo}|}$$

$\hat{\boldsymbol{u}}_{(1)} = \boldsymbol{T}_o \boldsymbol{u}'_{(1)}$ and it leads to $\boldsymbol{b}_i^{(1)} = \boldsymbol{b}_i'^{(1)} \boldsymbol{T}_o^{-1}$. Finally, from those relations attained above, the original matrix form of DARMA equation can be modified as

$$\boldsymbol{r} \otimes \hat{\boldsymbol{y}}(t) = \boldsymbol{\vartheta}^T \boldsymbol{\psi}(t)$$

where

$$\boldsymbol{\vartheta}^T = (\,\boldsymbol{K} \quad \boldsymbol{B}_0 \quad \boldsymbol{R}_1^T \quad \cdots \quad \boldsymbol{R}_p^T\,),\ \boldsymbol{\psi}(t) = \begin{pmatrix} \boldsymbol{I} \otimes \boldsymbol{1} \\ \tilde{\boldsymbol{F}}(t) \\ \boldsymbol{F}(t-1) \\ \vdots \\ \boldsymbol{F}(t-p) \end{pmatrix}$$

where

$$\boldsymbol{B}_0 = \begin{pmatrix} \boldsymbol{b}_0^{(1)} & \boldsymbol{b}_0^{(2)} \end{pmatrix},\ \boldsymbol{R}_i^T = \begin{pmatrix} \boldsymbol{A}_i & \boldsymbol{b}_i^{(1)} & \boldsymbol{b}_i^{(2)} \end{pmatrix},$$

$$\tilde{\boldsymbol{F}}(t) = \begin{pmatrix} \begin{pmatrix} r\,\boldsymbol{u}_{(1)}(t) & r'\hat{\boldsymbol{u}}_{(1)}(t) \end{pmatrix} \\ \boldsymbol{r} \otimes \boldsymbol{u}_{(2)}(t) \end{pmatrix},\ \boldsymbol{F}(t) = \begin{pmatrix} \boldsymbol{r} \otimes \boldsymbol{y}(t) \\ \begin{pmatrix} r\,\boldsymbol{u}_{(1)}(t) & r'\hat{\boldsymbol{u}}_{(1)}(t) \end{pmatrix} \\ \boldsymbol{r} \otimes \boldsymbol{u}_{(2)}(t) \end{pmatrix},$$

$$\boldsymbol{K} = \begin{pmatrix} \boldsymbol{k} & \boldsymbol{k}' \end{pmatrix},\ \boldsymbol{r} = \begin{pmatrix} r & r' \end{pmatrix},$$

$$\boldsymbol{u}_{(1)} = \begin{pmatrix} \Delta v_{POId} \\ \Delta v_{POIq} \end{pmatrix},\ \boldsymbol{u}'_{(1)} = \begin{pmatrix} \Delta v_{\text{mag}} \\ \Delta\theta_v \end{pmatrix},\ \boldsymbol{u}_{(2)} = \Delta\boldsymbol{w}\,.$$

where r and r' are weights that are simply chosen 1 and 1. The process of parameter identification is performed exactly the same way as the one using Woodbury matrix identify. Once all parameters are identified, the components in the numerator are given, for DARMA model with the input of dq-axis POI voltages

$$\boldsymbol{B}_0 = \begin{pmatrix} \boldsymbol{b}_0^{(1)} & \boldsymbol{b}_0^{(2)} \end{pmatrix},\ \boldsymbol{B}_i = \begin{pmatrix} \boldsymbol{b}_i^{(1)} & \boldsymbol{b}_i^{(2)} \end{pmatrix}$$

And, for the DARMA model with the inputs of POI voltage magnitude and angle

$$\boldsymbol{B}'_0 = \begin{pmatrix} \boldsymbol{T}_o\boldsymbol{b}_0^{(1)} & \boldsymbol{b}_0^{(2)} \end{pmatrix},\ \boldsymbol{B}'_i = \begin{pmatrix} \boldsymbol{T}_o\boldsymbol{b}_i^{(1)} & \boldsymbol{b}_i^{(2)} \end{pmatrix}$$

5.2.3 State Space Representation of DEM

Once the parameter vector $\boldsymbol{\vartheta}$ is properly obtained, the DEM is represented in a state-space form in order to utilize the DEM in power system studies, such as dynamic stability. The DEM is first represented in the observable canonical form of the discrete state space:

$$\boldsymbol{x}_s(k+1) = \boldsymbol{A}_{ds}\boldsymbol{x}_s(k) + \boldsymbol{B}_{ds}\boldsymbol{u}(k) \tag{5.2–12}$$

$$\boldsymbol{y}(k) = \boldsymbol{C}_{ds}\boldsymbol{x}_s(k) + \boldsymbol{D}_{ds}\boldsymbol{u}(k) \tag{5.2–13}$$

where

$$\boldsymbol{A}_{ds} = \begin{pmatrix} -\boldsymbol{A}_1 & \boldsymbol{I} & \cdots & \boldsymbol{0} \\ -\boldsymbol{A}_2 & \boldsymbol{0} & \cdots & \boldsymbol{0} \\ \vdots & \vdots & \ddots & \boldsymbol{I} \\ -\boldsymbol{A}_p & \boldsymbol{0} & \cdots & \boldsymbol{0} \end{pmatrix},\ \boldsymbol{B}_{ds} = \begin{pmatrix} \boldsymbol{B}_1 - \boldsymbol{A}_1\boldsymbol{B}_0 \\ \boldsymbol{B}_2 - \boldsymbol{A}_2\boldsymbol{B}_0 \\ \vdots \\ \boldsymbol{B}_p - \boldsymbol{A}_p\boldsymbol{B}_0 \end{pmatrix},\ \boldsymbol{C}_{ds} = \begin{pmatrix} \boldsymbol{I} & \boldsymbol{0} & \cdots & \boldsymbol{0} \end{pmatrix},\ \boldsymbol{D}_{ds} = \boldsymbol{B}_0\,,$$

$$\boldsymbol{x}_s(k) = \begin{pmatrix} \boldsymbol{x}(k)_{2\times 1} \\ \vdots \\ \boldsymbol{x}(k-p) \end{pmatrix}_{2p\times 1},\ \boldsymbol{u}(k) = \begin{pmatrix} \Delta \boldsymbol{V}_{POI}(k) \\ \Delta \boldsymbol{w}(k) \end{pmatrix}_{(2+n)\times 1},\ \boldsymbol{y}(k) = \Delta \boldsymbol{S}_{POI}(k)$$

The subscript "*ds*" denotes a discrete system. This discrete model is transformed into a corresponding continuous model by using a bilinear transformation (Tustin method) from the *s*-plane to the *z*-plane,

$$s \approx \frac{2}{T_s}\frac{z-1}{z+1} \tag{5.2–14}$$

In this study, the sampling time T_s is set to 0.1s. Applying (5.2–14) to (5.2–12) and (5.2–13), the DEM in a continuous state-space representation is

$$\dot{\boldsymbol{x}}_s(t) = \boldsymbol{A}_{cs}\boldsymbol{x}_s(t) + \boldsymbol{B}_{cs}\boldsymbol{u}(t) \tag{5.2–15}$$

$$\boldsymbol{y}(t) = \boldsymbol{C}_{cs}\boldsymbol{x}_s(t) + \boldsymbol{D}_{cs}\boldsymbol{u}(t) \tag{5.2–16}$$

where

$$\boldsymbol{A}_{cs} = k(\boldsymbol{A}_{ds} - \boldsymbol{I})(\boldsymbol{A}_{ds} + \boldsymbol{I})^{-1},$$

$$\boldsymbol{B}_{cs} = (k\boldsymbol{I} - \boldsymbol{A}_{ds})(\boldsymbol{A}_{ds} + \boldsymbol{I})^{-1}\boldsymbol{B}_{ds}\text{ , where } k = 2\ /\ T_s\ (T_s\text{: sampling time})$$

$$\boldsymbol{C}_{cs} = \boldsymbol{C}_{ds}\,,\ \boldsymbol{D}_{cs} = \boldsymbol{D}_{ds} - \boldsymbol{C}_{ds}(\boldsymbol{A}_{ds} + \boldsymbol{I})^{-1}\boldsymbol{B}_{ds}\,.$$

The subscript "*cs*" denotes a continuous system.

5.2.4 Constraint of Parameters

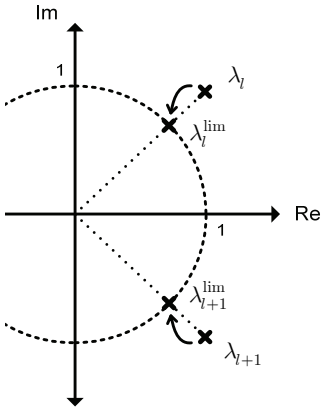

Fig. 4.4 Constraint of parameters

In the middle of parameter identification process, it might be necessary to perform the process stably by setting the roots of DAMRA equation within the unit circle (stable region). This can be done using Eigen-decomposition. Although the Eigen-decomposition requires comparatively large computation, the process can be carried out in a

short time with a computer. Thus, a direct approach of constraining parameters using the Eigen-decomposition is introduced here.

Let us assume that $\boldsymbol{\vartheta}_o(t)$ is the original parameter vector obtained at time instant t, which includes some parameters that make the identification process unstable. It is certain that the parameters making the process unstable are related to the recursive terms. For expressional simplicity, it is assumed that the parameter vector is permuted in the way of

$$\boldsymbol{\vartheta}'_o(t)^T = \begin{pmatrix} \boldsymbol{\vartheta}'_{oA}(t)^T & \boldsymbol{\vartheta}'_{oB}(t)^T \end{pmatrix}, \text{where } \boldsymbol{\vartheta}'_{oA}(t)^T = \begin{pmatrix} \boldsymbol{A}_1(t) & \cdots & \boldsymbol{A}_p(t) \end{pmatrix} \tag{5.2–17}$$

From the parameter vector, the following controllable canonical form is obtained

$$\boldsymbol{A}_o^{(t)} = \begin{pmatrix} -\boldsymbol{A}_1(t) & \cdots & -\boldsymbol{A}_{p-1}(t) & -\boldsymbol{A}_p(t) \\ \boldsymbol{I} & \ddots & \boldsymbol{0} & \boldsymbol{0} \\ \vdots & \cdots & \vdots & \vdots \\ \boldsymbol{0} & \cdots & \boldsymbol{I} & \boldsymbol{0} \end{pmatrix} \tag{5.2–18}$$

The Eigen-decomposition gives the diagonal eigenvalue matrix

$$\boldsymbol{\Lambda} = \boldsymbol{V}^{-1}\boldsymbol{A}_o^{(t)}\boldsymbol{V}, \text{where } \boldsymbol{\Lambda} = \mathrm{diag}\{\lambda_1 \quad \cdots \quad \lambda_l \quad \lambda_{l+1} \quad \cdots \quad \lambda_p\} \tag{5.2–19}$$

$$\boldsymbol{B}_\Lambda = \boldsymbol{V}^{-1}\boldsymbol{B}, \text{where } \boldsymbol{B} = \begin{pmatrix} \boldsymbol{I} & \cdots & \boldsymbol{0} \end{pmatrix}^T \tag{5.2–20}$$

Assuming that λ_l and λ_{l+1} are the unstable eigenvalues with imaginary parts so that the magnitudes of λ_l and λ_{l+1} are larger than 1, these eigenvalues are projected to the unit circle's boundary for the stable identification process, as figure 4.4 shows. In this case, the ratio of real and imaginary components of the eigenvalue is maintained.

$$\lambda_l^{\lim} = e^{j\alpha_l}, \text{where } \alpha_l = \mathrm{ang}(\lambda_l) \tag{5.2–21}$$

$$\lambda_{l+1}^{\lim} = (\lambda_l^{\lim})^* \tag{5.2–22}$$

Next, updated eigenvalue matrix is given

$$\boldsymbol{\Lambda}_{\lim} = \mathrm{diag}\{\lambda_1 \quad \cdots \quad \lambda_l^{\lim} \quad \lambda_{l+1}^{\lim} \quad \cdots \quad \lambda_p\} \tag{5.2–23}$$

Using the controllability matrix, the matrix can be transformed into

$$\boldsymbol{A}_{\lim}^{(t)} = \boldsymbol{Q}^{-1}\boldsymbol{\Lambda}_{\lim}\boldsymbol{Q} \tag{5.2–24}$$

where,

$$\boldsymbol{Q} = \begin{pmatrix} \boldsymbol{B}_\Lambda & \cdots & \boldsymbol{\Lambda}_{\lim}^n\boldsymbol{B}_\Lambda \end{pmatrix}, \ \boldsymbol{A}_{\lim}^{(t)} = \begin{pmatrix} -\boldsymbol{A}_1^{\lim}(t) & \boldsymbol{I} & \cdots & \boldsymbol{0} \\ \vdots & \vdots & \ddots & \vdots \\ -\boldsymbol{A}_{p-1}^{\lim}(t) & \boldsymbol{0} & \cdots & \boldsymbol{I} \\ -\boldsymbol{A}_p^{\lim}(t) & \boldsymbol{0} & \cdots & \boldsymbol{0} \end{pmatrix}$$

Finally, the constrained parameters for $\boldsymbol{\vartheta}'_{oA}(t)$ is obtained from the matrix of $\boldsymbol{A}_{\lim}^{(t)}$

$$\boldsymbol{\vartheta}_A^{\lim}(t)^T = \begin{pmatrix} \boldsymbol{A}_1^{\lim}(t) & \cdots & \boldsymbol{A}_p^{\lim}(t) \end{pmatrix} \tag{5.2–25}$$

Since the other parameters except those regarding to recursive terms should not be constrained in the process, only a part of parameter vector needs to be constrained. This problem can be solved using a projection method [78].

$$\boldsymbol{\vartheta}'(t) = \boldsymbol{\vartheta}'_o(t) + \boldsymbol{P}_1(t)\boldsymbol{P}_{11}(t)^{-1}(\boldsymbol{\vartheta}_A^{\lim}(t) - \boldsymbol{\vartheta}'_{oA}(t)) \tag{5.2–26}$$

where

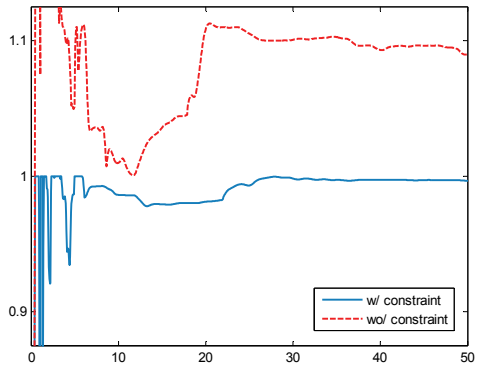

Fig. 4.5 Trajectory of DEM largest eigenvalue's magnitude

$$\boldsymbol{P}(t) = \begin{array}{c} \boldsymbol{P}_1(t) \\ \left(\begin{array}{cc} \boldsymbol{P}_{11}(t) & \boldsymbol{P}_{12}(t) \\ \boldsymbol{P}_{21}(t) & \boldsymbol{P}_{22}(t) \end{array}\right. \end{array} \vdots \left.\begin{array}{c} \\ \left(\begin{array}{c} \boldsymbol{\vartheta}'_{oA}(t) \\ \boldsymbol{\vartheta}'_{oB}(t) \end{array}\right) \end{array}\right)$$

$\boldsymbol{P}(t)$ is the covariance matrix in the equation (5.2–10). $\boldsymbol{P}_1(t)$ and $\boldsymbol{P}_{11}(t)$ are a column matrix and a fragment matrix corresponding to $\boldsymbol{\vartheta}'_{oA}(t)$, respectively. It needs to be cautious that the parameter vector was assumed permuted.

Figure 4.5 shows the result. The identification process is performed twice, with and without the constraint method. In the identification process, the order of DARAM model was chosen unnecessarily large with small forgetting factor and small number of batched samples so that the process is unlikely to be stable. The figure shows the trajectory of an eigenvalue with the largest absolute value. As seen, if the parameters are not constrained, the eigenvalue exceeds unity over the process so the parameters obtained are expected less useful. In contrast, when the parameters are constrained, the eigenvalue is always less than unity and the parameters obtained in the process are likely satisfactory.

5.2.5 Noise-Like Fast Dynamics Excursion

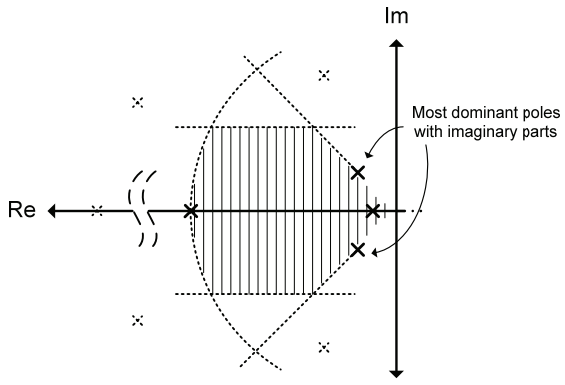

Fig. 4.6 Construction of region that eigenvalues are remained

When identifying the parameters of the DEM, setting the DEM to a high order might provide seemingly finer results such that the error between the original model and the DEM is lower. However, in this case, it is more likely that the DEM has redundant and unnecessarily fast dynamics that generate high-frequency noise. Therefore, if the order of the DEM is initially set high to capture as much dynamic performance as possible, the eigenvalues are examined after identifying the parameters of the DEM and then eigenvalues related to high frequency modes are removed using modal analysis since we are interested in the slow system electromechanical dynamics. The modal method is carried out by converting the DEM in continuous canonical form to the respective modal form and properly removing some of the eigenvalues. The way of eigenvalue removal was explained in sub-subsection 3.1.1.2.

There are reasons for this process: 1. The dynamics of the network are typically ignored in a slow dynamic study such that a static network model is used. However, the line inductance and capacitance in the network function as filters that eliminate high-frequency components in real circumstances. Thus, a DEM for slow dynamic study should not generate unnecessary fast dynamics that are expected to be damped out quickly and to not exist in the slow dynamic study. 2. Wind turbines, especially those with power converters, typically have a capacitor with a damping resistance at the terminal to prevent a high-frequency component from being injected into the main network. 3. Because of the aliasing effect that occurs when sampling the data, the existing frequency components greater than half the sampling frequency are unreliable. Thus, these frequency components need to be removed if the DEM is identified as generating fast dynamics.

The region is constructed by the modal method: the most dominant poles with imaginary parts were first identified. Then, a trajectory from the origin point to the eigenvalues is extended as shown in figure 4.6. Next step is to identify the least dominant eigenvalue to be kept. Then, an arc is constructed, of which center is the point of origin. The region that is bounded by the trajectories and the arc contains the eigenvalues of the reduced order DEM. One more consideration is when the frequency components are greater than half the sampling frequency, the described method could include inaccurate fast dynamics in the DEM. Thus, these frequency components need to be removed by restricting the described region between the horizontal lines in figure. 4.6, which are selected accordingly to the sampling frequency. This way, we can obtain the reduced order DEM suitable for power system dynamic studies.

5.2.6 Input and Output Modification

After the DEM has been developed, the DEM's input and output can be altered with simple matrix manipulation if necessary. For instance, the DEM can be modified so that real power and voltage magnitude are produced when reactive power and voltage angle are provided. Assuming that the inputs are POI voltage's magnitude and angle (with constant wind speeds) and the outputs are real and reactive powers,

$$\begin{pmatrix} \Delta P_{POI} \\ \Delta Q_{POI} \end{pmatrix} = \boldsymbol{C}_{cs}\boldsymbol{x}(k) + \boldsymbol{D}_{cs}\begin{pmatrix} \Delta v_{\mathrm{mag}} \\ \Delta \theta_v \end{pmatrix} \tag{5.2–27}$$

Manipulating the equation (5.3–27), the following two equations are obtained.

$$\begin{pmatrix} \Delta v_{\mathrm{mag}} \\ \Delta \theta_v \end{pmatrix} = \boldsymbol{K}_1\boldsymbol{x}(k) + \boldsymbol{K}_2\begin{pmatrix} \Delta Q_{POI} \\ \Delta \theta_v \end{pmatrix} \text{ and } \begin{pmatrix} \Delta P_{POI} \\ \Delta v_{\mathrm{mag}} \end{pmatrix} = \boldsymbol{C}'_{cs}\boldsymbol{x}(k) + \boldsymbol{D}'_{cs}\begin{pmatrix} \Delta Q_{POI} \\ \Delta \theta_v \end{pmatrix} \tag{5.2–28}$$

Substituting the first into an original state space equation gives new state space equation and the second is used for new output equation. Likewise, the DEM can also be modified in various forms of state space equations.

5.3 Nonlinear DEM Development

In this section, the nonlinear DEM is developed using a recurrent neural network. Neural networks include

nonlinear activation function in perceptron of hidden layers and thus provide some nonlinearity into the DEM [79]. On the other hand, the nonlinear functions make it difficult to determine whether or not the DEM stable. The DEM must be stable before applying it to power system dynamic study. Therefore, in order to avoid the problem, a recurrent network, of which output is bypassed to the output layer without linking it with the hidden layer, will be used. The following subsections explain the DEM development process.

5.3.1 Normalization

Neural network requires data normalization to produce better performance of both implementation and the training process. The network inputs and outputs are scaled by either the method of range or variance normalization. The normalization can be expressed as:

$$x_{\text{scaled}} = ax + b \tag{5.3–1}$$

The range normalization is performed by mapping the minimum and maximum of corresponding data to -1 and +1, respectively, and mapping the data between the extremes between -1 and +1, accordingly. For this method,

$$a = 2/(x_{\max} - x_{\min}),\ b = -(x_{\max} + x_{\min})/(x_{\max} - x_{\min}) \tag{5.3–2}$$

On the other hand, the variance normalization is carried out by subtracting the mean from corresponding data and dividing it by its standard deviation, where

$$a = 1/x_{\text{std}},\ b = -x_{\text{mean}}/x_{\text{std}} \tag{5.3–3}$$

5.3.2 Neural Network DEM Structure

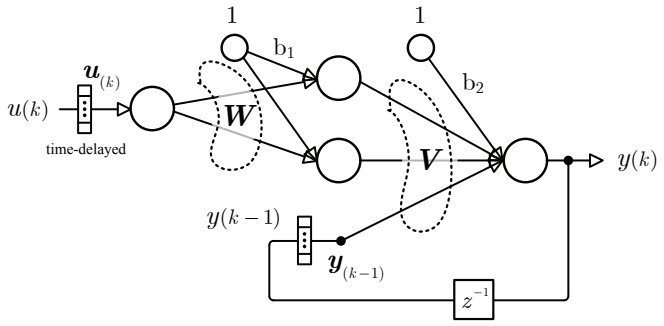

Fig. 4.7 Neural network DEM structure

Figure 4.7 shows the neural network DEM structure. Network input is $u(k)$ and is reproduced by being sample-delayed, according to DEM order. The output is also fed back by a sample-delaying and reproduced accordingly. The results are

$$\boldsymbol{u}_{(k)} = \begin{pmatrix} u(k) \\ \vdots \\ u(k-p) \end{pmatrix}_{2(p+1)\times 1},\ \boldsymbol{y}_{(k-1)} = \begin{pmatrix} y(k-1) \\ \vdots \\ y(k-p) \end{pmatrix}_{2p\times 1} \tag{5.3–4}$$

where $2p$ is the DEM order. The inputs and outputs of hidden layer are represented as

$$\boldsymbol{n}_{et} = \boldsymbol{W}_{h\times(2p+2)}\boldsymbol{u}_{(k)} + \boldsymbol{b}_1 \tag{5.3–5}$$

$$\boldsymbol{h}_o = f(\boldsymbol{n}_{et}) \tag{5.3–6}$$

where $\boldsymbol{n}_{et}$ is a hidden layer net input and $\boldsymbol{h}_o$ is a hidden layer output. $\boldsymbol{W}$ and $\boldsymbol{b}_1$ are weight matrices related to the reproduced network inputs and the bias term, respectively, and $f(\cdot)$ means activation function. Linear and nonlinear activation functions can be used together. h is the number of hidden layer perceptron. The outputs are

$$\boldsymbol{y}(k) = \boldsymbol{V}_{2\times(h+2p)}\boldsymbol{v} + \boldsymbol{b}_2 \tag{5.3–7}$$

where

$$\boldsymbol{V} = (\boldsymbol{V}_a \quad \boldsymbol{V}_b) \text{ and } \boldsymbol{v} = \begin{pmatrix} \boldsymbol{h}_o \\ \boldsymbol{y}_{(k-1)} \end{pmatrix}$$

where $\boldsymbol{V}$ is weight matrix related to hidden layer outputs and network outputs. $\boldsymbol{b}_2$ is weight for the bias term. As seen, the output is fed back without passing through a hidden layer perceptron. Therefore, the DEM stability can be checked by observing eigenvalues of DEM system matrix below, which provides the information for DEM convergence.

$$\boldsymbol{A}_{ds} = \begin{pmatrix} \boldsymbol{V}_b \\ (\boldsymbol{I} \quad \boldsymbol{0}) \end{pmatrix}_{2p\times 2p} \tag{5.3–8}$$

5.3.3 Network Training

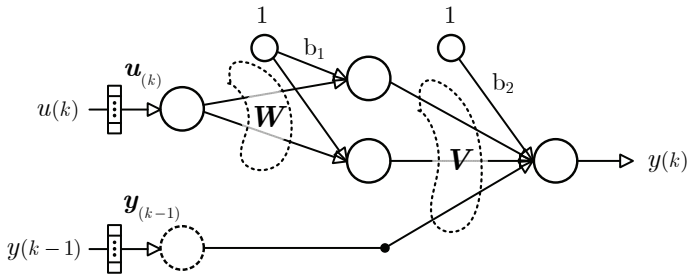

Fig. 4.8 Neural network for training process

Training is the process of obtaining the weight matrices $\boldsymbol{W}$, $\boldsymbol{V}$, $\boldsymbol{b}_1$, and $\boldsymbol{b}_2$. For training, a feed-forward network is used instead of a recurrent network. The network inputs are DEM inputs and outputs that are one sample delayed and reproduced according to DEM order. To identify the parameter matrices, a Levenberg-Marguardt algorithm is used. The procedure is as follows.

The error between each target and network output for pattern k is defined as

$$e_{k,j} = \frac{\lambda^{(N-k)}}{2N}(t_j(k) - y_j(k))^2, \text{ where } j = 1, 2 \tag{5.3–9}$$

The error vector is organized as

$$\boldsymbol{e} = \begin{pmatrix} \boldsymbol{e}_1 \\ \vdots \\ \boldsymbol{e}_N \end{pmatrix}, \text{ where } \boldsymbol{e}_k = \begin{pmatrix} e_{k,1} \\ e_{k,2} \end{pmatrix} \tag{5.3–10}$$

where N is total number of patterns (samples) for training and λ is the forgetting factor. The weight matrices in (5.3–5) and (5.3–7) are decomposed into several column vectors:

$$\boldsymbol{W} = \begin{pmatrix} \boldsymbol{w}_1 & \cdots & \boldsymbol{w}_{n_w} \end{pmatrix}_{h \times n_w (n_w = 2p+2)}, \; \boldsymbol{V} = \begin{pmatrix} \boldsymbol{v}_1 & \cdots & \boldsymbol{v}_{n_v} \end{pmatrix}_{2 \times n_v (n_v = h+2p)},$$

Then, the weight vector is organized accordingly.

$$\mathbf{w} = \begin{pmatrix} \boldsymbol{w}_1 \\ \vdots \\ \boldsymbol{w}_{n_w} \\ \boldsymbol{b}_1 \\ \boldsymbol{v}_1 \\ \vdots \\ \boldsymbol{v}_{n_v} \\ \boldsymbol{b}_2 \end{pmatrix}_{L \times 1 (L = n_w + h + n_v + 2)} \tag{5.3–11}$$

The variation of the weight vector is related to the error vector by a Jacobian matrix:

$$\boldsymbol{J} \Delta \mathbf{w} = -\boldsymbol{e} \tag{5.3–12}$$

Using the left inverse of the Jacobian matrix, the weight vector is iteratively updated:

$$\mathbf{w}^{(i+1)} = \mathbf{w}^{(i)} - (\mu I + \boldsymbol{J}_{(i)}^T \boldsymbol{J}_{(i)})^{-1} \boldsymbol{J}_{(i)}^T \boldsymbol{e}_{(i)} \tag{5.3–13}$$

where

$$\boldsymbol{J} = \begin{pmatrix} \frac{\partial e_{1,1}}{\partial \mathrm{w}_1} & \cdots & \frac{\partial e_{1,1}}{\partial \mathrm{w}_L} \\ \vdots & \ddots & \vdots \\ \frac{\partial e_{N,2}}{\partial \mathrm{w}_1} & \cdots & \frac{\partial e_{N,2}}{\partial \mathrm{w}_L} \end{pmatrix}$$

where i in the bracket is iteration number and $\boldsymbol{J}$ is the Jacobian matrix with respect to the error and the weight vectors. As noted in (5.3–13), by adding small residual μ, the left inverse of Jacobian matrix always exists and is called the Levenberg-Marguardt training method. One cumbersome issue in this method is calculating the Jacobian matrix obtained by back-propagation and the chain rule. It is explained in [79]. The parameter constraint can be performed in the same way explained in the subsection 5.2.4.

Although the nonlinear DEM provides more accurate performance in fitting with given training data, the neural network must be trained on large sets of training data to guarantee the well-generalized performance of the DEM: that is, the process needs huge computations. Besides, training the nonlinear neural network using the Levenberg-Marguardt algorithm requires large iteration process while the RLS method does not. Therefore, we have only introduced the nonlinear DEM as a comparable DEM development method in this study.

5.4 Simulations

The performance of the proposed linear DEM is verified by simulation tests. The simulation tests in this chapter, however, only focus on 1) the dynamic performance of the DEM and 2) the adaptiveness of the DEM identification.

The validity of the DEM's interaction with the power system will be verified in chapter 7.

- Nonlinear wind turbine models

To verify the adaptiveness of the DEM identification, the original system to collect data from it and to be compared with the DEM should be smoothly transitioned from one operational condition to another, and thus nonlinear models are required. In the simulation, nonlinear models of wind turbines are used to collect the data required for the DEM identification. The nonlinear model of wind turbines consists of several linear and nonlinear dynamic models and static models, which are interconnected and work together. The models are, for instance, static nonlinear wind model, linear dynamic drive train model, nonlinear dynamic generator model, nonlinear dynamic power converters model, power converters control part (digital), and pitch angle control part. These models were described in chapter 2, but none of nonlinear terms are linearized. Unlike linear models, it is highly difficult to aggregate nonlinear models into a single form due to nonlinear (or logical) components such as limiters in control parts. Therefore, separate multiple nonlinear models each of which are decomposed into two parts: linear dynamic models and nonlinear (or logical) parts.

Figure 4.1s offers an example of a nonlinear type 3 wind turbine model, which is constructed using Simulink in the MATLAB program. The figure shows a blade power model with pitch angle control, drive train model, generator model, converter model, and control part. In the blade power model, wind power captured by blades is a function of wind speed, rotor blade speed, and pitch angle. The pitch angle is generated by PI controller of which the

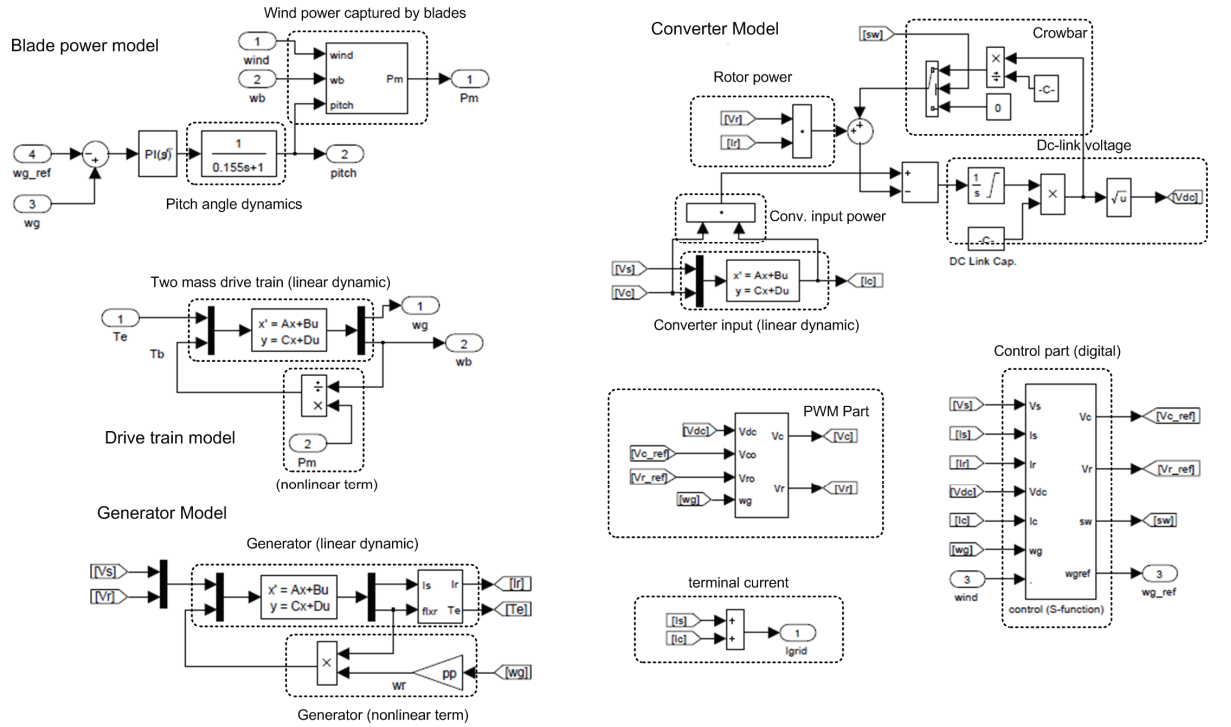

Fig. 4.1s Nonlinear models of a type 3 wind turbine (MATLAB)

output is restricted over zero. The dynamics of pitch angle mechanism is simplified with a first order low pass filter. Nonlinear dynamic models of generator and drive train consist of linear dynamic models and nonlinear terms fed back to the linear models. In the back-to-back converters, the dc-link voltage dynamics are modeled with additional nonlinear parts owing to the condition of dc being larger than zero and the crowbar connected in parallel at the dc-link capacitor. Also, the converter input and output voltages in magnitude are restricted by dc-link voltage, which is modeled using a PWM part. Terminal current is the sum of stator and converter input currents. The controls of the wind turbine are performed using the method introduced in the chapter 4, and they are digitally programmed with S-functions of MATLAB.

5.4.1 Test System

For the simulation, the WPP consists of 49 wind turbines (28 × type 1 and 21 × type 3) that are irregularly placed, as figure 4.2s shows. The base power for each turbine is 2 MVA, and the reactive power of any type 3 turbine is controlled to be 0.3 pu. Wind turbines standing in the first column in the wind direction initially face 13.5-m/s upstream wind speeds, and the other wind turbines behind the first column face wind speeds of approximately 11.5 to 12 m/s. The rated wind speed for the wind turbines is chosen to be 14 m/s; thus, all wind turbines have initial pitch angle of 0°. These wind turbines are clustered according to their types and wind speeds. In this work, the linkage clustering method is used, and the wind turbines are clustered in four groups such that the number of equivalent wind speeds is only four.

The nonlinear model of type 1 turbine has 9 state variables while type 3 has 12, including the pitch angle mechanism, and thus the WPP has 504 state variables.

The DEM for the WPP is identified by using a natural disturbance of wind. This DEM is adaptively adjusted according to variations in forthcoming wind speed.

To test the adaptive performance of the DEM, we assumed that upstream wind speed is increased from 13.5 m/s to 17 m/s, and the downstream wind speed is increased to approximately 15.5 m/s. In this case, all wind turbines have their pitch angles adjusted. Thus, the operating conditions are altered.

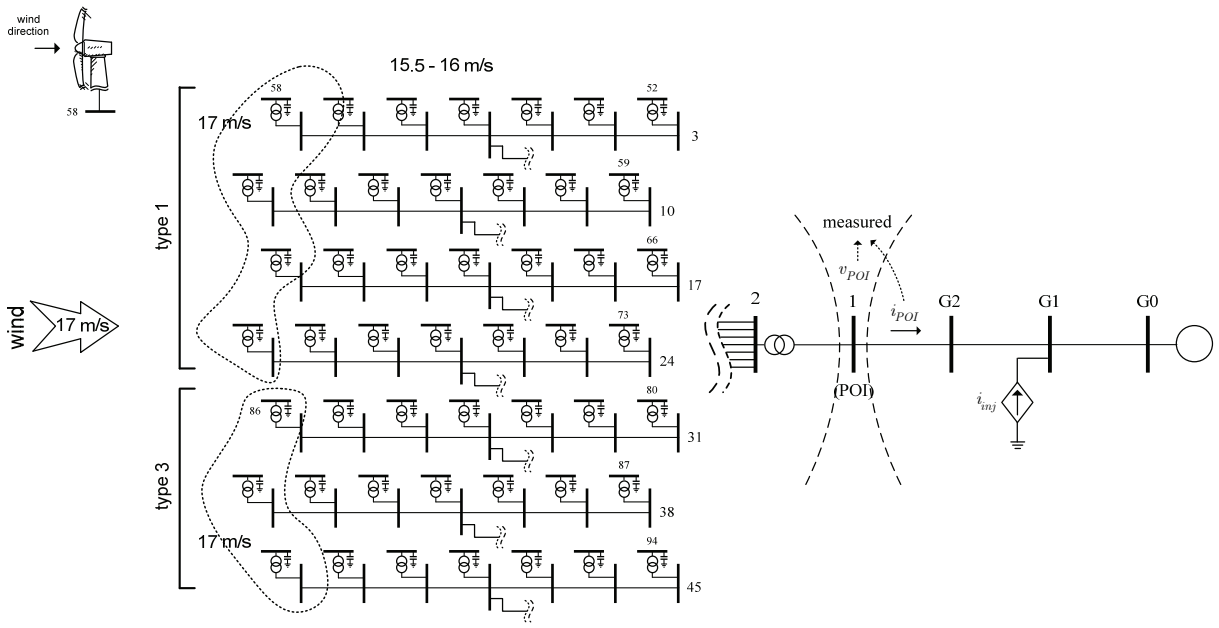

Fig. 4.2s WPP clustered into 4 groups

5.4.2 Results

Figure 4.3s shows the data for wind speed, real power, and reactive power of each of the 49 turbines. Figure 4.4s shows the voltages and powers at POI. These data are used in lieu of measurements.

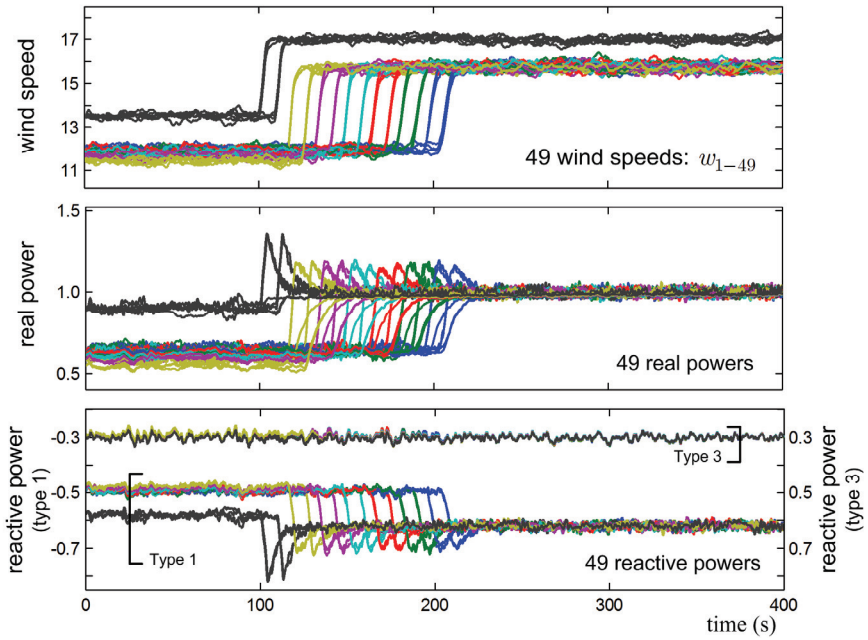

Fig 4.3s. 49 wind speeds (m/s), real and reactive powers generated by the 49 wind turbines.

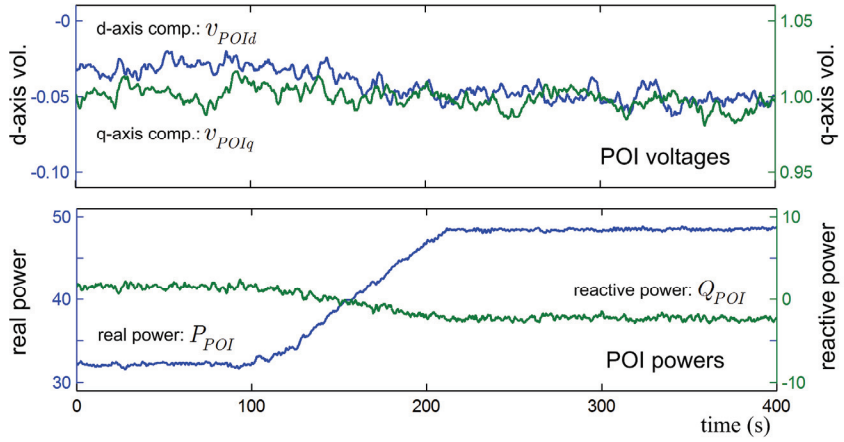

Fig. 4.4s. Voltages and powers at POI

Figure 4.5s shows the variations of the four equivalent wind speeds, the voltages and the powers at POI. These data are used as the inputs and outputs of the DEM. Figure 4.6s shows examples of trajectories of two parameters. When the parameters of the DEM change due to variations in wind speed, the DEM is updated with the new parameters.

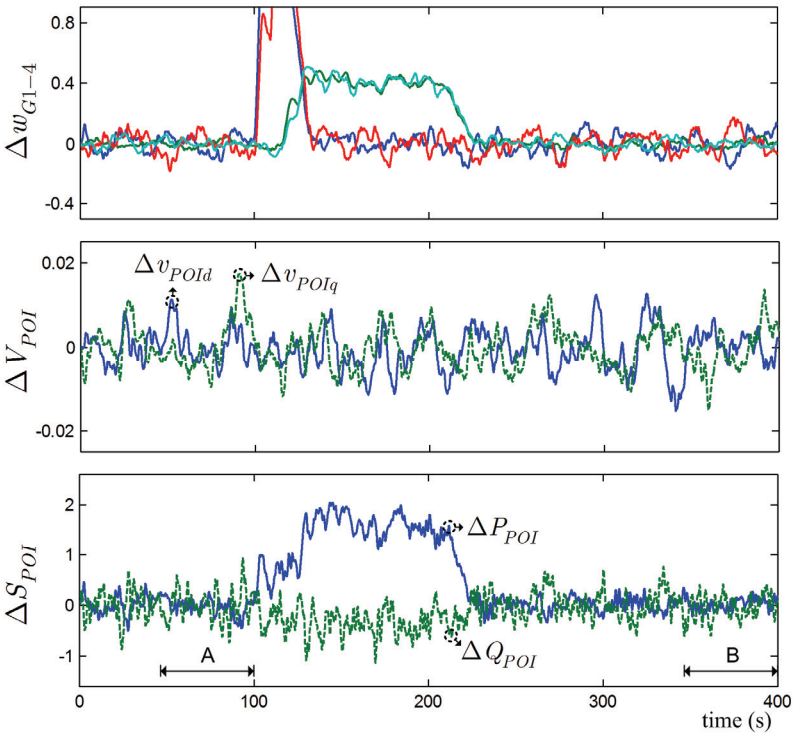

Fig. 4.5s. Data used as the inputs and outputs in the DEM identification process.

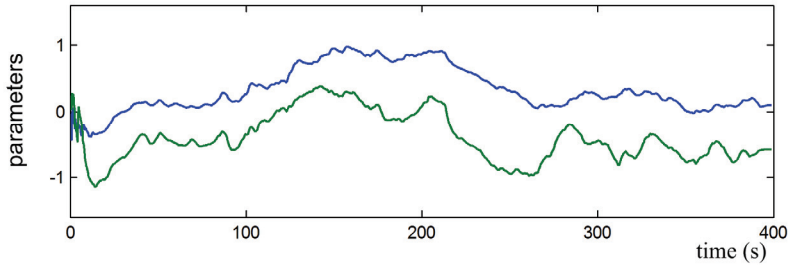

Fig. 4.6s. Trajectories of two parameters.

The DEM was tested under various operating conditions. Two of these tests are done for region of A and B in Figure 4.5s. Figure 4.7s shows the real and reactive powers at POI of the original nonlinear system and that of the DEM for region A. The figure also shows the error in both powers. Figure 4.8s shows the same test for region B. These tests show that the DEM is highly accurate and is adaptive.

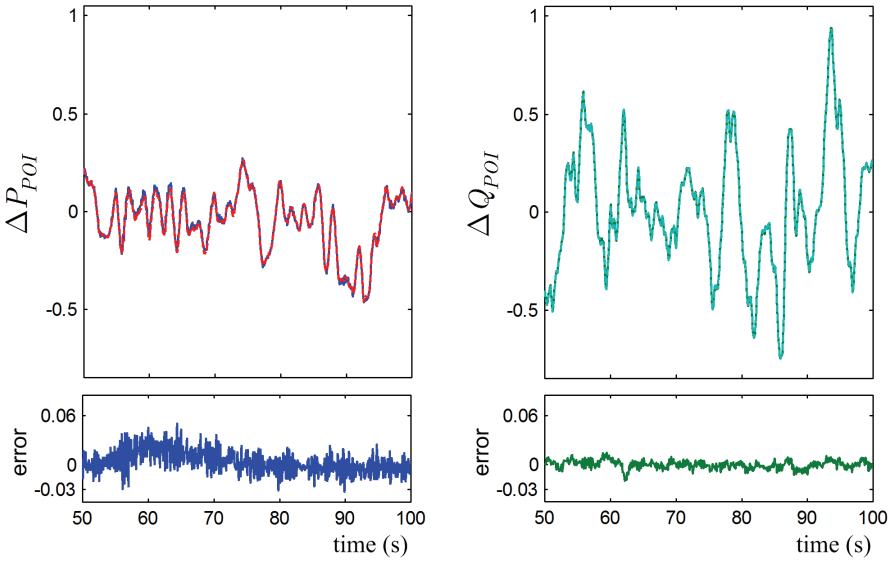

Fig. 4.7s. Dynamic performance of the DEM compared with the WPP for region A in Fig. 4.5s.

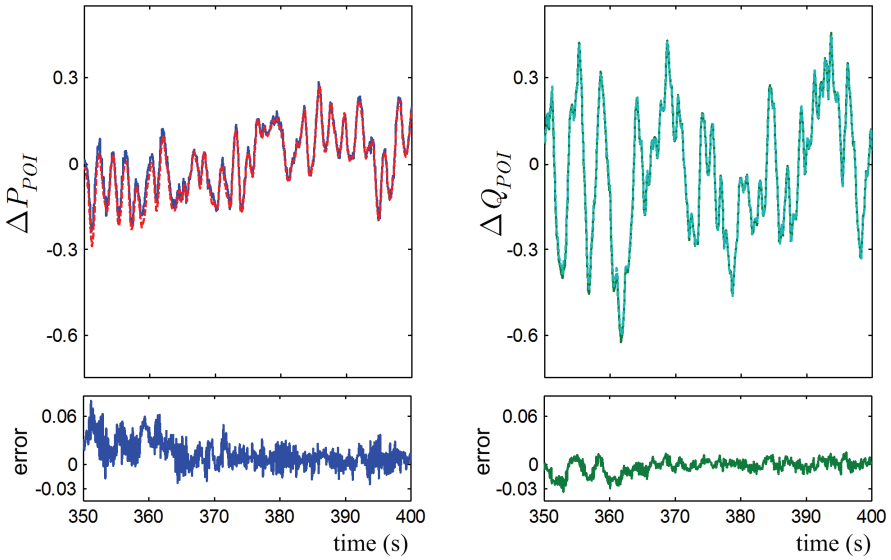

Fig. 4.8s. Dynamic performance of the DEM compared with the WPP for region B in Fig. 4.5s.

To test the validity of the DEM under different type of disturbance, we performed the test in figure 4.9s. The system is disturbed due to a sudden change in the POI bus voltage while the wind speeds are maintained constant. The parameters of the DEM are the same as those of the DEM in figure 4.8s. The results are shown in three different time durations. In subfigures C and D, we observe that the WPP and the DEM react differently; however, the dynamics relate to fast transients that are not important in this study. Besides, because the original system is nonlinear; it is expected to respond differently from the linear DEM. Nevertheless, subfigure C reveals, after the initial fast transients have subsided, the DEM matches the dynamics of the WPP, which proves the DEM is accurate under the different types of disturbances.

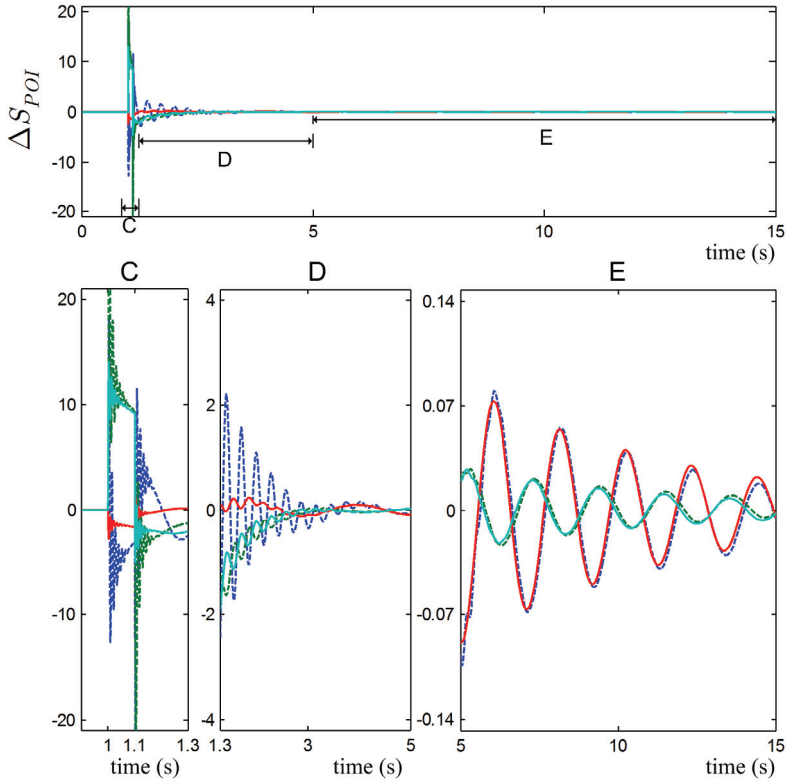

Fig. 4.9s Dynamic performance of the DEM compared with the WPP (nonlinear) when the POI voltage drops in magnitude by 0.1 pu for 0.1 s.

5.5 Conclusions

This chapter proposed a linear DEM development technique for a WPP system. It developed the linear DEM using the RLS method. The proposed technique was carried out adaptively and only required the data of the inputs and outputs to identify the DEM. Additionally, this chapter introduced a nonlinear DEM development technique using a neural network. It was noted that the nonlinear method requires huge computation in the training process so it was remained as a comparable method. Simulation results verified the validity of the proposed method showing that the proposed method significantly reduced the order of the system without sacrificing accuracy.

There are remained tests to confirm the DEM has the same effects on power system dynamics as the WPP. These tests, performed in chapter 7, will use the DEM interacted with power systems.

Chapter 6

Power System Modeling

This chapter models a power system in dq-representation. The dq-representation is categorized in two ways using different frames: a dq-frame (q-axis leading d-axis) and a qd-frame (d-axis leading q-axis). Power systems are typically modeled in the qd-frame. In the previous chapters, the WPP model has been developed in the dq-frame. To avoid confusion between the representations and to clarify the difference between dq-frame and qd-frame, all models of generator, governor, excitation system, power system stabilizer, and network in power systems are developed in the dq-frame.

The model of a generating unit consists of the models of generator, governor, excitation system, and power system stabilizer. The models of generating units and network are combined to represent a power system. Before integrating generating units with a network model, the stability of a network is checked using its dynamic model. Also, the stability of the power system is strengthened by applying power system stabilizers to some of the generating units in the power system. The adequacy of modeling and control method is tested using the IEEE 39 bus power system. Once the adequacy is proven, the power system developed in this chapter will be used in the next chapter to verify the validity of the WPP DEM.

6.1 Modeling of Generating Units

6.1.1 Modeling of Generating Units in Dq-frame

The modeling of a generating unit in dq-representation can be performed into two ways. In the first general way, the model of a generating unit is obtained using the Park's transformation that has q-axis lagging d-axis so that d- and q-axis components correspond to imaginary and real parts, respectively. In the other way, the model is expressed in a frame where the q-axis leading the d-axis. To distinguish the two presentations, the first is called qd-frame and the second is called dq-frame.

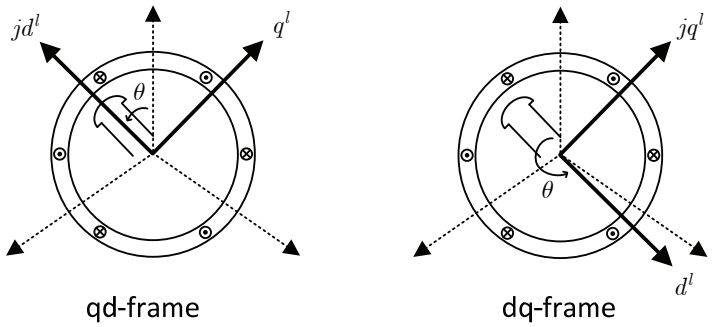

Fig. 5.1 Generator cross section represented in qd-frame and in dq-frame.

In the previous chapters, the WPP model has been developed in the dq-frame. To make it consistent with respect to the model representation, this chapter briefly introduces the model development of generating units in the dq-frame. A generating unit is typically developed with the Park's transformation in the qd-frame. There is not much difference between the models developed in either the qd- or dq-frame. However, the model developed in one of the frames has different signs from the other model in its model parameters. In both representations, the q-axis internal voltage should be aligned with the q-axis so that the q-axes in both frames are the same but their d-axes are in opposite. In other words, the d-axis aligns with the rotor but with a different part of pole. Rotating speeds of the rotor and the frame are the same. Figure 5.1 shows the difference between the qd- and dq-frame.

The voltage equation of a generator, which is represented in the qd-frame, is given from [80], [81] as

$$\Delta \boldsymbol{v}^{l(qd)} = -\big(\boldsymbol{R} + \omega_u \boldsymbol{N}^{(qd)}\big)\Delta \boldsymbol{i}^{l(qd)} - \frac{1}{\omega_B}\boldsymbol{L}^{(qd)}\Delta \dot{\boldsymbol{i}}^{l(qd)} \tag{6.1–1}$$

where

$$\boldsymbol{v}^{l(qd)} = \begin{pmatrix} v_{td}^{l(qd)} \\ v_{tq}^{l(qd)} \\ -v_F^{(qd)} \\ v_D^{(qd)}(=0) \\ v_Q^{(qd)}(=0) \end{pmatrix},\ \boldsymbol{i}^{l(qd)} = \begin{pmatrix} i_{td}^{l(qd)} \\ i_{tq}^{l(qd)} \\ i_F^{(qd)} \\ i_D^{(qd)} \\ i_Q^{(qd)} \end{pmatrix}$$

v_t and i_t are terminal voltage and armature current. v_F and i_F are field voltage and current. v_D, v_Q, i_D, and i_Q are the voltages and currents of d-axis and q-axis damping winding, respectively. The variables of terminal voltages and currents in the local frame have been denoted with superscript *l*. Reminding of the fact $f^{(qd)} = f_q^{(qd)} + jf_d^{(qd)}$ and $f^{(dq)} = f_d^{(dq)} + jf_q^{(dq)}$, the d- and q-axis components in the dq-frame can be changed from those in the qd-frame as

$$\begin{pmatrix} f_d^{(dq)} \\ f_q^{(dq)} \end{pmatrix} = \begin{pmatrix} -1 & 0 \\ 0 & 1 \end{pmatrix}\begin{pmatrix} f_d^{(qd)} \\ f_q^{(qd)} \end{pmatrix} \tag{6.1–2}$$

Because of the difference between the qd- and dq-frames, the terminal voltage $v_t^{(qd)}$ and armature current $i_t^{(qd)}$, which flows through the terminal, are needed to be changed. Using the transformation, the voltage equation in the qd-frame is transformed into one in the dq-frame

$$\Delta \boldsymbol{v}^{l} = -\big(\boldsymbol{R} + \omega_u \boldsymbol{N}\big)\Delta \boldsymbol{i}^{l} - \frac{1}{\omega_B}\boldsymbol{L}\Delta \dot{\boldsymbol{i}}^{l} \tag{6.1–3}$$

where

$$\boldsymbol{N} = \boldsymbol{P}\boldsymbol{N}^{(qd)}\boldsymbol{P}^{-1},\ \boldsymbol{L} = \boldsymbol{P}\boldsymbol{L}^{(qd)}\boldsymbol{P}^{-1},\ \boldsymbol{P} = \mathrm{diag}\{\text{-}1,\ 1,\ 1,\ 1,\ 1\}$$

Since the model of a generating unit is developed in its local frame rotating at the speed of its rotor, the angle difference between the local frame and the global frame, which will be called power angle, is required when interfacing with the other models that are also developed using their own local frames.

By subtracting the angle of global frame $\theta^g = \omega^g t + \theta_0^g$ from the angle of local frame $\theta^l = \omega t + \theta_0^l$, the equation of power angle δ is obtained

$$\tfrac{1}{\omega_B}\Delta\dot{\delta} = \Delta\omega - \Delta\omega^g, \text{ where } \delta = \theta^l - \theta^g \tag{6.1–4}$$

The power angle δ in the equation (6.1–4) is the same as the angle between the local frame and the global frame, where the global frame rotates in the synchronous speed ω^g. The synchronous speed is generally assumed constant ($\Delta\omega^g = 0$) when developing an individual generating unit's model. However, when interfacing the model with the other models, one of generating units will be selected as the reference unit so that the synchronous speed will be the

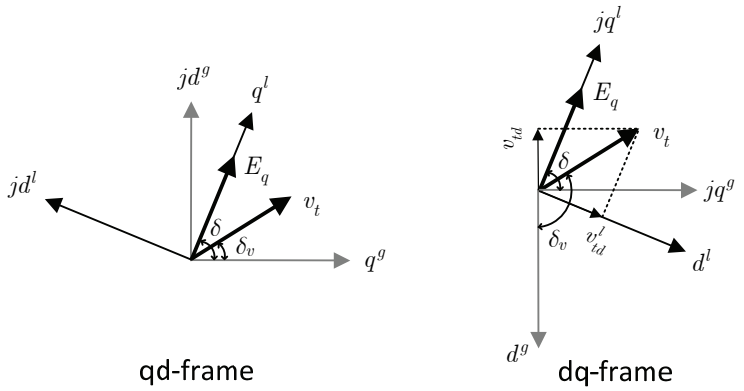

Fig. 5.2 Internal (q-axis) and terminal voltages represented in qd-frame and in dq-frame.

same as the reference unit's rotor speed. In this case, the power angle equation of the reference generating unit will be $\Delta\dot{\delta} = 0$ because its rotor speed is instantaneously the same as the synchronous speed. With torque equation given in [80], of which the signs are properly altered, a generating unit's dq-representation is obtained as

$$\dot{\boldsymbol{x}}_g^l = \boldsymbol{A}_g^l \boldsymbol{x}_g^l + \boldsymbol{B}_g^l \boldsymbol{u}_g^l \tag{6.1–5}$$

where

$$\boldsymbol{x}_g^l = (\Delta i_{td}^l \;\; \Delta i_{tq}^l \;\; \Delta i_F \;\; \Delta i_D \;\; \Delta i_Q \;\; \Delta\omega \;\; \Delta\delta)^T,$$

$$\boldsymbol{u}_g^l = (\Delta v_{td}^l \;\; \Delta v_{tq}^l \;\; \Delta v_F \;\; \Delta T_m)^T.$$

Once the power angle is given, the vectors of terminal voltages and currents can be expressed in the global frame and be interconnected with the other generating units by transmission lines. They can be transformed into the corresponding vectors in the global frame using the following equations.

$$v_{dq}^l = e^{-j\delta} v_{tdq} \text{ and } i_{dq} = e^{j\delta} i_{dq}^l \tag{6.1–6}$$

Linearizing the equations and expressing in matrix forms,

$$\begin{pmatrix} \Delta v_{td}^l \\ \Delta v_{tq}^l \end{pmatrix} = \begin{pmatrix} v_{tqo}^l \\ -v_{tdo}^l \end{pmatrix} \Delta\delta + \boldsymbol{T}^{-1}(\delta_o) \begin{pmatrix} \Delta v_{td} \\ \Delta v_{tq} \end{pmatrix} \tag{6.1–7}$$

$$\begin{pmatrix} \Delta i_{td} \\ \Delta i_{tq} \end{pmatrix} = \begin{pmatrix} -i_{tqo} \\ i_{tdo} \end{pmatrix} \Delta\delta + \boldsymbol{T}(\delta_o) \begin{pmatrix} \Delta i_{td}^l \\ \Delta i_{tq}^l \end{pmatrix} \tag{6.1–8}$$

where

$$\boldsymbol{T}(\delta_o) = \begin{pmatrix} \cos\delta_o & -\sin\delta_o \\ \sin\delta_o & \cos\delta_o \end{pmatrix},$$

$$\delta_o = \text{angle}(E_{qo}) - \pi / 2,$$

$$E_{qo} = v_{to} + jx_q i_{to}.$$

Using the equations (6.1–7) and (6.1–8), the model has been properly transformed into the one represented in the global frame as

$$\dot{\boldsymbol{x}}_g = \boldsymbol{A}_g \boldsymbol{x}_g + \boldsymbol{B}_g \boldsymbol{u}_g \tag{6.1–9}$$

where

$$\boldsymbol{x}_g = (\,\Delta i_{td}\ \ \Delta i_{tq}\ \ \Delta i_F\ \ \Delta i_D\ \ \Delta i_Q\ \ \Delta\omega\ \ \Delta\delta\,)^T\,,$$
$$\boldsymbol{u}_g = (\,\Delta v_{td}\ \ \Delta v_{tq}\ \ \Delta v_F\ \ \Delta T_m\,)^T$$

A generating unit generally includes turbine governor and excitation system. So, they should be included in the model. Their block diagrams are shown in figure 5.3 and 5.4.

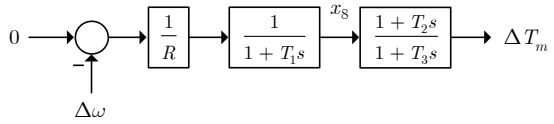

Fig. 5.3 Turbine governor

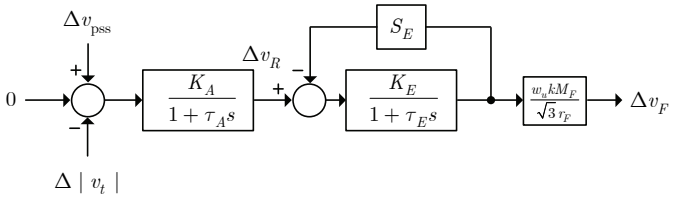

Fig. 5.4 Excitation system

The excitation system in figure 5.4 uses two different values in the place of the parameter S_E with respect to the exciter saturation, that is, a value for the desaturation mode and another value for the saturation mode. The mode is determined in terms of the magnitude of the internal voltage or the field voltage. The magnitude of terminal voltage to be feedback-controlled in the excitation system is linearized and interconnected with the equation (6.1–9) using

$$\Delta\left|v_t\right| = \tfrac{1}{\left|v_{to}\right|}(v_{tdo}\Delta v_{td} + v_{tqo}\Delta v_{tq}) \tag{6.1–10}$$

Finally, the model of a generating unit including turbine governor and excitation system is completed as

$$\dot{\boldsymbol{x}}_{gen} = \boldsymbol{A}_{gen}\boldsymbol{x}_{gen} + \boldsymbol{B}_{gen}\boldsymbol{u}_{gen} + \boldsymbol{B}_{\text{pss}}\Delta v_{\text{pss}} \tag{6.1–11}$$

where

$$\boldsymbol{x}_{gen} = (\,\boldsymbol{x}_g\ \ x_8\ \ x_9\ \ \Delta v_R\ \ \Delta v_F\,)^T,\ \boldsymbol{u}_{gen} = (\,\Delta v_{td}\ \ \Delta v_{tq}\,)^T$$

The number of state variables in this model is 11. Among these, the state variables of rotor speed and power angle are related to the dominant slow electromechanical dynamics. The dynamics related to the other state variables can be ignored and the model can be properly reduced by the aggregation technique.

$$\dot{\boldsymbol{x}}_{rg} = \boldsymbol{A}_{rg}\boldsymbol{x}_{rg} + \boldsymbol{B}_{rg}\boldsymbol{u}_{gen} + \boldsymbol{B}_{rg\text{-pss}}\Delta v_{\text{pss}} \tag{6.1–12}$$

$$\boldsymbol{y}_{gen} = \boldsymbol{C}_{rg}\boldsymbol{x}_{rg} + \boldsymbol{D}_{rg}\boldsymbol{u}_{gen} \tag{6.1–13}$$

where

$$\boldsymbol{x}_{rg} = \begin{pmatrix}\Delta\omega\\ \Delta\delta\end{pmatrix},\ \boldsymbol{y}_{gen} = \begin{pmatrix}\Delta i_{td}\\ \Delta i_{tq}\end{pmatrix}$$

6.1.2 Power System Stabilizer Design

The δ_m is the angle between the internal voltage and terminal voltage, which can be measured or estimated in real circumstances. It will be called 'local' power angle here. Ignoring the small armature resistance, this angle is the same as the angle between the air-gap flux and rotor flux. It is given

$$\delta_m = \delta - \delta_v' \text{ , where } \delta_v' = \delta_v - \pi / 2 \tag{6.1–14}$$

The local power angle might need to be indirectly controlled to stabilize the power system. The reason follows. To control the terminal voltage at a given value when load increases, it needs to produce more reactive power to recover the terminal voltage and to let more currents flow through armature winding. In this case, the voltage drop across the armature reactance increases due to the increased armature current and it leads to the local power angle increased. If the local power angle abruptly increases above a certain limit, it would lead to out-of-synchronization. Hence, terminal voltage control might need to be restricted in certain cases by controlling the rotor speed, which also represents the differential term of local power angle. For this reason, it is assumed that rotor speed and the local power angle are additionally controlled by Power System Stabilizer (PSS). However, controlling the local power angle completely at certain value would lead to make the generator not be able to produce more reactive power. Besides, in the case of load absorbing constant power, adding PSS could reduce the terminal voltage control capability and it might make the power system less stable. Therefore, the PSS control should be designed to control mainly rotor speed. Here, the controller will be designed using the linear quadratic regulator method. The dynamics of rotor speed and local power angle are both slow; either of them cannot be ignored. In this case, a model that includes both states is required.

The angle δ_v' is a function of d- and q-axis terminal voltages in the global frame and it is given as

$$\delta_v' = \tan^{-1}\left(\frac{-v_{td}}{v_{tq}}\right) \tag{6.1–15}$$

Linearizing the equations (6.1–14) and (6.1–15),

$$\Delta\delta_m = \Delta\delta - \Delta\delta_v' \tag{6.1–16}$$

where

$$\Delta\delta_v' = \boldsymbol{K}_\delta \begin{pmatrix} \Delta v_{td} \\ \Delta v_{tq} \end{pmatrix},\ \boldsymbol{K}_\delta = \frac{1}{|v_{to}|^2}\begin{pmatrix} -v_{tqo} & v_{tdo} \end{pmatrix}$$

As noticed in the equation, the angle is a function of both the power angle and the terminal voltages. So, this angle can change rapidly because the dynamics of terminal voltage could be fast and abrupt, while the power angle cannot, which leads to the conclusion that the dynamics of $\Delta\delta_v'$ could be ignored ($\Delta\dot{\delta}_v' = 0$). In this case, the original model can be simply modified by subtracting the term $\boldsymbol{K}_\delta$ from the input matrix and adding the term to the feed-through matrix as

$$\boldsymbol{B}_{rg}' = \boldsymbol{B}_{rg} - \begin{pmatrix} \boldsymbol{0} \\ \boldsymbol{K}_\delta \end{pmatrix},\ \boldsymbol{D}_{rg}' = \boldsymbol{D}_{rg} + \boldsymbol{C}_{rg}\begin{pmatrix} \boldsymbol{0} \\ \boldsymbol{K}_\delta \end{pmatrix} \tag{6.1–17}$$

On the other hand, the model also can be modified without ignoring the voltage dynamics by taking the network into account. It is a little more complicated than the simple method. Regarding the network, it is assumed that all loads are constant admittance loads so that the load buses are eliminated. Except for the bus to which targeted generating unit is connected, the other buses are considered infinite buses with constant voltages. Then, the following is obtained:

$$\begin{pmatrix} \Delta\boldsymbol{v}_{tdq} \\ \boldsymbol{0} \end{pmatrix} = \begin{pmatrix} \boldsymbol{Z}_{dq}^{(a)} & \boldsymbol{Z}_{dq}^{(b)} \\ \boldsymbol{Z}_{dq}^{(c)} & \boldsymbol{Z}_{dq}^{(d)} \end{pmatrix}\begin{pmatrix} \Delta\boldsymbol{i}_{tdq} \\ \Delta\boldsymbol{i}_{t-} \end{pmatrix} \tag{6.1–18}$$

where $\boldsymbol{v}_{tdq}$ is the dq-axis voltages of a bus to which the targeted generating unit is connected. The voltages are the same as the unit's terminal voltages. $\boldsymbol{i}_{tdq}$ is the injected dq-axis currents to the bus and they are the same as the

unit's armature currents. $\boldsymbol{i}_{t\_}$ are the currents injected to the other buses, which have constant voltages. Reducing the equation (6.1–18),

$$\boldsymbol{u}_{gen} = \boldsymbol{Z}_{dq}^{(eq)}\boldsymbol{y}_{gen}\text{, where } \boldsymbol{Z}_{dq}^{(eq)} = \boldsymbol{Z}_{dq}^{(a)} - \boldsymbol{Z}_{dq}^{(b)}(\boldsymbol{Z}_{dq}^{(d)})^{-1}\boldsymbol{Z}_{dq}^{(c)} \tag{6.1–19}$$

Using the equation (6.1–18) and (6.1–19), the terminal voltages are expressed in rotor speed and power angle as

$$\boldsymbol{u}_{gen} = (\boldsymbol{Y}_{dq}^{(eq)} - \boldsymbol{D}_{rg})^{-1}\boldsymbol{C}_{rg}\boldsymbol{x}_{rg}\text{, where } \boldsymbol{Y}_{dq}^{(eq)} = (\boldsymbol{Z}_{dq}^{(eq)})^{-1} \tag{6.1–20}$$

Recall $\Delta\delta_v' = \boldsymbol{K}_\delta\boldsymbol{u}_{gen}$ which leads to $\Delta\delta_v' = \bar{\boldsymbol{K}}_\delta\boldsymbol{x}_{rg}$, where $\bar{\boldsymbol{K}}_\delta = \boldsymbol{K}_\delta(\boldsymbol{Y}_{dq}^{(eq)} - \boldsymbol{D}_{rg}')^{-1}\boldsymbol{C}_{rg}$. The matrix to transform power angle to local power angle is obtained as

$$\boldsymbol{T} = \boldsymbol{I} - \begin{pmatrix} \boldsymbol{0} \\ \bar{\boldsymbol{K}}_\delta \end{pmatrix} \tag{6.1–21}$$

Using the transformation matrix, the original model can be modified as

$$\boldsymbol{x}_{rg}'' = \boldsymbol{A}_{rg}''\boldsymbol{x}_{rg}'' + \boldsymbol{B}_{rg}''\boldsymbol{u}_{gen} + \boldsymbol{B}_{rg\text{-pss}}''\Delta v_{\text{pss}} \tag{6.1–22}$$

$$\boldsymbol{y}_{gen} = \boldsymbol{C}_{rg}''\boldsymbol{x}_{rg}'' + \boldsymbol{D}_{rg}\boldsymbol{u}_{gen} \tag{6.1–23}$$

where

$$\boldsymbol{x}_{rg}'' = \begin{pmatrix} \Delta\omega \\ \Delta\delta_m \end{pmatrix}$$

Again, $\boldsymbol{u}_{gen} = (\boldsymbol{Y}_{dq}^{(eq)} - \boldsymbol{D}_{rg})^{-1}\boldsymbol{C}_{rg}''\boldsymbol{x}_{rg}''$ is newly given. Then, the model of the generating unit that includes the network can be expressed as

$$\dot{\boldsymbol{x}}_{rg}'' = \boldsymbol{A}_{rg}'''\boldsymbol{x}_{rg}'' + \boldsymbol{B}_{rg\text{-pss}}''\Delta v_{pss}\text{, where } \boldsymbol{A}_{rg}''' = \boldsymbol{A}_{rg}'' + \boldsymbol{B}_{rg}(\boldsymbol{Y}_{dq}^{(eq)} - \boldsymbol{D}_{rg})^{-1}\boldsymbol{C}_{rg}'' \tag{6.1–24}$$

Using this state space equation, a gain matrix $\boldsymbol{K}$ is derived by the linear quadratic regulator method. When choosing the weight matrix $\boldsymbol{Q}$, the weight related to the rotor speed will only be chosen, for instance,

$$\boldsymbol{x}_{rg}''^{T}\boldsymbol{Q}\,\boldsymbol{x}_{rq}''\text{ , where } \boldsymbol{Q} = \begin{pmatrix} w^2 & 0 \\ 0 & 0 \end{pmatrix} \tag{6.1–25}$$

In this case, the gain for local power angle generally is given 0. The gain matrix $\boldsymbol{K}$ will be applied to the excitation system, as figure 5.5 shows:

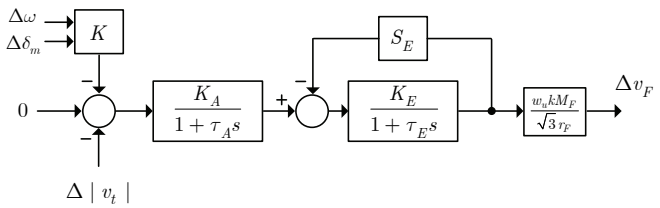

Fig. 5.5 Excitation system with PSS

Once the transformation matrix and gain matrix are both given, the generating unit with PSS can be expressed from the equations (6.1–12) as

$$\dot{\boldsymbol{x}}_{rg} = \bar{\boldsymbol{A}}_{rg}\boldsymbol{x}_{rg} + \boldsymbol{B}_{rg}\boldsymbol{u}_{gen} \tag{6.1–26}$$

where

$$\bar{\boldsymbol{A}}_{rg} = \boldsymbol{A}_{rg} - \boldsymbol{B}_{rg\text{-pss}}\boldsymbol{K}\boldsymbol{T},$$

By using this PSS control design method, where the local power angle assumed estimated, the linear quadratic regulator method can be successfully applied. In addition, it is possible to observe what effect controlling local power angle has against the stability of networked power system. However, since the gain for local power angle is typically zero, the transformation matrix might not be required when applying the PSS. If a method that uses eigenvalue sensitivity theory [82] is applied to control only the rotor speed, this transformation process to obtain the local power angle could be avoided.

When only the rotor speed is fed-backed with the gain K, the PSS control can be applied with a high pass filter in the form of $KF(s)$, where $F(s)$ is the transfer function of the filter that satisfies $\lim_{s\to\infty} F(s) = 1$ and $\lim_{s\to 0} F(s) = 0$; by the initial and final value theorems, the corresponding values of the filter for the step input are 1 and 0, respectively. This is equivalent to a PSS designed with a lead-lag compensator. By doing so, relatively high frequency components of the rotor speed are fed-back so that oscillating components except dc are damped out faster.

6.2 Network Design

6.2.1 Dynamic Network Model with Damping Resistance

Network model with pure capacitance is generally stable when loads are modeled with linear RLC components. However, if a certain type of load model is applied, such as a constant power load (CPL) model, the network dynamic model could be unstable since the capacitance acts as a source of resonance [83]. It might be necessary to add some damping resistance to the capacitance to stabilize the network.

There assumed exists capacitance regarding long distance transmission lines. One is natural capacitance existing between conductors and the other is capacitance between the conductors and ground. The capacitance is typically assumed attached at near buses. It might be able to think that the capacitance existing at the buses is connected to the ground by some earth resistance. However, the assumption of damping resistance being connected from the neutral point of capacitance to the ground is not enough to stabilize the network. That is proven by the following.

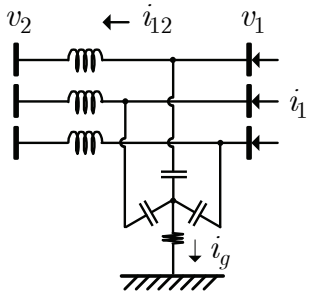

Fig. 5.6 Two bus system including capacitance with damping resistance of neutral point to the ground

In the figure, the current is injected to the bus 1 and bus 2 voltage is assumed controlled. When the neutral point of Y-connected three phase capacitance is linked to the ground by damping resistance, the ground current i_g is equal to the sum of three phase capacitance currents

$$i_g = i_{ca} + i_{cb} + i_{cc} \tag{6.2–1}$$

And, the phase voltage of bus 1 is equal to the sum of phase capacitance voltage and voltage between the neutral point and the ground, v_g

$$v_1^{abc} = v_c^{abc} + v_g \text{, where } \; v_g = R_g i_g \tag{6.2–2}$$

The three phase voltages and currents are transformed to dq0 components. Then, the dq0 components of capacitance voltage is given as

$$\begin{pmatrix} v_1^{dq} \\ v_1^0 \end{pmatrix} = \begin{pmatrix} v_c^{dq} \\ v_c^0 \end{pmatrix} + \begin{pmatrix} 0 \\ v_g \end{pmatrix} \tag{6.2–3}$$

where superscript 0 denotes zero-sequence component. With applying the dq0 'power invariant' transformation, the zero-sequence component of capacitance current is the same to the ground current

$$i_g = i_{c0} \tag{6.2–4}$$

Then, the voltage v_g can be expressed as

$$v_g = R_g i_{c0} \tag{6.2–5}$$

In addition, the dq0 capacitance currents are related to the dq0 components of injected current to the bus 1 and the line current as

$$i_c^{dq0} = i_1^{dq0} - i_{12}^{dq0} \tag{6.2–6}$$

Assuming that the injected currents are balanced so that its zero-sequence is zero, the following relation is obtained

$$i_c^0 = -i_{12}^0 \tag{6.2–7}$$

By Kirchhoff's laws, the equations of capacitance voltage and line current are given

$$C\begin{pmatrix} \dot{v}_c^{dq} \\ \dot{v}_c^0 \end{pmatrix} = \begin{pmatrix} -j\omega C & \\ & 0 \end{pmatrix}\begin{pmatrix} v_c^{dq} \\ v_c^0 \end{pmatrix} + \begin{pmatrix} i_c^{dq} \\ i_c^0 \end{pmatrix} \tag{6.2–8}$$

$$L\begin{pmatrix} \dot{i}_{12}^{dq} \\ \dot{i}_{12}^0 \end{pmatrix} = \begin{pmatrix} -j\omega L & \\ & 0 \end{pmatrix}\begin{pmatrix} i_{12}^{dq} \\ i_{12}^0 \end{pmatrix} + \begin{pmatrix} v_1^{dq} \\ v_1^0 \end{pmatrix} - \begin{pmatrix} v_2^{dq} \\ 0 \end{pmatrix} \tag{6.2–9}$$

Combining the equation (6.2–8) and (6.2–9) and organizing it using the equations of (6.2–3) to (6.2–7), the following is obtained.

$$\begin{pmatrix} C & & & \\ & L & & \\ & & C & \\ & & & L \end{pmatrix}\begin{pmatrix} \dot{v}_c^{dq} \\ \dot{i}_{12}^{dq} \\ \dot{v}_c^0 \\ \dot{i}_{12}^0 \end{pmatrix} = \begin{pmatrix} -j\omega C & -1 & & \\ 1 & -j\omega L & & \\ & & 0 & -1 \\ & & 1 & -R_g \end{pmatrix}\begin{pmatrix} v_c^{dq} \\ i_{12}^{dq} \\ v_c^0 \\ i_{12}^0 \end{pmatrix} + \begin{pmatrix} i_1^{dq} \\ 0 \\ 0 \\ 0 \end{pmatrix} - \begin{pmatrix} 0 \\ v_2^{dq} \\ 0 \\ 0 \end{pmatrix} \tag{6.2–10}$$

As seen in the equation, the dq components and zero-sequence component are completely decoupled. It means that the damping resistance only works and stabilizes the network with respect to some faults generating zero-sequence components into the network. To eliminate the stability issue regarding the capacitance resonance, which is related to high frequency components, and to stabilize the network in steady state, the damping resistance for each phase capacitance might be required. So, it is assumed that small damping resistance exist at every (or chosen) capacitance in the network. This assumption especially holds true when capacitor banks are connected to buses because they include small internal resistance as well. More importantly, some generating units using high-frequency power converters such as wind turbines equipped PWM converters often apply LCL filters that use damping resistances in

series with the capacitors. Therefore, the dynamic network model will be adequately developed with the use of damping resistance. A simple example is shown in the figure below.

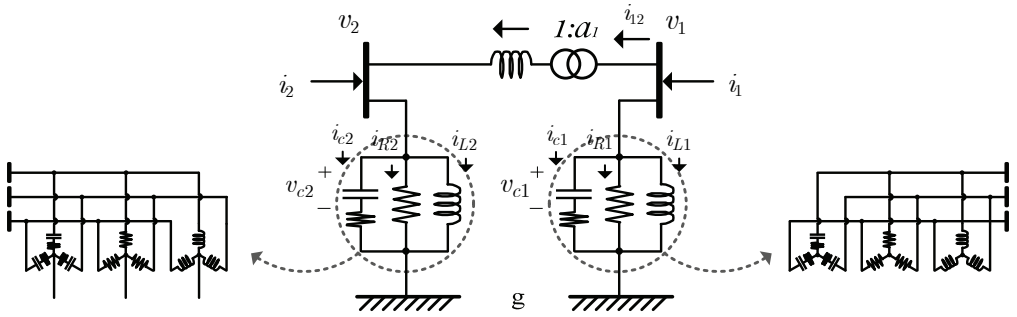

Fig. 5.7 Two bus system including capacitance with damping resistance.

In this figure, RL loads are Y-connected without grounding. However, their zero-sequence voltages are always zero so they can be assumed grounded. The capacitance existing at the bus 1 and 2 has damping resistance in series. Then, the bus voltages are equal to the voltages across the capacitance and damping resistance, which is given as

$$\begin{pmatrix} v_1^c \\ v_2^c \end{pmatrix} = \begin{pmatrix} v_{c1}^c \\ v_{c2}^c \end{pmatrix} + \boldsymbol{R}_c \begin{pmatrix} i_{c1}^c \\ i_{c2}^c \end{pmatrix} \tag{6.2–11}$$

where

$$\boldsymbol{R}_c = \mathrm{diag}\{\, R_{c1},\, R_{c2}\}$$

The capacitance voltage equations and the inductance current equations are expressed

$$\frac{1}{\omega_B}\begin{pmatrix} C_1 & \\ & C_2 \end{pmatrix}\begin{pmatrix} \dot{v}_{c1}^c \\ \dot{v}_{c2}^c \end{pmatrix} = \begin{pmatrix} -j\omega_u C_1 & \\ & -j\omega_u C_2 \end{pmatrix}\begin{pmatrix} v_{c1}^c \\ v_{c2}^c \end{pmatrix} + \begin{pmatrix} i_{c1}^c \\ i_{c2}^c \end{pmatrix} \tag{6.2–12}$$

$$\frac{1}{\omega_B} L_{\mathrm{line12}}\, a_1 \dot{i}_{12}^c = -j\omega_u L_{\mathrm{line12}}\, a_1 i_{12}^c + \begin{pmatrix} 1 \,/\, a_1 & -1 \end{pmatrix}\begin{pmatrix} v_{c1}^c \\ v_{c2}^c \end{pmatrix} + \begin{pmatrix} 1 \,/\, a_1 & -1 \end{pmatrix}\boldsymbol{R}_c \begin{pmatrix} i_{c1}^c \\ i_{c2}^c \end{pmatrix} \tag{6.2–13}$$

$$\frac{1}{\omega_B}\begin{pmatrix} L_1 & \\ & L_2 \end{pmatrix}\begin{pmatrix} \dot{i}_{L1}^c \\ \dot{i}_{L2}^c \end{pmatrix} = \begin{pmatrix} -j\omega_u L_1 & \\ & -j\omega_u L_2 \end{pmatrix}\begin{pmatrix} i_{L1}^c \\ i_{L2}^c \end{pmatrix} + \begin{pmatrix} 1 & 0 \\ 0 & 1 \end{pmatrix}\begin{pmatrix} v_{c1}^c \\ v_{c2}^c \end{pmatrix} + \begin{pmatrix} 1 & 0 \\ 0 & 1 \end{pmatrix}\boldsymbol{R}_c \begin{pmatrix} i_{c1}^c \\ i_{c2}^c \end{pmatrix} \tag{6.2–14}$$

The currents flowing through capacitance can be expressed

$$\begin{pmatrix} i_{c1}^c \\ i_{c2}^c \end{pmatrix} = (\boldsymbol{I} + \boldsymbol{R}_c \boldsymbol{R}^{-1})^{-1} \begin{pmatrix} g_1 \\ g_2 \end{pmatrix} \tag{6.2–15}$$

where

$$\begin{pmatrix} g_1 \\ g_2 \end{pmatrix} = -\boldsymbol{R}^{-1}\begin{pmatrix} v_{c1}^c \\ v_{c1}^c \end{pmatrix} + \begin{pmatrix} -1 \\ a_1 \end{pmatrix} i_{12}^c + \begin{pmatrix} -1 & 0 \\ 0 & -1 \end{pmatrix}\begin{pmatrix} i_{L1}^c \\ i_{L2}^c \end{pmatrix},$$

$$\boldsymbol{R} = \mathrm{diag}\{\, R_1,\, R_2\}$$

Using the binomial inverse theorem, the equation (6.2–15) can be modified

$$\begin{pmatrix} i_{c1}^c \\ i_{c2}^c \end{pmatrix} = \begin{pmatrix} g_1 \\ g_2 \end{pmatrix} - (\boldsymbol{R} + \boldsymbol{R}_c)^{-1}\boldsymbol{R}_c \begin{pmatrix} g_1 \\ g_2 \end{pmatrix} \tag{6.2–17}$$

As seen, the parts with the matrix $\boldsymbol{R}_c$ do not exist if $\boldsymbol{R}_c = \boldsymbol{0}$. These parts give more damping ability to the network so that it is more stable. By choosing the bus voltages as the outputs, the state space equation of network model can be modified from the equations (2.2–3) and (2.2–4) as

$$\dot{\boldsymbol{x}}_{\mathrm{nt1}}^c = \bar{\boldsymbol{A}}_{\mathrm{nt1}}^c \boldsymbol{x}_{\mathrm{nt1}}^c + \bar{\boldsymbol{B}}_{\mathrm{nt1}}^c \boldsymbol{u}_{\mathrm{nt1}}^c \tag{6.2–18}$$

$$\boldsymbol{y}_{\mathrm{nt1}}^c = \bar{\boldsymbol{C}}_{\mathrm{nt1}}^c \boldsymbol{x}_{\mathrm{nt1}}^c + \bar{\boldsymbol{D}}_{\mathrm{nt1}}^c \boldsymbol{u}_{\mathrm{nt1}}^c \tag{6.2–19}$$

where

$$\bar{\boldsymbol{A}}_{\mathrm{nt1}}^c = \boldsymbol{A}_{\mathrm{nt1}}^c + \boldsymbol{K}_1\boldsymbol{K}_3 \ ,$$

$$\bar{\boldsymbol{B}}_{\mathrm{nt1}}^c = \boldsymbol{B}_{\mathrm{nt1}}^c + \boldsymbol{K}_1\boldsymbol{B}_{\mathrm{in}} \ ,$$

$$\bar{\boldsymbol{C}}_{\mathrm{nt1}}^c = \boldsymbol{C}_{\mathrm{nt1}}^c + \boldsymbol{c}\boldsymbol{K}_2\boldsymbol{K}_3 \ ,$$

$$\bar{\boldsymbol{D}}_{\mathrm{nt1}}^c = \boldsymbol{c}\boldsymbol{K}_2\boldsymbol{B}_{\mathrm{in}}$$

where, $\boldsymbol{K}_1 = \omega_B \begin{pmatrix} \boldsymbol{C} & & \\ & \boldsymbol{L}_{\mathrm{line}}\boldsymbol{T}r & \\ & & \boldsymbol{L} \end{pmatrix}^{-1} \begin{pmatrix} -(\boldsymbol{R}+\boldsymbol{R}_c)^{-1}\boldsymbol{R}_c \\ -\boldsymbol{M}_{\mathrm{b}}^T\boldsymbol{K}_2 \\ -\boldsymbol{M}_{\mathrm{c}}^T\boldsymbol{K}_2 \end{pmatrix},$

$$\boldsymbol{K}_2 = \boldsymbol{R}_c(\boldsymbol{I} + \boldsymbol{R}^{-1}\boldsymbol{R}_c)^{-1}, \ \boldsymbol{K}_3 = (-\boldsymbol{R}^{-1} \quad \boldsymbol{M}_{\mathrm{a}} \quad \boldsymbol{M}_{\mathrm{c}})$$

Although the damping resistance helps for the stability issue regarding to high frequency resonance components, it also might work to reduce the stability margin in terms of slow dynamics. Therefore, damping resistance should be included very small in values.

The complex state space model can be transformed into dq-representation in the same way that is done in the chapter 2. Once it is proven that the network model is stable and the dynamics of voltages and currents in the network is faster than those of generating units, the dynamics for the network can be ignored and the static network model can be applied.

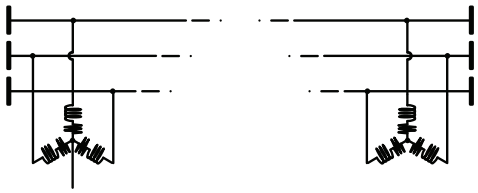

Fig. 5.8 Inductance with series resistance

In addition, unlike adding series damping resistance to the capacitance, adding series resistance to the inductance is straightforward. For instance, from the equation (6.2–14),

$$\frac{1}{\omega_B}\begin{pmatrix} L_1 & \\ & L_2 \end{pmatrix}\begin{pmatrix} \dot{i}_{L1}^c \\ \dot{i}_{L2}^c \end{pmatrix} = \begin{pmatrix} -R_{L1} - j\omega_u L_1 & \\ & -R_{L2} - j\omega_u L_2 \end{pmatrix}\begin{pmatrix} i_{L1}^c \\ i_{L2}^c \end{pmatrix} + \begin{pmatrix} 1 & 0 \\ 0 & 1 \end{pmatrix}\begin{pmatrix} v_{c1}^c \\ v_{c2}^c \end{pmatrix} + \begin{pmatrix} 1 & 0 \\ 0 & 1 \end{pmatrix}\boldsymbol{R}_c\begin{pmatrix} i_{c1}^c \\ i_{c2}^c \end{pmatrix}$$

6.2.2 Lumped Static Network Model with Power Loads

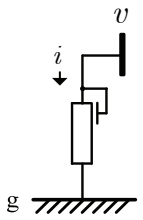

Fig. 5.9 Model of constant power load

This sub-subsection explains that lumped static network model with power injection where the power injection implies loads. The static network model plays an important role in developing the model of power systems since the stability of the power systems might change depending on the use of different types of static network models. We talk about two types of static network model here: one is a model with constant current loads (constant current model) and the other is a model with constant power loads (constant power model). For the constant current (or power) model, it could be assumed that the injected current (or power) does not vary in a normal condition whatever the bus voltage is so that the current (or power) variation of the load bus is zero. In this case, the network model can be reduced and that is just the same as eliminating the load from the network. This reduced model should be used for the study of power system stability. It needs to be noted that, because the respective variations of injected currents (or powers) into the corresponding load buses are zero while their real values are not actually zero, the reduced network model can only be applied to the power systems using linearized dynamic models.

Models of power loads (power equation) with both the characteristic of constant current and constant power are developed based on the following equation.

$$\begin{pmatrix} \Delta \boldsymbol{S}_g \\ \Delta \boldsymbol{S}_l \end{pmatrix} = \begin{pmatrix} \boldsymbol{V}_{\mathrm{o}}^{(g)} & \\ & \boldsymbol{V}_{\mathrm{o}}^{(l)} \end{pmatrix} \begin{pmatrix} \Delta \boldsymbol{I}_g \\ \Delta \boldsymbol{I}_l \end{pmatrix} + \begin{pmatrix} \boldsymbol{I}_{\mathrm{o}}^{(g)} & \\ & \boldsymbol{I}_{\mathrm{o}}^{(l)} \end{pmatrix} \begin{pmatrix} \Delta \boldsymbol{V}_g \\ \Delta \boldsymbol{V}_l \end{pmatrix} = \boldsymbol{F} \begin{pmatrix} \Delta \boldsymbol{V}_g \\ \Delta \boldsymbol{V}_l \end{pmatrix} \tag{6.2–20}$$

If the generating unit's outputs are chosen currents, the equation (6.2–20) is modified accordingly. The procedures of developing the models are different. For the constant current model, a reduced current equation is first obtained and then a power equation is developed using the current equation. Considering the admittance matrix is properly organized regarding generator buses and load buses, the current equation is expressed as

$$\text{Original: } \begin{pmatrix} \Delta \boldsymbol{I}_g \\ \Delta \boldsymbol{I}_l (=0) \end{pmatrix} = \begin{pmatrix} \boldsymbol{Y}_{11} & \boldsymbol{Y}_{12} \\ \boldsymbol{Y}_{21} & \boldsymbol{Y}_{22} \end{pmatrix} \begin{pmatrix} \Delta \boldsymbol{V}_g \\ \Delta \boldsymbol{V}_l \end{pmatrix} \tag{6.2–21}$$

$$\text{Reduced: } \Delta \boldsymbol{I}_g = \boldsymbol{Y}_{\mathrm{ccl}} \Delta \boldsymbol{V}_g \tag{6.2–22}$$

Since the operating points are identical for both the original and reduced current equations, power equation based on the constant current injection is simply expressed as

$$\Delta \boldsymbol{S}_g = \boldsymbol{V}_{\mathrm{o}}^{(g)} \Delta \boldsymbol{I}_g + \boldsymbol{I}_{\mathrm{o}}^{(g)} \Delta \boldsymbol{V}_g = \boldsymbol{F}_{\mathrm{ccl}} \Delta \boldsymbol{V}_g \tag{6.2–23}$$

From the equation (6.2–21), it is easily noticed that, although the variation of currents injected to load bus is zero ($\Delta \boldsymbol{I}_l = 0$), the variation of powers at the load bus is not zero ($\Delta \boldsymbol{S}_l \neq 0$) when the variation of load bus voltage is not zero ($\Delta \boldsymbol{V}_l \neq 0$). The power absorbed by constant current loads varies with load bus voltages. If the load bus voltages increase, it results in the increase of powers absorbed by the loads.

On the other hand, a power equation with constant power loads should be different because the power equation with constant current loads does not properly represent the constant power loads' characteristic. The power equation is firstly developed with the original current equation ($\Delta \boldsymbol{I}_l \neq 0$), and then it is reduced based on the assumption of $\Delta \boldsymbol{S}_l = 0$, as shown in the below

$$\text{Original: } \begin{pmatrix} \Delta \boldsymbol{S}_g \\ \Delta \boldsymbol{S}_{l(=0)} \end{pmatrix} = \begin{pmatrix} \boldsymbol{F}_{11} & \boldsymbol{F}_{12} \\ \boldsymbol{F}_{21} & \boldsymbol{F}_{22} \end{pmatrix} \begin{pmatrix} \Delta \boldsymbol{V}_g \\ \Delta \boldsymbol{V}_l \end{pmatrix} \tag{6.2–24}$$

$$\text{Reduced: } \Delta \boldsymbol{S}_g = \boldsymbol{F}_{\text{cpl}} \Delta \boldsymbol{V}_g \tag{6.2–25}$$

It should be noted that, although the forms of power equations for both constant current loads and constant power loads are identical, they have different parameters ($\boldsymbol{F}_{\text{cpl}} \neq \boldsymbol{F}_{\text{ccl}}$).

6.2.3 Fault Model

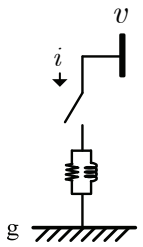

Fig. 5.10 Fault model

To demonstrate the dynamics of a power system when a fault happens, the fault model is required. When a bus is short circuited to the ground with zero-impedance line, infinite current flows through the faulted line and the bus voltage drops to zero for a short time until the fault is cleared. It is quite difficult to say that how much power is withdrawn from the bus because the power is a function of the bus voltage and the fault current. However, huge current flowing through the faulted line causes huge reactive power flowing from elsewhere to the point of the fault. So, it is assumed that huge reactive power is injected (withdrawn) when a fault happens. On the other hand, if the bus is short circuited to the ground with relatively high impedance line, it is clear that the fault can be modeled with power injected from the bus as load does. The power injected from a bus can be modeled the same as the equation (6.2–24).

Given generating units' state space equations,

$$\dot{\boldsymbol{x}}_g = \boldsymbol{A}_g \boldsymbol{x}_g + \boldsymbol{B}_g \Delta \boldsymbol{V}_g \tag{6.2–26}$$

The voltages of generating units are expressed with either of faulted bus voltages or powers injected,

$$\Delta \boldsymbol{V}_g = \boldsymbol{L}_a \boldsymbol{x} + \boldsymbol{L}_b \Delta \boldsymbol{V}_f \text{ or } \Delta \boldsymbol{V}_g = \boldsymbol{L}'_a \boldsymbol{x} + \boldsymbol{L}'_b \Delta \boldsymbol{S}_f \tag{6.2–27}$$

where $\Delta \boldsymbol{V}_f$ and $\Delta \boldsymbol{S}_f$ are voltage and power, respectively, at a faulted bus that could be any one of the buses, including load buses. By substituting (6.2–27) into (6.2–26), a state space equation for faulted condition is obtained. In normal conditions, unlike the fault model of power injection, the fault model using faulted bus voltages has the following relation that is derived with the assumption of $\Delta \boldsymbol{S}_f = 0$.

$$\Delta \boldsymbol{V}_f = -\boldsymbol{L}_c \boldsymbol{x} \tag{6.2–28}$$

$\Delta \boldsymbol{V}_f$ is forced to certain values when a fault happens and exists in a short time, otherwise $\Delta \boldsymbol{V}_f$ is reset to $-\boldsymbol{L}_c \boldsymbol{x}$ accordingly when the fault is cleared. On the other hand, $\Delta \boldsymbol{S}_f$ is forced to certain values when a fault happens, $\Delta \boldsymbol{S}_f$ is zero when the fault is cleared.

Normal condition (before and after a fault): $\dot{\boldsymbol{x}}_g = \boldsymbol{A}''_g \boldsymbol{x}_g$ ($\Delta \boldsymbol{S}_f = 0$)

Abnormal condition (during a fault): $\dot{\boldsymbol{x}}_g = \boldsymbol{A}'_g \boldsymbol{x}_g + \boldsymbol{B}'_g \Delta \boldsymbol{V}_f$ or $\dot{\boldsymbol{x}}_g = \boldsymbol{A}''_g \boldsymbol{x}_g + \boldsymbol{B}''_g \Delta \boldsymbol{S}_f$

6.3 IEEE 39 Bus Power System

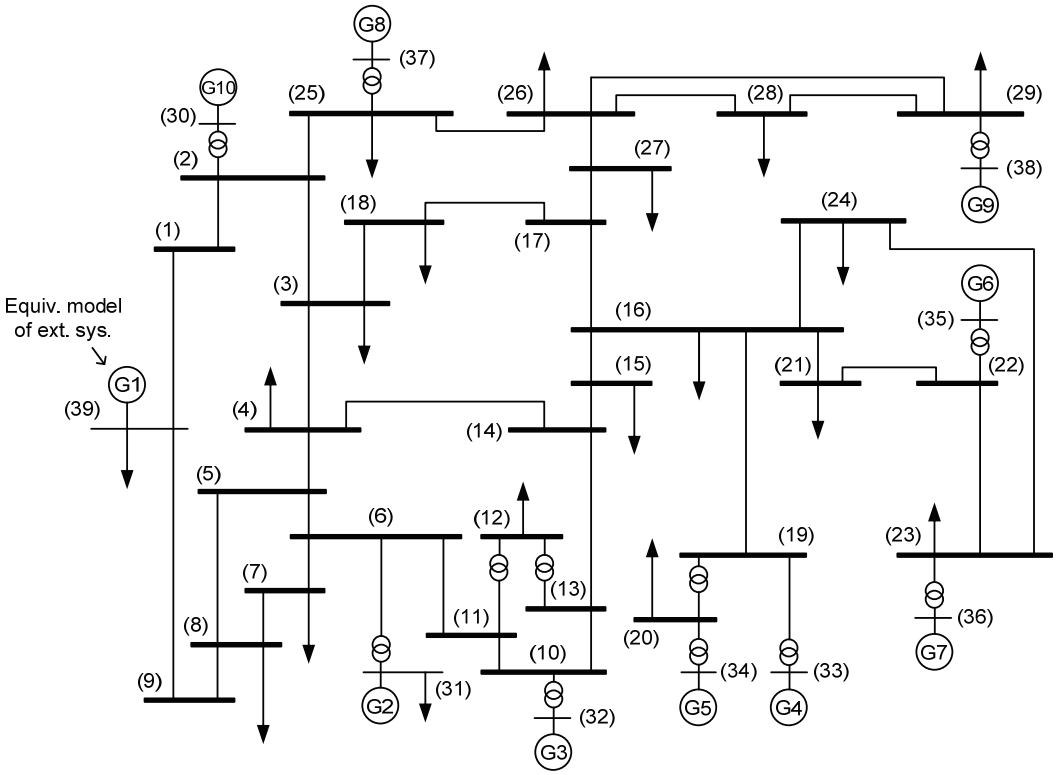

Fig. 5.11 New England power system

In this power system, the generating unit 2 is the reference unit, and the other 9 generating units' power angles are expressed on the basis of the generating unit 2's power angle that is always zero. The generating unit 1 is considered as an equivalent model of external systems so that this unit does not have the capability to control the terminal (bus) voltage.

6.3.1 Network Stability

Before integrating the generating units into the network, the network stability is first checked with its dynamic model. It is assumed that the buses with capacitance have series damping resistance of 10% (in pu) of the corresponding capacitance value, which is thought as naturally existing, and that the buses without capacitance have very small capacitance (10^{-9}) so that current hardly flows through the capacitance. Including the damping resistance can be performed with the equations (6.2–18, 19) as introduced in the previous section.

All loads are modeled with constant power loads (CPLs). Because $\Delta \boldsymbol{S} = 0$ for constant power loads, the load is modeled with,

$$\Delta \boldsymbol{I}_l = \boldsymbol{K} \Delta \boldsymbol{V}_l \text{, where } \Delta \boldsymbol{I}_l = \begin{pmatrix} \Delta i_{ld} \\ \Delta i_{lq} \end{pmatrix} \text{ and } \Delta \boldsymbol{V}_l = \begin{pmatrix} \Delta v_{ld} \\ \Delta v_{lq} \end{pmatrix}$$

where $\Delta \boldsymbol{I}_l$ and $\Delta \boldsymbol{V}_l$ are the input and output of the dynamic network model, respectively, and it creates a feedback loop. Thus, the constant power load is applied with low pass filter to avoid the stability issue concerned with high frequency components that might be generated by the feedback loop. The use of the filter is proper

because the equivalent reactance at low voltage side in distribution level is high enough to eliminate very high frequency components. Also, it might be thought that there exist some filters, in the distribution level, designed with an impedance matching method so that the equivalent impedance of a link, by which the network and the constant power load is connected, is only very small in relation to fundamental frequency; It is reminded that band-pass filtering in the three-phase frame (or the stationary dq-frame) is equivalent to low-pass filtering in the rotating dq-frame. Under these assumptions, the cut off frequency of 1st order low pass filter is chosen properly. Figure 5.12 shows the load model.

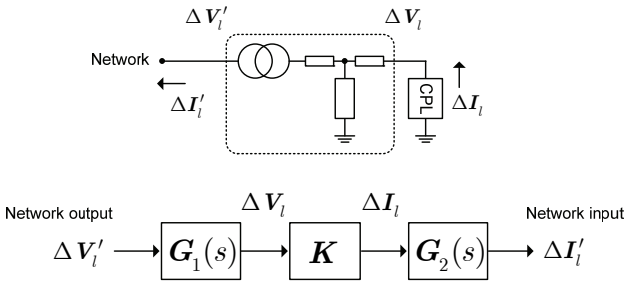

Fig. 5.12 Constant power load with low pass filters

In the power system, it is assumed that the generating unit 1 attached at the bus 39 is an equivalent model that represents the external system and that the unit does not have capability to control the voltage of bus 39. With this assumption, the network input to the bus 39 could be constant power and the other network inputs to the bus 30 to 38 are constant voltage sources. A test has been performed by varying the cut off frequency for CPLs. Table 5.1 shows the result.

Table 5.1 Network stability for varying cutoff frequency of low pass filters (LPF)

LPF cut off frequency	Real part of the most dominant eigenvalue
210 Hz	– 4.71
220 Hz	– 3.00
230 Hz	+ 0.61
:	:
400 Hz	+ 180.70

Because the network system in real circumstances is more complicated, the use of the result might be limited. However, at least, the result provides the observation that if dynamics generated by CPLs are fed to the network system without proper filtering, the network could become unstable.

Once the network system is proven stable, the dynamics of network model is ignored and lumped static network model can be used. The effects of low pass filtering do not exist in the steady state, which means the relation between the input and output of the filter is just 1. Thus, the network model is given

For generating unit model with current output: $\Delta \boldsymbol{I}_g = \boldsymbol{Y}_{\text{cpl}} \Delta \boldsymbol{V}_g$

For generating unit model with power output: $\Delta \boldsymbol{S}_g = \boldsymbol{F}_{\text{cpl}} \Delta \boldsymbol{V}_g$

It should be noted that the matrix $\boldsymbol{Y}_{\text{cpl}}$ is not the same as the admittance matrix. This static model is used to interconnect the generating units so that they compose a power system.

6.3.2 PSS Damping Ability

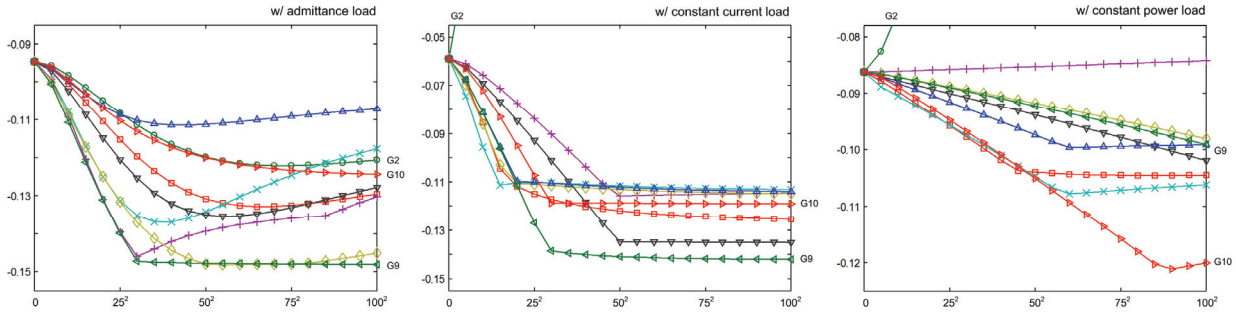

Fig. 5.13 Power system stability for weight variation of PSS design

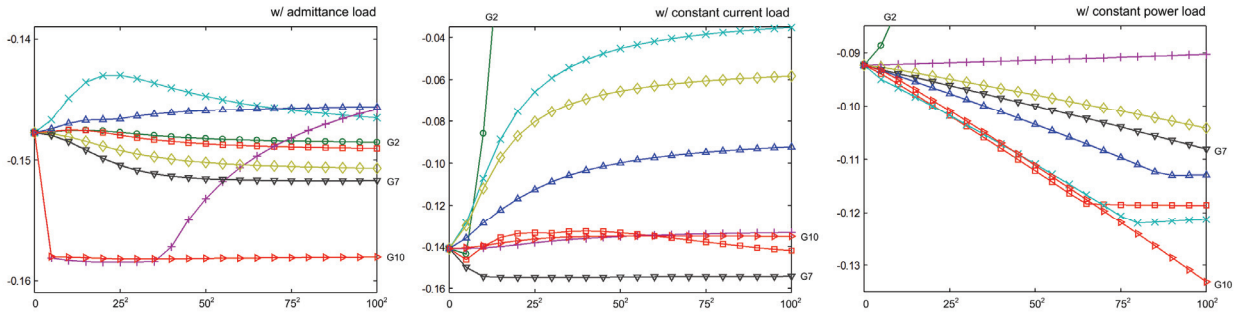

Fig. 5.14 Power system stability for weight variation of PSS design (w/ PSS applied to gen. unit 9)

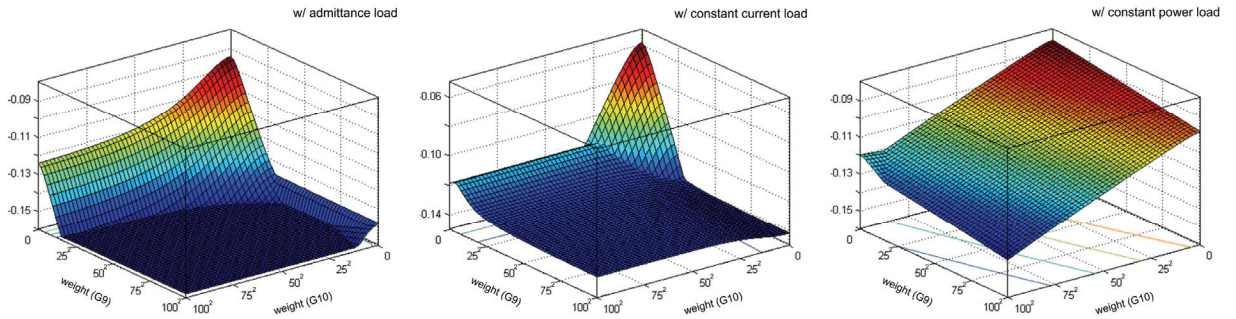

Fig. 5.15 Power system stability when PSS applied for gen. unit 9 and 10.

It is expected that applying PSS is to increase the power system's stability. However, it is not certain what effect PSS provides depending on the types of loads: admittance load, constant current load, and constant power load. Thus, the power system stability has been checked with applying PSS to one or two generating units except generating unit 1.

Firstly, in order to verify the effect of different types of loads in applying PSS, the network models with the three different loads have been used and PSS is designed using lumped static network model with the respective loads. In the figures, the x-axis is for the weight in the equation (6.1–25) and the y-axis is for the real value of the most dominant eigenvalue of the power system. Figure 5.13 shows the result that PSS is applied to one of 8 generating units one at a time, and weights are varied from (0, 0) to (100^2, 0). As seen in the figure 5.13, applying PSS gives more damping for all types of loads, but different results depending on the types. Additionally, it needs to be noted that applying PSS to generating unit 2 that is connected to swing bus, could make power system unstable if the type

of load is CCL or CPL. After all, it seems that PSS applied for generating unit 9 provides consistent damping to the power system with all three types of loads. Thus, PSS is first designed with 50^2 in weight and applied to the generating unit 9.

Second, generating unit 9 with PSS designed by the weight 50^2 is permanently applied and additional PSS is applied to one of 7 generating units one at a time in the same way. Figure 5.14 shows the result. With the aid of generating unit 9 with PSS, applying PSS on generating unit 10 gives more damping for the power system with admittance loads or CPLs than applying PSS on any other generating units. By comparison, applying PSS on the generating unit 7 gives better damping ability for power system with CCLs. Also, it is observed that, if PSS is applied to any of generating unit 2, 4, and 6 when the power system is composed of CCLs, it works negatively for system stability, even the power system could be unstable with PSS applied to generating unit 2. It is expected, in real circumstances, that applying PSS on more generating units does not guarantee better damping capability for power systems because the type and amount of loads in the power system might continuously change so that it might create some unexpected results. Therefore, for consistent damping capability for power system, it seems better to apply PSS on generating unit 10. As a result, it would be appropriate to apply PSS on one or two of generating units at most so that the power system is robust. Additionally, figure 5.15 shows the power system stability regarding to the weight variation of PSS design for generating units 9 and 10.

Table 5.2 Power system stability with three different load types

Gen. unit	PSS gain (Admittance Load)		PSS gain (CCL)		PSS gain (CPL)	
	$\Delta\omega$	$\Delta\delta_m$	$\Delta\omega$	$\Delta\delta_m$	$\Delta\omega$	$\Delta\delta_m$
G9 (weights: 50^2, 0)	– 46.86	0.002	– 47.16	0	– 47.17	0
G10 (weights: 100^2, 0)	– 80.92	– 0.360	– 93.37	0	– 96.05	0.001
Dominant eigenvalue	$-0.095 \pm j2.127 \rightarrow$ $-0.158 \pm j3.464$		$-0.059 \rightarrow$ $-0.135 \pm j3.460$		$-0.086 \rightarrow -0.133$	

The gains of PSS designed for generating units 9 and 10 with 3 types of loads, are shown in the table 5.2. By applying PSS, the real value of the most dominant eigenvalue of the power system is increased from – 0.095 to – 0.158, from – 0.059 to – 0.135, and from – 0.086 to – 0.133, respectively. It is noticed that the gain of local power angle for generating unit 10 PSS is not zero when admittance load is applied. This is because that, if loads in the power system are modelled with constant admittance, powers absorbed by the loads vary depending on bus voltages so that the loads do not require more currents when the bus voltages decrease. In this case, controlling terminal voltages of generating units is not as important as in the case of power systems composed of CCLs or CPLs, then controlling the local power angle might help in more stabilizing the power system. On the other hand, if the power system consists of CCLs or CPLs, applying PSS might reduce its stability because it generally compromises the performance of controlling terminal voltage.

Considering that power system consists of various types of loads, PSS might or might not be helpful in increasing damping ability of the power system. Therefore, the use of PSS control should be carefully determined depending on the types of loads.

- Dynamic Responses

The dynamic responses of the power system, which is modeled as explained in this chapter, are shown. It is assumed that fault happened at bus 17. The fault condition is generated by injecting real and reactive power in step for 0.1 second, which can be though as impulse inputs. The real and reactive powers injected are -10 pu and -1 pu, respectively. The dynamics of the individual generating unit's rotor speed and power angle are shown in figures 5.17, and 5.18, respectively.

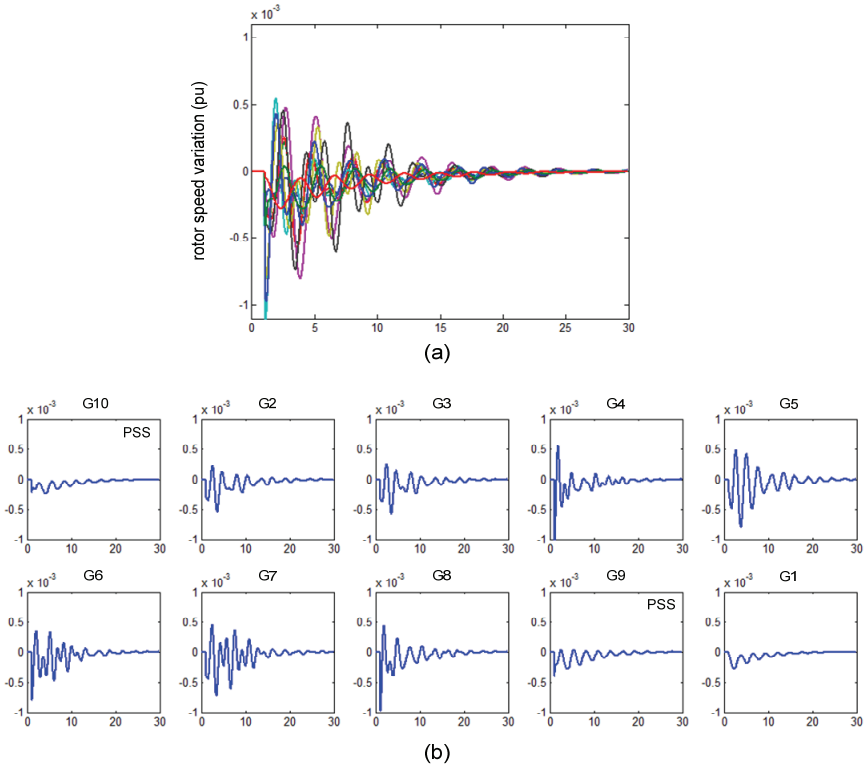

Fig. 5.16 Rotor speed variations of 10 gen. units shown (a) collectively and (b) individually

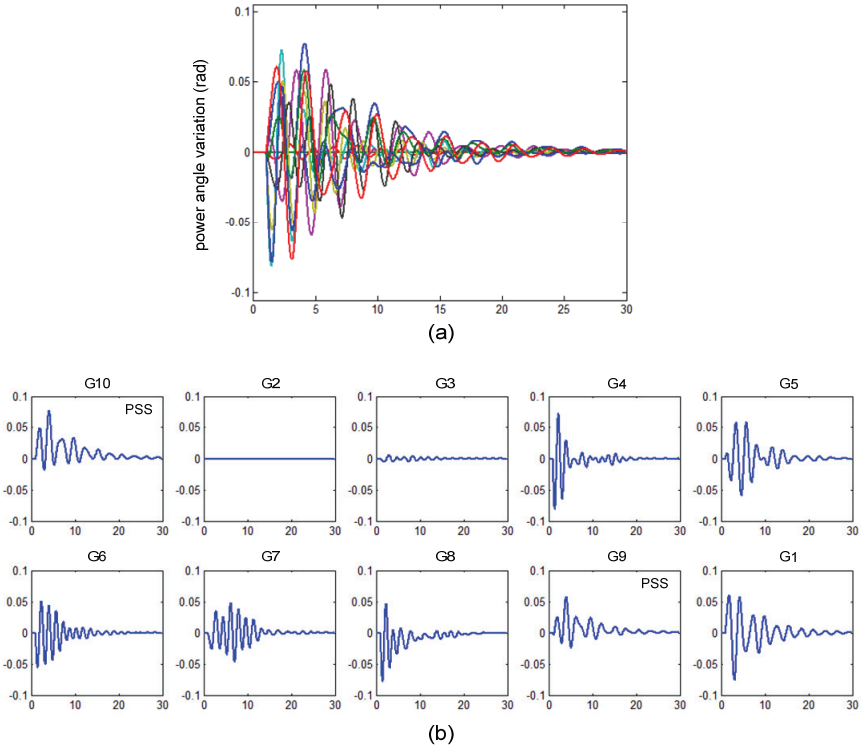

Fig. 5.17 Power angle variations of 10 gen. units shown (a) collectively and (b) individually

Figure 5.17 reveals that the generating units 9 and 10, which are equipped with PSS, have better damping with respect to the rotor speed.

Figure 5.18 shows that the generating unit 2 is the reference unit, which is the one connected at the swing bus, and thus it has always power angle of zero. The power angles of generating units 9 and 10 less abruptly change because their derivatives, the rotor speeds, are controlled with PSS.

6.4 Summary

This chapter has been assigned to introduce power system modelling. A model of generating units, which is represented in the rotating dq-frame that is aligned with the rotor of the corresponding generating units, was introduced. As generating units are often equipped with PSS to enhance the stability of power systems, PSS design was also presented. In addition, dynamic network model that was introduced in the chapter 2 is re-expressed with using damping resistance, which might be useful to study network stability. The dynamic network model could be replaced with static network model for power system dynamic study. Thus, static network models with different types of loads were developed. Finally, it was explained how a fault condition could be modeled using the models of the generating units and the network. After the explanations for the modelling process, IEEE 39 bus system was introduced. By using the system, it was shown that network stability could be altered unless dynamics of generating units and loads were properly damped. Also, it was shown that PSS would not always provide more damping on a power system, and thus PSS should be carefully applied. Finally, a simulation result was shown to observe how the power system response to an impulsive fault condition. The power system introduced in this chapter will be used as a basic power system for simulation tests in chapter 7.

Chapter 7

Simulations

7.1 Introduction of Basic Test System

This section introduces a power system for simulation tests to be made in the next sections. The simulation tests use linearized models of the power system. Unlike simulation tests using nonlinear power systems whose system parameters are updated at every time instance, the simulation tests to be made in this chapter use linearized power systems whose parameters are updated on the basis of events that cause the operating points to largely deviate from those initially given. For this reason, the process of the simulation tests is briefly explained.

7.1.1 Power System

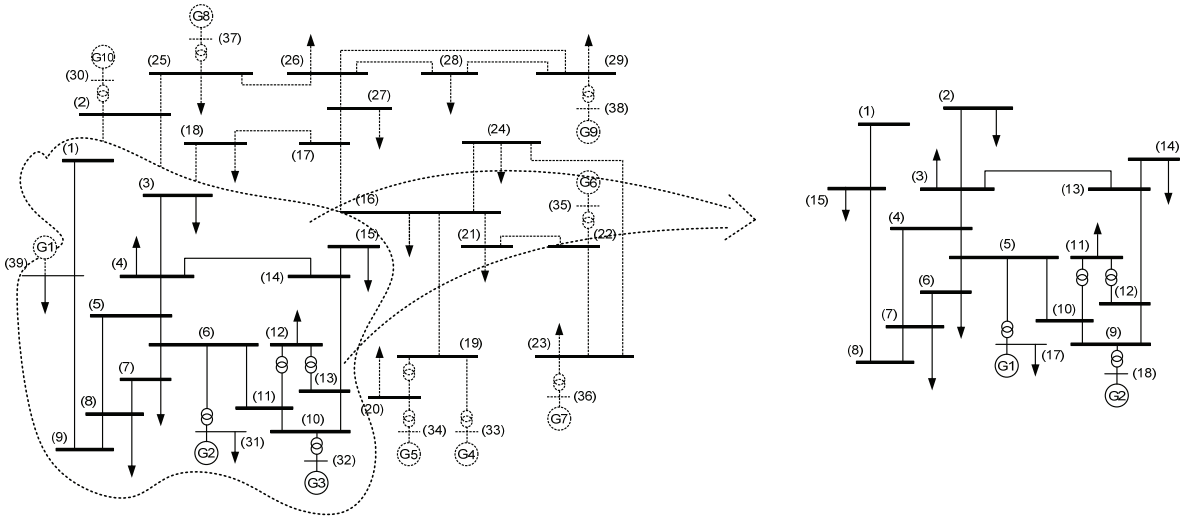

Fig. 6.1 IEEE 39 bus power system (left) and an isolated part of the system (right)

For the simulation tests, IEEE 39 bus power system explained in the chapter 6 is used. However, to study effectively the impact of WPP on the power system, the size of the WPP must be a good percentage of the total generation. Therefore, a small power system, which is obtained from the IEEE 39 bus power system, is applied: a part of the IEEE 39-bus power system is isolated by disconnecting the lines of bus 1 to 2, bus 3 to 18, and bus 15 to 16 and by removing the generating unit 1 from the bus 39. Figure 6.1 shows the IEEE 39 bus power system in the left and the isolated part in the right. In the new small power system, the buses are re-numbered accordingly. The bus 17 is the swing bus and the generating unit 1 is the reference unit.

In the new power system, an additional bus 16, which is connected to bus 15, is created (as a POI bus for WPPs to be attached later). In addition, a load is created and connected to bus 1. The amounts of loads are as shown in table 1. The resultant test system is shown in figure 6.2.

Table 1 Loads in test system

Bus 1 – 85.4 MW, 8.6 Mvar	Bus 2 – 336 MW, 54.6 Mvar	Bus 3 – 446 MW, 106 Mvar
Bus 6 – 244 MW, 84 Mvar	Bus 7 – 544 MW, 138 Mvar	Bus 11 – 20 MW, 80 Mvar
Bus 14 – 134 MW, 115 Mvar	Bus 15 – 40 MW, 0 Mvar	Bus 17 – 9.2 MW, 4.6 Mvar

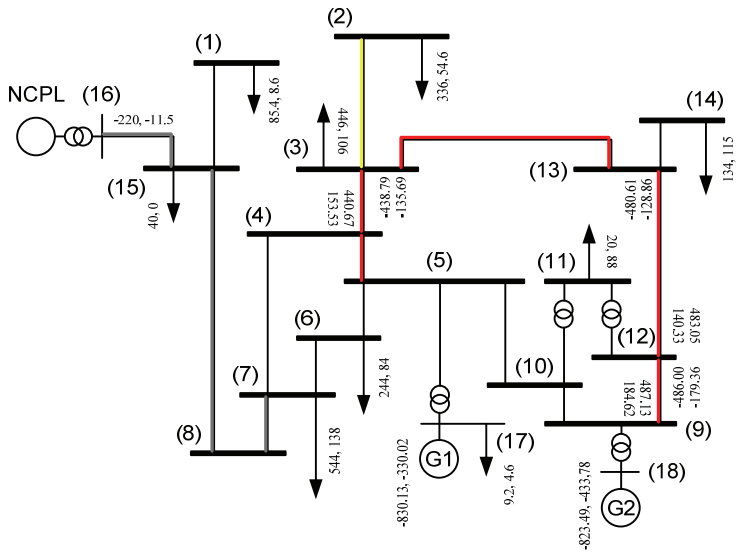

Fig. 6.2 Test system (base power: 100 MVA)

In the test system, all loads are constant power loads. It is assumed that negative constant power load (NCPL) is connected to bus 16 in lieu of WPP, and the negative power load is, for instance, chosen: 200 MW, 11.5 Mvar. Assuming that the two generating units have identical cost functions, optimal operating conditions are determined by solving optimal power flow problem. In a solution, generating unit 1 (swing bus) produces 830.13MW and 330.02Mvar and generating unit 2 produces 823.49MW and 433.78Mvar. The powers transferred through the lines are accordingly obtained by the solution as shown in figure 6.2.

Now, some possible fault scenarios in the test system are presented: First, it is well known that some of lines in a power system have critical roles in transferring powers from generating units to loads. If any of the lines are faulted, the whole power system might be troubled. In the test system, the lines of bus 3 to 4, bus 4 to 5, bus 9 to 12, bus 12 to 13, and bus 13 to 3 have large powers transferred through them, which is said to be bottlenecked. If any of them is disconnected, there might be problem in transferring the powers to the loads. Therefore, this case can be studied in simulation tests. Second, a line between buses in a power system actually consists of several lines, not just one. If the lines are not fully disconnected due to, sort of, circuit breaker malfunction so that some of the lines are remained, it results that the line impedance between the buses increases. For instance, in the test system, the largest load is connected to bus 2 among the loads at the end buses of 1, 2, 11, and 14. Assuming that the number of lines connecting bus 2 to 3 is four, no power is transferred to bus 2 if all lines are disconnected. On the other hand, if only some of the four lines are disconnected, more reactive power should be transferred to meet the demand because of the line impedance increased. This case can also be studied in simulation tests. In addition, lines of bus 7 to 8, bus 8 to 15, and bus 15 to 16 have a critical role to support voltage at bus 16. If a system which requires a voltage source such as WPP was connected at bus 16, the system would not be able to operate properly when any of the lines was disconnected. However, this case will not be studied because it is obvious WPP systems cannot survive unless they work with proper ride-through technique.

7.1.2 Process of Simulation

As the simulation tests are carried out by using dynamic models of generating units and WPP, which are linearized on operating points, by what sequences the tests are performed needs to be told in advance and explained in this subsection.

For the simulation tests, it is assumed that: 1) a fault occurs near a bus, and 2) the line between the bus and another one, that is, the line between where the fault occurred, is disconnected by circuit breaker 0.1 second after the fault.

With the assumptions, the tests are carried out by the sequence as: First, for given load conditions, real powers and voltage magnitudes of generating units are determined by solving optimal power flow problem, and the initial operating points are obtained. By using them, the models of generating units and WPP are obtained. Then, it is assumed that a fault occurs at a chosen bus, and powers are injected to the bus or voltage magnitude at the bus is forced to zero. After 0.1 second, the line connecting buses between the fault occurred is disconnected by circuit breaker and fault is cleared. Power flow problem (not optimal) is solved again for the altered operating conditions due to network change. Updated models of generating units and network are obtained according to the power flow solution, and they are applied in the simulation tests.

Table 2 Process of simulation to be performed

A	By solving optimal power flow problem, real powers and voltage magnitudes of generating units are determined, and the initial operating points are obtained. By using them, linearized models of generating units, wind power plant, and network are obtained.
B	A (faulted) bus is chosen. Then, powers due to the fault are injected to the bus or the corresponding bus voltage in magnitude is forced to zero, for a short time.
C	After the short time, it is assumed that a line linked from the faulted bus to another bus is disconnected by circuit breaker and the fault is cleared. Power flow problem (not optimal) is solved again for the altered operating conditions due to network change. Updated linearized models are obtained according to the power flow solution.
D	Updated models are applied to continue the simulation test.

An example of the simulation test is performed as the way explained above, which is also listed in table 2, and it is shown in figure 6.3. The instances of A, B, C, and D in the figure are the same as those in table 2. One thing to be noticed in the figure is that, because operating points of A and D are different by power flow solutions for different networks, real power from a generating unit is shown suddenly changed to meet the demand.

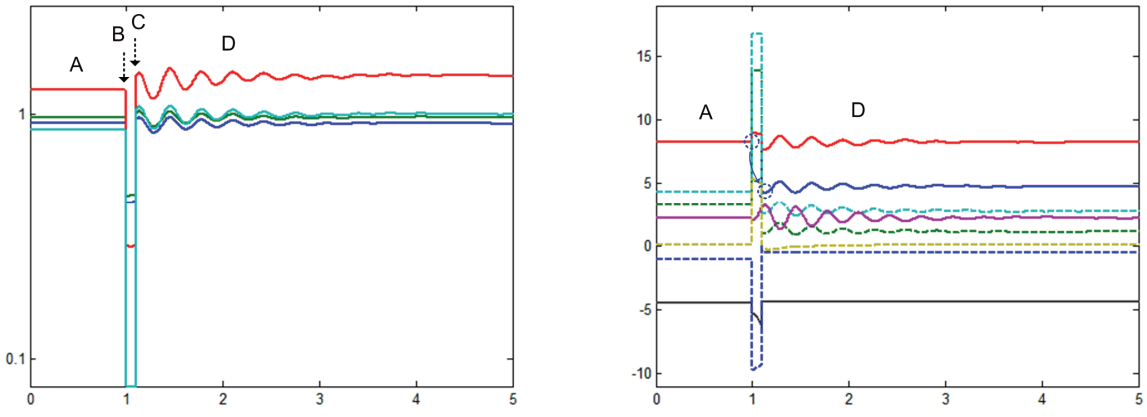

Fig. 6.3 Voltage magnitudes and powers at a bus near fault occurred and at buses of generating units and bus 16.

7.2 Simulation A

Now, simulation tests are performed using the power system introduced in section 7.1. This section is allocated for tests using the DEM developed in the chapter 3. For the tests, a WPP model using the local-frame network model 1: refer to subsection 2.2.2.2 and the corresponding DEM are applied. To interface the WPP model and its DEM into the power system, the method of modeling in POI voltage-oriented frame introduced in subsection 2.2.3 is used.

7.2.1 Test system

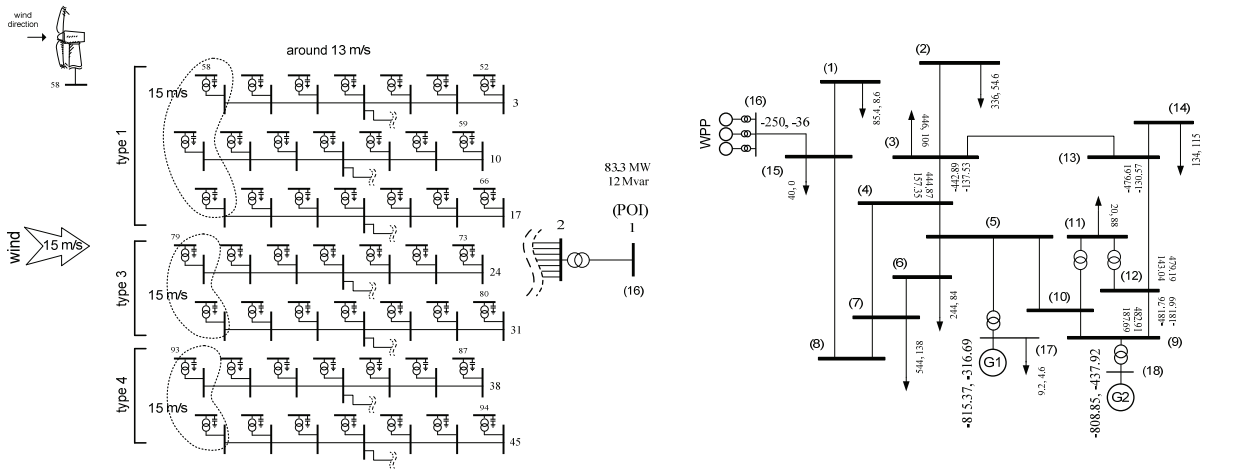

Fig. 6.4 Test system for simulation A

Test system for simulation is shown in figure 6.4. The WPP consists of 49 wind turbines (21 × type 1, 14 × type 3, and 14 × type 4) that are irregularly placed, as shown in the left of figure 6.4. The WPP system is the same as that used for the simulation tests in the chapter 3. The first column turbines directly facing the wind experience a wind speed of 15 m/s, while the other turbines experience only about 13 m/s owing to the wind wake effect. The rate wind speed for wind turbines is chosen 14m/s and the pitch angles are adjusted if the wind speeds exceed this value.

The power generated from one WPP at the wind speed is 83.3 MW with 12 Mvar, and it is assumed that two additional identical WPPs are connected to bus 16, which is done by amplifying the output power of the original WPP threefold. In the right of figure 6.4, it is seen a test system with a base power of 100 MVA in which two generating units with identical cost functions were assumed; the optimal operating conditions of these were determined by solving the optimal power flow problem. Based on the solution, generating unit 1 (at the swing bus) produced 815.37 MW with 316.69 Mvar and unit 2 produced 808.85 MW with 437.92 Mvar.

The performance of the DEM proposed in the chapter 3 is verified by using the test system shown in figure 6.4. The wind turbines were clustered by respective types and wind powers, producing six groups and, correspondingly, six equivalent wind turbines. The slow dynamic model of the WPP is used and it has 203 state variables, while the DEM has 24 state variables.

To determine whether the DEM produced the same effect on the power system as the WPP, the rotor speed variations in generating units 1 and 2 were observed when a fault occurred and was cleared.

7.2.2 Results

First, it is assumed that a fault occurred at bus 3 and that the lines of bus 2 to 3 were disconnected 0.1 s after the fault. No power was transferred to the load connected at the bus 2, and thus powers generated from unit 1 and 2

were reduced accordingly by a solution of power flow problem (not optimal).

Figure 6.5 shows the rotor speed variations of generating units and the rotor-blade speed variations of turbines in the WPP (figure (a)) and in the DEM (figure (b)).

Figures (c) and (d) show the generator speed variations and rotor-blade speed variations of type 1 turbines in the WPP and in the DEM.

Figures (e) and (f) show the generator speed variations and rotor-blade speed variations of type 3 turbines in the WPP and in the DEM.

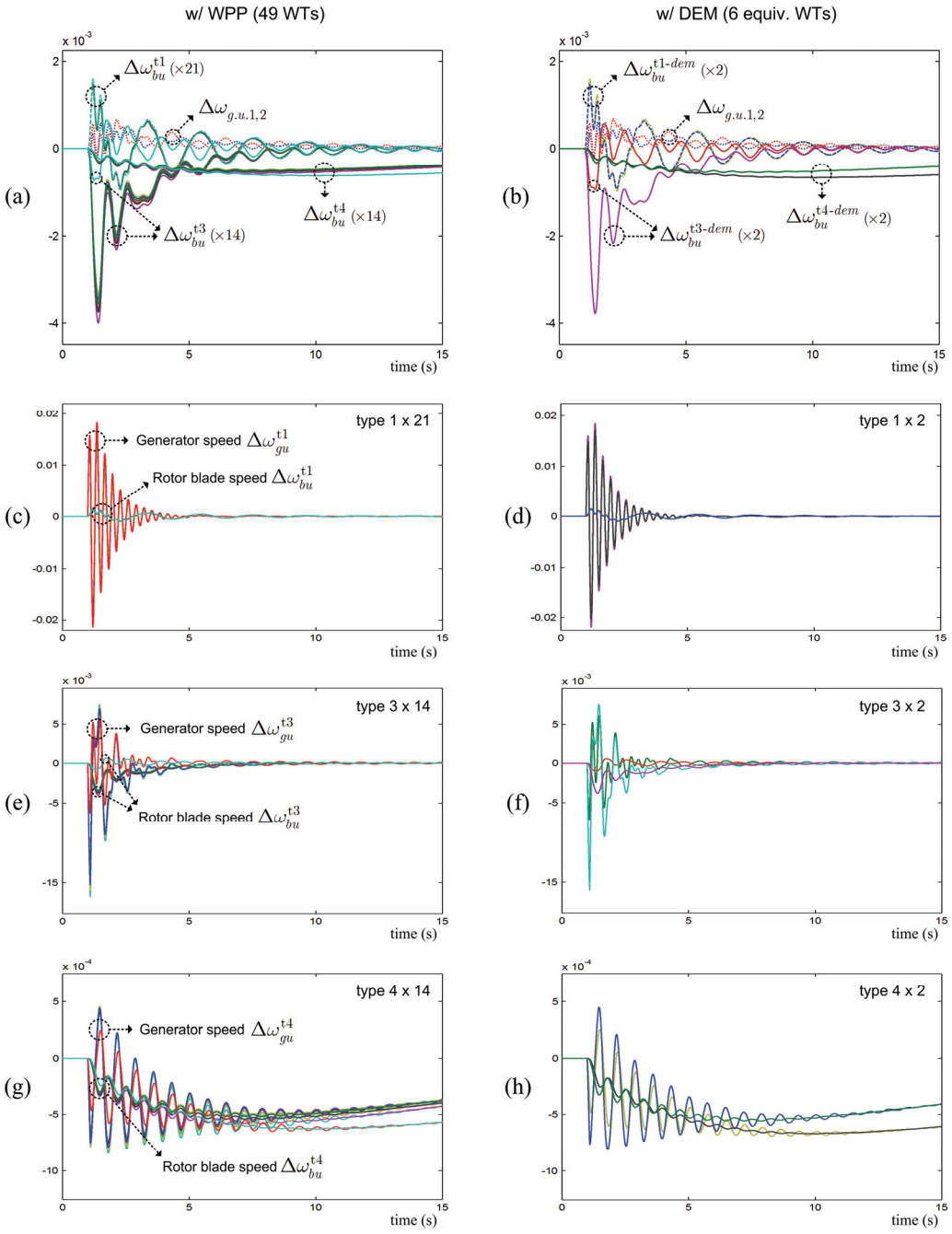

Fig. 6.5 Rotor speed variations of generating units and rotor-blade speed variations of turbines in WPP - (a) and in DEM - (a), generator and rotor-blade speed variations of type 1, 3, and 4 turbines in WPP - (c), (e), and (g) and in DEM - (d), (f), and(h).

Figures (g) and (h) show the generator speed variations and rotor-blade speed variations of type 4 turbines in the WPP and in the DEM.

Figure 6.6 shows the rotor speed variations of generating unit 1 and 2, which are the same as those shown in figure 6.5 (a) and (b). It is seen that, for both the WPP and DEM, the variations in rotor speed converged over time. The right figure shows the dominant eigenvalues of the power system before and after the fault; the eigenvalue at the origin is for the reference generating unit's angle and it does not affect the system stability so ignored. It is seen that the most dominant eigenvalue is moved to the left side, which means the power system become more stable, and also that the most dominant eigenvalues of the power system are at the same place for both results of using the WPP and using the DEM.

Second, it is assumed that three of the four lines from bus 2 to bus 3 were disconnected, causing the impedance on the remaining line to increase fourfold. In this case, the generating unit 1 and 2 should generate more reactive power to meet the load connected at the bus 2, and it causes the damping ability of generating units to decrease so that the power system is unstable. Figure 6.7 shows the variations in rotor speed slowly diverged over time for both the WPP and the DEM. Here, it is observed that the dominant eigenvalue determining the system stability is moved into the graph from the right side. This is explained by the trajectory of the eigenvalues shown in the figure 6.8, which is obtained by increasing gradually the impedance of the transmission line of but 2 to 3 from 1 to the infinite value. When the impedance increases, two eigenvalues move to the right side in the shape of arc, which represents the system becoming unstable. At certain point, one moves to the left and the other moves very fast to the right infinity. When the impedance becomes large, the one that moved to the right infinity is canceled by a zero that is supposed to exist at the right infinity and appears again at the left infinity. When the impedance becomes very large to be considered almost the infinite value, which represent the lines are fully disconnected, the other one that moved to the left comes into the left half-plane, and thus the system become stable.

Third, a fault occurred at bus 3 and the lines from bus 3 to bus 4 were disconnected. No power was transferred through the lines, and thus powers generated from unit 1 and 2 were changed accordingly. Figure 6.9 shows the rotor speed variations of generating unit 1 and 2 diverged slowly over time, for both the WPP and the DEM. The right figure shows the dominant eigenvalue accountable for the power system being unstable, which moved into the graph from the right side. However, this is the different case from the previous ones because the eigenvalue moves much slower in the similar trajectory as the one shown in figure 6.8 by the line impedance increasing. Thus, even if the line impedance quite increases, for instance twenty or even thirty times, the power system will be still stable. In addition, the figure shows that the dominant eigenvalues of the power system with the DEM are the same as those with the WPP.

Fourth, a fault occurred at bus 13 and the lines from bus 3 to bus 13 were disconnected. Figure 6.10 shows the rotor speed variations of generating units 1 and 2 converged after making a small overshoot over time, for both the WPP and the DEM. In the right figure, the most dominant eigenvalue is moved a little to the left side but two dominant eigenvalues which is expected accountable for the overshoot were moved to the right side with decreased damping ratio.

Fifth, a fault occurred at bus 5 and the lines from bus 4 to bus 5 were disconnected. Figure 6.11 shows the rotor speed variations of generating units 1 and 2 diverged fast, for both the WPP and the DEM. The right figure shows the three eigenvalues were moved into the right half-plane for both results with the WPP and with the DEM.

Sixth, a fault occurred at bus 12 and the lines from bus 9 to bus 12 were disconnected. Figure 6.12 shows the rotor speed variations of generating units 1 and 2 diverged fast, for both the WPP and the DEM. The right figure shows the dominant eigenvalue accountable for the power system being unstable moved from the right side.

Seventh, a fault occurred at bus 13 and the lines from bus 12 to bus 13 were disconnected. Figure 6.13 shows the rotor speed variations of generating units 1 and 2 diverged slowly over time, for both the WPP and the DEM. The movements of the eigenvalues are similar as the sixth case, and the dominant eigenvalues of the power system with the DEM are the same as those with the WPP.

These all results confirm that the DEM has the same effects consistent with those of the WPP on the power system.

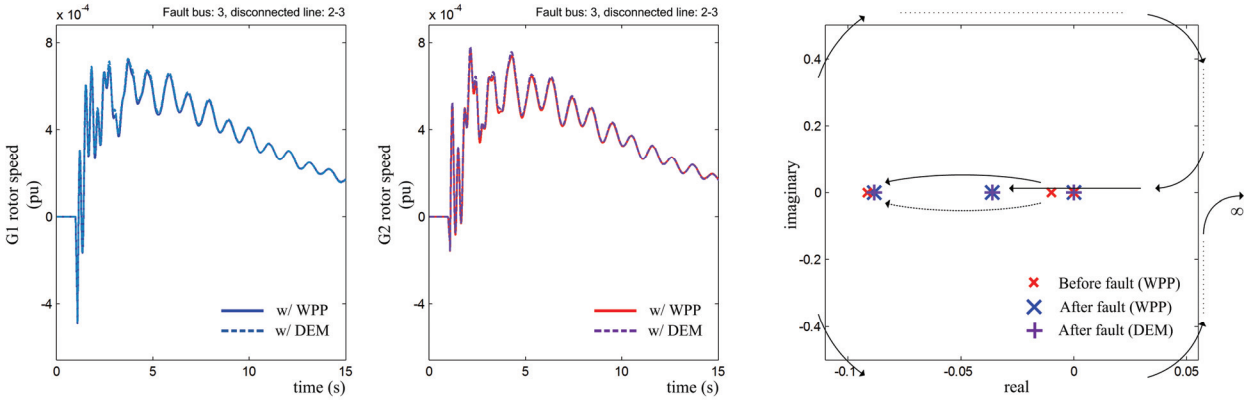

Fig. 6.6 Rotor speed variations of generating unit 1 (the left) and 2 (the middle) when a fault occurred at bus 3 and is cleared by fully tripping lines of bus 2 to 3: with using the WPP and with using the DEM. The dominant eigenvalues of the power system (the right): before and after the fault.

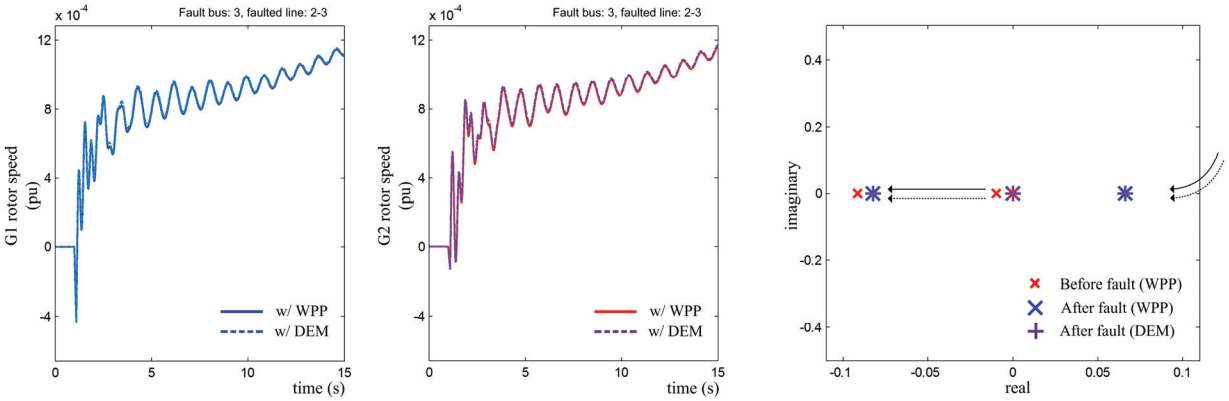

Fig. 6.7 Rotor speed variations of generating unit 1 (the left) and 2 (the middle) when a fault occurred at bus 3 and is not fully cleared by partially tripped lines of bus 2 to 3: with using the WPP and with using the DEM. The dominant eigenvalues of the power system (the right): before and after the fault.

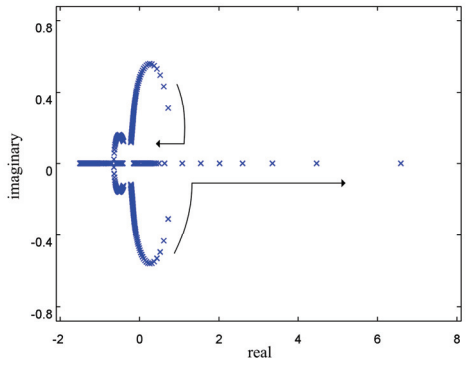

Fig. 6.8 Trajectory of the dominant eigenvalues of the power system where the impedance of transmission line between bus 2 and 3 is gradually increased from 1 to infinite value.

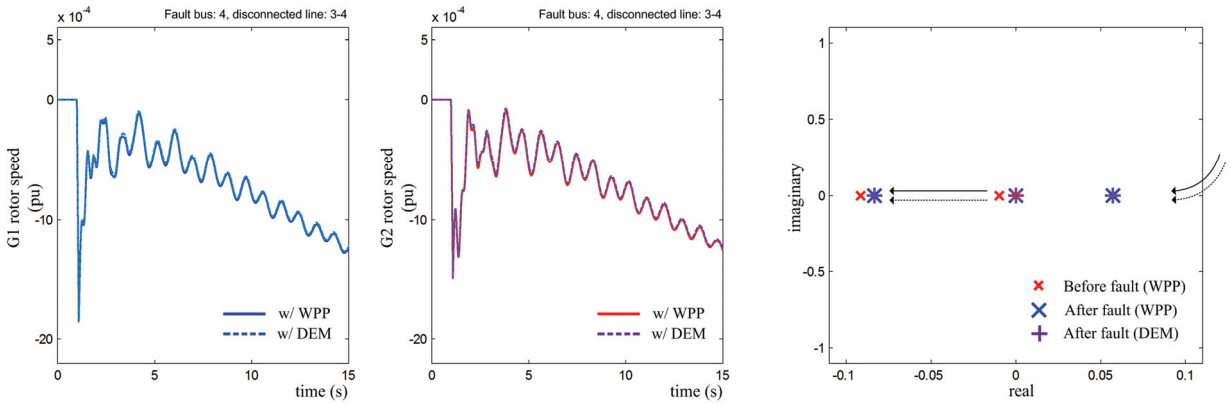

Fig. 6.9 Rotor speed variations of generating unit 1 (the left) and 2 (the middle) when a fault occurred at bus 4 and is cleared by fully tripping lines of bus 3 to 4: with using the WPP and with using the DEM. The dominant eigenvalues of the power system (the right): before and after the fault.

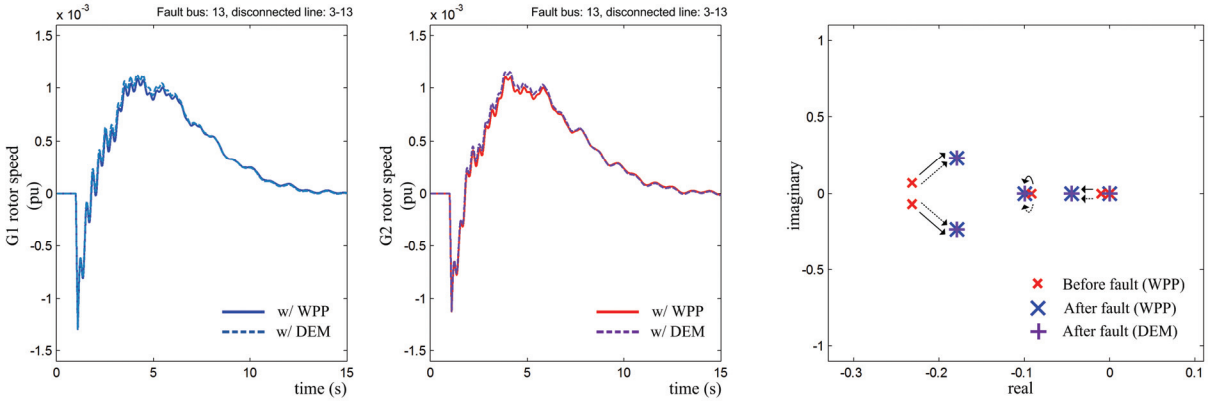

Fig. 6.10 Rotor speed variations of generating unit 1 (the left) and 2 (the middle) when a fault occurred at bus 13 and is cleared by fully tripping lines of bus 3 to 13: with using the WPP and with using the DEM. The dominant eigenvalues of the power system (the right): before and after the fault.

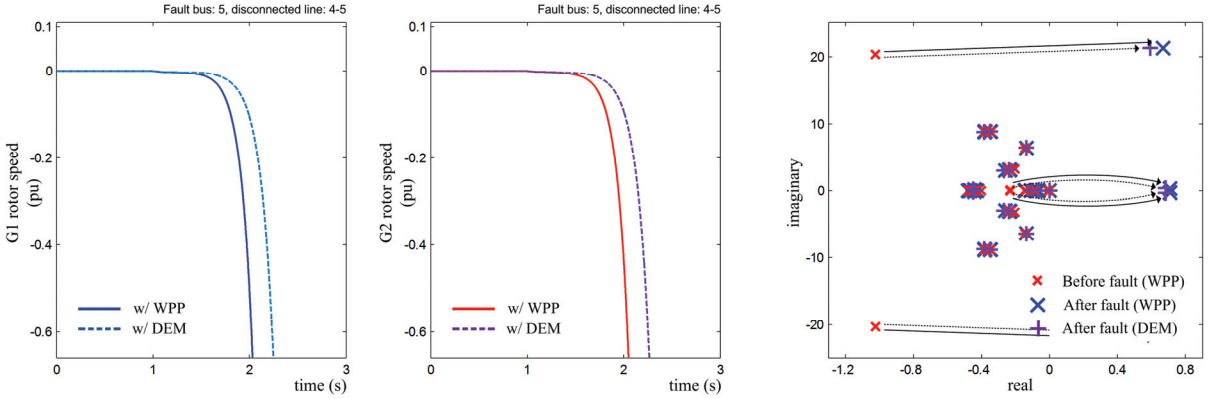

Fig. 6.11 Rotor speed variations of generating unit 1 (the left) and 2 (the middle) when a fault occurred at bus 5 and is cleared by fully tripping lines of bus 4 to 5: with using the WPP and with using the DEM. The dominant eigenvalues of the power system (the right): before and after the fault.

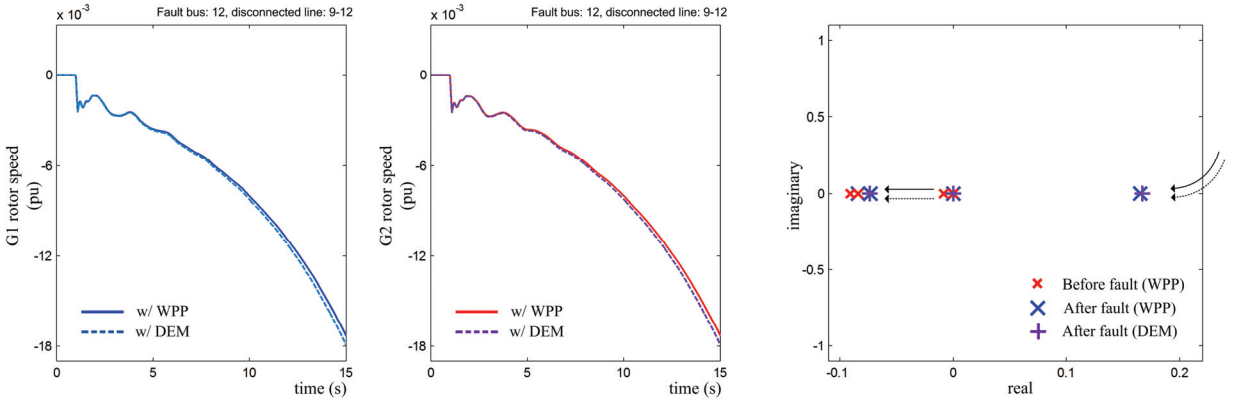

Fig. 6.12 Rotor speed variations of generating unit 1 (the left) and 2 (the middle) when a fault occurred at bus 12 and is cleared by fully tripping lines of bus 9 to 12: with using the WPP and with using the DEM. The dominant eigenvalues of the power system (the right): before and after the fault.

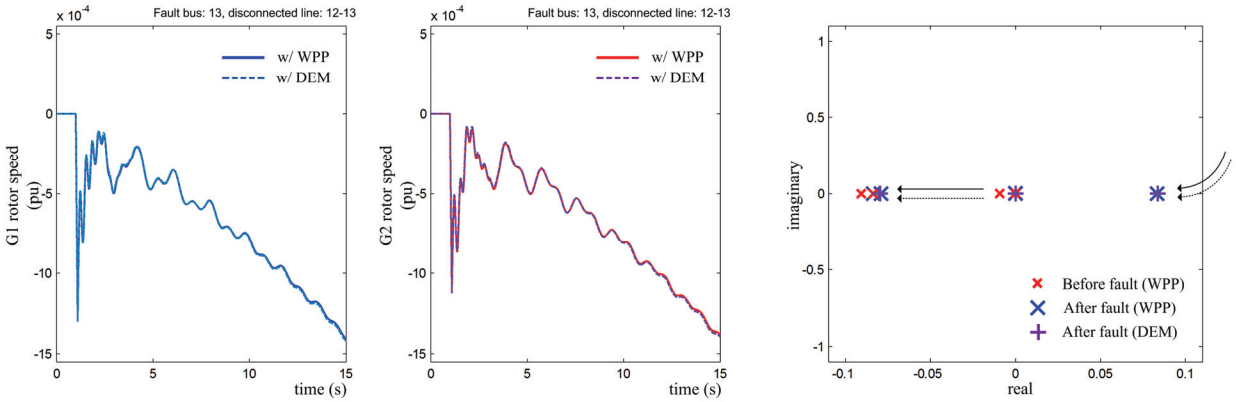

Fig. 6.13 Rotor speed variations of generating unit 1 (the left) and 2 (the middle) when a fault occurred at bus 13 and is cleared by fully tripping lines of bus 12 to 13: with using the WPP and with using the DEM. The dominant eigenvalues of the power system (the right): before and after the fault.

7.3 Simulation B

This section presents simulation tests using the DEM developed in chapter 5. For the tests, a WPP model using the local-frame network model 1 is applied and the corresponding DEM is obtained using the data generated with the full detailed of the WPP model. To interface the WPP model and its DEM into the power system, the method in subsection 2.2.3 is used.

7.3.1 Test system

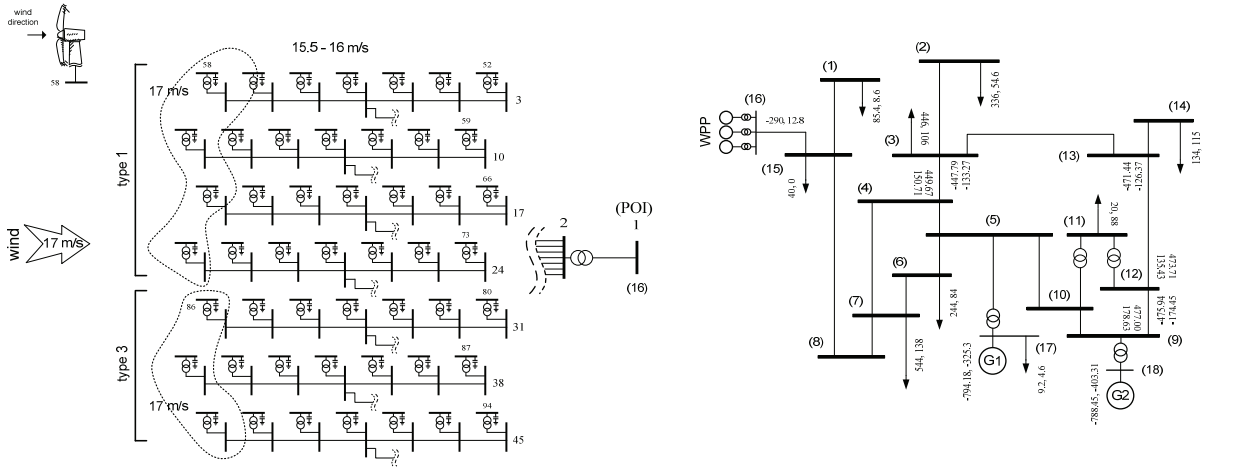

Fig. 6.14 Test system for simulation B

Test system for simulations is shown in figure 6.14. The WPP consists of 49 wind turbines (28 × type 1 and 21 × type 3) that are irregularly placed, as shown in the left of figure 6.14. The first column turbines directly facing the wind experience a wind speed of 17 m/s, while the other turbines experience only about 15.5 - 16 m/s owing to the wind wake effect. The rate wind speed for wind turbines is chosen 14m/s and thus all turbines have their pitch angles adjusted. The system parameters of the WPP are the same as those used for the simulation test in chapter 5. However, while the WPP used in chapter 5 was nonlinear model, in this subsection, the WPP is linearized on the operating points with respect to the wind speeds and used for the simulation tests. The DEM is also derived using the linearized WPP.

The power generated from one WPP at the wind speed is 96.7 MW with -4.27 Mvar, and it is assumed that two additional identical WPPs are connected to bus 16, which is done by amplifying the output power of the original WPP threefold. In the right of figure 6.14, it is seen a test system with a base power of 100 MVA in which two generating units with identical cost functions were assumed; the optimal operating conditions of these were determined by solving the optimal power flow problem. Based on the solution, generating unit 1 (at the swing bus) produced 794.18 MW with 325.3 Mvar and unit 2 produced 788.45 MW with 403.31 Mvar.

The performance of the DEM proposed in chapter 5 is verified by using the test system shown in figure 6.14. The wind turbines were clustered by respective types and wind powers, producing six groups and, correspondingly, six equivalent wind turbines. The slow dynamic model of the WPP is used and it has 203 state variables, while the DEM has 9 state variables.

To determine whether the DEM produced the same effect on the power system as the WPP, the rotor speed variations in generating units 1 and 2 were observed when a fault occurred and was cleared.

7.3.2 Results

First, it is assumed that a fault occurred at bus 3 and that the lines of bus 2 to 3 were disconnected 0.1 s after the fault. No power was transferred to the load connected at the bus 2, and thus powers generated from unit 1 and 2 were reduced accordingly. By the reduced powers, the damping abilities of generating units were expected to increase. Figure 6.15 shows the rotor speed variations of generating unit 1 and 2. It is seen that, for both the WPP and DEM, the variations in rotor speed converged over time. The right figure shows the eigenvalues of the corresponding power systems, where one is with using the WPP and the other is with using the DEM. Although there is a very small displacement between the most dominant poles, which determine the system stability, of the power systems, it is negligible in terms of the stability issue.

Second, it is assumed that three of the four lines from bus 2 to bus 3 were disconnected, causing the impedance on the remaining line to increase fourfold. In this case, the generating units 1 and 2 should generate more reactive power to meet the load connected at bus 2, and it causes the damping ability of generating units to decrease so that the power system is unstable. Figure 6.16 shows the variations in rotor speed diverged fast over time for both the WPP and the DEM and the right figure shows the dominant eigenvalues of the corresponding power systems. Here, one thing is noticed that the power system with the WPP has two more dominant eigenvalues compared to the power system with the DEM. It is expected that the dynamics of the power system appear by the combination of these two dominant and the most dominant eigenvalues, but the divergence is mostly determined by the most dominant eigenvalue in this case. As seen the power system with the WPP has the smaller dominant eigenvalue than that with the DEM, and thus it diverged slower than the power system with the DEM.

Third, a fault occurred at bus 3 and the lines from bus 3 to bus 4 were disconnected. No power was transferred through the lines, and thus powers generated from unit 1 and 2 were changed accordingly. Figure 6.17 shows the rotor speed variations of generating unit 1 and 2 diverged slowly over time, for both the WPP and the DEM. The right figure shows the dominant eigenvalue moved from the right side, which is accountable for the power system being unstable. The figure also shows that the dominant eigenvalues of the power system with the DEM are the same as those with the WPP.

Fourth, a fault occurred at bus 13 and the lines from bus 3 to bus 13 were disconnected. Figure 6.18 shows the rotor speed variations of generating units 1 and 2 converged over time, for both the WPP and the DEM. In the right figure, the most dominant eigenvalue was moved to the left side and one existed out of the graph was moved to the right side, so they become complex eigenvalues. This figure also confirms that the eigenvalues of the power systems with the WPP and DEM moved in the same pattern.

Fifth, a fault occurred at bus 5 and the lines from bus 4 to bus 5 were disconnected. Figure 6.19 shows the rotor speed variations of generating unit 1 and 2 diverged slowly oscillating over time, for both the WPP and the DEM. The right figure also confirms that the dominant eigenvalues of the power sistem with the DEM moved the same as those with the WPP.

Sixth, a fault occurred at bus 12 and the lines from bus 9 to bus 12 were disconnected. Figure 6.20 shows the rotor speed variations of generating unit 1 and 2 slowly diverged, for both the WPP and the DEM. The right figure shows that the movements of the dominant eigenvalues are similar as the fifth case, but they moved to the right side more.

Seventh, a fault occurred at bus 13 and the lines from bus 12 to bus 13 were disconnected. Figure 6.21 shows the rotor speed variations of generating units 1 and 2 with using the WPP, and with using the DEM. The variations diverged very fast over time for both the WPP and the DEM. As seen in the right figure, the most dominant eigenvalue moved far to the right side in the right half-plane.

Lastly, we might mistakenly conclude the DEM performance is relatively inaccurate by the result shown in the figure 6.16, 20, and 21 owing to the small dissimilarities between the curves. However, when any of states in power system diverge quickly, it results in large difference in the state even by very small difference in system parameters of the WPP and the DEM. Thus, it will be adequate to check if the power system with the DEM becomes stable or unstable in a manner consistent with the WPP to confirm the DEM's validity.

More tests were carried out to confirm the consistent effects of the DEM on the power system. Figure 6.22 show the results for six different faults. The results shows that the variations in the rotor speed, with using the WPP and

with using the DEM, are dynamically alike (slightly more or less), and the results confirm that the DEM is valid on power system dynamic study.

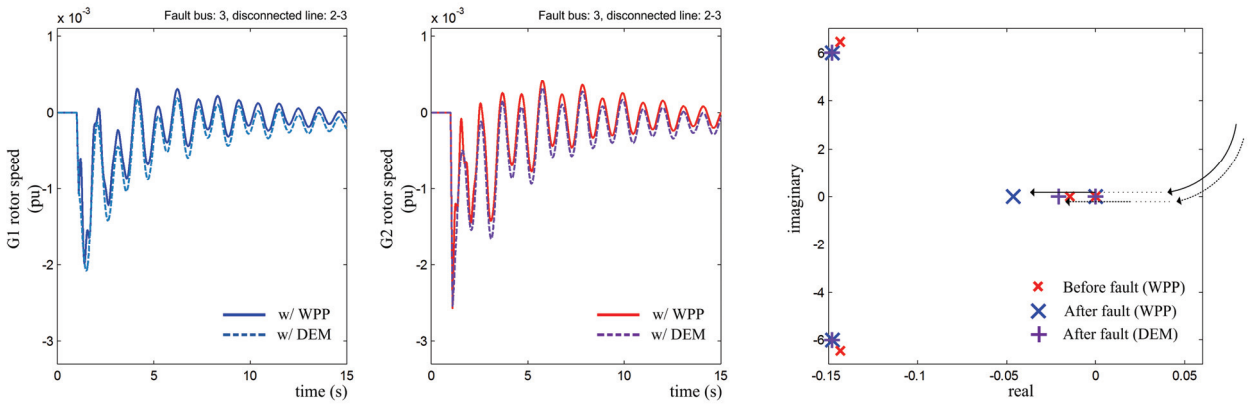

Fig. 6.15 Rotor speed variations of generating unit 1 (the left) and 2 (the middle) when a fault occurred at bus 3 and is cleared by fully tripping lines of bus 2 to 3: with using the WPP and with using the DEM. The dominant eigenvalues of the power system (the right): before and after the fault.

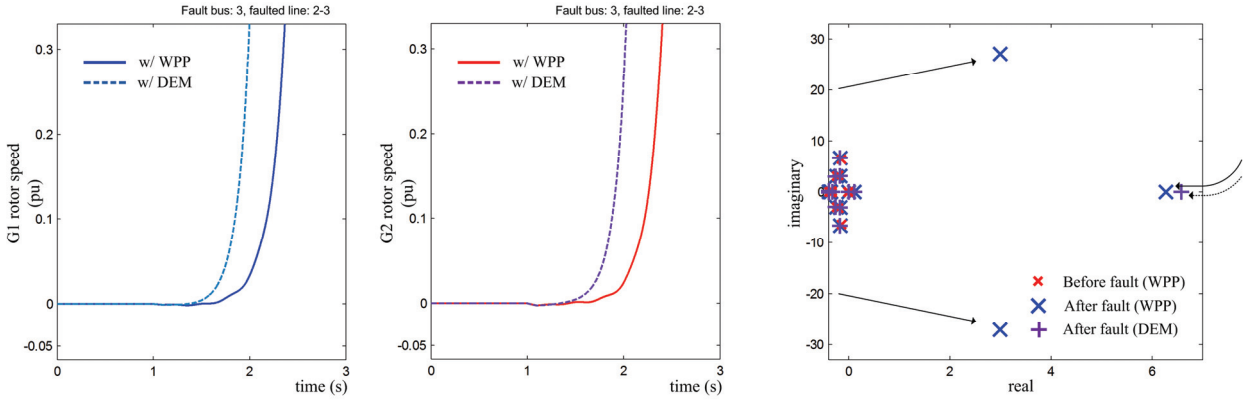

Fig. 6.16 Rotor speed variations of generating unit 1 (the left) and 2 (the middle) when a fault occurred at bus 3 and is not fully cleared by partially tripped lines of bus 2 to 3: with using the WPP and with using the DEM. The dominant eigenvalues of the power system (the right): before and after the fault.

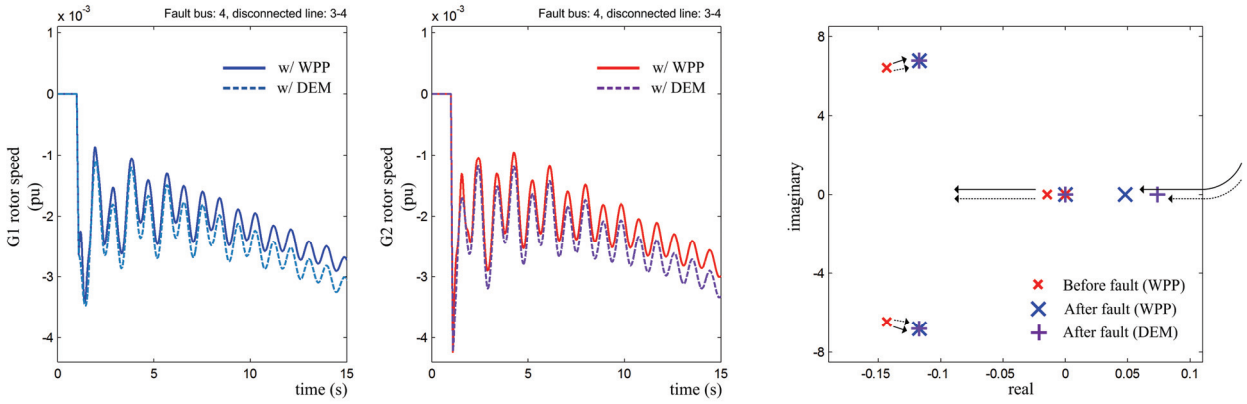

Fig. 6.17 Rotor speed variations of generating unit 1 (the left) and 2 (the middle) when a fault occurred at bus 4 and is cleared by fully tripping lines of bus 3 to 4: with using the WPP and with using the DEM. The dominant eigenvalues of the power system (the right): before and after the fault.

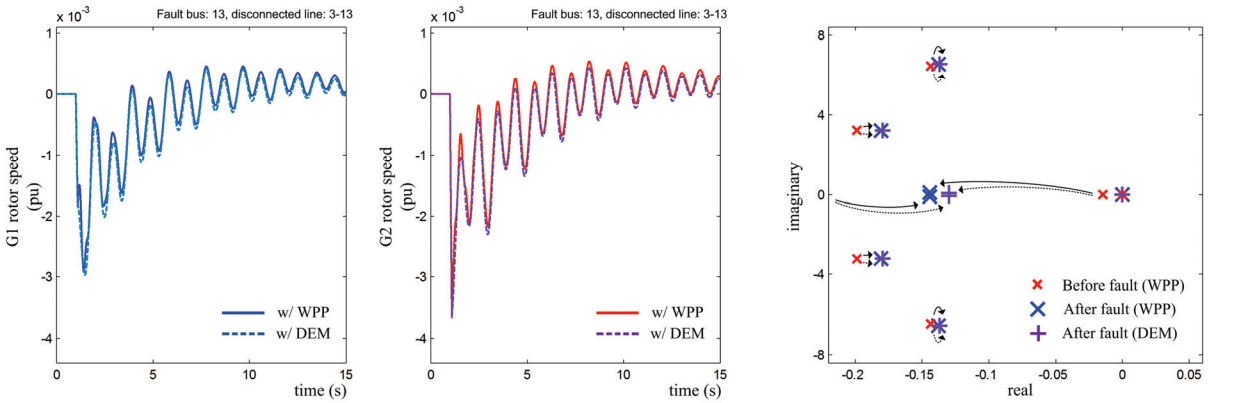

Fig. 6.18 Rotor speed variations of generating unit 1 (the left) and 2 (the middle) when a fault occurred at bus 13 and is cleared by fully tripping lines of bus 3 to 13: with using the WPP and with using the DEM. The dominant eigenvalues of the power system (the right): before and after the fault.

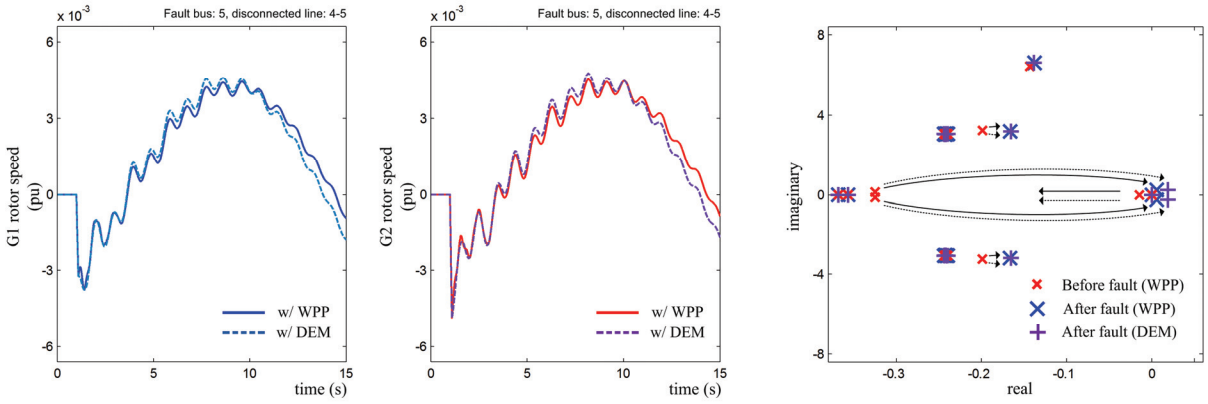

Fig. 6.19 Rotor speed variations of generating unit 1 (the left) and 2 (the middle) when a fault occurred at bus 5 and is cleared by fully tripping lines of bus 4 to 5: with using the WPP and with using the DEM. The dominant eigenvalues of the power system (the right): before and after the fault.

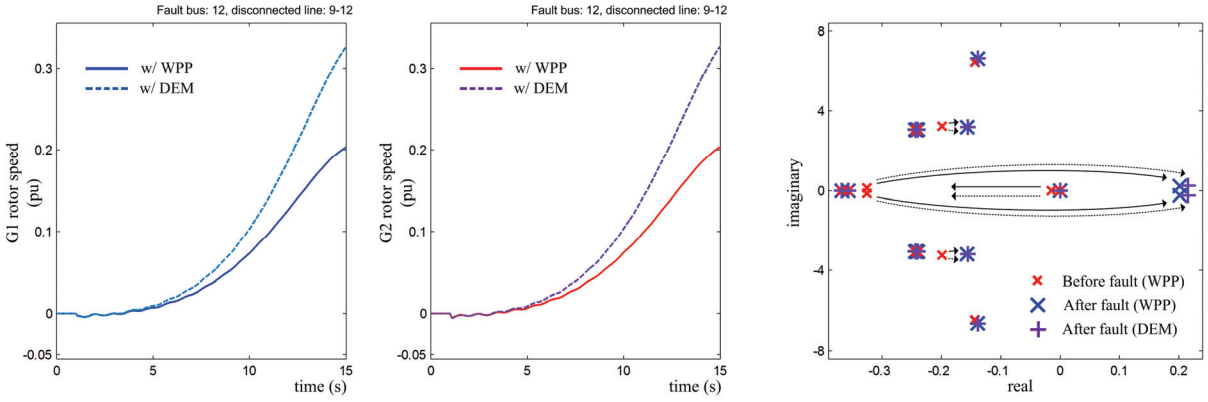

Fig. 6.20 Rotor speed variations of generating unit 1 (the left) and 2 (the middle) when a fault occurred at bus 12 and is cleared by fully tripping lines of bus 9 to 12: with using the WPP and with using the DEM. The dominant eigenvalues of the power system (the right): before and after the fault.

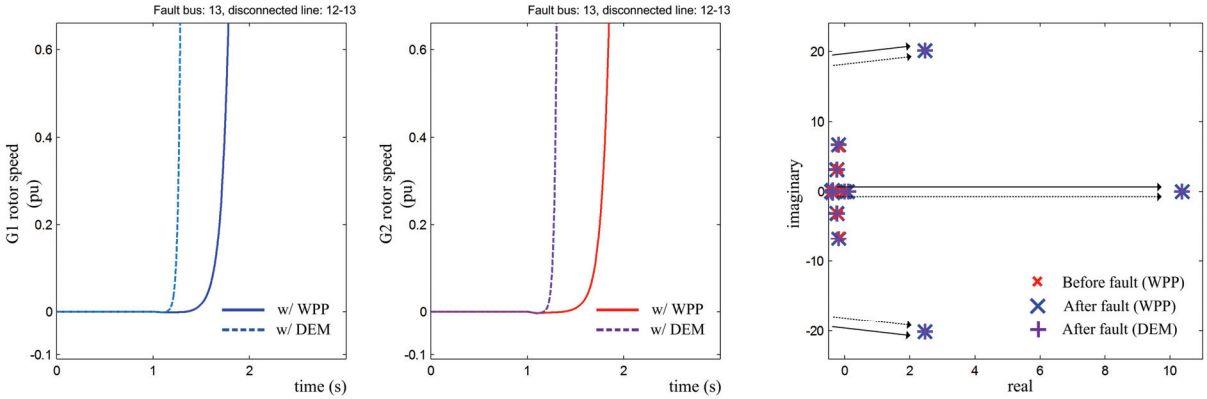

Fig. 6.21 Rotor speed variations of generating unit 1 (the left) and 2 (the middle) when a fault occurred at bus 13 and is cleared by fully tripping lines of bus 12 to 13: with using the WPP and with using the DEM. The dominant eigenvalues of the power system (the right): before and after the fault.

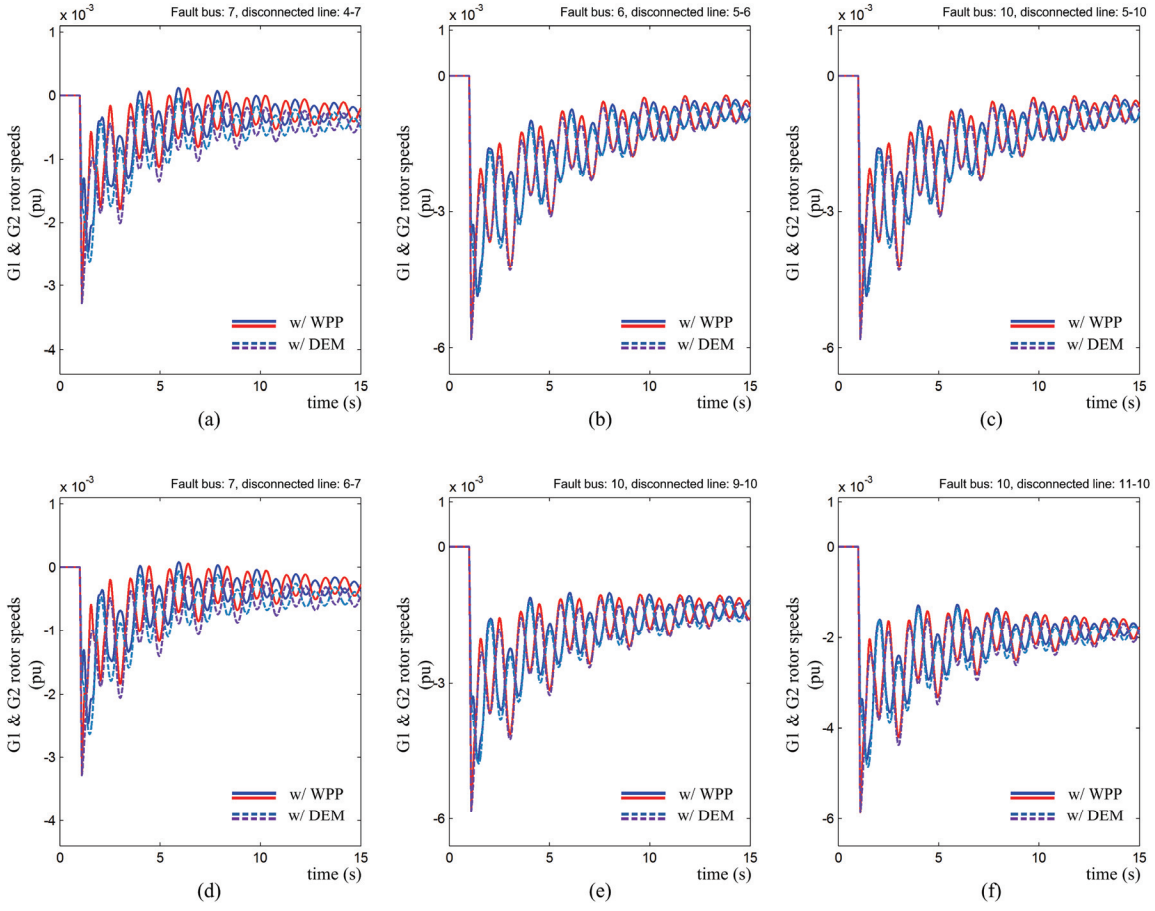

Fig. 6.22 Rotor speed variations of generating unit 1 and 2, when a fault occurred (a) at bus 7: line 4-7, (b) at bus 6: line 5-6, (c) at bus 10: line 5-10, (d) at bus 7: line 6-7, (e) at bus 10: line 9-10, and (f) at bus 10: line 11-10.

7.4 Conclusions

In this chapter, simulation tests to verify the validity of the DEMs were finalized. Firstly, basic power system to be used for the simulation tests was introduced. The power system was derived on the basis of IEEE 39 bus power system introduced in the chapter 6. In addition, it is explained how the simulation tests were processed. Unlike nonlinear power systems whose system parameters are updated at every time instance, a linear power system uses updated system parameters on the basis of events which cause operating points to largely deviate from initially given conditions. Thus, to make it clear how the simulation tests are carried out, the process of the simulation was explained with an example.

The sections of simulation A and B were allocated to prove the validity of the DEMs, specifically, when they were interacted with a power system. In simulation A, the DEM developed in the chapter 3, on the basis of aggregation technique, was used. In simulation B, the DEM developed in the chapter 5, on the basis of parameter identification technique, was used. The simulation tests were conducted by comparing the dynamics of the WPP and the DEM under several fault conditions. The simulation testing of the DEMs confirmed that they have the same effects on power system dynamics as a WPP model.

The simulation results showed that the both proposed DEMs significantly reduced the order of the system without sacrificing accuracy. The usefulness of the DEMs increases with the number of wind turbines in the WPP, and they are expected to be useful not only for WPP design but also for power system dynamic study.

Chapter 8

Conclusions

As the number of large-scale wind power plants increase, their significant impacts on existing power system became inevitable, and thus large-scale wind power plants are required to contribute for the stable operation of the power system as conventional generating units. However, because the wind power plants are basically different from the conventional power plants in terms of structure, operation, and dynamics, lots of efforts to understand their fundamental characteristic, problems, and requirements for stable operations have been made over numerous researches. Dynamic study for wind power plants, in particular, is an important area because stable operation for both wind power plants and power system cannot be achieved without understanding their dynamic characteristics. Therefore, dynamic equivalent models of wind power plants are required for dynamics study of power system including wind power plants.

As the dominant electromechanical dynamics are mostly slow frequency components due to the inter-area power transfer, power system dynamics are studied in terms of slow dynamics, and thus dynamic equivalent models of wind power plants are required to be developed to serve the purpose. This study was dedicated to develop fair dynamic equivalent models of wind power plants. The study extended over six chapters, each making contributions with a specific purpose.

- Chapter 2 has been allocated to develop dynamic models of wind power plants. As dynamics of wind power plant are created by dynamics of individual wind turbines and their interactions, accurate dynamic models of wind turbines and models of networked cables between them were developed. Furthermore, dynamic models of wind turbines in their local frames and network models matching for the dynamic models were established. The models of wind turbines and network were combined to complete a dynamic model of wind power plants.
- As the dynamic model developed in chapter 2 embodied complicated structure of wind power plants, the model became very complex. Therefore, reduced dynamic equivalent models (DEMs) of wind power plants (WPPs) were developed in chapter 3. In chapter 3, the concepts of equivalent model development using an aggregation technique were first introduced, and slow dynamic equivalent model of wind turbines was presented by using the aggregation technique. Also, how to develop an equivalent model representing multiple slow dynamic models of wind turbines was mentioned. Equivalent network models matching the equivalent models were developed. Finally, the equivalent models of multiple wind turbines and network models were combined to represent a DEM of a WPP.
- Wind power plants are centrally regulated to contribute to the stable operation of power system. The central regulation can be achieved under the condition that all wind turbines are accurately tracking the references created from the control center of the wind power plants. Inadequately designed controllers decrease the damping in slow electromechanical dynamics, and thus the controlled system could be unstable when they interact with other systems. Therefore, a fair control design for individual wind turbines is required, and it was achieved in chapter 4. In chapter 4, Linear Quadratic Integral Regulator (LQIR) method was introduced and the gain matrix for the LQIR method was derived by solving linear programming, which was configured using the DEM developed in chapter 3, in a Linear Matrix Inequality (LMI) frame. The control design introduced in this chapter was used for simulation tests in this study.
- In chapter 5, a linear DEM development technique based on measurements at point of interconnection as well

as equivalent wind speeds was introduced, which does not require the knowledge of system parameters and operating status. The DEM was adaptively developed using Recursive Least Square (RLS) method. In addition, nonlinear DEM development technique using neural network was introduced as a comparable method. It was noted that the linear DEM gives well-generalized performance while the nonlinear DEM requires large computation and training process. The adaptiveness and dynamic performance of the DEM was verified by simulation tests at the end of the chapter.

- To verify the validity of the DEM proposed in chapter 3 and 5, a model of power systems was essential for simulation tests that interacted with power systems. Thus, power system modelling was introduced in chapter 6. Since the DEM was developed in the rotating dq-frame, models of generating units and network in power system were represented in the dq-frame as well. Generating units sometimes includes power system stabilizer (PSS) to enhance stability of power system, and thus PSS design was also introduced. It was shown that network stability could be checked using dynamic network models. Although the dynamic network models are generally stable because the network simply consists of resistance, inductance, and capacitance, they could be unstable if high frequency components were injected into the network due to improper control or system structure. It was proved with simple tests using a dynamic network model. As static network models can be used in cases where a dynamic network model is stable under the assumptions of improper high frequency components damped out fast, lumped (reduced) static network models with three different types of loads were introduced: 1) admittance loads, 2) constant current loads, and 3) constant power loads. It was shown that the lumped network model could be useful when applying either constant current loads or constant power loads. Also, the effects of PSS on power system using network models with different loads were briefly studied. At the end of the chapter, by using IEEE 39 bus system, an example of dynamics in power system by a fault condition was shown.
- In chapter 7, it was proved the proposed DEMs are valid with respect to dynamic study on power systems interacted. Firstly, a basic power system was introduced, and then the DEM performances were compared with those of the WPP, where both interacted with the power system. The simulation tests were carried out under several fault conditions, and simulation testing of the DEMs confirmed that they have the same effects on power system dynamics as the WPP.

This entire study has been devoted to develop accurate dynamic models of wind power plants and the corresponding dynamic equivalent models, and to verify their validities. The dynamic equivalent models were achieved by using two different development methods: 1) equivalent slow dynamic models for groups of wind turbines within the wind power plant were developed and aggregated into an equivalent static network model to formulate a low-order DEM for a WPP, 2) a low-order DEM was adaptively developed using the RLS identification method on the basis of measurements of voltage and power at point of interconnection, and wind speeds. This study carefully verified the validity of the DEMs with simulation experiments. The proposed DEMs are highly beneficial when the number of turbines in a WPP is very large. We conclude the DEMs are useful not only for wind power plant design but also for power system dynamic study.

References

[1] L. Wang, M. Klein, S. Yirga, and P. Kundur, "Dynamic reduction of large power systems for stability studies," *IEEE Trans. Power Syst.*, vol. 12, no. 2, pp. 889-895, May 1997.

[2] G. Troullinos, J. Dorsey, H. Wong, and J. Myers, "Reducing the Order of Very Large Power System Models", *IEEE Trans. Power Syst.*, vol. 3, no.1, pp. 127-133, Feb. 1988.

[3] Y. Mansour, E. Vaahedi, A.Y. Chang, B.R. Coms, B.W. Garrett, K. Demaree, T. Athay, K. Cheung, "B.C. Hydro's On-line Transient Stability Assessment (TSA) Model Development, Analysis, and Post-processing", *IEEE Trans. Power Syst.*, vol. 10, no. 1, pp. 241-253, Feb. 1995.

[4] J. H. Chow, J. Cullum, and R. A. Willoughby, "A sparsity-based technique for identifying slow-coherent areas in large power systems," *IEEE Trans. Power App. Syst.*, vol. 103, no. 3, Mar. 1984.

[5] B. Avramovic, P. V. Kokotovic, J. R. Winkelman, and J. H. Chow, "Area decomposition for electromechanical models of power systems," *Automatica*, vol. 16, no. 6, pp. 637-648, Nov. 1980.

[6] J. H. Chow, F. F. Wu, and J. A. Momoh, *Applied Mathematics for Restructured Electric Power Systems: Optimization, Control, and Computational Intelligence*. Springer, 2005.

[7] U. D. Annakkage, N. K. C. Nair, Yuefeng Liang, A. M. Gole, V. Dinavahi, Bjorn Gustavsen, Taku Noda, Hassan Ghasemi, A. Monti, Mah Matar, R. Iravani, and J. A. Martinez, "Dynamic system equivalents: a survey of available techniques," *IEEE Trans. Power Del.*, vol. 27, no. 1, pp. 411-420, Jan. 2012.

[8] European SmartGrid Technology Platform, "Vision and strategy for Europe's electricity networks of the future," EU Commission, Directorate-General for Research, Information and Communication Unit, Brussels, Belgium, 2006.

[9] U.S. Federal Energy Regulatory Commission (FERC), "Smart grid policy," DOE: Washington, D.C., Docket No. PL09-4-000, July 2009.

[10] U.S. Department of Energy, "20% wind energy by 2030: increasing wind energy's contribution to U.S. electricity supply," 2008.

[11] European Wind Energy Association, "Pure power – wind energy targets for 2020 and 2030," Nov. 2009.

[12] North American Electric Reliability Corporation (NERC), "Accommodating high levels of variable generation," NERC: Princeton, NJ, Apr. 2009.

[13] European Wind Energy Association: "Economics of wind energy," Mar. 2009.

[14] E. Fagan, S. Grimes, J. McArdle, P. Smith, and M. Stronge, "Grid code provisions for wind generators in Ireland," IEEE Power Eng. Soc. General Meeting, vol. 2, pp 1241-1247, 2005.

[15] I. Erlich and U. Bachmann, "Grid code requirements concerning connection and operation of wind turbines in Germany," IEEE Power Eng. Soc. General Meeting, vol. 2, pp 1253-1257, 2005.

[16] R. M. Zavadil and J. C. Smith, "Status of wind-related US national and regional grid code activities," IEEE Power Eng. Soc. General Meeting, vol. 2, pp 1258-1261, 2005.

[17] F. Iov, R. Teodorescu, F. Blaabjerg, B. Andresen, J. Birk, and J. Miranda, "Grid Code Compliance of Grid-Side Converter in Wind Turbine Systems", IEEE 37th Power Electr. Specialists Conf., June 2006.

[18] M. P. Palsson, T. Toftevaag, K. Uhlen, and J. O. G. Tande, "Large-scale wind power integration and voltage stability limits in regional networks," IEEE Power Eng. Soc. Meeting, vol. 2, pp. 762-769, 2002.

[19] F. Ghassemi and K.-L. Koo, “Equivalent network for wind farm harmonic assessments,” *IEEE Trans. Power Del.*, vol. 25, no. 3, pp. 1808-1815, July 2010.

[20] M. A. El-Sharkawi, "Choice of model and topology for external equivalent systems," *IEEE Trans. Power App. Syst.*, pp. 3761–3768, Dec. 1983.

[21] R. Podmore, “Identification of coherent generators for dynamic equivalents”, *IEEE Trans. Power App. Syst.*, vol. pas-97, pp. 1344-1354, July/Aug. 1978.

[22] R. Nath, S.S. Lamba, K.S. Prakasa Rao, “Coherency based system decomposition into study and external areas using weak coupling”, *IEEE Trans. Power App. Syst.*, vol. 104, pp. 1443-1449, June, 1985.

[23] J.H. Chow, R. Galarza, P. Accari, and, W.W. Price, “Inertial and Slow Coherency Aggregation Algorithms for Power System Dynamic Model Reduction”, *IEEE Trans. Power Syst.*, vol. 10, no. 2, pp. 680-685, May 1995.

[24] R. A. Date and J. H. Chow, “Aggregation properties of linearized two-time-scale power network,” *IEEE Trans. Circuits Syst.*, vol. 38, no. 7, pp. 720-730, July 1991.

[25] J. Machowski, J. W. Bialek, and J. R. Bumby, *Power System Dynamics 2nd edition: Stability and Control.* New York: Wiley, 2008.

[26] A. J. Germond and R. Podmore, “Dynamic aggregation of generating unit models,” *IEEE Trans. Power App. Syst.*, vol. 97, pp. 1060-1069, July/Aug. 1978.

[27] M. L. Ourari, L.-A. Dessaint, and V.-Q. Do, “Dynamic equivalent modeling of large power systems using structure preservation technique,” *IEEE Trans. Power Syst.*, vol. 21, no. 3, pp. 1284-1295, Aug. 2005.

[28] B. C. Moore, “Principle component analysis in linear systems: controllability, observability, and model reduction,” *IEEE Trans. Automat. Contr.*, vol. 26, no. 1, pp. 17-32, Feb. 1981.

[29] R. J. Newell, M. D. Risan, L. Allen, I. S. Rao, and D. L. Stuehm, “Utility experience with coherency-based dynamic equivalents of very large systems,” *IEEE Trans. Power App. Syst.*, vol. 104, no. 11, pp. 3056–3063, Nov. 1985.

[30] S. B. Yusof, G. J. Rogers, and R. T. H. Alden, “Slow coherency based network partitioning including load buses,” *IEEE Trans. Power Syst.*, vol. 8, no. 3, pp. 1375–1382, Aug. 1993.

[31] S. Geeves, “A modal-coherency technique for deriving dynamic equivalents,” *IEEE Trans. Power Syst.*, vol. 3, no. 1, pp. 44–51, Feb. 1988.

[32] V. Akhmatov and H. Knudsen, “An aggregated model of a grid-connected, large-scale, offshore wind farm for power stability investigations – importance of windmill mechanical system,” *Elect. Power Energy Syst.*, vol. 24, pp. 709-717, Dec. 2002.

[33] H. A. Pulgar-Painemal and P. W. Sauer, “Towards a wind farm reduced-order model,” *Electric Power Syst. Research*, vol. 81, pp. 1688-1695, Dec. 2011.

[34] J. Usaola, P. Ledesma, J. M. Rodriguez, J. L. Fernandez, D. Beato, R. Iturbe, and J. R. Wilhelmi, “Transient stability studies in grids with great wind power penetration. Modelling issues and operation requirements,” IEEE Power Eng. Soc. General Meeting, vol. 3, pp. 1534-1541, July 2003.

[35] L. M. Fernandez, C. A. Garcia, J. R. Saenz, and F. Jurado, “Reduced model of DFIGs wind farms using aggregation of wind turbines and equivalent wind,” IEEE Electrotechnical Conf., 2006.

[36] E. Muljadi, C. P. Butterfield, A. Ellis, J. Mechenbier, J. Hochheimer, R. Young, N. Miller, R. Delmerico, R. Zavadil, and J. C. Smith, “Equivalencing the collector system of a large wind power plant,” IEEE Power Eng. Soc. General Meeting, 2006.

[37] E. Muljadi, S. Pasupulati, A. Ellis, and D. Kosterov, “Method of equivalencing for a large wind power plant with multiple turbine representation,” IEEE Power Energy Soc. General Meeting, pp. 1-9, July 2008.

[38] L. M. Fernandez, J. R. Saenz, and F. Jurado, “Dynamic models of wind farms with fixed speed wind turbines,” *Renew. Energy*, vol. 31, pp. 1203-1230, Dec. 2006.

[39] L. M. Fernandez, F. Jurado, and J. R. Saenz, “Aggregated dynamic model for wind farms with doubly fed induction generator wind turbines,” *Renew. Energy*, vol. 33, pp. 129-140, Dec. 2008.

[40] D. N. Hussein, M. Matar, and R. Iravani, “A type-4 wind power plant equivalent model for the analysis of electromagnetic transients in power systems,” *IEEE Trans. Power Syst.*, vol. 28, no. 3, pp. 3096-3104, Aug. 2013.

[41] L. Wang and K.-H. Wang, "Dynamic stability analysis of a DFIG-based offshore wind farm connected to a power grid through an HVDC link," *IEEE Trans. Power Syst.*, vol. 26, no. 3, pp. 1501-1510, Aug. 2011.

[42] J. Brochu, C. Larose, and R. Gagnon, "Validation of single- and multiple equivalents for modeling wind power plants," *IEEE Trans. Energy Convers.*, vol. 26, no. 2, pp. 532-541, June 2011.

[43] J. Brochu, C. Larose, and R. Gagnon, "Generic equivalent collector system parameters for large wind power plants," *IEEE Trans. Energy Convers.*, vol. 26, no. 2, pp. 542-549, June 2011.

[44] Y. Jin and P Ju, "Dynamic equivalent modeling of FSIG based wind farm according to slip coherency," Int. Conf. on Sustainable Power Generation and Supply, 2009.

[45] F. Kanellos and N. Hatziargyriou, "Dynamic equivalents of distribution networks with embedded wind parks," IEEE Power Tech Conf. Proc., Bologna, Italy, 2003.

[46] Z. Meng and F. Xue, "An investigation of the equivalent wind method for the aggregation of DFIG wind turbines," Power and Energy Engineering Conf. (APPEEC), 2010.

[47] R. Castro and J. Ferreira de Jesus, "Wind park reduced-order model using singular perturbations theory," *IEEE Trans. Energy Convers*., vol. 11, pp. 735–741, 1996.

[48] A. Morton, "Model aggregation of wind farms and other ensemble systems," Australasian Universities Power Engineering Conf. (AUPEC), 2007.

[49] S. Heier, *Grid Integration of Wind Energy Conversion Systems.* NY: Wiley, 1998.

[50] Generic Type-3 Wind Turbine-Generator Model for Grid Studies, Version 1.1, WECC Wind Generator Modeling Group, Sep. 2006.

[51] B. Boukhezzar and H. Siguerdidjane, "Nonlinear control on a variable speed wind turbine using a two-mass model," *IEEE Trans. Energy Convers*., vol. 26, no. 1, pp. 149–162, Mar. 2011.

[52] A. E. Fitzgerald and C. Kingsley, *Electric Machinery*. McGraw-Hill, 1961.

[53] O. Anaya-Lara, N. Jenkins, J. Ekanayake, P. Cartwright, and M. Hughes, *Wind Energy Generation: Modeling and Control*. Wiley, 2009

[54] P. Ledesma and J. Usaola, "Doubly fed induction generator model for transient stability analysis," *IEEE Trans. Energy Convers*., vol. 20, pp. 388–397, 2005.

[55] L. Yazhou, A. Mullane, G. Lightbody, and R. Yacamini, "Modeling of the wind turbine with a doubly fed induction generator for grid integration studies," *IEEE Trans. Energy Convers*., vol. 21, pp. 257–264, 2006.

[56] J. Ekanayake, L. Holdsworth, W. XueGuang, and N. Jenkins, "Dynamic modeling of doubly fed induction generator wind turbines," *IEEE Trans. Power Syst*., vol. 18, pp. 803–809, 2003.

[57] S. Auddy, R. Varma, and M. Dang, "Field validation of a doubly fed induction generator (DFIG) model," IEEE Elect. Power Conf. (EPC 2007), 2007, pp. 484–489.

[58] L. A. Fajardo-R, A. Medina, and F. Iov, "Dynamics of 'abc' and 'qd' constant parameters induction generator model: wind park application," Int. Conf. on Elect. Machines and Systems (ICEMS 2009), 2009, pp. 1–6.

[59] S. Chellapilla and B. Chowdhury, "Dynamic model of induction generators for wind power studies," IEEE Power Eng. Soc. General Meeting, 2003.

[60] W. Qiao, R. G. Harley, and G. K. Venayagamoorthy "Dynamic modeling of wind farms with fixed-speed wind turbine generators," IEEE Power Eng. Soc. General Meeting, 2007.

[61] R. Pena, J. C. Clare, and G. M. Asher, "Doubly fed induction generator using back-to-back PWM converters and its application to variable-speed wind-energy generation," IEE Proc. Elect. Power Applicat., vol. 143, no. 3, pp. 231-241, May 1996.

[62] L. M. Tolbert, F. Z. Peng, and T. G. Habetler, "Multilevel converters for large electric drives," *IEEE Trans. Ind. Applicat.*, vol. 35, no. 1, pp. 36-44, Jan. 1999.

[63] D.-E. Kim and D.-C. Lee, "Feedback linearization control of grid-interactive PWM converters with LCL input filters," *Journal of Power Electron.*, vol.9, no.2, pp. 288-299, 2009.

[64] J. W. Kolar, T. Friedlli, J. Rodriguez, and P. W. Wheeler, "Review of three-phase PWM AC-AC converter topologies," *IEEE Trans. Ind. Electron.*, vol. 58, no. 11, pp. 4988-5006, Nov. 2011.

[65] D.-W. Chung, J.-S. Kim, and S.-K. Sul, "Unified voltage modulation technique for real-time three-phase power conversion," *IEEE Trans. Ind. Applicat.*, vol. 34, no. 2, pp. 374-380, Mar. 1998.

[66] H. Akagi, E. H. Watanabe, and M. Aredes, *Instantaneous Power Theory and Applications to Power Conditioning*. Piscataway, NJ: IEEE Press, 2007, pp. 41–104.

[67] M. Aoki, "Control of large-scale dynamic systems by aggregation," *IEEE Trans. Automat. Contr.*, vol. 13, no. 3, pp. 246-253, June 1968.

[68] M. Aoki, "Some approximation methods for estimation and control of large scale systems," *IEEE Trans. Automat. Contr.*, vol. 23, no. 2, pp. 173-182, Apr. 1978.

[69] B. C. Moore, "Principle component analysis in linear systems: controllability, observability, and model reduction," *IEEE Trans. Automat. Contr.*, vol. 26, no. 1, pp. 17-32, Feb. 1981.

[70] S. Wußow, L. Sitzki, and T. Hahm, "3D-simulation of the turbulent wake behind a wind turbine," *Journal of Physics: Conf. Series*, vol. 75, no.1, Aug. 2007.

[71] R. J. Barthelmie, O. Rathmann, S. T. Frandsen, K. Hansen, E. Politis, J. Prospathopoulos, K. Rados, D. Cabezon, W. Schlez, J. Phillips, A Neubert, J. G. Schepers, S. P. van der Pijl, "Modelling and measurements of wakes in large wind farms," *Journal of Physics: Conf. Series*, vol. 75, no.1, Aug. 2007.

[72] F. Gonzalez-Longatt, P. Wall, and V. Terzija, "Wake effect in wind farm performance: steady-state and dynamic behavior," *Renew. Energy*, vol. 39, pp. 329-338, Dec. 2012.

[73] F. Koch, M. Gresch, F. Shewarega, and I. Erlich, "Consideration of wind farm wake effect in power system dynamics simulation," IEEE Power Tech, Russia, pp. 1-7, June 2005.

[74] D.-E. Kim and D.-C. Lee, "Feedback linearization control of three-phase UPS inverter systems," *IEEE Trans. Ind. Electron.*, vol.57, no.3, pp. 963-968, Mar. 2010.

[75] P. Dorato, C. T. Abdallah, and V. Cerone, *Linear Quadratic Control: An Introduction*. Prentice Hall, 1995.

[76] D. D. Siljak, D. M. Stipanovic, and A. I. Zecevic, "Robust decentralized turbine/ governor control using linear matrix inequalities," *IEEE Trans. Power Syst.*, vol. 17, no. 3, pp. 715-722, Aug. 2002.

[77] M. Grant and S. Boyd, CVX: Matlab software for disciplined convex programming, version 2.0 beta. http://cvxr.com/cvx, Sept. 2012.

[78] G. C. Goodwin and K. S. Sin, *Adaptive Filtering Prediction and Control*. NY: Dover, 2009.

[79] B. M. Wilamowski and J. D. Irwin, *The Industrial Electronics Handbook 2nd edition*: *Intelligent Systems*. CRC Press, 2011.

[80] P. M. Anderson and A. A. Fouad, *Power System Control and Stability 2nd edition*. Wiley, 2003.

[81] Y.-N. Yu, *Electric Power System Dynamics*, AP, 1983.

[82] H.-K. Nam, Y.-K, Kim, K.-S. Shim, and K. Y. Lee, "A new Eigen-sensitivity theory of augmented matrix and its applications to power system stability analysis," *IEEE Trans. Power Syst.*, vol. 15, no. 1, pp. 363-369, Feb. 2000.

[83] M. Liserre, F. Blaabjerg, and S. Hansen, "Design and control of an LCL-filter-based three-phase active rectifier," IEEE Trans. Ind. Applicat., vol. 41, no. 5, pp. 1281-1291, Spt./Oct. 2005.

[84] L. Y. Pao and K. E. Johnson, "A tutorial on the dynamics and control of wind turbines and wind farms," American Control Conf., pp. 2076-2089, June 2009

[85] J. H. Laks, L. Y. Pao, and A. D. Wright, "Control of wind turbine: past, present, and future," American Control Conf., pp. 2096-2103, June 2009

[86] T. Ahmed, K. Nishida, and M. Nakaoka, "Advanced control of PWM converter with variable-speed induction generator," *IEEE Trans Ind. Applicat.*, vol. 42, no. 4, pp. 934-945, July/Aug. 2006.

[87] D. Roiu, R. I. Bojoi, L. R. Limongi, and A. Tenconi, "New stationary frame control scheme for three-phase PWM rectifiers under unbalanced voltage dips conditions," *IEEE Trans. Ind. Applicat.*, vol. 46, no. 1, Jan./Feb. 2010.